MICROGRID MULTI-DISTRIBUTED ENERGY RESOURCES FOR POWER MANAGEMENT NETWORK STABILITY

BILAL MOUNEIR SAEED EID

FACULTY OF ENGINEERING
UNIVERSITY OF MALAYA
KUALA LUMPUR

2016

University of Malaya

MICROGRID MULTI-DISTRIBUTED ENERGY RESOURCES FOR POWER MANAGEMENT NETWORK STABILITY

BILAL MOUNEIR SAEED EID

THESIS SUBMITTED IN FULFILMENT
OF THE REQUIREMENTS
FOR THE DEGREE OF DOCTOR OF PHILOSOPHY

FACULTY OF ENGINEERING
UNIVERSITY OF MALAYA
KUALA LUMPUR

2016

University of Malaya

UNIVERSITI MALAYA

ORIGINAL LITERARY WORK DECLARATION

Name of Candidate: **Bilal Mouneir Saeed Eid**

Matrix No.: **KHA110061**

Name of Degree: **Doctor of Philosophy (PhD)**

Title of Thesis: **MICROGRID MULTI-DISTRIBUTED ENERGY RESOURCES FOR POWER MANAGEMENT NETWORK STABILITY**

Field of Study: **Electrical Engineering / Renewable Energy and Power Systems**

I do solemnly and sincerely declare that:

(1) I am the sole author/writer of this Work;
(2) This work is original;
(3) Any use of any work in which copyright exists was done by way of fair dealing and for permitted purposes and any excerpt or extract from, or reference to or reproduction of any copyright work has been disclosed expressly and sufficiently and the title of the Work and its authorship have been acknowledged in this Work;
(4) I do not have any actual knowledge nor do I ought reasonably to know that the making of this work constitutes an infringement of any copyright work;
(5) I hereby assign all and every rights in the copyright to this Work to the University of Malaya ("UM"), who henceforth shall be owner of the copyright in this Work and that any reproduction or use in any form or by any means whatsoever is prohibited without the written consent of UM having been first had and obtained;
(6) I am fully aware that if in the course of making this Work I have infringed any copyright whether intentionally or otherwise, I may be subject to legal action or any other action as may be determined by UM.

Candidate's Signature Date

Subscribed and solemnly declared before,

Witness's Signature Date

Name:
Designation:

University of Malaya

ABSTRACT

The increased demand for power that has to be transferred over long distances within increasing load growth makes the integration of Distributed Energy Resources (DERs) a fast and effective solution. DERs are able to reduce the electrical and physical distances between load and generator, transmission and distribution power losses, and the carbon emission levels. They can also eliminate bottlenecks from distribution and transmission lines. DERs are able to improve reactive power to enhance grid voltage profile and power stability, and utilize waste heat better, postponing the necessity to establish new transmission lines and huge power generation plants. Increased penetration of DERs into conventional power systems, however, increases control challenges. Such challenges can be overcome by a microgrid, whose many features include integrating DERs without interrupting the grid operation, enabling power systems to observe and control faults more effectively, reducing the damage caused by DER outages, feeding critical loads continually, allowing load shedding and automated switching through control algorithms so outages and power restoration time are shortened, allowing either grid-connected or islanded operation, and improving system reliability and flexibility through DER's many options. This work examines the structure of microgrids and reviews their classifications and the literatures discussing their control objectives. It finds that the use of microgrids enhances a conventional power system's grid smartness. It summarizes microgrid control objectives and their most common problems and solutions. It also proposes a single-stage power converter for electronically coupled distributed generation; the converter is able to track the maximum power point and yield unity power factor. A model for the Photovoltaic (PV) array and three-phase grid-connected inverter shows the control parameters. The inverter's controller uses inner and outer control loops to control the injected current and DC voltage. The inner control loop controlling the current by converting the input

University of Malaya

from the abc frame to the dq0 frame then yield the desired reactive power value. The outer voltage control loop tracks the maximum power point through a dynamic reference DC-voltage technique. The active power produced by the single-stage and double-stage power converters are compared (the single-stage converter showed higher efficiency). A dynamic reference voltage is proposed and the variable and the fixed DC reference voltages are compared for their active power yields in the proposed single-stage converter system. The impact on the active and reactive powers, by ambient disturbances such as solar radiation with severe disturbances, and variable PV cell temperature, are investigated. The active and reactive power flows and the voltages of the system at three distances of distribution line are investigated and verified by Matlab/Simulink.

In low-voltage networks with a high penetration of Renewable Energy Sources (RESs), various disturbances may occur such as voltage fluctuation, frequency deviation, high reverse power flow, and high circulating reactive power. This work also proposes a large-scale microgrid grid-connected system of PV and Fuel cell (FC) sources for improving the voltage profiles. Three microgrid configurations were tested using the proposed control strategy to determine the reactive power generated by RESs. The test conditions considered load disturbances, variations in solar radiation(in case one), feeder removal and partial shading (in case two). In other test conditions, we validated a voltage regulator implemented for an FC inverter. The voltage stability was improved at the load bus by maintaining the voltage within acceptable limits. All three microgrid configurations exhibited similar active power losses, but only one of the microgrid configurations had a rapid response time and low circulating reactive power. The results of this study demonstrate the effectiveness of connecting an FC source (i.e., the dispatchable source) to the load bus for regulating the voltage. The effectiveness and superior performance of the proposed configuration verified by comparison with other configurations using Matlab/Simulink.

University of Malaya

ABSTRAK

Permintaan yang semakin meningkat untuk kuasa yang boleh dipindah pada jarak yang jauh dalam meningkatkan pertumbuhan beban menjadikan integrasi pengagihan sumber tenaga (DERs), penyelesaian yang cepat dan berkesan. DERs mampu mengurangkan jarak fizikal dan elektrik antara beban degan janakuasa dan penghantaran dan pengagihan kuasa yang hilang serta tahap pelepasan karbon juga dapat dikurangkan. Mereka juga menunda keperluan mewujudkan talian penghantaran baru dan loji penjanaan kuasa yang besar. Walau bagaimanapun, peningkatan penembusan DERs ke dalam sistem kuasa menyebabkan cabaran untuk mengawalnya menjadi lebih besar. Cabaran tersebut boleh diatasi dengan microgrid yang mempunyai pelbagai ciri istimewa termasuklah integrasi DERs tanpa mengganggu operasi grid-umum, membolehkan sistem kuasa dipantau dan kerosakan dapat dikawal dengan efektif, mengurangkan kerosakan disebabkan gangguan DER, menghantar beban yang kritikal secara berterusan, membolehkan penurunan beban dan suis automatik melalui pengawalan algoritma, jadi masa gangguan elektrik dan pemulihan kuasa dapat dipendekkan, mengaktifkan sama ada grid-bersambung atau operasi yang terpisah, dan meningkatkan kebolehpercayaan sistem dan fleksibiliti melalui pelbagai pilihan DER. Kajian ini meneliti struktur microgrid dan menyemak klasifikasi mereka. Manakala bahagian literatur membincangkan objektif yang dikawal. Kajian ini mendapati bahawa penggunaan microgrids meningkatkan kecekapan sistem tenaga grid konvensional. Ia merumuskan objektif kawalan microgrid dan permasalahan yang selalu timbul dan jalan penyelesaiannya. Turut dicadangkan adalah penukaran kuasa satu fasa untuk elektronik serta penjanaan teragih; pengubah dapat mengesan titik kuasa maksimum dan menghasilkan penyatuan faktor kuasa. Model untuk jajaran fotovoltan (PV) dan grid-bersambung-tiga-fasa songsang mengoptimumkan parameter kawalan. Pengawal songsang menggunakan gelung kawalan dalaman dan luaran untuk mengawal para-

University of Malaya

meter. Gelung kawalan dalaman menukar input dari bingkai abc ke bingkai dq0 untuk menghasilkan penyatuan faktor kuasa. Gelung kawalan voltan luaran mengesan titik kuasa maksimum melalui teknik terbaru yang menggunakan microgrid pada tahap kawalan utama (kawalan setempat). Kuasa aktif menghasilkan satu peringkat dan dua peringkat kuasa penukar dibandingkan (penukar satu peringkat menunjukkan tahap kecekapan yang lebih tinggi). Voltan rujukan dinamik dicadangkan dan pemboleh ubah dan rujukan voltan DC tetap dibandingkan untuk penghasilan kuasa aktif mereka dalam sistem penukar satu peringkat yang dicadangkan. Kesan ke atas kuasa yang aktif dan reaktif, dengan gangguan persekitaran seperti radiasi solar dengan gangguan yang teruk, dan pemboleh ubah suhu sel PV telah dikaji. Aliran kuasa aktif dan reaktif serta voltan dalam system pada pada tiga jarak garis pengagihan dikaji dan disahkan dengan Matlab/Simulink. Kajian ini juga mencadangkan sistem PV microgrid berskala besar dan sumber Sel Bahan Api (FC) untuk menambah baik kestabilan rangkaian pengagihan. Tiga konfigurasi microgrid telah diuji dengan strategi kawalan yang dicadangkan untuk kuasa reaktif yang dihasilkan oleh sumber tenaga yang boleh diperbahrui (RESs). Keadaan ujian termasuklah gangguan beban dan pelbagai radiasi matahari dan penyingkiran pengantara dan teduhan separa. Keadaan ini juga adalah untuk ujian pengesahan pengatur voltan yang dilaksanakan dalam FC songsang. Kualiti dan kestabilan rangkaian pengagihan voltan rendah bertambah baik, seperti yang ditunjukkan oleh voltan pada bus beban. Ketiga-tiga konfigurasi microgrid menunjukkan kehilangan kuasa aktif yang sama. Konfigurasi microgrid kedua menunjukkan masa tindak balas yang pantas dan peredaran kuasa yang rendah. Kajian ini diuat secara umum untuk memperluas penggunaannya kepada mana-mana konfigurasi grid. Keberkesanan dan keunggulan konfigurasi yang dicadangkan berbanding lagi dua konfigurasi disahkan dengan menggunakan Matlab/Simulink.

University of Malaya

ACKNOWLEDGEMENTS

I would like to express my heart's gratitude to those who provided scientific guidance, and continuous support to this project. In particular, I owe thanks to my supervisor Professor Nasrudin Abd Rahim, for many valuable guidance and support, who assisted me appreciatively in his spacious knowledge of Power Conversion and Renewable Energy field. I have also become indebted to the scholarly work of my co-supervisor Dr Jeyraj Selvaraj in his great encouragement and support. This project could not have been achieved without continued honest support, endless patience that have gifted to me from my great parents. My heartfelt thanks goes to my wife, Doaa, for her constantly unwavering support, which makes this dream in reality. I also place on record, my deep gratitude to my two little kids, Mouneir and Ezedeen, whose innocent souls have inspired me throughout the all stages of this work. My special thanks also go to all administrative staff in UMPEDAC and Faculty of engineering, those who help thankfully to let this work have been produced.

University of Malaya

TABLE OF CONTENTS

University of Malaya

University of Malaya

University of Malaya

LIST OF FIGURES

University of Malaya

University of Malaya

University of Malaya

University of Malaya

University of Malaya

LIST OF TABLES

University of Malaya

LIST OF SYMBOLS AND ACRONYMS

V_{ref}	reference voltage.
η	Diode quality factor of PV model.
ζ	damping ratio.
I_{SC}	Short Circuit Current.
I_{mp}	Maximum Power Current.
I_{ph}	Light-generated photo-current.
I_{rsc}	Diode reverse saturation current.
P_{mp}	Maximum Power.
R_s	Series resistance of PV model.
R_{sh}	Parallel resistance of PV model.
T_c	cell temperature.
V_{OC}	Open Circuit Voltage.
V_{mp}	Maximum Power Voltage.
3C	Circular Chain Control.
AC	Alternative Current.
ALS	Average Load Sharing.
B_b	main bus.
B_{FC}	fuel cell bus.
B_L	load bus.
B_{pv1}	photovoltaic bus.
B_{pv}	photovoltaic buses.
CCS	Current Control Strategy.
CERTS	Consortium for Electric Reliability Technology Solutions.
DC	Direct Current.
DER	Distributed Energy Resource.
DNO	Distribution Network Operator.
E*	voltage at no load.
f	Frequency.
f_{fl}	Full load frequency.
f_{nl}	No load frequency.
FC	Fuel cell.
FFC	Feeder Flow Control.
FPD	Frequency Vs. Active Power Droop.
FR	Frequency regulation.
IC	Incremental Conductance.
k_{ii}	Integral Constant.
k_{ip}	Proportional Constant.
LC	Local Controller.
LS	Load sharing.
LSCM	Load shedding controller module.
MC	Matrix Converter.
MGCC	Microgrid Central Controller.
MMO	Multi-Master Operation.
MO	Market Operator.
MPP	Maximum Power Point.
MPPT	Maximum Power Point Tracking.
MS	Master-Slave.
NOCT	nominal operating cell temperature.

University of Malaya

nP	power variation.
P	Active power.
P&O	Perturb and Observe.
PCC	Point of Common Coupling.
PLL	phase locked loop.
PMS	power management system.
PV	Photovoltaic.
Q	Reactive power.
Q_c	Capacitive reactive power.
Q_L	Inductive reactive power.
RES	Renewable Energy Source.
RMS	root mean square.
SM	Synchronous machine.
SMO	Single-Master Operation.
SP	Set point.
tFOCT	tropical field operation cell temperature.
THD	Total Harmonic Distortion.
UPC	unit output power control.
V	Voltage.
V_L	Load voltage.
V_o	Output voltage.
VPD	Voltage Power Droop.
VQD	Voltage Vs.Reactive Power Droop.
VR	Voltage regulation.
VSC	Voltage Source Converter.
VSI	Voltage Source Inverter.
Z_L	Load impedance.
Z_{Line}	Line impedance.
Z_o	Output impedance.

University of Malaya

LIST OF APPENDICES

University of Malaya

CHAPTER 1: INTRODUCTION

1.1 Background

Possibility of increased blackouts can be due to both economical and physical reasons, e.g., (1) increased demand for power that had to be transferred over long distances resulting in huge amounts of lost power, (2) continual load growth unparalleled by sufficient investment into power transmission systems, and (3) extreme swings from one day to the next in power flow dispatch making conventional off-line planning useless. These push power systems to their physical limits, with a possibility of compromising grid reliability. A more intensive on-line analysis is required, to improve grid control reliability (Khosrow Moslehi, 2006). Some of the features of DERs are able to reduce the electrical and physical distances between load and sources and to improve reactive power to enhance grid voltage profile and power quality. They can also eliminate bottlenecks from distribution and transmission lines, reduce transmission and distribution losses. DERs are able to utilize waste heat better, postponing the necessity to establish new transmission lines and huge power generation plants, and keep carbon emission levels low (Knazkins, 2004; Piagi & Lasseter, 2006; Shamshiri, Chin Kim, & Chee Wei, 2012; Sontidpanya, Radman, & Craven, 2011). Control of a Voltage Source Inverter (VSI) in a multiple-DER microgrid is different compared to a single grid-connected DER which is controlled by Current Control Strategy (CCS). Challenges to having multiple-DERs include: (1) CCS unable to function during islanded mode because there is no dominant source of energy (Katiraei & Iravani, 2006; Mao, Liuchen, & Ding, 2008) and (2) multiple-DERs have multiple power generation characteristics and capacities, therefor the microgrid needs rapid regulation more in islanded mode than in grid-connected mode (Mao et al., 2008). An increased presence of DERs, especially in a distribution network (medium-voltage or

University of Malaya

low-voltage), may cause problems such as voltage rise and unstable network voltage and frequency either during operation of the DERs or upon their sudden tripping (Carvalho, Correia, & Ferreira, 2008; N. D. Hatziargyriou & Sakis Meliopoulos, 2002; Mao et al., 2008; Masters, 2002). The microgrid paradigm is that a group of microsources and loads with some form of energy storage operate as a controllable system, providing heat and power to local communities, which is able to overcome the aforementioned problems (Duan, Gong, Li, & Wang, 2008). Microgrid features include;

- integration of DERs without interrupting public-grid operation, thus a lot of DERs can be installed without reforming or rewiring the distribution network (Duan et al., 2008; R. H. Lasseter, 2011; R. Lasseter & Piagi, 2006);
- enabling power systems to observe and control faults more effectively, and reduce the damage caused by a DER outage; this boosts the power system's smart grid capability (N. D. Hatziargyriou & Sakis Meliopoulos, 2002; J. Lopes, Hatziargyriou, Mutale, Djapic, & Jenkins, 2007; Shamshiri et al., 2012);
- allowing load transfer and automated switching through control algorithms to shorten outage and power restoration time, and keeping the faulted section of the distribution line isolated until utility crews locate the fault location (Canada, 2012; J. Lopes et al., 2007; Shamshiri et al., 2012);
- allowing to run in either grid-connected or islanded mode according to economy or a planned disconnection, or to restore the grid power quality when it drops below certain standards (Alsayegh, Alhajraf, & Albusairi, 2010; Duan et al., 2008; Kamel, Chaouachi, & Nagasaka, 2011; Serban & Serban, 2010);
- improving system reliability and flexibility, through the many options of DERs (Driesen & Katiraei, 2008; Piagi & Lasseter, 2006; Silva, Morais, & Vale, 2012;

University of Malaya

Yunwei, Vilathgamuwa, & Poh Chiang, 2004);

- using DER waste heat to improve generation efficiency (Ahn et al., 2010; Blaabjerg, Chen, & Kjaer, 2004; Kroposki et al., 2008; Mao et al., 2008; R. H. Lasseter, 2011);

Due to these advantages, significant changes around the world are taking place to integrate more Renewable Energy Resources (RES) into electrical systems. A county like Germany has already supplied 25 % of their electrical consumption from DERs (von Appen, Braun, Stetz, Diwold, & Geibel, 2013). The aforementioned features do have drawbacks, especially if the RESs are forming a significant portion of the DERs. High penetration of RESs can cause negative effects includes voltage rise, circulating current, unstable network voltage and frequency, and reverse power flow in the transmission lines (von Appen et al., 2013; Carvalho et al., 2008; N. D. Hatziargyriou & Sakis Meliopoulos, 2002; Masters, 2002). These drawbacks are more likely to occur when the RESs are connected to low voltage distribution networks (von Appen et al., 2013; Farhangi, 2010). The following section presents microgrids integration challenges.

1.2 Problem Statement

Microgrid system presents electrical challenges such as contain three phase, single phase and variety of electronically coupled sources which need different control approaches (Salam, Mohamed, & Hannan, 2008). Microgrids can cause several technical problems in its operation and control. Factors affecting choice of the required control and operation strategies of a microgrid include power quality restrictions, DER type and depth of penetration, load characteristics, and load market sharing strategies. Thus significantly different control approaches in microgrid are required. And the reasons are as follow (Z. Chen, 2012; Katiraei, Iravani, Hatziargyriou, & Dimeas, 2008; R. H. Lasseter, 2011; Ustun, Ozansoy, & Zayegh, 2011):

University of Malaya

- Most DERs are electronically coupled units with different steady-state and dynamic characteristics from those of conventional generator units.
- Imbalance, due to single-phase loads, is more common in microgrids.
- DERs within microgrids significantly involve “uncontrollable” sources such as wind and PV units.
- In microgrids, short-term and long-term energy storage devices can affect control and operation.
- Microgrids are forced by economics to rapidly accommodate connection and disconnection of DER units and loads during system operation.
- Microgrids are sometimes required to prioritize service to critical loads.
- Microgrids need to preset the power quality levels.

Abovementioned microgrid requirements causes problems for the system, such as; deviation in the line frequency, circulating reactive current (Azmi, Adam, Ahmed, Finney, & Williams, 2013; De Brabandere et al., 2007a), unbalanced reactive power flow, unbalanced Z_{line} (Kamel et al., 2011; R. H. Lasseter, 2002; Piagi & Lasseter, 2006), high Total Harmonic Distortion (THD), ineffective control methods, failed in islanding mode detection and overcurrent flow in the system (Serban & Serban, 2010; Tuladhar, Jin, Unger, & Mauch, 2000; Turitsyn, Sulc, Backhaus, & Chertkov, 2011). Figure 1.1, summarizes the challenges associated with microgrid operation, and categorize each problem under the related factor.

1.2.1 Microgrid Configuration and Structure

As some papers considers the microgrid configuration effects on power flow control (Ahn et al., 2010), however previous studies did not deeply investigate how different

University of Malaya

Microgrid Challenges		
	Voltage (amplitude and frequency)	-Deviation of the line frequency
		-Circulating reactive current
	P and Q Power sharing	-Unbalanced Q flow
		-Unbalanced Z_{line}
		-High THD
		-Droop method not effective
	Protection	-Overcurrent flow
		-Failed in islanding detection
	Microgrid topology and configuration	-Large scale DERs
		-Power conversion systems
		-Distance between DERs
		-Microgrid point of connection to public grid

Figure 1.1: Challenges associated with microgrid operation.

microgrid configurations can influence; voltage profile, active and reactive power flow.

Although, conventional DERs with battery can constitute the microgrid as proposed in (Koohi-Kamali, Rahim, & Mokhlis, 2014; Elsied, Oukaour, Gualous, & Hassan, 2015), however, the RESs integration are associated with more challenges, such as; intermittent power source and non-dispatchable power supply (J. Wu et al., 2015). Many RESs aggregation have been studied (von Appen et al., 2013; Shahnia, Majumder, Ghosh, Ledwich, & Zare, 2010; Ahn et al., 2010; Rekik, Abdelkafi, & Krichen, 2015), the PV with FC combination is one of the most attractive combination for RESs (Khanh, Seo, Kim, & Won, 2010; Elsied et al., 2015) the operation effectiveness without battery is required to be investigated.

1.2.2 Power Conversion System

A power conversion system is designed to transfer power from the Direct Current (DC) source to the AC utility. Power conversion systems can be classified into two types

University of Malaya

depending on the number of power processing stages: single-stage (Ozdemir, Altin, & Sefa, 2014; Xiao, Edwin, Spagnuolo, & Jatskevich, 2013), and two-stage power conversion systems (Eid, Rahim, Selvaraj, & El Khateb, 2014; El Khateb, Rahim, Selvaraj, & Uddin, 2013, 2014; Bastos, Aguiar, Goncalves, & Machado, 2014). The latter is the most common configuration for electronically-coupled distributed energy resources (DER). A two-stage conversion system has two converters. The one on the PV side extracts maximum power from the PV and the other is a synchronized inverter connected to the utility side, which controls the active and reactive power dispatched. In a single-stage approach, the inverter solely handles the requirements of the power conversion system. Although single-stage conversion needs a bulky line transformer, it offers advantages such as high conversion efficiency, simplified topology, low cost, and compactness (Yazdani et al., 2011; Jang & Agelidis, 2011; Alajmi, Ahmed, Adam, & Williams, 2013; Das & Agarwal, 2012).

1.2.3 Distance Between DERs and PCC

The distance between DER and the PCC can affect system power flow due to many different reasons such as; line power losses, resonant effect, communication between parallel DERs and short circuit current (M. C. Chandorkar, Divan, & Adapa, 1993; Ustun et al., 2011). The location of the DER, which is determined mostly by environmental and economic factors, may not be close to the PCC. Therefore, the effect of variable distribution line distance between DERs and PCC is required to be studied.

1.2.4 Large Scale RESs in Microgrid

The penetration of RESs in power system increased dramatically last few years. Even though, micro-RESs used widely in microgrids due to their simplicity and low capital cost, the large scale RESs attracted investors and operators attention due to their competitive features such as; high clean energy integration and lower cost per installed

University of Malaya

watt. Many large scale projects implemented worldwide integrated different types of DERs, storage device and loads. Therefore, the large scale microgrid parameters and components are required to be studied to present their effects on low voltage distribution network.

1.2.5 Microgrid Point of Connection with grid

The electrical power system lines and buses have different voltage profile and active and reactive power flow. To connect a microgrid system to a grid the critical lines and buses have to be specified. Microgrid connection to a properly chosen bus, reduce the total power losses of the grid and increase the grid stability. The standard IEEE 30-bus test system represents the grid as many previous works shows (Saadat, 2002; Zabaiou, Dessaint, & Kamwa, 2014). The effectiveness of microgrid connection to IEEE 30-bus test system is required to be study.

1.2.6 Voltage and Frequency Control

When a cluster of DERs connected to the loads operates, the problem of voltage stability appears. Either mode of operation requires different controlling approaches. It is necessary to regulate the voltage during islanded operation by using a voltage versus reactive power droop controller for local reliability and stability, while regulating current during grid-connected operation. A dynamic analysis of generation control scheme consisting of active power-frequency and reactive power-voltage controllers for the inverter based distributed generations. These droop-based controllers that allow decentralized operation of the microgrid without communication needed between the DERs and Microgrid Central Controller (MGCC). The fast and accurate voltage and frequency control are fundamental requirements for successful operation at low voltage networks. The control of storage unit in microgrid is not enough to manage/restore voltage and frequency near the set values. Besides that, controllable loads and DERs (e.g. PV, FCs and microtur-

University of Malaya

bines) would take part in voltage and frequency control according to their voltage and frequency droops. Because of low lines impedance, the circulating reactive current problem frequently appears, this my deviate the voltage of the system (R. H. Lasseter, 2011; Z. Chen, 2012). The aforementioned challenges have to be solved to enable the plug and play functionality of connection for DERs in distribution network.

1.2.7 P and Q Power Sharing

Power sharing management is an important task during both grid-connected and islanded modes. Power sharing is required to ensure each DER supplies its pre-set proportion at steady-state (Zhang, Huang, Jiang, & Wu, 2010), minimum system power losses, operating within the DERs limit (Peng, Li, & Tolbert, 2009; Rocabert et al., 2012; Moreira, Resende, & Peas Lopes, 2007; Green & Prodanović, 2007), high level of power quality, low harmonic distortion (Mazumder, Tahir, & Acharya, 2008; M. Chandorkar & Divan, 1996; Hanaoka, Nagai, & Yanagisawa, 2003), and specific value of voltage, system operation within the stability margin (Barklund, Pogaku, Prodanovic, Hernandez-Aramburo, & Green, 2008; De Brabandere et al., 2007b; Sao & Lehn, 2008). The aforementioned criteria have to be considered to achieve smooth operation for microgrid.

1.2.8 Protection

Microgrid protection is one of the important challenges facing the implementation of the microgrids. Once a microgrid is formed, it is important to assure that the loads, lines and the DERs are protected. Two alternative current limiting algorithms are available to prevent from overcurrent flow and protection of microgrid during utility-voltage sags (Miveh, Mirsaeidi, & Gandomkar, 2012). A protection scheme based on directional is a good solution for microgrids as (Salam et al., 2008) proposed. Directional overcurrent relays are used to protect the lines during both grid-connected and islanded operation. The protection question is; how to have the same protection strategies for both grid-connected

University of Malaya

and islanded operation. Microgrid is interfaced to distribution network by a fast static switch to protect a microgrid in both modes of operation against all types of faults.

1.2.8 (a) Islanding

It is necessary for the microgrid to operate in autonomous mode. Autonomous mode may be intentional or unintentional due to prescheduled maintenance or grid disturbance or outage. By operating in islanded mode, microgrids must be able to supply critical load without interruption, run at specific values for voltage and power, extract the maximum power from the DERs. Islanding mode detection is an important control function to handle. Fast and accurate isolation are essential to achieve an effective power management (J. A. P. Lopes, Moreira, & Madureira, 2006; Madureira, Moreira, & Lopes, 2005; Sao & Lehn, 2006; Savaghebi, Jalilian, Vasquez, & Guerrero, 2013).

1.3 Research Objectives

The main goal of this work is to contribute to the expandability of the microgrids, through the development of suitable stability criteria. The stability criteria should be applicable to microgrids that may grow and deal with different circumstances. The main objectives of this work are as follow;

- to investigate the difference between double stage and single stage power conversion systems in terms of efficiency, reliability and Maximum Power Point Tracking (MPPT) capability;
- to enhance the voltage stability in presence of large penetration of DERs, various operating modes, resistive and inductive load and distance effect;
- to investigate different microgrid configurations with different DERs types (such as; dispatchable and non-dispatchable DERs), with concluding the best structure in terms of power and voltage stability at the Point of Common Coupling (PCC);

University of Malaya

- to extend distributed control of active and reactive power to ancillary functions of getting the MPPT without using DC-DC converter and operating at unity power factor mode;

1.4 Scope of Work

Microgrid with multi DERs and local loads were studied in this work. A grid connected microgrid without backup energy storage systems were designed. PV and FC sources with single stage power conversion system were developed. Three large-scale microgrid configurations have been investigated for their effects to distribution networks under conditions of solar radiation with severe disturbances, load disturbance, feeder removal, and partial shading. Each microgrid, comprising PV and FC sources with a local load, was connected to a low voltage distribution network. Active and reactive powers dispatched from the sources and importer/exported to the grid were studied to show the effectiveness of power management strategies.

1.5 Methodology

The methodology of this research began through deeply studying the previous works. The power conversion systems are the controllable part of the DERs, this make them the important part to began this research with. In this work a single-stage power conversion system was used. Single-stage power conversion systems offer advantages such as high conversion efficiency, simplified topology, low cost, and compactness (Yazdani et al., 2011; Alajmi et al., 2013; Das & Agarwal, 2012). Then a study for similar microgrid projects were achieved, which guide the researcher to choose the suitable DERs for this work. After that the concept of the proposed microgrid with large scale PV sources, FC source, local loads, inverters and grid were modeled and simulated by using MATLAB/Simulink. For the purpose of studying the power management effect of the network stability three microgrid configurations were designed. Each configuration studied un-

University of Malaya

der many cases. The cases investigated are; radiation variation, load variation, dynamic DC reference voltage, feeder removal and voltage regulator. During these cases the active power, reactive power and the RMS voltage are measured and studied. Then a comparison between the different configurations was taken place, with concluding the findings.

1.6 Thesis Outline

The following chapters of the thesis are organized as follows: Chapter 2 presents an overview of microgrid control methods and objectives. Microgrid controlling layers are explained, and the three main controlling functions are summarized; Chapter 3 compared between single and double stage power conversion systems, and illustrates the three phase inverter modeling. Moreover, the simulation used to show the effectiveness of the inverter voltage and current controllers at variable radiation and temperature; Chapter 4 presents three microgrid configurations and compare the voltage regulation and power flow with variable cases (such as; radiation variation, load variation, feeder removal and partial shading), the simulation results and discussion are described; then Chapter 5 concludes the work.

University of Malaya

CHAPTER 2: AN OVERVIEW OF MICROGRID CONTROL METHODS AND OBJECTIVES

2.1 Introduction

This chapter examines the system control used for grid connected and islanded operation (e.g., voltage and frequency regulation, load sharing optimization and active reactive power dispatching). As there is no synchronous machine in most microgrids to achieve demand and supply balancing, the inverters are used for balancing. Voltage source inverter (VSI) is used to provide a reference for voltage and frequency that enables microgrids to operate in islanded mode (J. A. P. Lopes et al., 2006; Georgakis, Papathanassiou, Hatziargyriou, Engler, & Hardt, 2004). The current control strategy plays the main role in power flow performance enables microgrids to operate in grid connected mode (Kadri, Gaubert, & Champenois, 2011).

2.2 Microgrid Configuration

The Consortium for Electric Reliability Technology Solutions (CERTS) definition of microgrid is cluster of DERs, storage systems, and loads which can operate in either grid-connected mode or islanded mode (R. H. Lasseter, 2011). Figure 2.1 shows a basic Microgrid structure. The electrical system consists of three radial feeders that are connected to the grid, the point of connection is the PCC. MGCC is the main controller in microgrid. It is responsible for stabilizing the active and reactive powers dispatched from each DER and also the voltage and frequency at PCC. The circuit breaker installed at each feeder start-point provides the critical feeders (which contain the DERs and the critical loads) with the capability to supply the loads separately from the grid. Local Controller (LC) controls the DERs production and storage units and some of the local loads. In a centralized operation LCs receive set-points from the MGCC, whereas in a decentralized

University of Malaya

one they make decisions locally (Mao et al., 2008; Z. Chen, 2012; Jiayi, Chuanwen, & Rong, 2008).

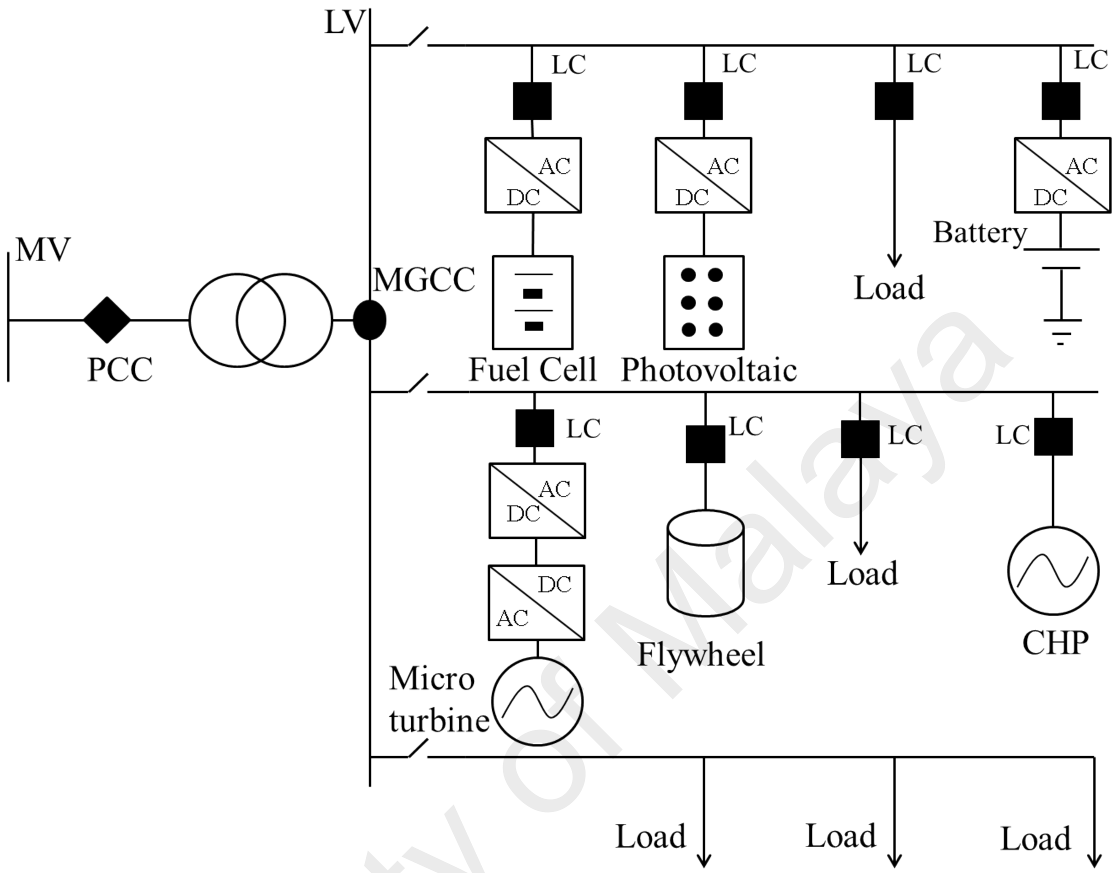

Figure 2.1: Microgrid basic structure.

2.3 Control Layers

The microgrid control system has to ensure that all the control functions, e.g., supply of electrical and/or thermal energy, continuous feeding of the critical loads, energy-market participation, auto-reconnection after failure, etc. (J. Guerrero, Vasquez, Matas, Castilla, & de Vicuna, 2009). The control objectives can be achieved through either centralized or decentralized control, and through three control layers as shown in Figure 2.2. Some authors (Mao et al., 2008; Dimeas & Hatziargyriou, 2005) call the supervisory control architecture as a multi-agent controller. Previous works (Katiraei et al., 2008; Z. Chen, 2012; Bo, Xuesong, & Jian, 2012; Tuladhar et al., 2000) summarized the control levels as follow:

University of Malaya

- Distribution Network Operator (DNO) and Market Operator (MO)
- Microgrid Central Controller (MGCC)
- Local Controller (LC), which can be either Source Controller or Micro Load Controller.

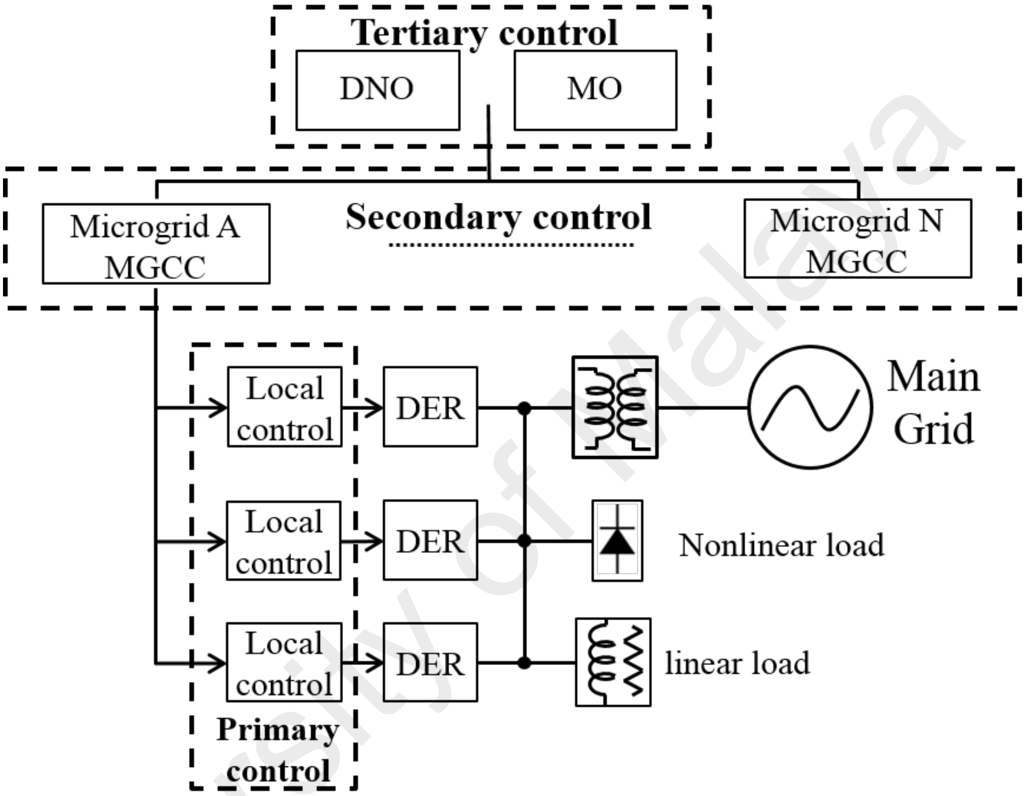

Figure 2.2: General architecture of hierarchical microgrid control system (multi-agent controller).

DNO is necessary where there is more than one microgrid in the distribution system. Also, for the Market Environment of a specific area, one MO or more is responsible for market management of the microgrid. Both DNO and MO are part of the grid; they do not belong to the microgrid. The second level is MGCC, which is the main integrator of the DER clusters in a microgrid. It is responsible in stabilizing voltage and frequency at PCC, and responsible for the active and reactive powers dispatched from each DER (Ustun et al., 2011; Bo et al., 2012). The LCs are the lower level of control sometimes known as peer-to-peer (Mao et al., 2008). They control the DERs and some of the local loads, and balancing the active and reactive powers were dispatched for the DER. They have a certain intelligence level thus can make decisions locally in a decentralized operation model (whereas in a centralized model the LCs receive set points from the MGCC) (Katiraei et al., 2008; N. Hatziargyriou et al., 2005; R. Lasseter & Piagi, 2006; Engler, 2005). Figure 2.2 shows the DNO, MGCC and LCcontrol layers.

2.4 Control Strategies

There are two main control strategies proposed for microgrids during islanded mode: (a) SMO and (b) MMO (J. A. P. Lopes et al., 2006; Moreira et al., 2007). Both use VSI to provide a reference for voltage and frequency (Georgakis et al., 2004) and a convenient secondary load-frequency control must be considered to maintain the frequency between the specified limits and run the DER economically (Kamel et al., 2011; J. A. P. Lopes et al., 2006; Madureira et al., 2005).

2.4.1 Single-Master Operation (SMO)

This approach has one inverter acting as VSI (the master) and others as followers (the slaves). When the main power supply is lost, the slaves take voltage reference from the master and operate in PQ mode. The LCs receive set points from the MGCC to maintain generation of active and reactive powers at the specified values. The part within the thick dashed lines in Figure 2.3 illustrates SMO scheme (J. A. P. Lopes et al., 2006; Moreira et al., 2007).

2.4.2 Multi-Master Operation (MMO)

Figure 2.3 also illustrates MMO approach, in which several inverters act as VSI (the master). The VSI can be connected to storage devices or to DERs. Other inverters with PQ control may also coexist. The generation profile can be modified by the MGCC, which can define new set points for the LCs.

University of Malaya

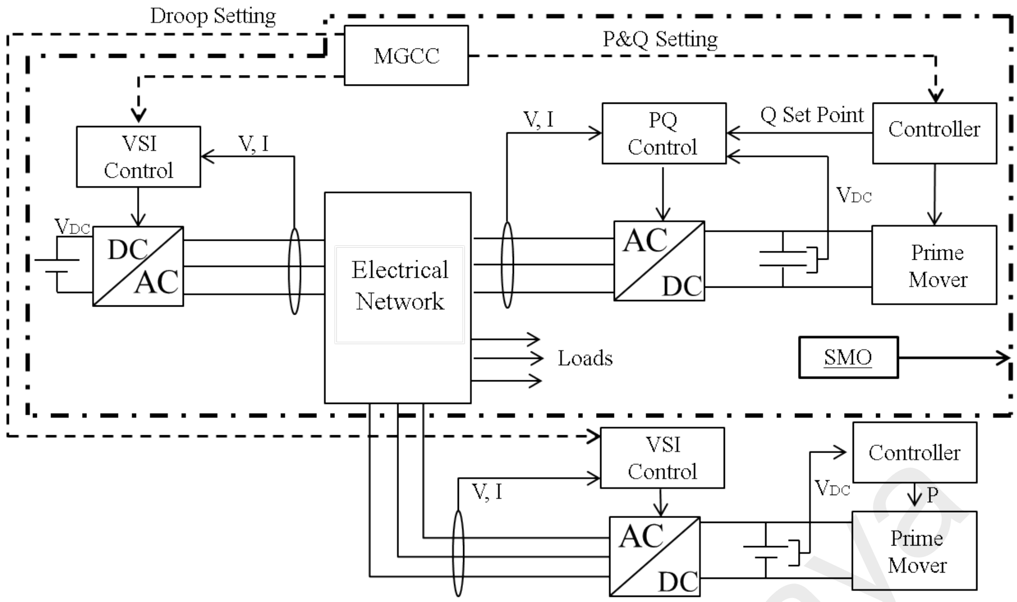

Figure 2.3: MMO Control, with SMO inside the dashed lines.

2.5 Wire and Non-Wire Interconnections

Instantaneous load sharing in microgrid is achieved through two main control schemes. The control schemes are classified according to their control-wire interconnections (Z. Chen, 2012; Gurrero, De Vicuna, & Uceda, 2007). One of the two is active load sharing technique, which has parallel-connected microgrid converters, including; Master-Slave (MS) (Holtz, Lotzkat, & Werner, 1988; Holtz & Werner, 1990; Lee et al., 1998; Pei, Jiang, Yang, & Wang, 2004; Tamai & Kinoshita, 1991; Y. J. Cheng & Sng, 2006), centralized (Iwade et al., 2003; Martins, Carvalho, & Araujo, 1995) Average Load Sharing (ALS) (Sun, Lee, & Xu, 2003; He, Xing, & Hu, 2004; Tan, Lin, Zhang, & Ying, 2003), current limitation (Chiang, Lin, & Yen, 2004), and Circular Chain Control (3C) (Chiang et al., 2004; T.-F. Wu, Chen, & Huang, 2000). These control schemes critically need intercommunication lines, which can decrease system reliability and expandability, though they enable good voltage regulation and accurate current sharing (J. M. Guerrero, Hang, & Uceda, 2008; Tuladhar et al., 2000). The other control scheme for parallel inverters is based mainly on droop method (Serban & Serban, 2010; Rocabert et al., 2012; Mazumder et al., 2008; M. C. Chandorkar et al., 1993; M. Chandorkar & Divan, 1996; Zanxuan &

Wenlong, 2004; Borup, Blaabjerg, & Enjeti, 2001; Chiang, Yen, & Chang, 2001). This technique adjusts the output voltage and frequency in functions of active power (P) and reactive power (Q) delivered by the inverter (Hanaoka et al., 2003; Barklund et al., 2008; Delghavi & Yazdani, 2012). Droop method uses only local power measurements, so better reliability and flexibility is achieved in the physical location of the units (J. Guerrero, de Vicuña, Matas, Castilla, & Miret, 2004; Katiraei et al., 2008).

2.6 Control Function

Published works on microgrid have been mostly about the control functions and strategies (Katiraei & Iravani, 2006; J. A. P. Lopes et al., 2006; Green & Prodanović, 2007; Eid, 2012). The next part of this thesis reviews the techniques and strategies for control of DER converters in a microgrid system. The two modes of operation for microgrids are equally important, however, each mode has his own challenges i.e; synchronization in grid connected mod and controlling without dominant source in islanded mode (Delghavi & Yazdani, 2012).

2.6.1 Voltage Stability

Terms relating to voltage stability include voltage quality, voltage regulation, voltage distortion and voltage profile. Voltage stability in microgrid is to maintain the voltage amplitude stable at a level required by the system. A voltage controller at each DER unit provides local stability. Without local voltage control, systems with high penetrations of DER might experience voltage and/or reactive power oscillations (Piagi & Lasseter, 2006; R. H. Lasseter, 2011). Voltage stability in islanded mode has been much studied (Yunwei et al., 2004; Piagi & Lasseter, 2006; Katiraei et al., 2008; R. H. Lasseter, 2011; Rocabert et al., 2012; Moreira et al., 2007; Bo et al., 2012; Pogaku, Prodanovic, & Green, 2007; Delghavi & Yazdani, 2012). The concept of voltage control can be expanded to include voltage balancing between the three phases (Prodanovic & Green, 2006).

University of Malaya

2.6.1 (a) *Factors Affecting Voltage Stability*

Control is more complicated in low-voltage distribution networks, because of their resistive nature, which may cause coupling between the active power and the voltage (instead of the frequency) (Pogaku et al., 2007). Load characteristics can affect microgrid performance in e.g., voltage stability and transient stability (Z. Chen, 2012). There are reactive currents circulating between the DERs. The problem is prominent in a microgrid because the impedance between the DERs is not large enough to prevent the circulating current. A possible solution is the use of a voltage-vs-reactive-power controller, which at capacitive reactive power (Q_C) should reduce the set point of the local voltage and at inductive reactive power (Q_L) should increase it. The maximum allowable set point voltage is up to maximum reactive power ($Q_{C,max}$) at capacitive reactive power, and ($Q_{L,max}$) at inductive reactive power as shown in Figure 2.4 (a). At nominal voltage (V_o) the reactive power is (Q_o), when reactive power increases to ($Q_{L,max}$) the voltage drops to minimum voltage (V_{min}) (see Figure 2.4 (b)) (Piagi & Lasseter, 2006; R. H. Lasseter, 2011; R. Lasseter & Piagi, 2006; Yunwei et al., 2004; Hien, Mithulananthan, & Bansal, 2013). PV generator can be used as synchronous generator to compensate reactive power through the inverter (Azmi et al., 2013; Turitsyn et al., 2011). Distance between the loads and the DERs can also affect the voltage stability, because line impedance varies with the distance, causing an unbalanced flow of reactive power (J. Guerrero, Matas, De Vicuna, Berbel, & Sosa, 2005; Aman, Jasmon, Mokhlis, & Bakar, 2012; R. H. Lasseter, 2011).

2.6.1 (b) *Control Techniques and Strategies*

- Nested control-loops: The term refers to two control loops (Yunwei et al., 2004; Green & Prodanović, 2007; Prodanovic & Green, 2006): inner and outer. The inner loop is placed around the inductor and the VSI to form a controlled current source (current control loop), whereas the outer one is a voltage control loop, which works on the voltage error, setting the required current for the inner loop. Voltage control loop aims to provide good tracking of slow changes in the output voltage reference signal and to minimize the output voltage errors caused by load output current disturbances (Peng et al., 2009; Green & Prodanović, 2007; Prodanovic & Green, 2006).

- Microgrid central controller MGCC: As mentioned in section 2.3 there are three control layers in microgrids and MGCC is the second layer, responsible in keeping voltage at PCC between specific limits (Shamshiri et al., 2012; Mao et al., 2008; Katiraei et al., 2008; Kroposki et al., 2008; Z. Chen, 2012; J. A. P. Lopes et al., 2006; Moreira et al., 2007; N. Hatziargyriou et al., 2005).

- Voltage (V)/Frequency (f) inverter control: This is not a new control technique. It has been used (Bo et al., 2012) to illustrate that during islanded mode, voltage and frequency are controlled by the DER converter.

- Voltage control loop: Despite this term's frequent use (Song, Chung, & Enjeti, 2004; Sao & Lehn, 2006; Delghavi & Yazdani, 2012; De Brabandere et al., 2007b; J. Guerrero, Vasquez, Matas, de Vicuña, & Castilla, 2011; Kim, Yu, & Choi, 2008) it represents neither control technique nor strategy but only describes the controller which control's voltage.

- Voltage Vs.Reactive Power Droop (VQD) controller: This control strategy is one of the most famous and important strategies used to control voltage (Piagi & Lasseter, 2006; R. H. Lasseter, 2011; Kroposki et al., 2008; Z. Chen, 2012; J. Guerrero et al., 2011). It mainly ensures that the circulating reactive current between the sources does not exceed the DER ratings (maximum capacitive reactive power ($Q_{C,max}$) and maximum inductive reactive power ($Q_{L,max}$)). A droop controller for voltage

University of Malaya

Vs reactive power is thus required, increasing the local voltage set point when the DER generates inductive reactive power (conversely, the set point reduces when Q becomes capacitive). The maximum allowable set point voltage is up to maximum reactive power ($Q_{C,max}$) at capacitive reactive power, and ($Q_{L,max}$) at inductive reactive power as shown in Figure 2.4 (a). At nominal voltage (V_o) the reactive power is (Q_o), when reactive power increases to ($Q_{L,max}$) the voltage drops to minimum voltage (V_{min}) (see Figure 2.4 (b)) (Piagi & Lasseter, 2006; R. H. Lasseter, 2011; R. Lasseter & Piagi, 2006; Yunwei et al., 2004; Hien et al., 2013).

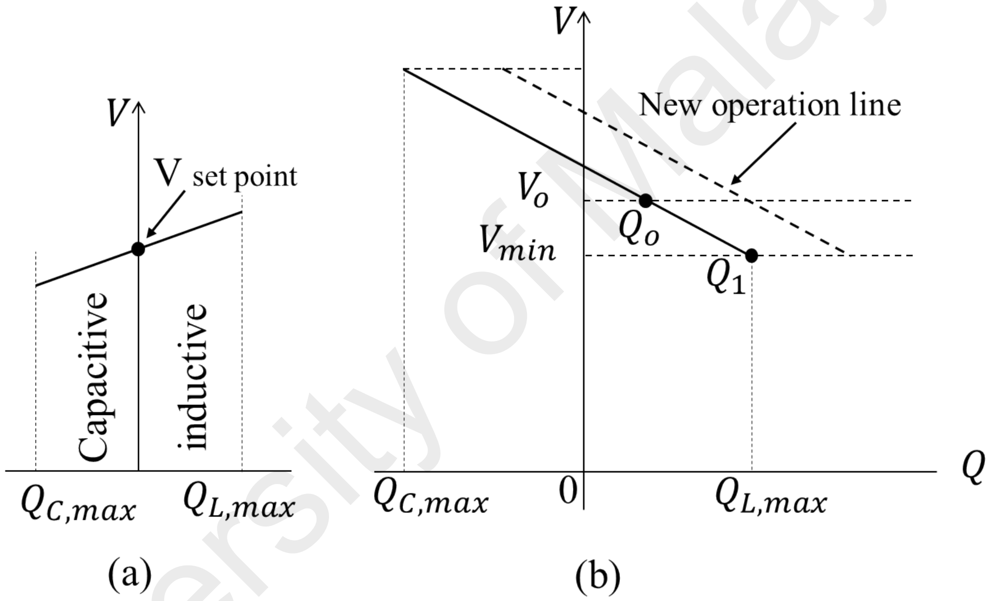

Figure 2.4: (a) Voltage set point to remove circulating reactive current; (b) Voltage Vs reactive power controller.

- Current-Controlled Matrix Converter (MC): One of the purposes of this controller (Marei, 2012) is to regulate voltage at the load terminals. It must thus feed a specific amount of current to the load, and therefore controls the load current, keeping the terminal voltage at the desired level.

- Voltage Power Droop (VPD): Unlike VQD controller, VPD technique shows that Microgrid voltage depends on active power balancing and not on reactive power (Sao & Lehn, 2008, 2006). Reference (Sao & Lehn, 2006) suggests a control scheme that allows a single Voltage Source Converter (VSC) to operate in an intentional islanding mode but not parallel with other VSCs in the same islanded microgrid. This is a problem overcome by VPD/FQB controllers (Sao & Lehn, 2008) that allow control of multiple VSCs in the same microgrid.

2.6.2 Frequency

In islanded mode, the DERs have to control the microgrid frequency cooperatively and synchronously with each other. As there is no dominant source during islanded mode, frequency control and synchronization is a challenge (Mao et al., 2008; Katiraei et al., 2008; Katiraei & Iravani, 2006), (Peng et al., 2009). In a conventional power system, synchronous machines play a main role in achieving synchronization and frequency stability - a role that microgrid inverters must now assume (J. A. P. Lopes et al., 2006; Moreira et al., 2007). The line frequency range should not exceed the pre-set values. The minimums and maximums of the frequency ranges (Serban & Serban, 2010) are 48Hz to 51Hz for 50Hz grids and 59.3Hz to 60.5Hz for 60Hz grids. Microgrid frequency has been much studied (N. D. Hatziargyriou & Sakis Meliopoulos, 2002; Engler, 2005; Katiraei & Iravani, 2006; J. Guerrero, Matas, de Vicuña, Castilla, & Miret, 2007; Katiraei et al., 2008; Duan et al., 2008; Serban & Serban, 2010; Ahn et al., 2010; Ustun et al., 2011; Rocabert et al., 2012; Bo et al., 2012) with the general aim of overcoming the frequency instability caused by the factors listed below.

2.6.2 (a) Factors Affecting Frequency Stability

- Battery voltage exceeding the pre-set value through overcharging; this affects demand and supply balancing, causing frequency disturbance at PCC (Serban & Serban, 2010; Georgakis et al., 2004).

- Variation in load or generation; this affects line frequency, because demand has to

University of Malaya

be same as the supply instantaneously (Duan et al., 2008; Ahn et al., 2010; Zhang et al., 2010).

- Unintentional islanding may cause frequency deviation as some imported or exported power will be lost suddenly (Ustun et al., 2011).

2.6.2 (b) Control Techniques and Strategies

- Frequency Vs. Active Power Droop (FPD)

  Real power versus system frequency is the most famous and popular technique (Piagi & Lasseter, 2006; Mao et al., 2008; Katiraei et al., 2008; Serban & Serban, 2010, 2010; R. H. Lasseter, 2011; Peng et al., 2009; Rocabert et al., 2012; Bo et al., 2012). It uses microgrid frequency to balance system-generated active power. It is proven to be robust and seamlessly adapts to power system variations. The relation between frequency and real power of each DER can be expressed as:

$$f_1 = f_o - K^U(P_1 - P_o) \tag{2.1}$$

  Where K^U is the droop constant of unit output power control (UPC) mode, f_1 and P_1 are respectively the new frequency and the DER output power, and f_o and P_o are the initial operation points. When the load increases, the DER output power also increases, associating with frequency reduction as Equation 2.1 shows. Figure 2.5, shows the FPD characteristic. There are two DERs (a and b), operating at f_o. When the power shares of any DER increases for any reasons (e.g., intentional or unintentional islanding or a demand hike), the new operating points for power become P_{a1} and P_{b1} instead of P_{ao} and P_{bo}. Frequency thus sags to a new value f_1, which is below the lower limit. Consequently then, a new operating line for each unit forms to return the system to the pre-set frequency values.

University of Malaya

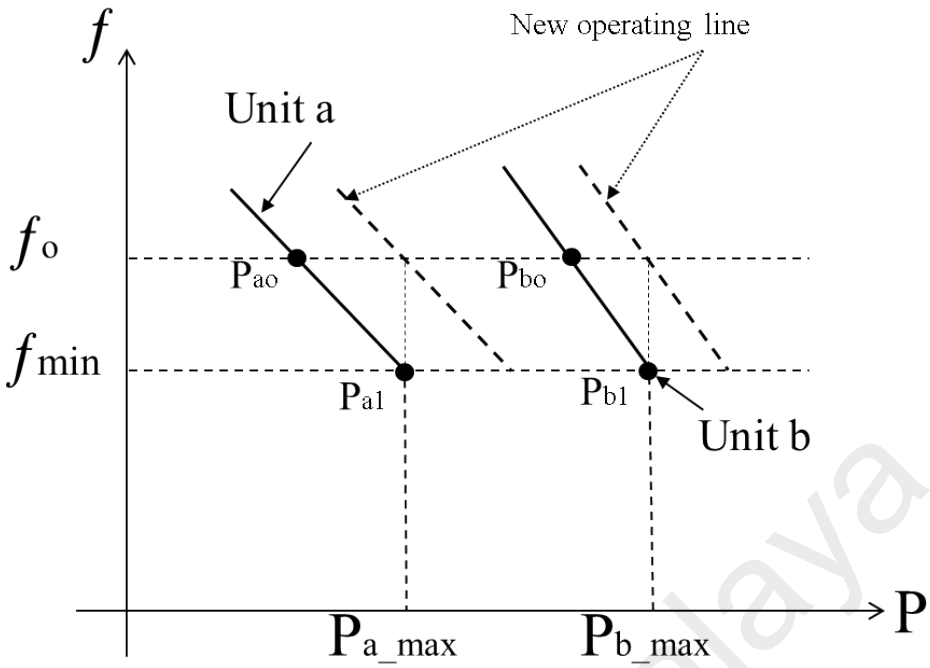

Figure 2.5: Frequency Vs. active power droop characteristics.

- Current-Controlled MC

  One of the tasks of this controller (Marei, 2012) is to keep the frequency constant. To do so, the MC feeds the load a specific amount of current, i.e., current control forces the MC current to follow the reference value, keeping the frequency constant within the source rating.

- Frequency-Reactive Power Boost FQB Controller

  This is the proposed technique, in which the frequency depends on the reactive power (whereas power balancing determines microgrid voltage) and which is in stark contrast with a conventional power system. Because there is no generator with rotational inertia in microgrids, the PCC capacitor dynamics have to control the relation between frequency and reactive power (Carvalho et al., 2008; Ustun et al., 2011; Sao & Lehn, 2008, 2006).

University of Malaya

2.6.3 Load-Sharing Q and P

An essential criterion of a power management system (PMS) is to consider the load sharing among DERs, to minimize system power losses (Katiraei & Iravani, 2006). Load sharing ensures that each DER supplies its pre-set proportion at steady-state (Zhang et al., 2010). It becomes more complicated in microgrids as there are multiple- DERs. Many have studied power sharing (Katiraei et al., 2008; Katiraei & Iravani, 2006; N. D. Hatziargyriou & Sakis Meliopoulos, 2002; Serban & Serban, 2010; Ahn et al., 2010; Ustun et al., 2011; Kroposki et al., 2008; Peng et al., 2009; Rocabert et al., 2012; De Brabandere et al., 2007b; Zhang et al., 2010; Colet-Subirachs, Ruiz-Alvarez, Gomis-Bellmunt, Alvarez-Cuevas-Figuerola, & Sudria-Andreu, 2012) and show that the main PMS considerations are:

- Minimizing system power loss during load sharing (Yunwei et al., 2004; Piagi & Lasseter, 2006; Mao et al., 2008).
- Considering the many limits of each DER, including type, generation cost, maintenance interval, and environmental impact (Moreira et al., 2007; Green & Prodanović, 2007; Mazumder et al., 2008).
- Maintaining power quality including keeping the harmonic distortion low and maintaining the voltage profile (Z. Chen, 2012; Hanaoka et al., 2003; J. Guerrero et al., 2007).
- Restoring voltage/frequency during and after transients (Prodanovic & Green, 2006).
- Improving the dynamic response (J. Guerrero et al., 2009; Barklund et al., 2008; Pogaku et al., 2007; Delghavi & Yazdani, 2012).
- Maintaining system operation within the stability margin (Sao & Lehn, 2008; Savaghebi et al., 2013).

University of Malaya

Among the three levels of control in microgrids, the secondary control (MGCC) is responsible for load sharing (Mao et al., 2008; J. Guerrero et al., 2009; Colet-Subirachs et al., 2012, 2012; Prodanovic & Green, 2006). Because the voltage source presents low output impedance, an accurate synchronization system is extremely necessary to operate many VSCs in parallel. Load-sharing among a cluster of VSCs operating in islanded mode in a microgrid is a function of the value of their output impedances (Rocabert et al., 2012).

2.6.3 (a) Factors Affecting Load-Sharing Accuracy

- The resistive nature (low X/R ratio) of distribution networks affects accuracy of load sharing (J. A. P. Lopes et al., 2006; Moreira et al., 2007; J. Guerrero et al., 2007; Barklund et al., 2008; Pogaku, 2006). Table 2.1, shows the line R/X ratios for different line voltages (Engler, 2005).

- Variation of the output impedance (Kroposki et al., 2008; J. Guerrero et al., 2007; Savaghebi et al., 2013).

- Variation of the inverter filter parameters; this may affect power sharing if the voltage is not controlled by MGCC (Prodanovic & Green, 2006).

- Harmonic current (which should be taken into account when sharing nonlinear loads, to balance active and reactive power) (J. Guerrero et al., 2005; Colet-Subirachs et al., 2012).

- The distance between the DERs in a microgrid; this can change the inverter output and line impedance, affecting load sharing (J. Guerrero et al., 2005).

Many literatures propose controlling power-sharing without any wire connection between the DERs.

University of Malaya

Table 2.1: Typical Line Impedance Values

Type of line	R(Ω/Km)	X(Ω/Km)	$R/X(p.u)$
Low Voltage line	0.642	0.083	7.7
Medium Voltage line	0.161	0.19	0.85
High Voltage Line	0.06	0.191	0.31

2.6.3 (b) Control Techniques and Strategies

- Droop control method is based on the well-known correlation between active power flows with frequency and reactive power with voltage. The relation shows that when active power increases through load increase, the frequency will decrease; the opposite happens when load decreases. Droop method allows DERs to share active power automatically by measuring the local variables, ensuring system reliability and flexibility (M. C. Chandorkar et al., 1993; J. Guerrero et al., 2007; Pogaku et al., 2007; Zhang et al., 2010; Savaghebi et al., 2013).

  Many droop method control schemes have been proposed for linear load-sharing (Tuladhar et al., 2000; M. C. Chandorkar et al., 1993; Tuladhar, Jin, Unger, & Mauch, 1997; Borup et al., 2001; Hua, Liao, & Lin, 2002; Barsali, Ceraolo, Pelacchi, & Poli, 2002; Chung et al., 2005). There are, however, still only a few controllers for sharing nonlinear loads (Tuladhar et al., 1997; Borup et al., 2001). In (Tuladhar et al., 1997), the proposed controller achieved load-sharing by adjusting the output-voltage bandwidth with the distortion components present. This way the harmonic voltage components were drooped, encouraging the DERs to share the current harmonics. In another way (Borup et al., 2001), to produce a proportional droop in the corresponding harmonic voltage term, every single term of the harmonic current was used. Despite the many advantages of droop method, its drawbacks limit its applications. Its accurate power sharing affects frequency and voltage, it has slow transient response (as it requires low-pass filters), its shar-

University of Malaya

ing of harmonic current is unbalanced, and it is highly affected by inverter output impedance and line impedance (J. M. Guerrero et al., 2008; Coelho, Cortizo, & Garcia, 1999; J. Guerrero et al., 2007; Colet-Subirachs et al., 2012). The drawbacks are overcome as follows.

- Improvements to Conventional Droop Method: As dependency on droop method increased in microgrids, some improvements for this technique are summarized as follow:

  – Virtual output impedance; this technique is widely used to achieve accurate load-sharing in microgrids (Rocabert et al., 2012; Tuladhar et al., 2000; Chiang et al., 2001; J. Guerrero et al., 2009; De Brabandere et al., 2007b; Colet-Subirachs et al., 2012; Savaghebi et al., 2013). It emulates lossless resistors of reactors to fix the output impedance of the units, eliminating the effect of the output and line impedances on load sharing and improving the steady-state and transient responses of the parallel-connected inverters. Other, virtual reactors and resistors (Alsayegh et al., 2010; Kakigano, Miura, Ise, & Uchida, 2006) have been included into droop method, with the additional purpose of sharing the harmonic-current content properly (Colet-Subirachs et al., 2012).

  – $D-\omega d$ droop characteristic: this method presents droop characteristics between the different frequency components of the controlled signal (the Alternative Current (AC) voltage) and the active power, the reactive power, and the distorted power (Tuladhar et al., 2000; Marwali, Jung, & Keyhani, 2004; P.-T. Cheng, Chen, Lee, & Kuo, 2009). The use of VQD is avoided and the line-impedance effect eliminated. $D-\omega d$ droop can also compensate the distorted powers that result from non-linear and unbalanced loads. ωd is the drooping frequency component caused by the distorted power.

University of Malaya

- Proper design of the output impedance; this can reduce the impact caused by change in the line impedance (J. M. Guerrero, GarciadeVicuna, Matas, Castilla, & Miret, 2005; J. Guerrero et al., 2007). Although the inverter output impedance can be designed well, the line impedance is still unknown, causing unbalanced flow of reactive power (Tuladhar et al., 1997).
- Injection of high-frequency signals; unbalanced flow of reactive power in the system can be solved by injecting high-frequency signals into the power lines (Tuladhar et al., 2000). Such an injection, however, limits the power rating of the DER units and increases voltage distortion at their outputs (Z. Chen, 2012; Tuladhar et al., 2000; J. Guerrero et al., 2005).
- A central voltage controller; it regulates the voltage profile preventing the system from being affected by both variations in the inverter filter parameters or voltage controller gains neither the steady-state voltage control nor the power sharing (Prodanovic & Green, 2006).
- Overcoming the problem of high R/X ratio; the resistivity of the low-voltage networks makes precise load sharing unachievable (J. A. P. Lopes et al., 2006; Moreira et al., 2007; Barklund et al., 2008). In terms of voltage harmonic mitigation, handling of short circuits, and effectiveness of frequency and voltage control, the approach proposed in (J. Guerrero et al., 2005; De Brabandere et al., 2007b) is superior than existing methods as it takes into account the R-to-X distribution-line ratio.
- Sharing of harmonic current, as proposed by (J. Guerrero et al., 2005; Colet-Subirachs et al., 2012); this technique prevents power from circulating during sharing of nonlinear loads. The harmonic currents are considered so the active and reactive powers can be balanced more accurately than they are in

University of Malaya

conventional droop method.

– Soft-start operation; necessary to avoid initial current peak and create a seamless hot-swap operation (Tuladhar et al., 2000).

– Load voltage control; this is a new load sharing strategy used instead of conventional load frequency based power dispatching scheme when system uses a fixed frequency (Zhang et al., 2010). The output voltage of each DER is adjusted to keep the load voltage stable. It makes for a simple and effective system.

- Frequency Active Power Droop / voltage Reactive Power Droop (FPD/VQD) control VPD/FQB control has been reported in many papers (Piagi & Lasseter, 2006; Katiraei et al., 2008; Serban & Serban, 2010; Ahn et al., 2010; Ustun et al., 2011; R. H. Lasseter, 2011; Colet-Subirachs et al., 2012). Figure 2.4 and 2.5; illustrate voltage Vs. reactive power controller and frequency Vs. active power droop characteristic, respectively. Droop method uses the conventional power flow Equations (2.15), (2.16) are derived from Figure 2.6 as in (Rocabert et al., 2012; J. Guerrero et al., 2009):

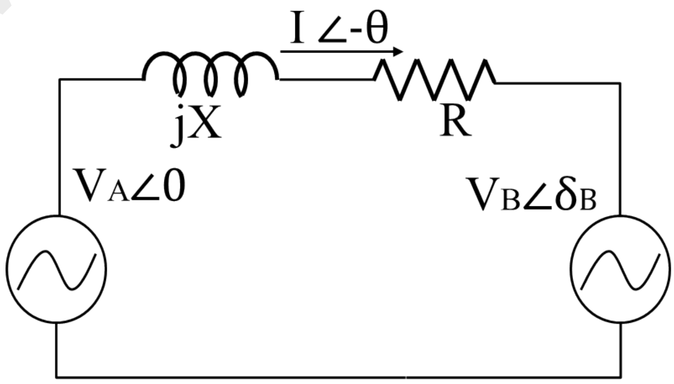

Figure 2.6: Equivalent circuit for distribution network.

Power equations:

$$p(t) = v(t)i(t) = V_m I_m cos(wt+\theta)cos(wt+\theta) \tag{2.2}$$

where: V$_m$ I$_m$ are the maximum values of voltage and current.

$$p(t) = V_m I_m[\frac{1}{2}cos(wt+\theta_v - wt - \theta_i) + \frac{1}{2}cos(wt+\theta_v + wt + \theta_i)] \tag{2.3}$$

$$\theta = \theta_v - \theta_i$$

$$p(t) = V_m I_m[\frac{1}{2}cos(\theta) + \frac{1}{2}cos(2(wt+\theta_v) - \theta)] \tag{2.4}$$

$$V = \frac{V_m}{\sqrt{2}}$$

$$I = \frac{I_m}{\sqrt{2}}$$

$$cos(2(wt+\theta_v) - \theta) = cos2(wt+\theta_v)cos\theta + sin2(wt+\theta_v)sin\theta$$

$$p(t) = |V||I|cos(\theta)[1 + cos2(wt+\theta_v)] + |V||I|sin\theta sin2(wt+\theta_v) \tag{2.5}$$

Equation 2.5 can divided to two components; first one represents the energy dispatched to the circuit, and the second one is the circulating energy stored and absorbed from the circuit's inductors and capacitors. P and Q equations equate:

$$p_R(t) = |V||I|cos(\theta)[1 + cos2(wt+\theta_v)]$$

University of Malaya

$$p_R(t) = |V||I|cos(\theta) + |V||I|cos(\theta)cos2(wt + \theta_v) \quad (2.6)$$

$$p_X(t) = |V||I|sin\theta sin2(wt + \theta_v) \quad (2.7)$$

For $p_R(t)$ the first term is the average energy dispatched to the circuit, where the second term is a sinusoidal signal with twice of the source frequency. The average of the second term is zero. So the average of $p_R(t)$ equals to the first term, as Equation 2.8 below shows:

$$P = |V||I|cos(\theta) \quad (2.8)$$

The term shown in Equation 2.7 represents the power stored or absorbed from the inductive and capacitive components in the circuit. The sinusoidal wave with the twice of the source frequency has an average value equals to zero. The amplitude of this term is:

$$Q = |V||I|sin\theta \quad (2.9)$$

From Equations (2.8), (2.9) the apparent power S can be driven as below:

$$S = P + jQ = |V||I|cos(\theta) + j|V||I|sin\theta$$

$$S = |V||I|cos(\theta) + j|V||I|sin\theta$$

as θ equals $\theta = \theta_v - \theta_i$ not the summation of the angle $\theta = \theta_v + \theta_i$, the apparent power equals the conjugate of the current and the power flow equation driven from

University of Malaya

Figure 2.6 is as below:

$$S = V_A I_{AB}^* \tag{2.10}$$

Where

$$I_{AB} = \frac{|V_A|\angle\delta_A - |V_B|\angle\delta_B}{|Z|\angle\theta} = \frac{|V_A|}{|Z|}\angle(\delta_A - \theta) - \frac{|V_B|}{|Z|}\angle(\delta_B - \theta) \tag{2.11}$$

So S equals:

$$S = |V_A|\angle\delta_A[\frac{|V_A|}{|Z|}\angle(\theta - \delta_A) - \frac{|V_B|}{|Z|}\angle(\theta - \delta_B)] \tag{2.12}$$

$$S = \frac{|V_A|^2}{|Z|}\angle\theta - \frac{|V_A||V_B|}{|Z|}\angle(\theta + \delta_A - \delta_B) \tag{2.13}$$

$$S = P + jQ \tag{2.14}$$

$$P_{AB} = \frac{|V_A|^2}{|Z|}\cos\theta - \frac{|V_A||V_B|}{|Z|}\cos(\theta + \delta_A - \delta_B) \tag{2.15}$$

$$Q_{AB} = \frac{|V_A|^2}{|Z|}\sin\theta - \frac{|V_A||V_B|}{|Z|}\sin(\theta + \delta_A - \delta_B) \tag{2.16}$$

$$\delta = \delta_A - \delta_B \tag{2.17}$$

Two important assumptions can take place to simplify the equations: Assumption I: In medium-voltage and high-voltage systems, the inductive components of the line impedance are very high compared with the resistive components (Engler, 2005), so

University of Malaya

the resistance can be neglected and the system considered as having a pure inductive output impedance (R=0, Z = X and θ = 90 deg). The active and reactive powers are thus:

$$P = \frac{|V_A||V_B|}{|X|}\sin\delta \tag{2.18}$$

$$Q = \frac{|V_A||V_B|}{|X|}\cos\delta - \frac{|V_B|^2}{|X|} \tag{2.19}$$

θ = the phase of the output impedance

δ = the phase angle between the inverter output and the microgrid voltages.

Assumption II: The angle δ is small, so sin δ almost equals δ and cos $\delta \approx 1$. Consequently,

$$P = \frac{|V_A||V_B|}{|X|}\delta \tag{2.20}$$

$$Q = \frac{|V_B|(|V_A| - |V_B|)}{|X|} \tag{2.21}$$

$$P_A = \frac{|V_A|}{R^2 + |X|^2}[R(|V_A| - |V_B|cos\delta) + |X||V_B|\sin\delta] \tag{2.22}$$

$$Q_A = \frac{|V_A|}{R^2 + |X|^2}[-R|V_B|sin\delta + |X|(|V_A| - |V_B|\cos\delta)] \tag{2.23}$$

Where P and Q are respectively the active and reactive powers, and V_A and V_B are respectively the voltages in buses A and B. Figure 2.7 shows a simplified system,

University of Malaya

in phasor diagram.

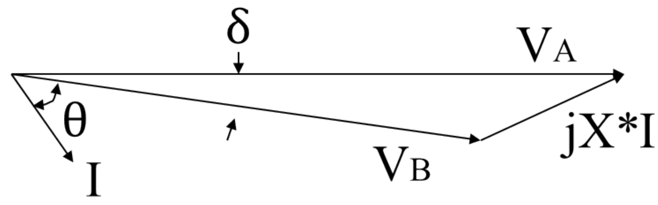

Figure 2.7: Distribution network, in phasor diagram.

- VPD/FQB controller Low-voltage microgrids are known to be resistive. This is considered so good control can be achieved. The distance between the DERs makes wire interconnections difficult, so droop control is used. In VPD/FQB controller, there is direct relation between voltage and active power and between frequency and reactive power (Serban & Serban, 2010; J. Guerrero et al., 2007; Sao & Lehn, 2008). Figure 2.8 (a), shows that when power increases, voltage reduces, so to get the voltage in any operating time the power variation (nP) is subtracted from the voltage at no load (E*). Figure 2.8 (b) relates reactive power with frequency. The reactive power ranges from positive Q_{max} at the inductive load to -Q_{max} at the capacitive load. The controller can measure the frequency by adding the frequency at no load (ω*) plus the change in reactive power (mQ).

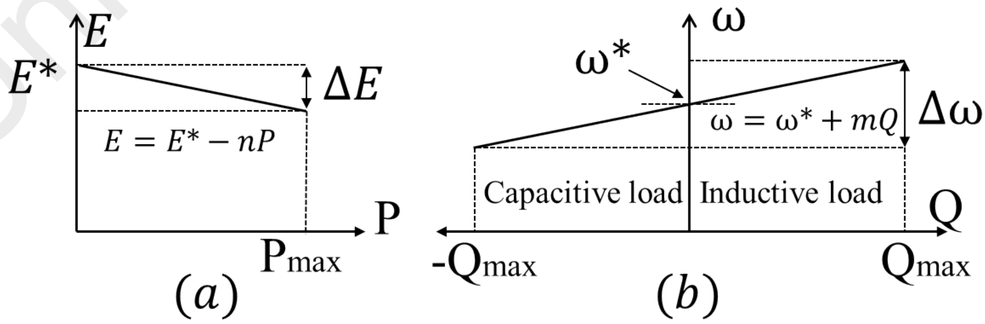

Figure 2.8: Resistive impedance curves for (a) Voltage Vs. active power; (b) Frequency Vs. reactive power.

Table 2.2 summarizes the equations used for droop method, for different output impedances (inductive and resistive) (J. Guerrero et al., 2005).

Table 2.2: Droop method strategy based on output impedance

Output impedance	Resistive, $Z = R, \angle 0$	Inductive, $Z = jX, \angle 90$
Active power	$P = \frac{\lvert V_A \rvert \lvert V_B \rvert}{X} \sin\delta$	$P = \frac{\lvert V_A \rvert \lvert V_B \rvert}{X} \delta$
Reactive power	$Q = \frac{\lvert V_A \rvert \lvert V_B \rvert}{\lvert X \rvert} \cos\delta - \frac{\lvert V_B \rvert^2}{\lvert X \rvert}$	$Q = \frac{\lvert V_B \rvert (\lvert V_A \rvert - \lvert V_B \rvert)}{\lvert X \rvert}$

2.7 Power Flow Analysis

Power flow analysis plays a key role in power system planning, operation and stability investigation. Power flow equations are shown in (2.15) and (2.16). Since in any complex power system the number of lines connected to each bus are normally more than one, so the power flow equations can be extended to :

$$P_i = \sum_{j=1}^{n} |V_i||V_j||Y_{ij}|cos(\theta_{ij} - \delta_i + \delta_j) \tag{2.24}$$

$$Q_i = -\sum_{j=1}^{n} |V_i||V_j||Y_{ij}|sin(\theta_{ij} - \delta_i + \delta_j) \tag{2.25}$$

where i is the bus number where the power is calculated, n is the sum of the lines connected to the bus, j is the bus number connected the bus i. Y_{bus} is the admittance matrix which obtained by inversing the impedance matrix Z_{bus}. The diagonal elements of Y_{bus} is known as the self-admittance:

$$Y_{ii} = \sum_{j=0}^{n} y_{ij} \qquad j \neq i \tag{2.26}$$

where the off-diagonal elements are:

$$Y_{ij} = -y_{ij} \tag{2.27}$$

where the y_{ij} is the admittance between buses i and j.

University of Malaya

There were many methods used for power flow analysis. In case of nonlinear equations (as in power system case) the Newton Raphson method has been widely used to solve the power flow equations for large power system, due to their fast quadratic convergence (Saadat, 2002). In power systems there are three types of buses; slack bus, load bus and voltage regulation bus. In slack bus the voltage amplitude and angle are specified, in load bus active and reactive power are specified and in voltage regulation bus active power and voltage amplitude are specified. So for voltage regulation buses one equation can be obtained from Equation 2.25, while for the load buses two equations can be obtained from Equations (2.24) and (2.25). Expanding Equations (2.24) and (2.25) in Taylor's series and neglecting all higher order terms produces the following set of linear equations:

$$\begin{bmatrix} \Delta P_i \\ \vdots \\ \Delta P_n \\ \Delta Q_i \\ \vdots \\ \Delta Q_n \end{bmatrix} = \begin{bmatrix} \frac{\partial P_i}{\partial \delta_i} & \cdots & \frac{\partial P_i}{\partial \delta_n} & \frac{\partial P_i}{\partial V_i} & \cdots & \frac{\partial P_i}{\partial V_n} \\ \vdots & \ddots & \vdots & \vdots & \ddots & \vdots \\ \frac{\partial P_n}{\partial \delta_i} & \cdots & \frac{\partial P_n}{\partial \delta_n} & \frac{\partial P_n}{\partial V_i} & \cdots & \frac{\partial P_n}{\partial V_n} \\ \frac{\partial Q_i}{\partial \delta_i} & \cdots & \frac{\partial Q_i}{\partial \delta_n} & \frac{\partial Q_i}{\partial V_i} & \cdots & \frac{\partial Q_i}{\partial V_n} \\ \vdots & \ddots & \vdots & \vdots & \ddots & \vdots \\ \frac{\partial Q_n}{\partial \delta_i} & \cdots & \frac{\partial Q_n}{\partial \delta_n} & \frac{\partial Q_n}{\partial V_i} & \cdots & \frac{\partial Q_n}{\partial V_n} \end{bmatrix} \begin{bmatrix} \Delta \delta_i \\ \vdots \\ \Delta \delta_n \\ \Delta V_i \\ \vdots \\ \Delta V_n \end{bmatrix} \tag{2.28}$$

The Jacobian matrix forms the linearize relationship between small changes in voltage angle ($\Delta\delta_i$) and voltage amplitude (ΔV_i) with small changes in active and reactive power (ΔP_i) and (ΔQ_i). The Jacobian matrix elements obtained from the partial derivative of the Equations (2.24) and (2.25), respect to ($\Delta\delta_i$) or (ΔV_i). The power residuals ($\Delta P_i^{(k)}$) and ($\Delta Q_i^{(k)}$) are the difference between scheduled and calculated power P^{sch}, $P_i^{(k)}$, as below:

$$\Delta P_i^{(k)} = P_i^{sch} - P_i^{(k)} \tag{2.29}$$

$$\Delta Q_i^{(k)} = Q_i^{sch} - Q_i^{(k)} \tag{2.30}$$

The new estimate for voltage angle and amplitude are:

$$\delta_i^{(k+1)} = \delta_i^{(k)} + \Delta\delta_i^{(k)} \tag{2.31}$$

$$|V_i^{(k+1)}| = |V_i^{(k)}| + \Delta|V_i^{(k)}| \tag{2.32}$$

2.8 Grid Connected Control Modes

Grid-connected DERs are widely used nowadays. Grid-connected sources are required to synchronize with the grid voltage and frequency. Sections below summarize grid-connected control techniques.

2.8.1 Unit Output Power Control (UPC)

DER uses this control mode to dispatch the power at pre-set desired value (R. Lasseter & Piagi, 2006; Serban & Serban, 2010). Figure 2.9 illustrates the UPC method, the voltage at the interconnection point and the DER output current are measured and fed back to the LC. By applying this method the dispatched power from DER is constant regardless of the load variation, since the power mismatch can be compensated by the grid.

2.8.2 Feeder Flow Control (FFC) mode

Feeder Flow Control (FFC) mode of operation uses to make the active power flows in the feeder constant at the point where the DER unit is installed. The DER output power controlled by (FL$_{ref}$) to match the value of the load without affecting the feeder power flow. Figure 2.10 shows the grid connected DER controlled by FFC, voltage at

University of Malaya

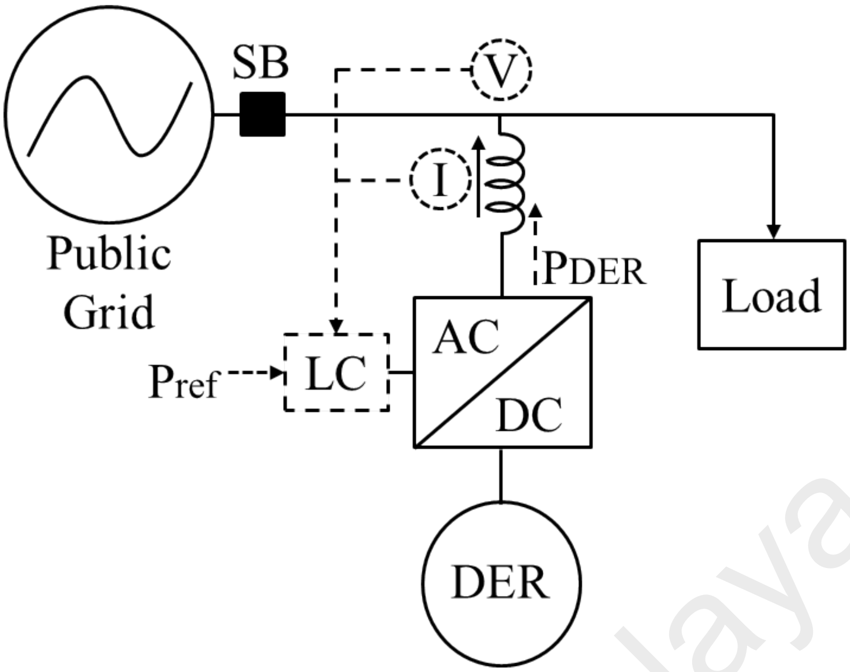

Figure 2.9: Unit output power control.

interconnection point and feeder power flow measured and fed back to the LC the DER increases its output power until it satisfies the load demand. to supply the load by the mismatched amount of power.

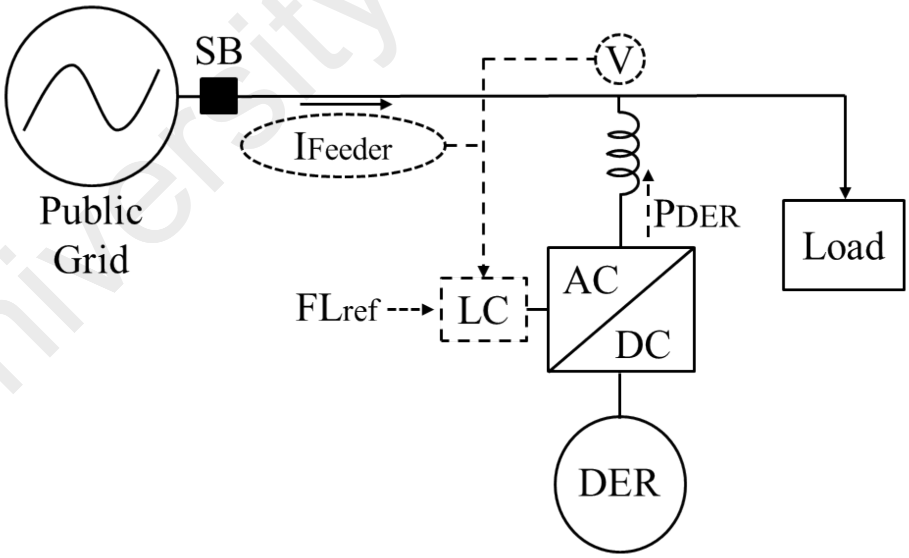

Figure 2.10: Feeder flow control mode.

University of Malaya

Table 2.3: Summary of microgrid Control Objectives, Problems, and Solutions

Control objective	What's the problem	The reason of the problem: When (changing)	The reason of the problem: Why (permanent)	The solution	Explanation	References
Accurate LS*, accurate FR	Deviation of the Line Frequency	Surplus energy charges the battery	Unbalanced supply and demand affecting FR	Control the direction of P according to battery VR	–	(Serban & Serban, 2010)
VR	Circulating reactive current	Z_L, Z_{line} and Z_o change	Low Z_L between DERs	Change the local voltage SP	Increase SP at Q_L, reduce SP at Q_c	(Piagi & Lasseter, 2006)
Accurate LS, accurate VR	Unbalanced Q flow	Unbalanced Z_{line}	–	Inject high frequency signals through the power lines	Disadvantageous limiting of the power rating of the DERs	(Mihalache, 2003)
Accurate LS, accurate VR	Unbalanced Q flow	Unbalanced Z_{Line}	–	Add external data communication signals	Disadvantages of low reliability, low expandability	(P.-T. Cheng et al., 2009)
Accurate LS, for linear and nonlinear loads	Unbalanced Z_{Line}	The distance between the DERs changes	Z_{Line} changes with distance	Proper design of Z_o	–	(J. M. Guerrero et al., 2005)
Accurate LS, for linear and nonlinear loads	Unbalanced Z_{Line}	The distance between the DERs changes	Z_{Line} changes with distance	Adaptive virtual Z_o	Good Q sharing regardless of Z_L	(Z. Chen, 2012)
Accurate LS, for linear and nonlinear loads	High THD	Supplying a nonlinear load	Large impedance value (seen by the current harmonics)	Adaptive virtual Z_o (two behaviors: 1)inductive; 2)resistive)	1) around the output voltage frequency; 2) at high-or DER current harmonics	(Ito & Iyama, 1997)
LS, so the sum of Z_o & Z_{Line} has to be balanced	Droop method not effective	Unbalanced Z_o	Z always affecting P and Q	Adaptive virtual Z_o	Emulating lossless resistors or reactors	(Kamel et al., 2011)
LS, so the sum of Z_o Z_{Line} has to be balanced	Droop method not effective	–	Z always affecting P and Q	Interface inductor between inverter and load	Disadvantages: heavy and bulky	(M. C. Chandorkar et al., 1993)

University of Malaya

Control objective	What's the problem	The reason of the problem When (changing)	 Why (permanent)	The solution	Explanation	
LS and FR	FPD scheme no longer feasible	Fixed frequency	Control of P must be by frequency	New LS strategy	This change inverter V_o and V_L remains constant	(J. Guerrero et al., 2011)
FR	Frequency deviation	Unequal instantaneous supply and demand	P=(Δ P/ Δ f)*(f_{nl}-f_{fl})	Change the no-load generator speed or the power dispatch	–	(Duan et al., 2008)
FR	Deviating frequency and voltage	Unintentional islanding	Loss of load or imported power	LSCM immediately trips a significant number of load fee DERs	Load-shedding controller module (LSCM)	(De & Ramanarayanan, 2010)
VR and LS	Control of VR and LS becomes complicated	Resistive nature of distributed network	R cannot be neglected anymore	VPD controller	Direct relation between V and P	(J. Guerrero et al., 2009)
To accomplish all microgrid control functions	Failure in any of the functions mentioned in 2.5	–	–	Three-layer control: DNO, MGCC, LC	Primary, secondary and Tertiary control layers	(Mao et al., 2008)
Instantaneous and equal LS, and good VR	Failure in any of the LS criteria mentioned in 2.6	Load nature and changeable energy demand	Load-changing affecting P and Q	Centralized load sharing technique Average load sharing (ALS) Current limitation control Circular chain control (3C)	Wire interconnections (based on active LS techniques)	(Y.-K. Chen, Wu, Wu, & Ku, 2003; T.-F. Wu et al., 2000; Bo et al., 2012)
Instantaneous and equal LS, and good VR				Master–slave (MS)	No-wire interconnections (higher reliability, higher flexibility)	

University of Malaya

Control objective	What's the problem	The reason of the problem When (changing)	 Why (permanent)	The solution	Explanation	
Accurate LS	Harmonics and unbalanced powers poorly compensated	Nonlinear and unbalanced loads	Low X/R ratio of distribution Z_{Line}	Frequency components and (P), (Q) and distortion power (D)	D-ωd droop characteristic / Injection of high-frequency signals	(Skjellnes, Skjellnes, & Norum, 2002; Zhang et al., 2010; Pogaku, 2006)
				Adaptive virtual Z_o	Virtual impedance has no power losses and can provide plug & play operation to DER	
FR and LS to achieve economical generation	Frequency deviation	Unintentional islanding, and no SM to balance demand and supply	Unbalanced demand and supply	Single-master and multi-master operations (SMO and MMO)	–	(Kamel et al., 2011)

*Table abbreviations: Active power (P), Reactive power (Q), Voltage regulation (VR), Frequency regulation (FR), Load sharing (LS), Inductive reactive power (Q_L), Capacitive reactive power (Q_c), Set point (SP), Load impedance (Z_L), Line impedance (Z_{Line}), Output impedance (Z_o), Output voltage (V_o), Load voltage (V_L), No load frequency (f_{nl}), Full load frequency (f_{fl}), Load shedding controller module (LSCM), Synchronous machine (SM).

University of Malaya

2.9 Summary

As this study illustrates, there are three microgrid control functions: voltage regulation (VR), frequency regulation (FR), and load sharing (LS). Table 2.3 summarizes the problems of microgrid control and their solutions. The microgrids have many attractive features that make its research promising and boost its competitiveness in penetrating renewable energy. Microgrid architecture and classifications have been reviewed in this chapter, along with the control techniques and strategies. Challenges to microgrids operation include maintaining the voltage regulated, optimal power sharing which ensures minimum power losses, high power quality hence low harmonic distortion, and operating the DERs on their preset values after any disturbance occurs. A robustly controlled microgrid ensures seamless import/export of active and reactive powers by the main grid and continuous supply of the critical load during islanded mode. These lead to a flexible and smart power system.

University of Malaya

CHAPTER 3: POWER CONVERSION SYSTEMS FOR GRID CONNECTED DERS

3.1 Introduction

Many advanced researches have been carried out for integrating the distributed renewable energy resources into electrical power systems. Their features include zero carbon dioxide emission, low running cost, low maintenance cost, and high abundance; encouraging many governments to pass ambitious policies of up to 20% increase or more of renewable energy resources in power supply resources (Schenk & Stokes, 2013). PV is one promising renewable energy option, increasingly being integrated into distribution networks. Despite the advantages of PV resources, there are a few challenges that hinder their widespread exploitation. Power source intermittence is one complex challenge afflicting integration. As for grid-connected PV systems, removing battery backup reduces costs and increases efficiency, but increases the challenge of solar radiation intermittence. The controller must have the ability to overcome input and output power disturbances that arise when a PV distributed source is connected to the grid (Yun Tiam, Kirschen, & Jenkins, 2004; Acuna, Morán, Weishaupt, & Dixon, n.d.; Dixon, Moran, Rodriguez, & Domke, 2005; Srivastava, Kumar, & Schulz, 2012). Given that nearly 90% of all grid disturbances occur in the distribution networks (Farhangi, 2010), the move towards distributed generation integration has had to focus on how to enhance grid reliability and quality within the distribution networks (Srivastava et al., 2012). Fast response equipments could be installed to overcome these problems, but the cost will be covered by the grid operators not the owner of the PV panel who is benefiting from it (Turitsyn et al., 2011). Therefore power conversion systems can be used to achieve a smooth power transfer from the DC PV source to the AC grid.

University of Malaya

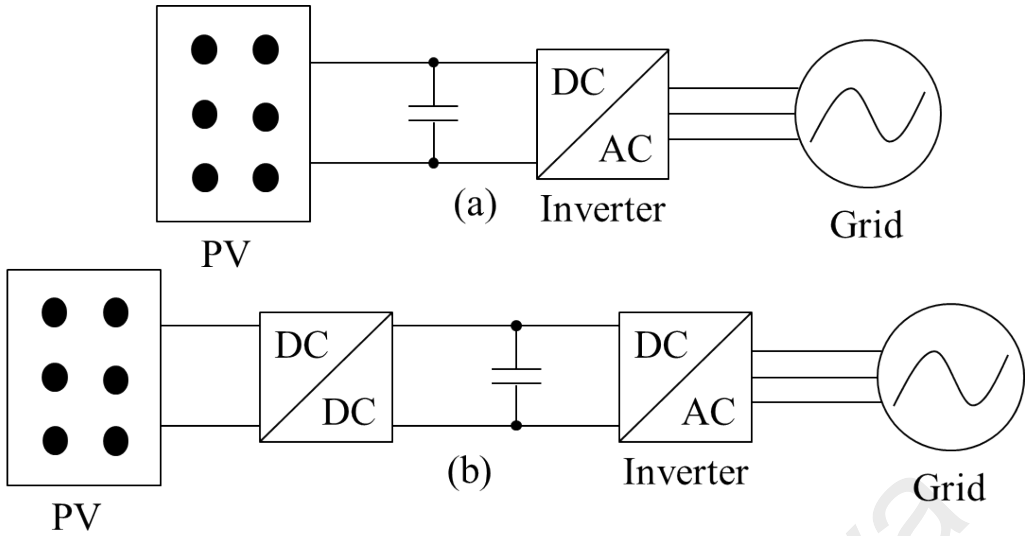

Figure 3.1: (a) Single-stage power-conversion system and (b) a two-stage power-conversion system.

Power conversion systems can be classified into two types, depending on the number of power processing stages: single-stage (Ozdemir et al., 2014; Z. Chen, 2012; Du, Jiang, Erickson, & Lasseter, 2014; Das & Agarwal, 2012; Xiao et al., 2013), and two-stage power conversion systems (Ponnaluri, Linhofer, Steinke, & Steimer, 2005; Eid et al., 2014; Balathandayuthapani, Edrington, Henry, & Cao, 2012; El Khateb et al., 2014) (the latter being the most common structure for electronically-coupled DER) (see Figure 3.1). Two-stage conversion systems have two converters; one on the PV side which extracts maximum power from the PV, the other is a synchronized inverter connected to the public-grid side, which controls the active and reactive power dispatched. In a single-stage approach, the inverter is used alone to meet the power conversion system's requirements. Single-stage power conversion systems offer advantages such as high conversion efficiency, simplified topology, low cost, and compactness (Yazdani et al., 2011; Jang & Agelidis, 2011; Alajmi et al., 2013; Das & Agarwal, 2012). A comparison between double and single stage conversion systems have been curried out in below sections.

University of Malaya

3.2 Double Stage Conversion Systems

Figure 3.1 (b) shows the PV power source connected to a grid via two stage power conversion system. A DC-DC converter using a maximum power point tracking (MPPT) technique to extract the maximum power from PV panels. Then the inverter convert the DC to AC. The inverter switching technique producing pulses generates regulated voltage at the DC link and running the inverter at a desired power factor, and achieve the synchronism with the grid. The power conversion stages are explained as below.

3.2.1 First Stage DC-DC Boost Converter

There are many MPPT techniques can be used to extract the maximum power from the PV solar systems by changing the switch's status (on and off). During switching connection time (on) the inductor's current rises so it is storing energy, while during disconnection time (off) the stored energy delivers to the load (Abusorrah et al., 2013). Many techniques may control the switching time, such as; Constant Voltage, Fixed Duty Cycle, Incremental Conductance (IC), Perturb and Observe (P&O) (de Brito, Sampaio, Luigi, e Melo, & Canesin, 2011; Tsang & Chan, 2013). The Constant Voltage method using the empirical results indicating that the value of voltage that extracts maximum power is 70 % to 80 % of the open circuit voltage, although it is fast and easy to implement method, however it is not accurate enough because the percentage changes with temperature changes. The Fixed Duty Cycle method does not require any feedback, because it uses a fixed duty cycle value. P&O and IC methods may have difficulty finding the Maximum Power Point (MPP), when used in large scale PV systems where multiple local maxima occur (Kish, Lee, & Lehn, 2012; Hussein, Muta, Hoshino, & Osakada, 1995). Moreover, P&O can not work well when the insolation varies quickly with time (Li, Gao, Wang, & Liu, 2013; Chong & Zhang, 2013). However, IC method has the advantage over P&O as it has the ability to determine the MPP without oscillation around the value (Norton et al., 2011).

University of Malaya

3.2.2 Second Stage DC-AC Inverter

In two-stage conversion system, the function of the inverter is to convert the DC to AC. There are two other associated tasks achieved by the DC-AC inverter, i.e; stabilizing DC link voltage (DC voltage regulator) and operating at the desired power factor (Current Regulator) (Norton et al., 2011; Tsang & Chan, 2013).

3.3 Single Stage Conversion Systems

In this work a single stage DC-AC inverter is used as a power converter. Its function is to track the DC link voltage that extracts maximum power from the PV and dispatches zero reactive power to the grid. The proposed control technique (for VSIs) achieves fast dynamic response through an outer dc link voltage control loop and an inner current control loop. The current control strategy plays the main role in power flow performance. It uses the d q reference frame which is able to eliminate steady-state error and, through decoupled control has a fast transient response (Kadri et al., 2011).

3.3.1 Circuit Description and Modeling

Figure 3.2 shows a PV source connected to a three-phase grid via a single-stage power conversion system, namely an inverter. The inverter has two control loops: an inner loop to control the reactive power and maintain unity power factor, and an outer loop to control reference DC voltage so as to remain at a voltage that extracts maximum power from the PV.

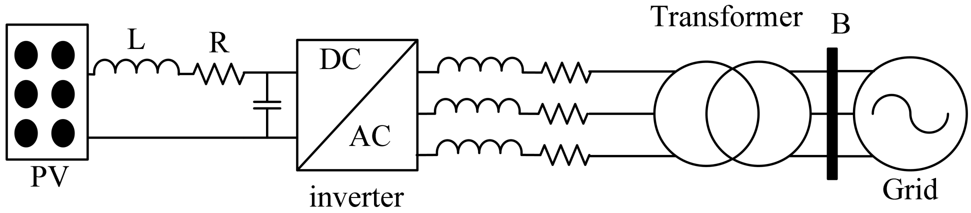

Figure 3.2: Photovoltaic arrays connected to the grid.

Pulse width modulation (PWM) technique is the inverter switching. The switches frequency is significantly higher than the line frequency. PWM produces pulses to comply with; MPPT, unity power factor, and synchronization with the grid. The inverter output is connected to the secondary side of a step up transformer. The transformer's primary is connected to the high voltage grid. The measurement block measures the output voltage and current at bus B. The controllable part in this system is the inverter. More details about the inner and outer loops are presented in section 3.3.3.

3.3.1 (a) PV Modeling

The solar cell is the energy producing part of the PV panel. Figure 3.3 shows an equivalent circuit for a solar cell (Yazdani et al., 2011; Kadri et al., 2011; Balathandayuthapani et al., 2012). It can be represented by a current source connected in parallel with a diode.

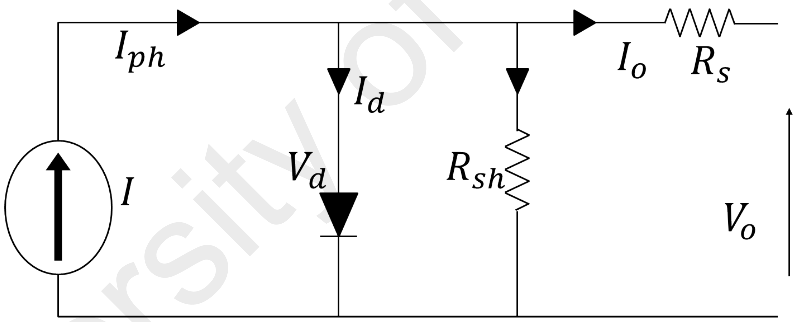

Figure 3.3: PV cell equivalent circuit.

The output current I_o is given by:

$$I_o = I_{ph} - I_d - \frac{V_d}{R_{sh}} \tag{3.1}$$

I_{ph} is the photocurrent V_d is the diode voltage, R_{sh} is the equivalent shunt resistance and I_d is the diode current which equals:

$$I_d = I_{rsc} * ((\exp \frac{q.V_d}{\eta .k.T}) - 1) \tag{3.2}$$

University of Malaya

I_{rsc} is the diode reverse saturation current, q is the electron charge 1.6* 10^{-19} C, k is Boltzman's constant 1.38 * 10^{-23} J/K, η is the diode quality factor, T is the PV panel temperature. The output voltage V_o is given by:

$$V_o = V_d - I_o R_s \tag{3.3}$$

where R_s is the series resistance. In general, the output current I_o of the solar cell is:

$$I_o = I_{ph} - I_{rsc} * ((\exp \frac{q.(V_o + I_o R_s)}{\eta.k.T}) - 1) - \frac{(V_o + I_o R_s)}{R_{sh}} \tag{3.4}$$

R_s is usually low and R_{sh} high; so it can be neglected. Equation 3.4 can be simplified to:

$$I_o = I_{ph} - I_{rsc} * ((\exp \frac{q.V_o}{\eta.k.T}) - 1) \tag{3.5}$$

During open circuit, the output current I_o equals zero. Furthermore, the shunt resistance is considered to be very large, so the open-circuit voltage (V_{oc}) from Equation 3.5 is:

$$V_{oc} = (\frac{\eta.T.k}{q}) \ln(\frac{I_{ph}}{I_{rsc}} + 1) \tag{3.6}$$

During short circuit, the output voltage V_o equals zero and I_{rsc} can be neglected, so the output short-circuit current (I_{sc}) from Equation 3.4 is:

$$I_{sc} = \frac{I_{ph}}{(1 + \frac{R_s}{R_{sh}})} \tag{3.7}$$

The output power equation is:

$$P = V_o I_o = V_o (I_{ph} - I_d - \frac{V_d}{R_{sh}}) \tag{3.8}$$

University of Malaya

The relation between I_{ph} and sun radiation is:

$$I_{ph} = \frac{G * \eta_c}{V_d} \tag{3.9}$$

η_c is solar cell efficiency. The solar radiation G is:

$$G = \phi * E \tag{3.10}$$

where ϕ is the photon flux, which represents the number of photons per unit time per unit area. E is photon energy, obtainable from:

$$E = \frac{hc}{\lambda} \tag{3.11}$$

where h is Planck's constant 6.626*10^{-34} j.s, c is the light speed in a vacuum 3*10^8 m/s, and λ the wavelength.

3.3.1 (b) VSI Modeling

The three-phase VSI connected to a grid is shown in Figure 3.4.

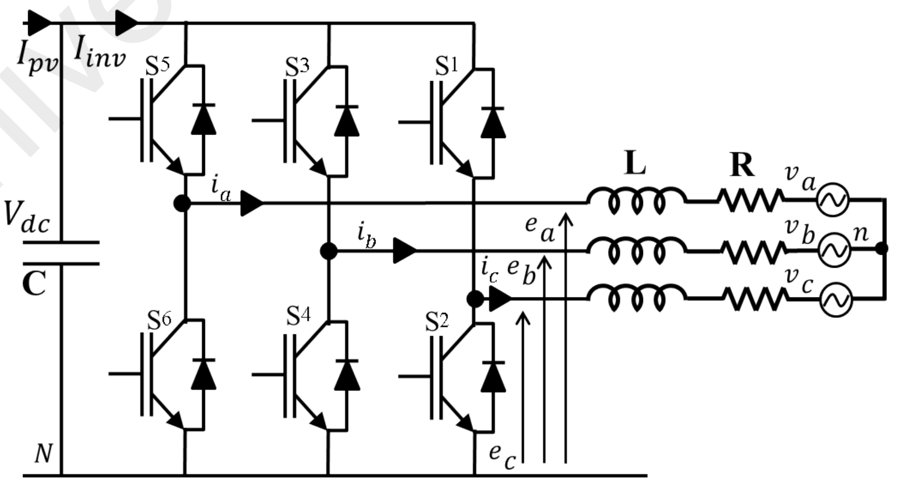

Figure 3.4: Three-phase voltage source inverter.

To achieve VSI modeling, the assumption of symmetrical and sinusoidal three phase

University of Malaya

voltage is adopted as shown in (3.12):

$$\begin{Bmatrix} v_a = V_m cos(wt) \\ v_b = V_m cos(wt - \frac{2}{3}\pi) \\ v_c = V_m cos(wt + \frac{2}{3}\pi) \end{Bmatrix} \tag{3.12}$$

Where V_m is the peak value of the voltage, so the VSI model in the abc frame is:

$$\begin{Bmatrix} e_a = L\frac{di_a}{dt} + i_a R + v_a + v_{nN} \\ e_b = L\frac{di_b}{dt} + i_b R + v_b + v_{nN} \\ e_c = L\frac{di_c}{dt} + i_c R + v_c + v_{nN} \\ I_{pv} = C\frac{dv_{dc}}{dt} + i_{inv} \end{Bmatrix} \tag{3.13}$$

R, L and C are the resistor, inductor and capacitor respectively shown in Figure 3.4, from (3.13)

$$v_{nN} = \frac{1}{3}(e_a + e_b + e_c) \tag{3.14}$$

The inverter's switching function $d_k^*(k = 1,3,5)$ is defined as

$$d_k^* = \begin{Bmatrix} 1, \ if\ S_k\ is\ on\ and\ S_{k+1}\ is\ \ off \\ 0, \ if\ S_k\ is\ off\ and\ S_{k+1}\ is\ \ on \end{Bmatrix} \tag{3.15}$$

The voltage values per phase are calculated based on switch position at that period from the Equation below:

$$e_a - V_{nN} = V_{dc}(d_1^* - \frac{d_1^* + d_3^* + d_5^*}{3}) \tag{3.16}$$

University of Malaya

Therefore, the model can be written as in Equation 3.17

$$\begin{Bmatrix} L\frac{di_a}{dt} = -i_aR - v_a + (d_1^* - \frac{d_1^*+d_3^*+d_5^*}{3})v_{dc} \\ L\frac{di_b}{dt} = -i_bR - v_b + (d_3^* - \frac{d_1^*+d_3^*+d_5^*}{3})v_{dc} \\ L\frac{di_c}{dt} = -i_cR - v_c + (d_5^* - \frac{d_1^*+d_3^*+d_5^*}{3})v_{dc} \\ C\frac{dv_{dc}}{dt} = I_{pv} - (d_1^*i_a + d_3^*i_b + d_5^*i_c) \end{Bmatrix} \tag{3.17}$$

For PWM inputs Equation 3.17 can be separated into high-frequency and low-frequency components following Fourier analysis. The low-frequency component is the same as Equation 3.17, with the switching functions d^* being replaced by continuous duty ratios $d_k^*(k = 1,3,5)$, containing $\in [0,1]$ is considered further in (R. Wu, Dewan, & Slemon, 1991)

The model described by Equation 3.17 are time varying and nonlinear. Control can be facilitated by transforming the model into a synchronous orthogonal frame rotating at the utility angular frequency ω. The positive-sequence components at the fundamental frequency become constant and the resultant time-varying transformation is given by Equation 3.18.

$$T_{dq0}^{abc} = \frac{2}{3}\begin{bmatrix} cos(wt) & cos(wt - \frac{2}{3}\pi) & cos(wt + \frac{2}{3}\pi) \\ sin(wt) & sin(wt - \frac{2}{3}\pi) & sin(wt + \frac{2}{3}\pi) \\ \frac{1}{2} & \frac{1}{2} & \frac{1}{2} \end{bmatrix} \tag{3.18}$$

From Equations (3.17) and (3.18) an expression in dq frame for the whole dynamic model is:

$$\begin{bmatrix} \frac{di_d}{dt} \\ \frac{di_q}{dt} \\ \frac{dv_{dc}}{dt} \end{bmatrix} = \begin{bmatrix} -\frac{R}{L} & \omega & \frac{d_d}{L} \\ -\omega & -\frac{R}{L} & \frac{d_q}{L} \\ -\frac{d_d}{C} & -\frac{d_q}{C} & 0 \end{bmatrix}\begin{bmatrix} i_d \\ i_q \\ v_{dc} \end{bmatrix} + \begin{bmatrix} -\frac{1}{L} & 0 & 0 \\ 0 & -\frac{1}{L} & 0 \\ 0 & 0 & \frac{1}{C} \end{bmatrix}\begin{bmatrix} v_d \\ v_q \\ I_{pv} \end{bmatrix} \tag{3.19}$$

University of Malaya

where:

i_d is d axis grid currents;

i_q is q axis grid currents;

v_d is d axis grid voltages;

v_q is q axis grid voltages;

d_d is d axis duty ratios;

d_q is q axis duty ratios;

3.3.2 Nominal Operating Cell Temperature

The cell temperature (T_c) plays the main role in assessing the efficiency of a solar cell. The value of T_c is calculated based on ambient temperature and solar radiation values as well as the nominal operating cell temperature (NOCT). NOCT is defined as the temperature element in a solar cell exposed at 800 W/m^2 of solar radiation, 20°C of ambient temperature, and a wind speed of 1 m/s. As these conditions may vary depending on the climate zone nature, the paper (Ya'acob et al., 2014) proposed a new condition called tropical field operation cell temperature (tFOCT) suitable for tropical zones like Malaysia. The results show that the suitable weather conditions for measuring the tFOCT are 886 W/m ^{2} of solar radiation, 34°C of ambient temperature, and a wind speed of 3.2 m/s, Concluding that the recommended tFOCT value is 52.5°C. Therefore the T_c obtain as follows:

$$T_c = T_a + G * \frac{(tFOCT - 34°C)}{886W/m^2} \tag{3.20}$$

where T_c and T_a are the cell and the ambient temperatures respectively, G is the instant solar radiation.

The experimental tests for the PV panels detect that the efficiency decreases with T_c increases. From Equations (3.1) and (3.2) the output current I_o increases slightly with

University of Malaya

the temperature, while temperature affects various other terms in Equation 3.6, net effect of temperature is that it decreases the V_{oc} linearly. The drop in V_{oc} with temperature is mainly related to the increase in the diode reverse saturation current I_{rsc} which is strongly depends on the temperature. The common rule for the I_{rsc} and T_c relation is that the I_{rsc} doubles for every 10°C rise in T_c (Bogart Jr, 1986). Therefore, the relation between diode saturation current and temperature can be expressed as Equation 3.21

$$I_{rsc} = I_{rsc,STC} * 2^{(\frac{T_c - 298^\circ}{10})} \tag{3.21}$$

Where $I_{rsc,STC}$ is the diode saturation current at the standard test condition (STC).

3.3.3 System Controllers

3.3.3 (a) Phase locked loop (PLL)

PLL uses to generate an output signal whose phase is same as the phase of input signal. The input are the three phases grid voltage and the output is the phase angle of one of the three phases.

3.3.3 (b) Outer Loop Controller

The third equation in model 3.19 represents the voltage control. At unity power factor (i_q=0), this equation can be simplified to:

$$C\frac{dv_{dc}}{dt} = i_{pv} - i_d d_d \tag{3.22}$$

The error $e = V_{dc,ref} - V_{dc}$ passes through a PI-type regulator as depicted in Figure 3.5 to regulate the dc voltage to a fixed value. The controller used to balance the power between the DC-link and the grid as well as to determine the amount of current injected into or absorbed by the grid (Bastos et al., 2014). In Figures. 3.5 and 3.6, the voltage loop is an outer loop whereas the current loop is an inner loop. The internal loop can be

University of Malaya

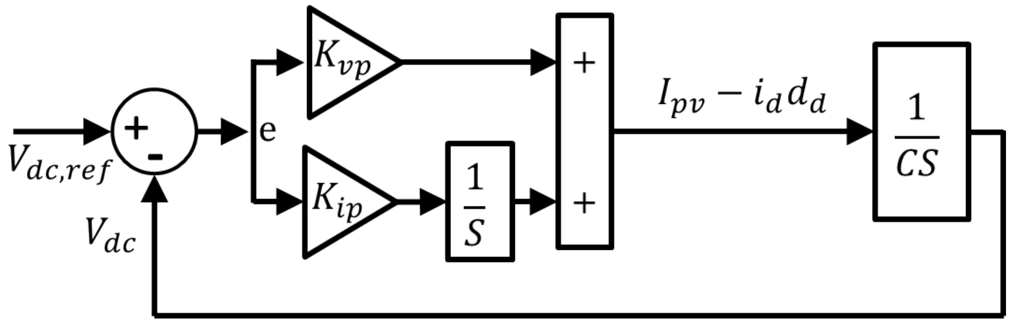

Figure 3.5: Voltage loop control.

designed for short settling time and fast error correction. Thus, the outer and inner loops can be considered decoupled and can be linearized. The closed-loop transfer function of the dc voltage regulation, obtained from Figure 3.5, can be expressed in the following form:

$$\frac{V_{dc}(s)}{V_{dc,ref}(s)} = \frac{k_{vp}}{C}\frac{\frac{k_{vi}}{k_{vp}} + S}{S^2 + \frac{k_{vp}}{C}S + \frac{k_{vi}}{C}} \tag{3.23}$$

The damping ratio (ζ) is $\zeta = (k_{vp})/2C\sqrt{k_{vi}/C}$, and $\omega_{nv}^2 = k_{vi}/C$. Thus the voltage regulator parameters are:

$$k_{vp} = 2\zeta C\omega_{nv}, k_{vi} = C\omega_{nv}^2 \tag{3.24}$$

3.3.3 (c) Inner Loop Controller

Model expressed by Equation 3.19 shows that there is cross-coupling between the d and q components, where dynamic performance of the regulator is affected by this cross-coupling (Kadri et al., 2011). Therefore, for better performance, decoupling the two axes is necessary, which can be accomplished by feedforward decoupling control method. Assuming:

$$\left\{\begin{aligned} v_{rd} &= -V_d + d_d V_{dc} + \omega L i_q \\ v_{rq} &= -V_q + d_q V_{dc} - \omega L i_d \end{aligned}\right\} \tag{3.25}$$

University of Malaya

Then from the model given by Equations (3.19), the system expressions become

$$\left\{\begin{array}{c} \frac{di_d}{dt} = -\frac{R}{L}i_d + \frac{1}{L}v_{rd} \\ \frac{di_q}{dt} = -\frac{R}{L}i_q + \frac{1}{L}v_{rq} \\ \frac{dv_{dc}}{dt} = \frac{I_{pv}}{C} - \frac{V_d+v_{rd}}{CV_{dc}}i_d - \frac{V_q+v_{rq}}{CV_{dc}}i_q \end{array}\right\} \tag{3.26}$$

Equation 3.26 eliminates the cross-coupling variables. Therefore, the currents i_d and i_q can be controlled independently by acting upon inputs V_d and V_q, respectively. Moreover, by using a PI-type compensation, zero steady-state error and a fast dynamic response can be achieved. The current regulator diagram is shown in Figure 3.6. The sampling and hold delay can be neglected, since the line frequency is much less than the switching frequency.

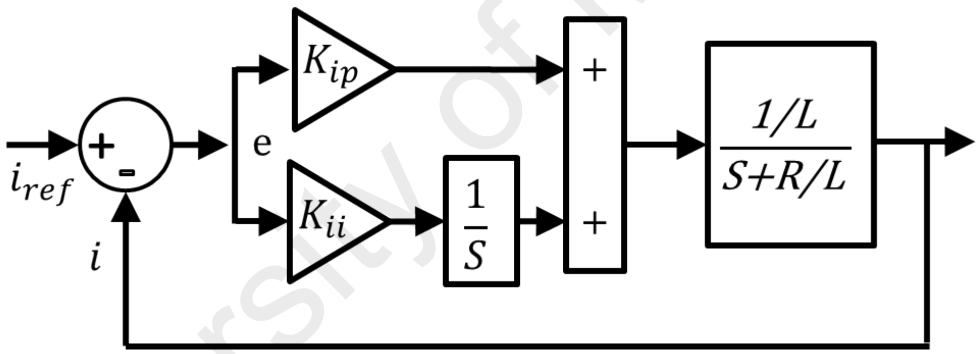

Figure 3.6: Current loop control with constant irradiation.

Proportional Constant (k_{ip}) and Integral Constant (k_{ii}) for current control are shown in Figure 3.6. The reference current signal and the feedback current are respectively i_{ref} and i. The figure is suitable for both the i_d and i_q loops. From the figure, the closed-loop transfer function of the dq current loops is:

$$\frac{i_q(s)}{i_{q,ref}(s)} = \frac{i_d(s)}{i_{d,ref}(s)} = \frac{k_{ip}}{L}\frac{\frac{k_{ii}}{k_{ip}}+S}{S^2+\frac{k_{ip}+R}{L}S+\frac{k_{ii}}{L}} \tag{3.27}$$

The ζ is $\zeta = (k_{ip}+R)/2L\sqrt{k_{ii}/L}$, and $\omega_{ni}^2 = k_{ii}/L$. Thus the voltage regulator parameters are:

$$k_{ip} = 2\zeta\omega_{ni}L - R, k_{ii} = L\omega_{ni}^2 \tag{3.28}$$

3.4 Simulation Results and Discussions for Single Stage

The outer voltage control loop regulates the DC link voltage to extract maximum power from the PV (see Figure 3.7). DC-measured voltage ($V_{dc,mes}$), DC-measured current ($I_{dc,mes}$) are the inputs of the MPPT, which continuously compares the present and past values of power, voltage and current, then appropriately increases or decreases the reference voltage ($V_{dc,ref}$). Proportional and integral (PI) controllers are used, producing the output $I_{d,ref}$, which feeds the inner loop controller input.

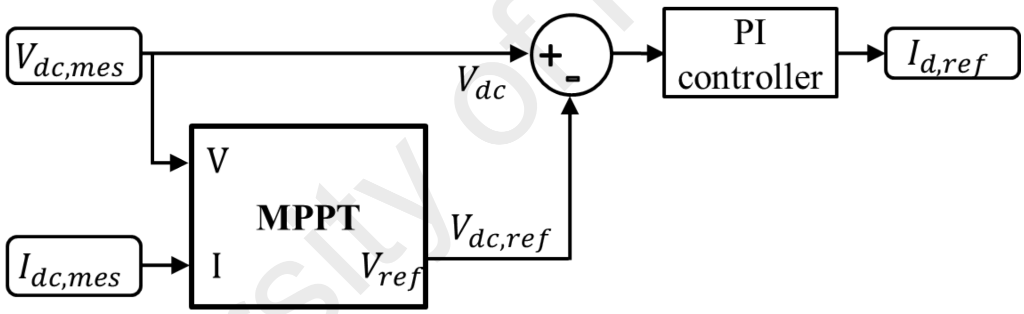

Figure 3.7: DC voltage regulator.

Figure 3.8 shows the inner loop controller function, which controls the reactive power dispatched to the utility, reference reactive power ($I_{q,ref}$) is set to zero to maintain unity power factor. $V_{abc,B}$ and $I_{abc,B}$ are the three-phase voltage and current measured at bus B as shown in Figure 3.2. The PLL block converts them from the three-phase reference frame to dq0 reference frame. The values are then used by the reactive power regulator to give the V_d, V_q that operate the system in a unity power factor mode. These signals are used by the PWM generator to produce the desired switch pulses. The control systems use a sample time of 100 μs in the voltage and current controllers and also the PLL synchronization unit. However, the sampling time for the power system is shorter;

University of Malaya

taking 10μ s to make the simulation run faster. The value of $I_{d,ref}$ comes from the outer loop.

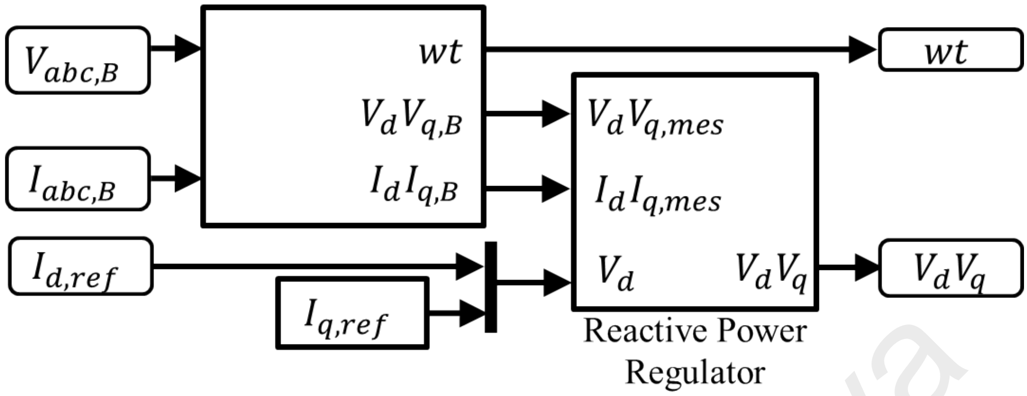

Figure 3.8: Reactive power regulator (inner loop).

The system runs for 5 s in all the cases. The radiation was varied as shown in Table 3.1.

Table 3.1: The solar radiation on the PV panel

Solar radiation W/m^2	Time (s)	
	From	To
1000	0	2
500	2	4
900	4	5

SunPower SPR-305-WHT PV panels were used. The number of series-connected modules per string is 5, while the number of parallel strings is 66. At 1000 W/m^2 the panels provide 100 kW, with the open circuit voltage (V_{oc}), short circuit current (I_{sc}), voltage at maximum power (V_{mp}), and current at maximum power (I_{mp}) being 64.2 V, 5.96 A, 54.7 V, and 5.58 A, respectively. Parameters of PV module used in this work are shown in appendix A.

3.4.1 Proposed Voltage Reference Value

- **Variable radiation**

University of Malaya

This study proposes a variable voltage reference (V_{ref}) instead of fixed (Eid, Rahim, & Selvaraj, 2013); the reference voltage value changes as in Figure 3.9. This technique increases the active power extracted from system, as shown in Figure 3.10; the black dashed line (which is the proposed technique) dispatches higher power than the fixed reference (blue continuous) at all solar radiation levels. The correlation between Figures (3.9) and (3.10) show that the reference voltage decreased when the radiation reduced in order to increase the extracted active power at the certain radiation level.

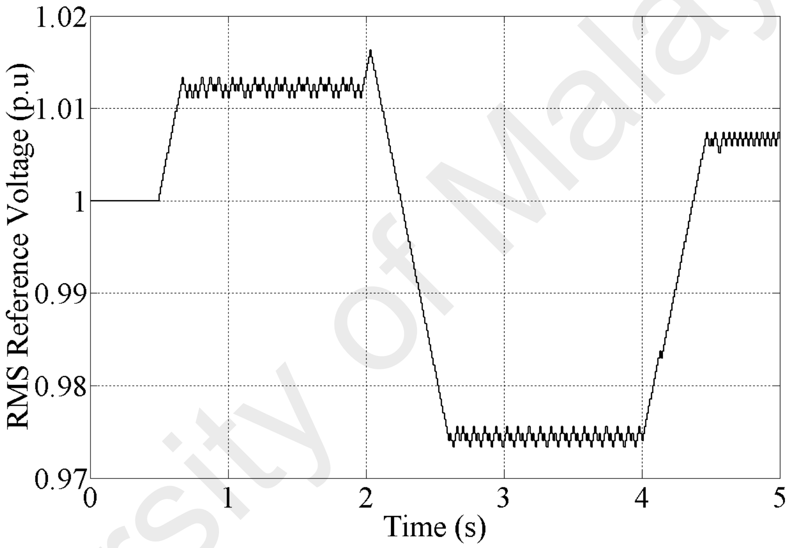

Figure 3.9: RMS reference voltage during variable radiation.

- **Variable temperature**

Figure 3.11 shows the active power dispatched to the grid with variable temperature. The T_c increased from 25° C to 65°C during the first 8 s then it decreased gradually. Although, the active power decrease with increasing of the T_c, the proposed technique (dashed black line) achieves higher dispatching active power at steady state compared the continuous blue line (which uses fixed DC voltage reference). Figure 3.12, illustrates the voltage reference changes with the variable temperature. The correlation between Figures 3.11 and 3.12 show that the reference

University of Malaya

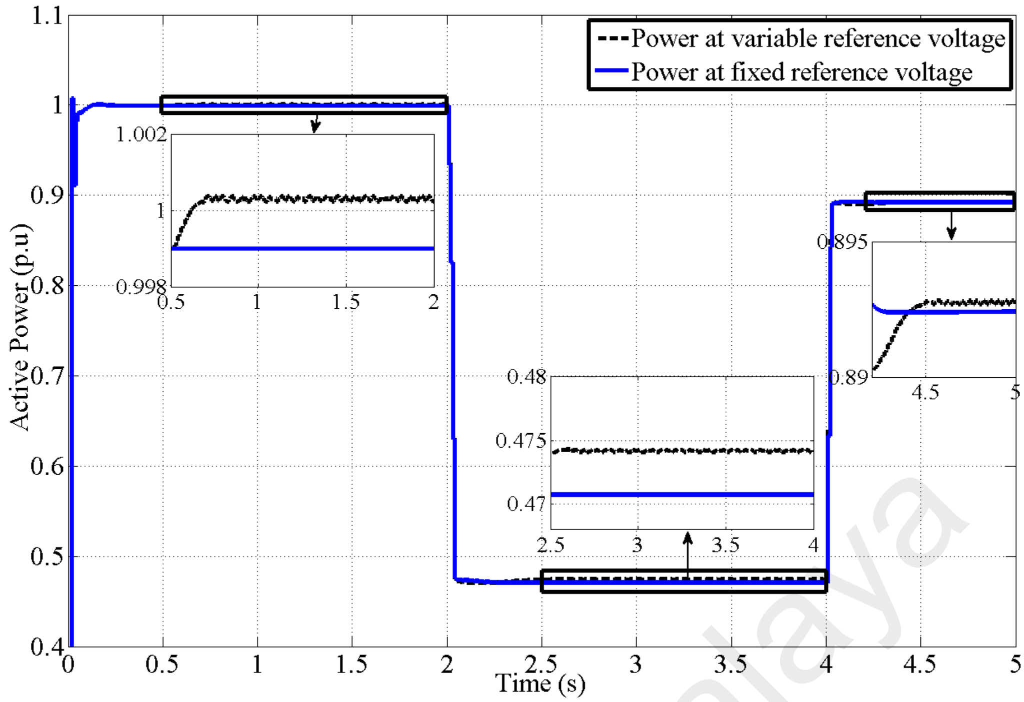

Figure 3.10: Active power dispatched to the grid, with variable and fixed voltage references.

voltage decreased when the temperature increase in order to increase the extracted active power at the certain temperature level.

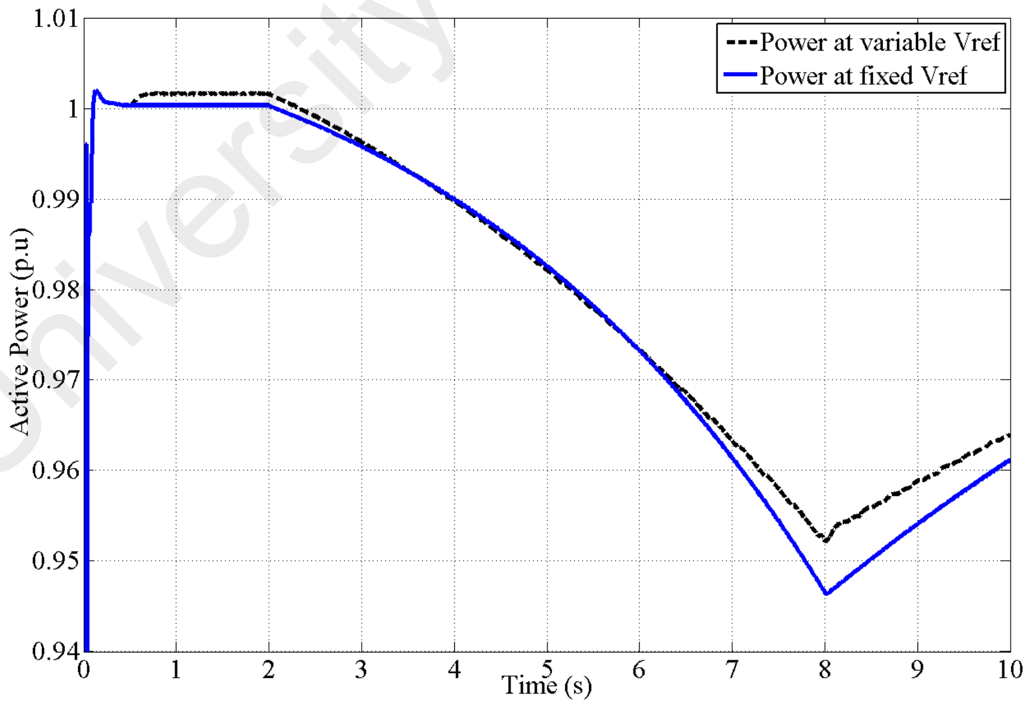

Figure 3.11: Active power dispatched to the grid with variable temperature.

University of Malaya

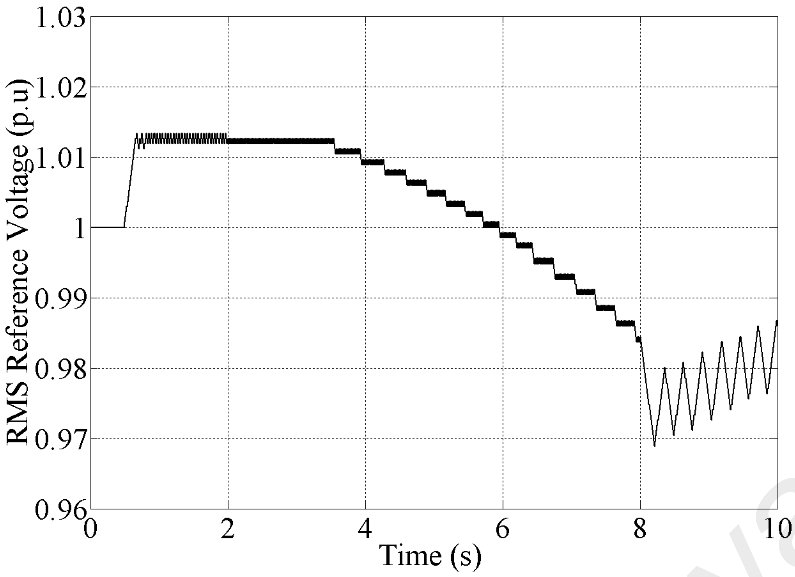

Figure 3.12: RMS reference voltage during variable temperature.

3.4.2 Power Flow at Single and Two Stages Power Conversion

As active power flows from the PV to the utility, losses occur in the conversion system. This work proposes a single-stage power conversion system, whose efficiency is higher than the two stage power conversion system (Eid et al., 2013). Figure 3.13 shows the active power exported to the grid with single-stage (dashed line) and two stages (continuous line). The base active power is 100 kW. The power from single-stage is higher for the three solar radiation levels, showing that the efficiency with single-stage power conversion is higher.

3.4.3 Reactive Power

As in some previous works (Balathandayuthapani et al., 2012), the system dispatches unity power factor, and the reactive power injected into the grid is set to zero. Figures 3.14 shows the reactive power dispatched to the grid during variable solar radiation, and variable temperature. The reactive power disrupts at 2 s and 4 s when the solar radiation changes, but the controller overcomes the disturbance and returns the reactive power back to zero. The base reactive power is 100 kVAr.

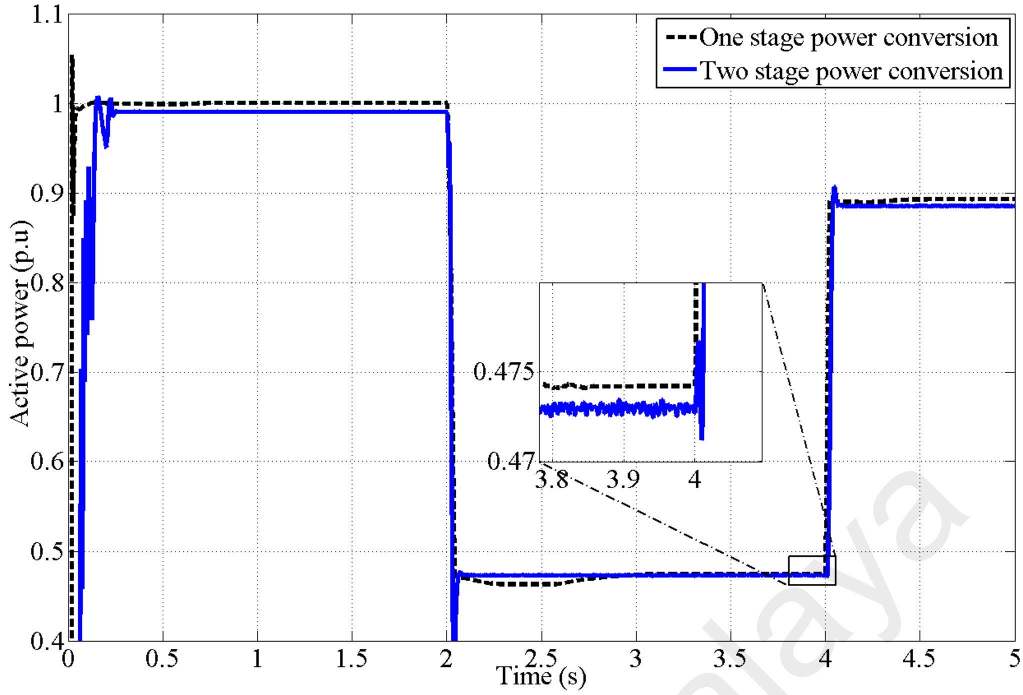

Figure 3.13: The active power in single-stage and two-stage power conversion systems.

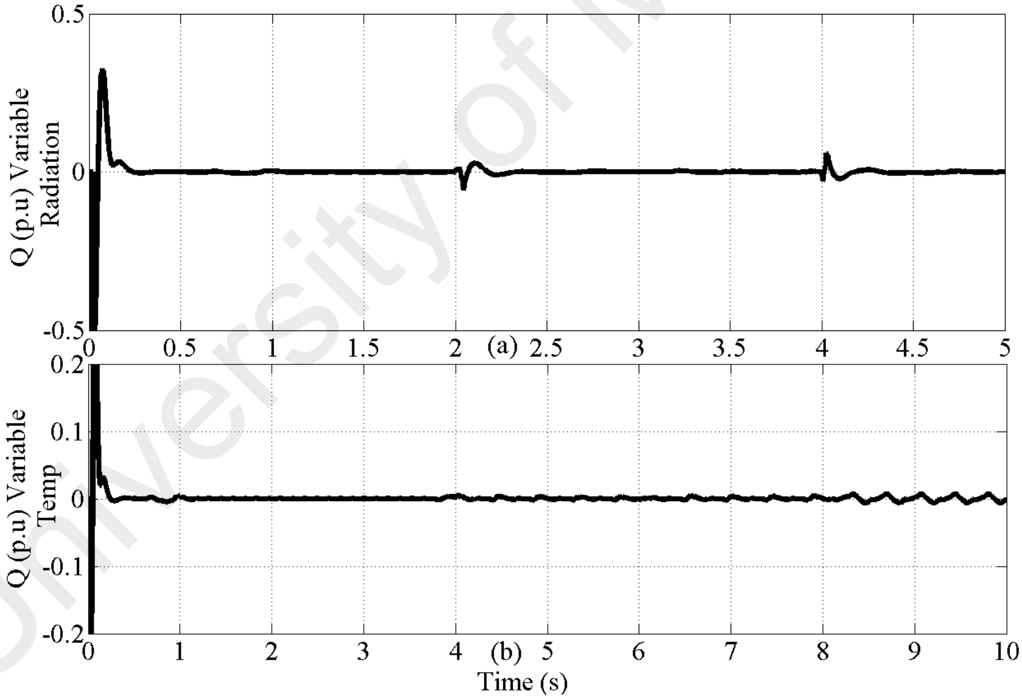

Figure 3.14: The reactive power dispatched from the PV system to the grid with variable: (a) solar radiation and (b) temperature

3.4.4 Voltage and Current

Figures 3.15 and 3.16 show the line-to-ground RMS voltage and current at the PCC. The voltage line to line at grid is 25 kV so the voltage base phase is 14.433 kV and the apparent power base is 100 kVA. The RMS voltage is stable around 1.4 kV. The

University of Malaya

current base value is 3.35 A. Figure 3.16 shows the current imported to the grid, which is directly proportional to the active power provided by the PV source. Current reaches to the minimum between 2 s to 4 s due to the drop of solar radiation during that period of time.

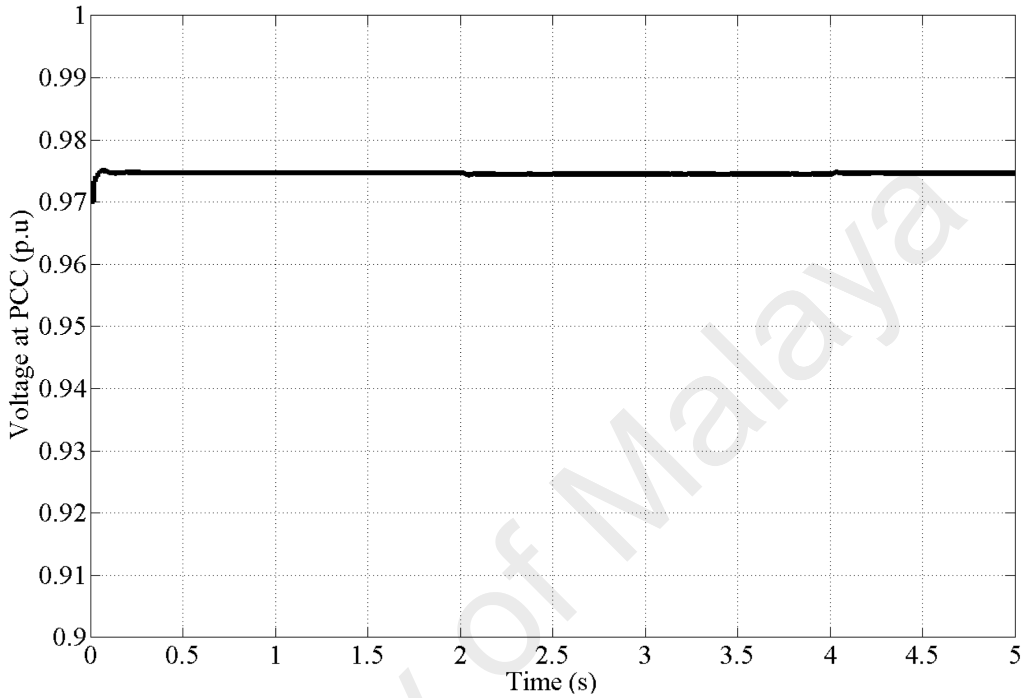

Figure 3.15: Voltage rms p.u at the PCC.

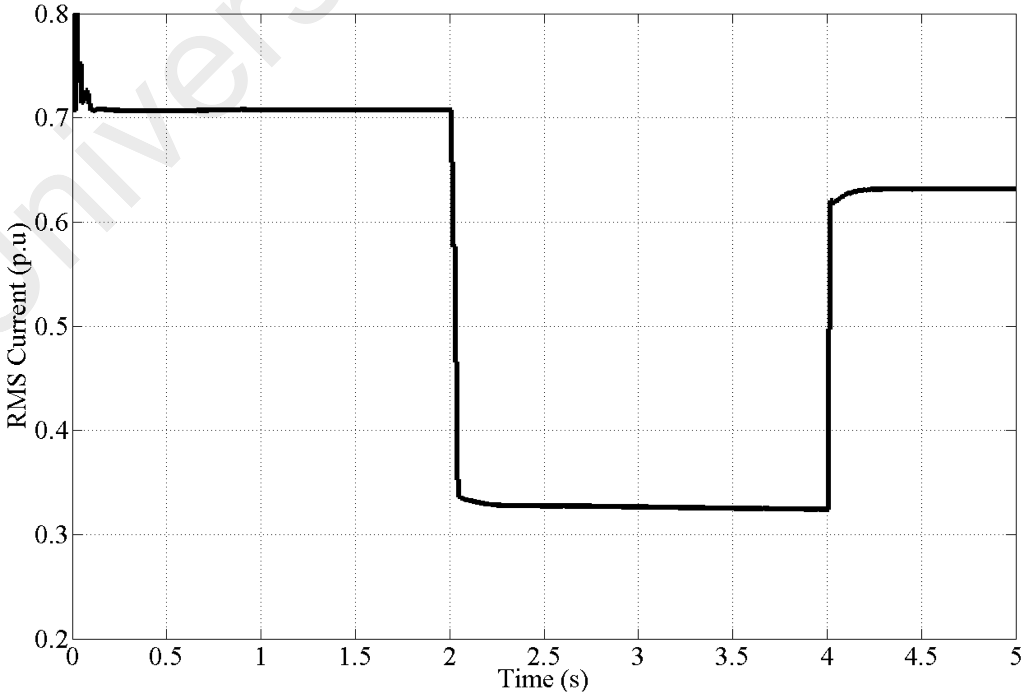

Figure 3.16: Current rms p.u at the PCC.

University of Malaya

3.5 Large Scale DER with Different Distribution Line Distance

The penetration of renewable DERs into power systems increased dramatically in the past few years. Even though micro-DERs are used widely in microgrids due to their simplicity and low capital cost, large-scale DERs have been used due to their competitive features such as high integration of clean energy and lower cost per installed watt. Despite these attracting features, the geographical and electrical drawbacks start to grow with the size of the PV DER as it reaches few MWs in a single location. This may result in high instability for distribution network mainly due to weather disturbances (Mirhosseini, Agelidis, & Ravishankar, 2012). In this section a large scale grid-connected PV DER is studied. The impact of different ambient disturbances such as varying weather conditions, solar radiation with severe disturbances, and variable PV cell temperature on the active and reactive power yields. The active and reactive power flow and voltage of the system at three different distances of distribution line have been investigated.

Figure 3.17 shows a PV DER connected to a three-phase utility via a single-stage power conversion system, namely an inverter. The three phase inverter has two loops: an inner loop to control the reactive power, and an outer loop to control reference DC voltage ($V_{dc,ref}$) so as to remain at a voltage that extracts maximum power from the PV. Coupling inductors connect the inverter to inverter bus (B_{inv}). The distance between B_{inv} and bus b (B_b) is represented by π model (distribution line) to study the effect of distribution line impedance. The distribution line impedance has impact on voltage regulation, power flow and circulating reactive current. A local load is connected to load bus (B_L). A transformer connects the system to the grid. The transformer's primary is connected to the medium voltage utility 11 kV.

University of Malaya

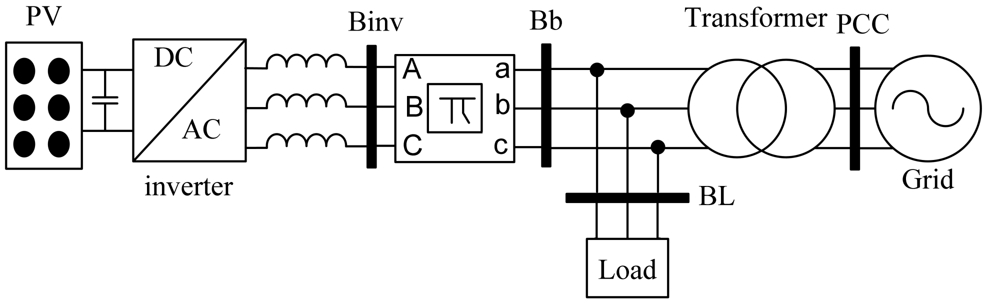

Figure 3.17: Grid connected PV source with local load.

3.5.1 Distribution Line Length Effect

The circuit simulated in Figure 3.17 has been used to investigate the distribution line length effect. SunPower SPR-305-WHT PV DER have been used, the PV source parameters are shown in appendix A. The number of series-connected modules per string is 17, while the number of parallel strings is 200. The panels produce 1.037 MW at 1000 W/m^2 radiation. Solar radiation was changed during the simulation as illustrated in Table 3.2. The local load is 0.5 MW at initial condition, then 0.1 MW and 0.1 MVar are added at 4 s, then are removed at 6 s. π model represents the distribution line between B_{inv} and B_b. The active and reactive power flow, and voltage are studied for three distribution line distances 10 m, 100 m, 200 m as discussed below.

Table 3.2: The solar radiation to study different distances

Radiation W/m^2	Time (s)	
	From	To
1000	0	2
500	2	8
900	8	10

3.5.2 For 10 m Distribution Line

In this case the distance between B_{inv} and B_b is 10 m and the distribution line has been presented by π model. Figure 3.18 shows the active power at buses corresponding to PCC, B_b, B_L and B_{inv} coupled with a 10 m distribution line. The summary of the values at all five stages which are initial value, radiation droop, load increase, load decrease, and radiation increase, are illustrated in Table 3.3. At all stages, B_{inv} has the highest active power. B_b has the same value since the distance is almost zero resulting in a negligible power loss at distribution line. When the load increases at B_L, some of the power is transferred to the load instead of being exported to the utility, which eventually causes drop in active power at PCC.

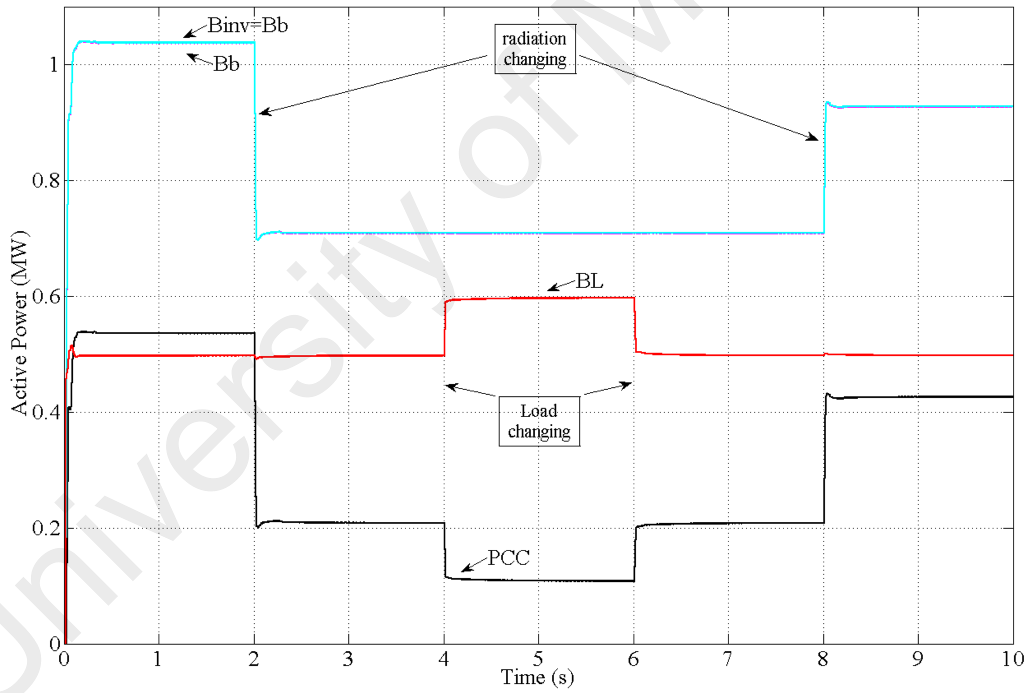

Figure 3.18: Active power at buses corresponding to PCC, B_b, B_L and B_{inv} coupled with a 10 m distribution line.

Figure 3.19 shows the reactive power at buses corresponding to PCC, B_b, B_L and B_{inv} with a 10 m long distribution line. The summary of the values at all five stages are illustrated in Table 3.3. For all the cases, the reactive power at B_{inv} is the highest, which used to regulate the voltage at B_L, then the non consumed reactive power at local load

University of Malaya

exports to the utility. The deviation between B_{inv} and B_b shows the reactive power losses in the distribution line. The deviation between B_b and PCC shows the reactive power consumed in the transformer at zero reactive load.

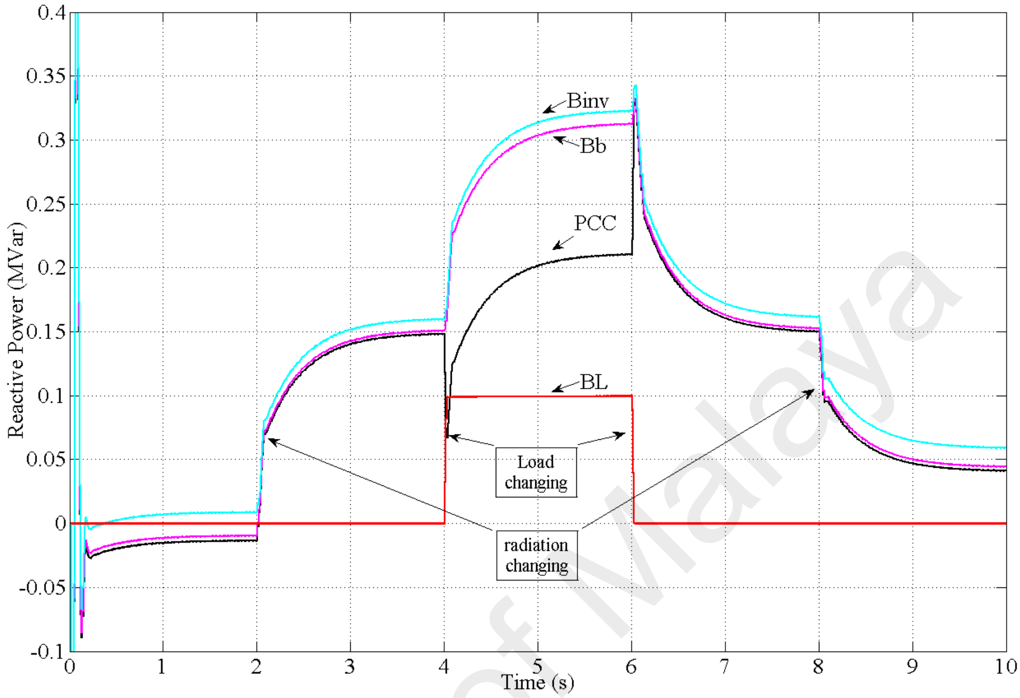

Figure 3.19: Reactive power at buses corresponding to PCC, B_b, B_L and B_{inv} with a 10 m distribution line.

Figure 3.20 shows the RMS voltage of phase A at buses corresponding to PCC, B_b, B_L and B_{inv} at 10 m distance. The summary of the values at all five stages are illustrated in Table 3.3. At all cases voltage at B_L is regulated at 239 V, B_b has almost the same value. Voltage at B_{inv} is a bit higher mainly between 4 s and 6 s due to increasing the amount of reactive power consumed at the load. The voltage at PCC is stable as well.

University of Malaya

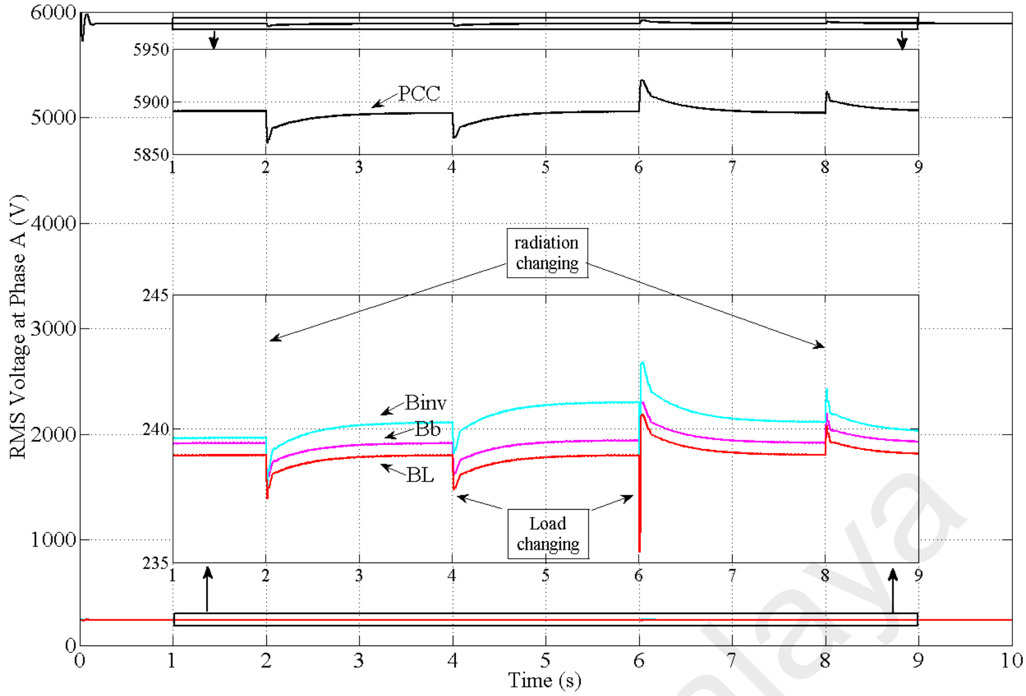

Figure 3.20: RMS Voltage for phase A at buses PCC, B_b, B_L and B_{inv} with 10 m distribution line.

Table 3.3: Summary of active power, reactive power and voltage values at 10 m distance

Item	Initial value	Radiation droop	Load increase	Load decrease	Radiation increase
P_{pcc} (MW)	0.536	0.2085	0.1085	0.2083	0.4261
P_{inv} (MW)	1.0378	0.7093	0.7093	0.7093	0.9276
P_{Bb} (MW)	1.037	0.7088	0.7088	0.7088	0.927
P_{BL} (MW)	0.4975	0.4975	0.597	0.4975	0.4975
Q_{pcc} (MVar)	-0.0133	0.1484	0.2106	0.15	0.041
Q_{inv} (MVar)	0.0087	0.16	0.323	0.1615	0.059
Q_{Bb} (MVar)	-0.0095	0.151	0.3126	0.1525	0.0445
Q_{BL} (MVar)	0	0	0.0995	0	0
V_{pcc} (V)	5890.9	5889	5890.5	5889.2	5890.4
V_{inv} (V)	239.7	240.22	241	240.23	239.8
V_{Bb} (V)	239.45	239.45	239.55	239.45	239.45
V_{BL} (V)	239	239	239	239	239

3.5.3 For 100 m Distribution Line

In this case the distance between B_{inv} and B_b is 100 m. Figure 3.21 shows the active power for buses corresponding to PCC, B_b, B_L and B_{inv} at 100 m distance from the PV source. The summary of the values at all five stages are illustrated in Table 3.4. At all stages, B_{inv} has the maximum active power, while B_b is slightly less due to the power losses at the 100 m distribution line. The load at B_L is 0.5 MW which is increased to

University of Malaya

0.6 MW at 4 s. When the load is increased at B_L the power exported to the utility (PCC) drops to its minimum.

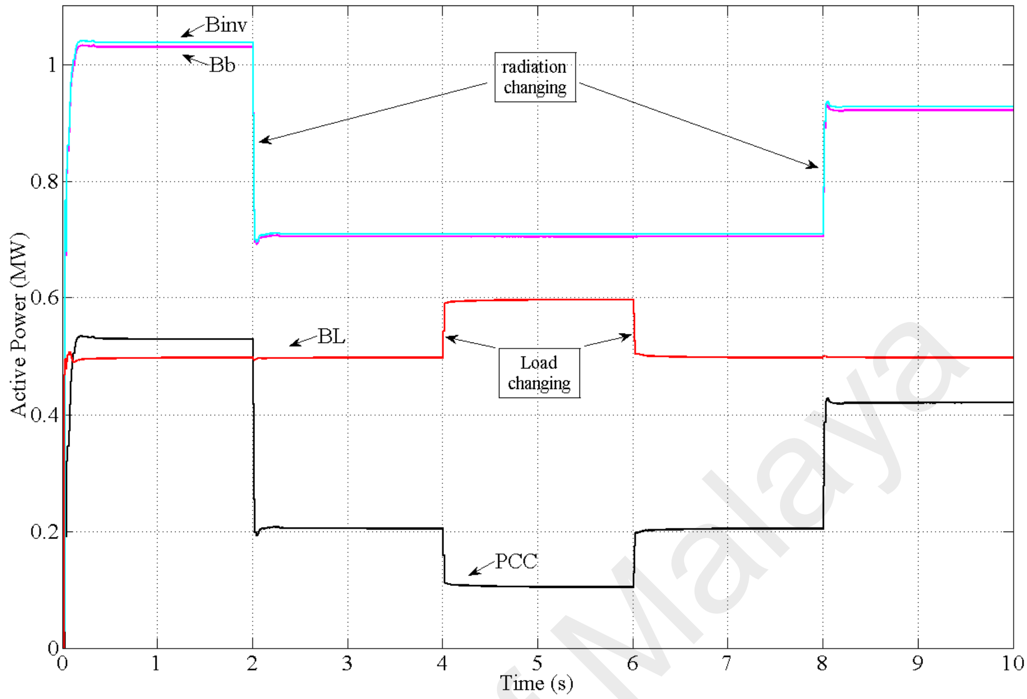

Figure 3.21: Active power at buses corresponding to PCC, B_b, B_L and B_{inv} coupled with a 100 m distribution line.

Figure 3.22 shows the reactive power at buses corresponding to PCC, B_b, B_L and B_{inv} with a 100 m long distribution line. The summary of the values at all the five stages are illustrated in Table 3.4. At all cases the reactive power at B_{inv} is the highest, which used to regulate the voltage at B_L, while the non consumed reactive power at local load exports to the utility. The deviation between B_{inv} and B_b shows the reactive power losses in the distribution line. The deviation between B_b and PCC shows the reactive power consumed in the transformer at zero reactive load.

Figure 3.23 shows the RMS voltage for phase A at buses corresponding to PCC, B_b, B_L and B_{inv} with a 100 m long distribution line. The summary of the values at all five stages; are illustrated in Table 3.4. At all cases voltage at B_L is regulated at 239 V and B_b has almost the same value. Voltage at B_{inv} is higher than that at B_L and B_b particularly between 4 s and 6 s due to rise in active power load. The voltage at PCC is stable around

University of Malaya

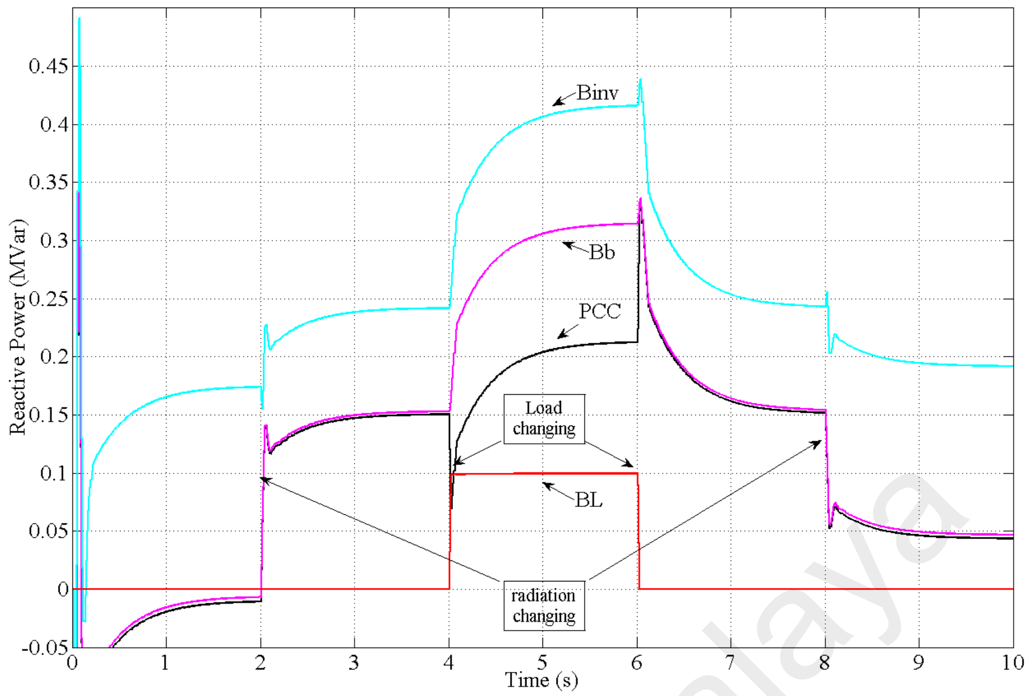

Figure 3.22: Reactive power at buses corresponding to PCC, B_b, B_L and B_{inv} with a 100 m distribution line.

5890 V (10.2 kv line to line).

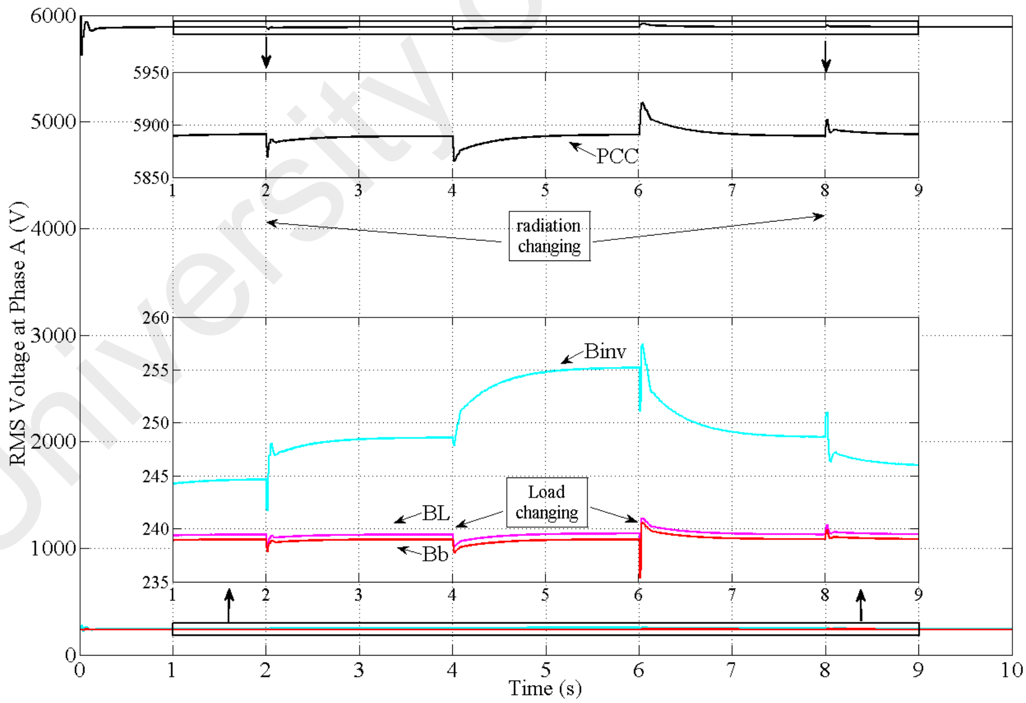

Figure 3.23: RMS Voltage value for phase A at buses PCC, B_b, B_L and B_{inv} with 100 m distribution line.

University of Malaya

Table 3.4: Summary of active power, reactive power and voltage values at 100 m distance

Item	Initial value	Radiation droop	Load increase	Load decrease	Radiation increase
P_{pcc} (MW)	0.5289	0.2048	0.1044	0.2048	0.42046
P_{inv} (MW)	1.0377	0.7093	0.7093	0.7093	0.9276
P_{Bb} (MW)	1.0298	0.7055	0.7047	0.7055	0.9213
P_{BL} (MW)	0.4975	0.4975	0.5968	0.4975	0.4975
Q_{pcc} (MVar)	-0.0106	0.1505	0.2126	0.1517	0.0436
Q_{inv} (MVar)	0.1742	0.2418	0.4161	0.2432	0.1919
Q_{Bb} (MVar)	-0.0067	0.1531	0.3145	0.1542	0.0468
Q_{BL} (MVar)	0	0	0.0995	0	0
V_{pcc} (V)	5890.8	5889	5890.4	5889.2	5890.3
V_{inv} (V)	244.66	248.61	255.3	248.7	245.89
V_{Bb}(V)	239.45	239.45	239.55	239.46	239.45
V_{BL} (V)	239	239	239	239	239

3.5.4 For 200 m Distribution Line

In this case the distance between B_{inv} and B_b is 200 m. Figure 3.24 shows the active power at buses corresponding to PCC, B_b, B_L and B_{inv} for a 200 m long distribution line. The summary of the values at all five stages are illustrated in Table 3.5. At all stages B_{inv} has the maximum active power, while the active power at B_b is a bit less due to the power losses over the 200 m distribution line. The load at B_L was 0.5 MW which is increased to 0.6 MW at 4 s. When the load is increased at B_L, less power is exported to the utility (PCC).

Figure 3.25 shows the reactive power at buses corresponding to PCC, B_b, B_L and B_{inv} for a 200 m long distribution line. The summary of the values at all five stages; are illustrated in Table 3.5. The maximum reactive power is required to be dispatched from B_{inv} is at 4 s when the radiation is at the minimum and the reactive load is at the maximum. Reactive power at B_b is significantly less due to longer distribution line. A significant amount of the reactive power exported to the utility reveal that only 0.1 MVar is required to be consumed at B_L, while the rest is produced to regulate the voltage at the desired value.

Figure 3.26 shows the RMS voltage for phase A at buses PCC, B_b, B_L and B_{inv} for a

University of Malaya

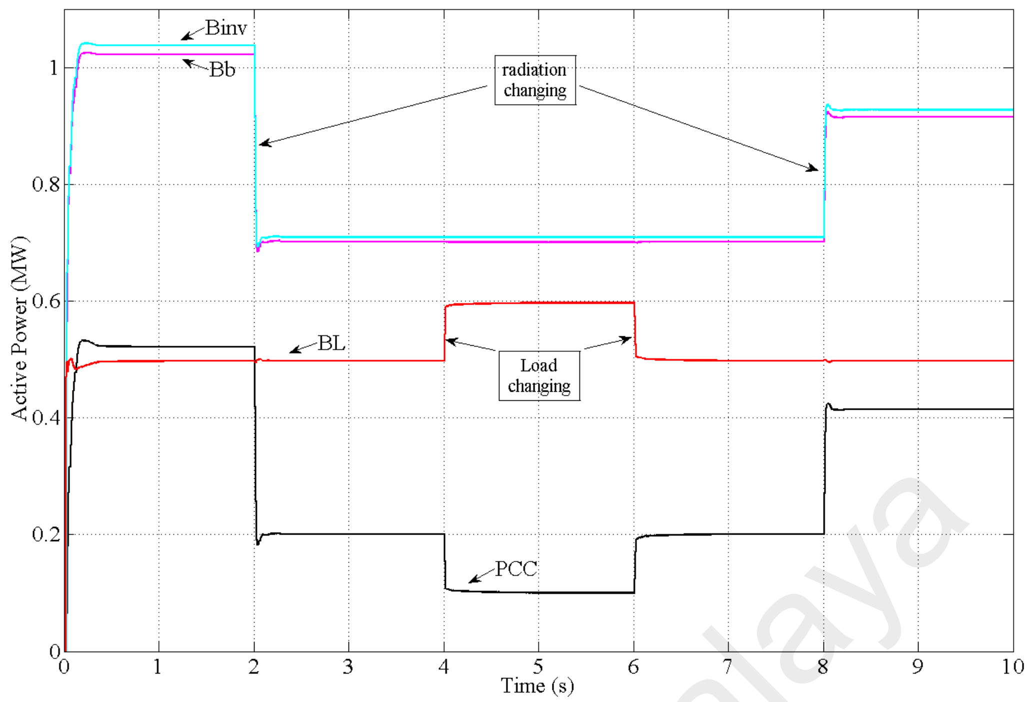

Figure 3.24: Active power at buses corresponding to PCC, B_b, B_L and B_{inv} coupled with a 200 m distribution line.

200 m lond distribution line. The summary of the values at all five stages are illustrated in Table 3.5. The voltages at B_L and B_b are regulated at the desired values 239 V. The voltage at B_{inv} is dynamic based on the required reactive power dispatch in order to obtain the desired voltage at B_L. Voltage at PCC is stable around 5890 V (10.2 kV line to line).

3.5.5 Results Comparison and Discussions

Figure 3.27 shows the active power dispatched to PCC for the three distribution line distances; 10 m (blue), 100 m (red), and 200 m (green) at the five stages. The amount of power dispatched mainly depends on the sun radiation, whereas the distance effect is not significant. At all the stages, the highest power dispatch to the utility happens for 10 m distance (blue).

Figure 3.28 illustrates the reactive power dispatched from B_{inv} for three distribution line distances at five experimental stages. At stage 1, almost zero reactive power is required to be dispatched for 10 m (blue). When the distance is increased, the reactive power required to regulate the voltage at B_L increases dramatically. In the case of radia-

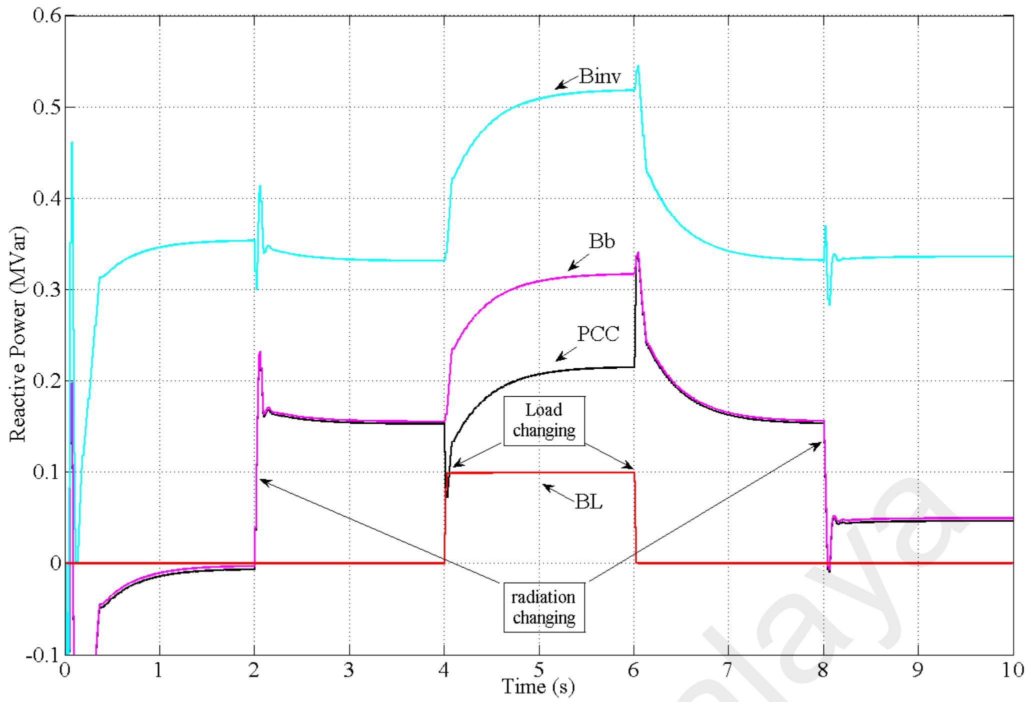

Figure 3.25: Reactive power at buses corresponding to PCC, B_b, B_L and B_{inv} with a 200 m distribution line.

tion variation the deviations between reactive power for the three distances at stages 2 and 4 are not similer as in stages 1 and 5. This is, due to the decrease in the power transfer over the distribution line when the radiation decreases. At stage 3, when the radiation is at the minimum and the reactive load is at the maximum, the maximum reactive power is required to fulfill the voltage regulation requirement. The increase in the dispatched reactive power is higher than the new amount of reactive load demand due to the increase of reactive power consumed at distribution line.

Figure 3.29 shows the active power losses for the three distances at the five stages. Stages 1 and 5 incur a significant increase in the amount of power losses with the increase in the distance, since the highest amount of power is transferred at these stages. When the load increase at stage 3, the increase in the losses compared to stages 2 and 4 is not significant.

Figure 3.30 shows the reactive power losses for the three distances at the five stages. At stages 1 and 5 incur a significant increase in the amount of power losses with the

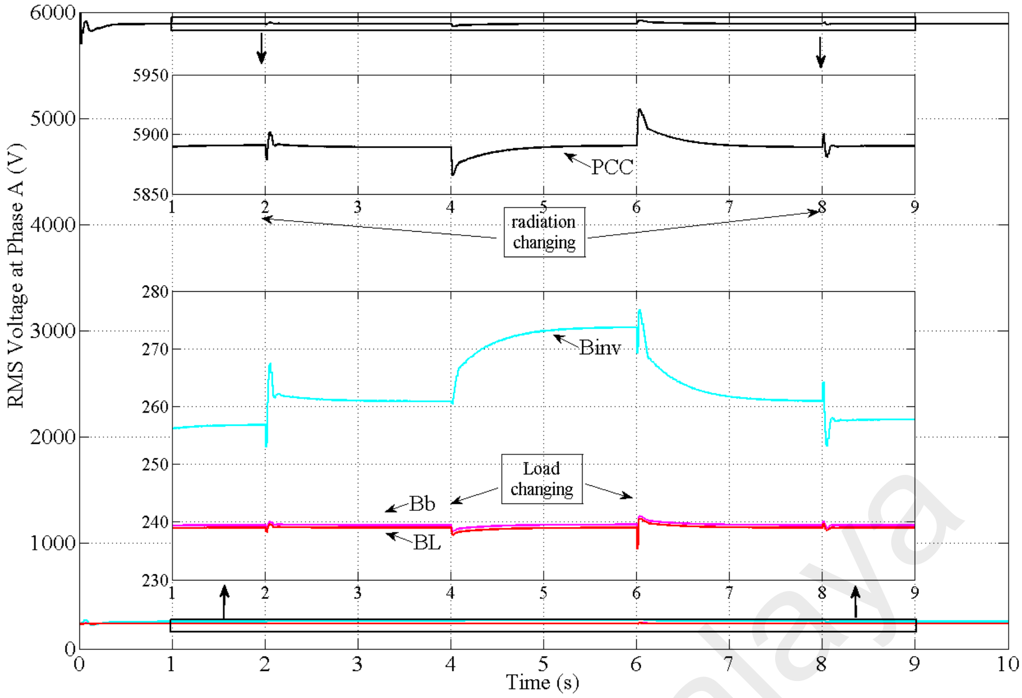

Figure 3.26: RMS Voltage value for phase A at buses PCC, B_b, B_L and B_{inv} with 200 m distribution line.

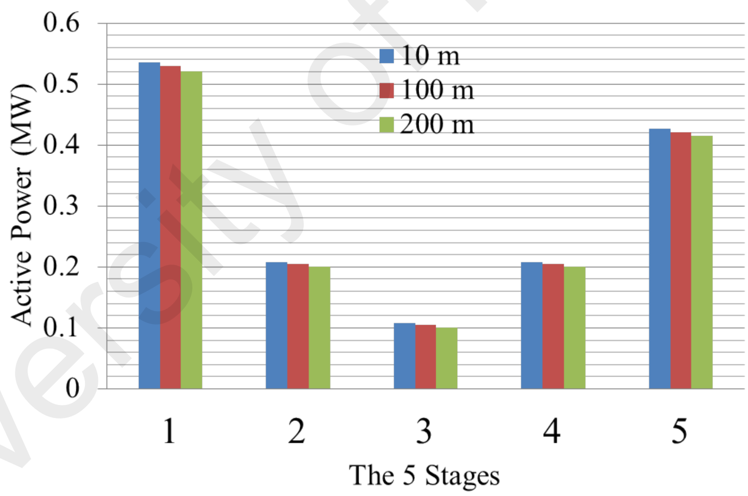

Figure 3.27: Active Power dispatched to PCC at the distances 10, 100, 200 m.

increase in the distance, since the highest amount of power is transferred at these stages. When the load increases at stage 3, the increase in the losses compared to stages 2 and 4 is not significant.

Figure 3.31 shows the RMS voltages for the three distances at the five stages. The voltage at B_L is stable revealing the effectiveness of the controller. When the distance of distribution line is increased more reactive power is required to be dispatched from the

University of Malaya

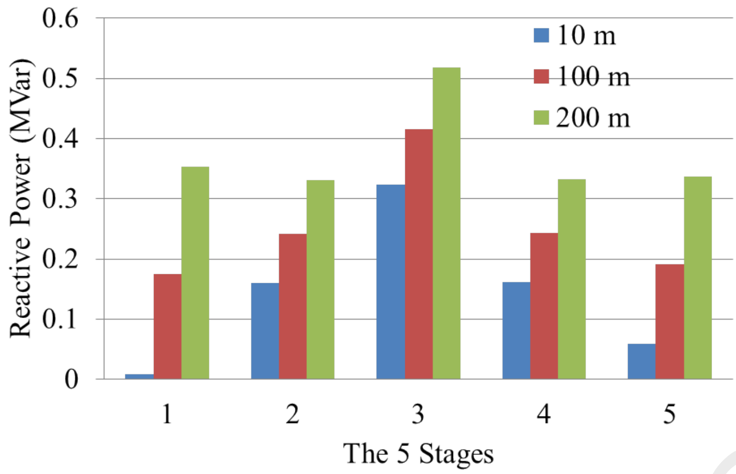

Figure 3.28: Reactive power dispatched from B_{inv} at the distances 10, 100, 200 m.

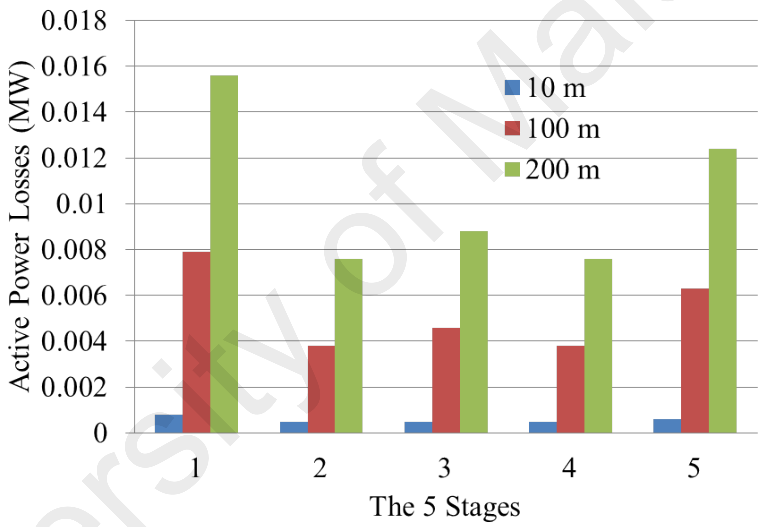

Figure 3.29: Active power losses at distribution line between B_{inv} and B_b.

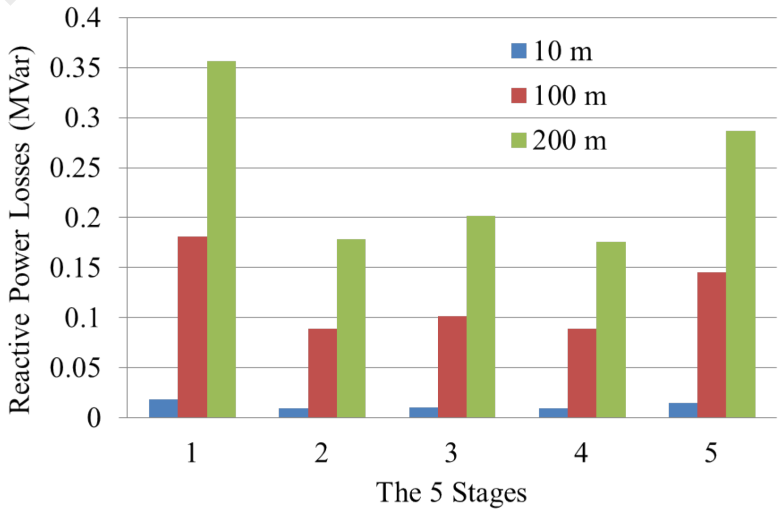

Figure 3.30: Reactive Power Losses in distribution line for the three distances.

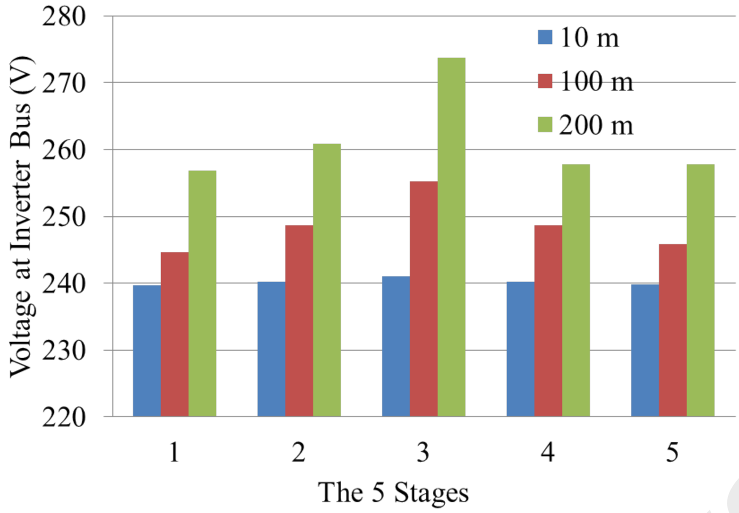

Figure 3.31: RMS Voltage at phase A for different distances.

B_{inv}. Since the distribution network is inductive, the reactive power dispatched is directly proportional to voltage.

Table 3.5: Summary of active power, reactive power and voltage values at 200 m distance

Item	Initial value	Radiation drop	Load		Radiation increase
			increase	decrease	
P_{pcc} (MW)	0.5213	0.2011	0.1001	0.2011	0.4144
P_{inv} (MW)	1.0378	0.7093	0.7093	0.7093	0.9276
P_{Bb} (MW)	1.0222	0.7017	0.7005	0.7017	0.9152
P_{BL} (MW)	0.4975	0.4975	0.597	0.4975	0.4975
Q_{pcc} (MVar)	-0.0066	0.1553	0.2147	0.1535	0.0465
Q_{inv} (MVar)	0.3536	0.3315	0.5184	0.3322	0.3362
Q_{Bb} (MVar)	-0.0028	0.1528	0.3169	0.156	0.0495
Q_{BL} (MVar)	0	0	0.0995	0	0
V_{pcc} (V)	5890.8	5889.05	5890.41	5889.1	5890.3
V_{inv} (V)	256.81	260.88	273.71	257.78	257.8
V_{Bb} (V)	239.45	239.45	239.54	239.45	239.45
V_{BL} (V)	239	239	239	239	239

3.6 Summary

In this chapter, a large scale PV DER with a single-stage power conversion system was studied. An inverter was the only power conversion component which achieved two tasks: maximum power point tracking (MPPT) and controlling reactive power dispatching. A variable reference voltage was implemented to extract the maximum power from the system. This technique extracted higher active power from PV panel during variable

University of Malaya

solar radiation and variable cell temperature. Reactive power was controlled by internal controller of the inverter which achieved regulated voltage at local load B_L. Effect of the distance between PV DER at B_{inv} and B_b was studied at 10 m, 100 m and 200 m with variable sun radiation and variable local load. Even though the voltage controller was able to regulate the voltage for 200 m distance, however the power losses at the distribution line is significant enough to override the decision to connect the PV DER to a higher distribution voltage like 11 kV.

University of Malaya

CHAPTER 4: EFFECTS OF DIFFERENT CONFIGURATIONS OF MICROGRID WITH LARGE-SCALE DERS

RES have many advantages compared with other DERs, including high abundance, zero carbon-dioxide emissions, low running costs, and low maintenance costs (Mehta & Singh, 2013). These advantages are increasingly encouraging the integration of RES into electrical systems throughout the world. Thus, Germany already supplies 25% of its electrical consumption through RES (von Appen et al., 2013). However, the high penetration of RES can have negative effects in terms of voltage increases, circulating current, network voltage instabilities, and reverse power flow in the transmission lines (von Appen et al., 2013; Carvalho et al., 2008). These problems are more apparent when RES are connected to a low-voltage distribution network (which is usual when a feed-in tariff mechanism is in place) (von Appen et al., 2013; Farhangi, 2010). Various RES combinations have been studied (von Appen et al., 2013; Ahn et al., 2010), but combining photovoltaic (PV) and fuel cell (FC) energy sources is one of the most attractive (Khanh et al., 2010), and it is investigated in the present study. RES integration is associated with the problem of intermittence, which can be overcome by adding a controllable battery to the microgrid (Koohi-Kamali et al., 2014; Elsied et al., 2015). However, using a battery increases the cost and decreases the efficiency and plug-and-play capability. Moreover, the battery's life cycle is much shorter than that of the other components in the system. Therefore, intermittent sources such as PV sources need to be combined with DERs with a rapid response rate, such as that in a FC, so the system can smooth out intermittent PV power generation (Khanh et al., 2010).

Previous studies have investigated the effects of different microgrid configurations on power flow control (Ahn et al., 2010). Active power and frequency control principles have been described for multiple DERs in grid-connected and islanded modes (Ahn et al., 2010). Different control modes such as unit output-power control and feeder flow control (FFC) have been introduced for controlling active power. Furthermore, various configurations have been considered for DERs, including investigations under the following system conditions: 1) load variation during grid-connected operation and islanded operation, and 2) loss of mains (disconnected from the grid). A previous study demonstrated that the FFC mode is advantageous for the grid and the microgrid itself with variations in the load (Ahn et al., 2010); however, only dispatchable power sources were used and simulation results were only obtained for one configuration without considering the voltage profile and the circulating reactive power at each bus.

Two configurations were studied by (Mikati, Santos, & Armenta, 2013), where each configuration comprised two subsystems with a control system, a wind turbine, a PV array, and a load in every subsystem. The first configuration could exchange power inside the microgrid whereas the other exchanged all of its power directly with the grid. The analysis conducted by (Mikati et al., 2013) aimed to compare power transfers with the main grid in these two configurations, as well as investigating how connecting the subsystems affected the grid in terms of dependency and the contribution of renewables to the load, but this study did not consider the voltage profile or the effect of reactive power injection. In (Teimourzadeh Baboli, Shahparasti, Parsa Moghaddam, Haghifam, & Mohamadian, 2014), hybrid AC and DC microgrids were studied by considering the time-dependent impacts on the network over 24 hours. A general architecture was proposed for a hybrid microgrid with the following advantages: enhanced nodal reliability due to the availability of alternative resources, simple deployment for DC generators, low cost, and loss of a DC subgrid. However, (Teimourzadeh Baboli et al., 2014) only studied one configuration without considering the reactive power flow and voltage stability of the buses. In (Hong & De Leon, 2015), an auto-loop microgrid was used to reconfigure the distribution system to perform tie recloser functions. The auto-loop microgrid

University of Malaya

could import/export power to the feeders, thereby providing high flexibility compared with ordinary auto-loops. However, (Hong & De Leon, 2015) did not study the configuration inside the microgrid or investigate the effects of different types of DERs, while they did not consider the relationship between voltage stability at the point of connection and the power flow. The voltage control strategies for PV sources connected to low-voltage networks were described by (von Appen et al., 2013), who proposed a reactive power injection technique as a rapid and cost-effective solution. However, (von Appen et al., 2013) did not study the combination of PV and FC sources in a microgrid, or the active and reactive power flow in the buses inside the microgrid. To overcome these problems, a microgrid system with power flow management and voltage regulation was proposed. A microgrid usually comprises a group of sources and a load, which operate as a controllable system to provide power to a local community (Eid et al., 2014). In the present study, a reactive power injection technique has been investigated, and determined the influence of grid-connected microgrid configurations on the voltage profiles, active power flow, and reactive power flow. Three microgrid configurations have been investigated with variations in solar radiation and load, feeder removal, and partial shading. A large-scale microgrid system comprising PV and FC sources with a reactive power control strategy has been developed to improve the voltage regulation in the distribution network. All three microgrid configurations exhibited similar active power losses, but only one of the microgrid configurations (the second) had a rapid response time and low circulating reactive power.

The distance between DER and the PCC can affect system power flow through line power losses, resonance, communication between parallel DERs, and short-circuit current (M. C. Chandorkar et al., 1993; Ustun et al., 2011). The location of the DER may not be close to the PCC (the location is mostly determined by environmental and economic factors). The effect of distribution-line distance is studied in this work. The distribution

University of Malaya

line is represented by π model. Three microgrid configurations are investigated against variations in solar radiation and load, feeder removal, and partial shading. The effect of connecting a microgrid system to an IEEE 30-bus test system, which reduced power loss of the power system, is discovered.

4.1 Microgrid Configurations

One of the most attractive combination for renewable energy resources is PV with FC as mentioned previously (Rahman & Tam, 1988; Khanh et al., 2010). This study combine PV and FC, with a local load connected to the grid. The study investigates how the different microgrid configuration can influence; voltage profile, power factor, power flow and frequency. Three different microgrid configurations are investigated in this work. The three configurations are presented here as Figures. 4.1, 4.2, and 4.3. Configuration 1 (Figure 4.1), consists of the PV source, FC source, and load are connected to the main bus (B_b). Configuration 2 (Figure 4.2) consists of the FC source (a dispatchable power supply) is connected to the load bus (B_L) and the PV source was connected to B_b. Configuration 3 (Figure 4.3) consists of the FC source is connected to B_b and the PV is connected to B_L. Transformer (T) steps up the microgrid voltage from 415 V (line-to-line) to 11 kV at the PCC on the grid side. The FC and PV sources described in Sections 4.1.3 and 4.1.4 are used in all three configurations. The initial local load is 2 MW. Distribution line impedance (Z_L), represented by the π model, illustrates the effect of the distribution line length.

4.1.1 FC Modeling

FC converts the chemical energy in hydrogen (H_2) and oxygen (O_2) into electrical energy, with the basic reactions at two electrodes of an solid oxide fuel cells (SOFC)

University of Malaya

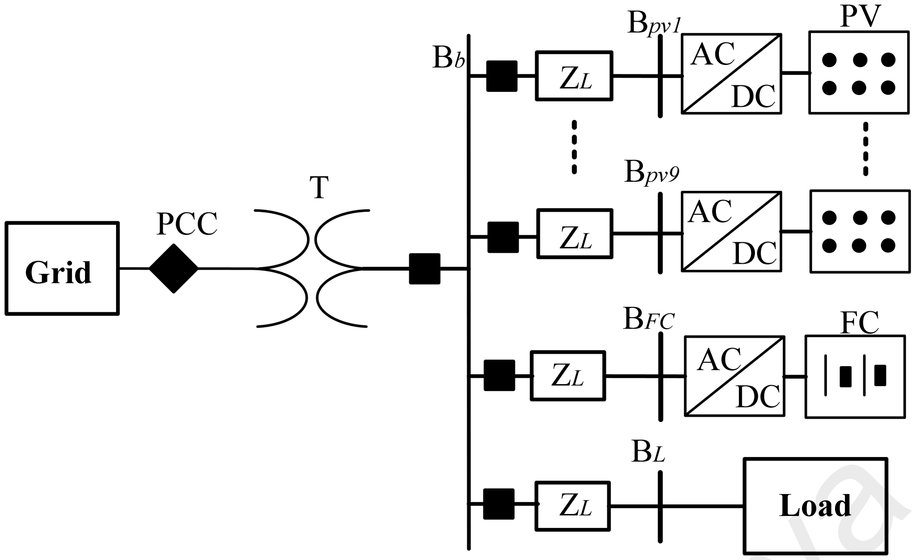

Figure 4.1: Configuration 1.

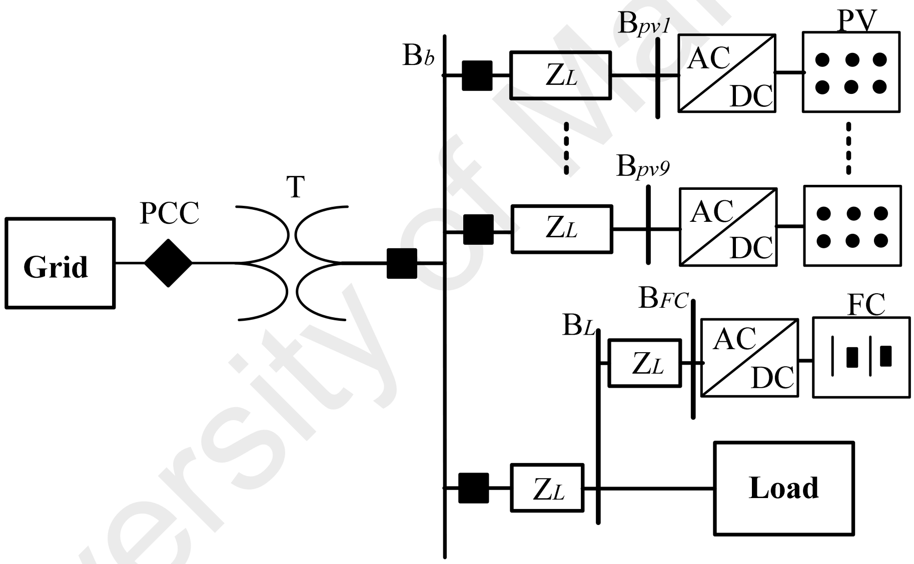

Figure 4.2: Configuration 2.

being (Wang & Nehrir, 2007):

$$\begin{aligned} &Anode: H_2 + O^{=} \rightarrow H_2O + 2e^{-} \\ &Cathode: \frac{1}{2}O_2 + 2e^{-} \rightarrow O^{=} \end{aligned} \tag{4.1}$$

Figure 4.4 shows the process of producing the electrical energy. The reaction produces electrons at the anode. The electrons then pass through the load to the cathode. The

University of Malaya

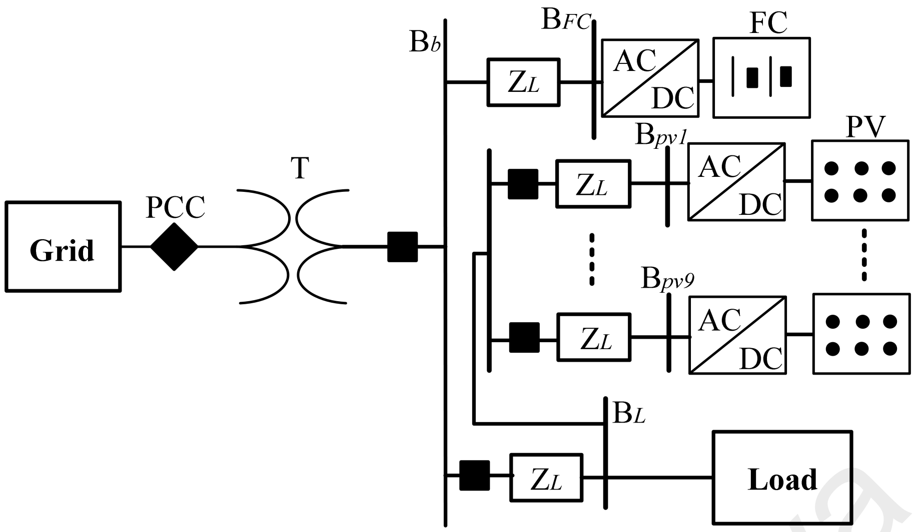

Figure 4.3: Configuration 3.

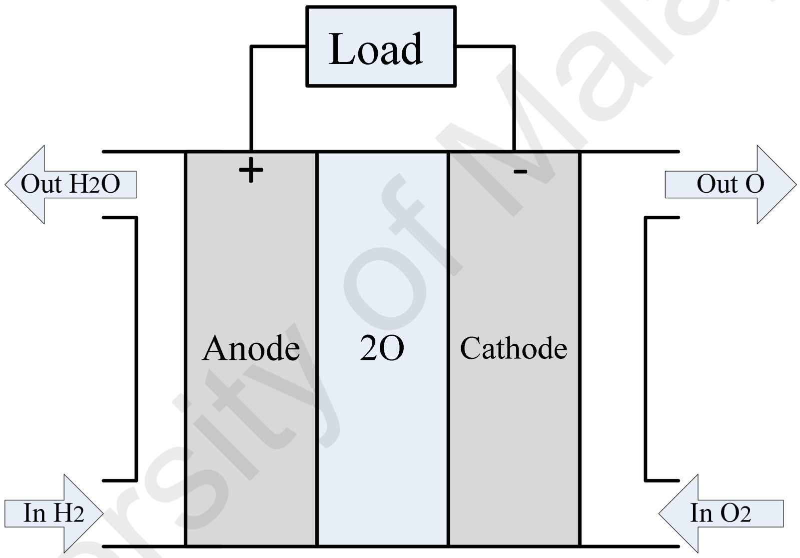

Figure 4.4: Fuel cell process of producing electrical energy.

equivalent circuit for the FC electrical side is shown in Figure 4.5. The voltage across the capacitor (C) is:

$$V_{C,cell} = (i - C\frac{dV_{C,cell}}{dt})(R_{act,cell} + R_{conc,cell}) \tag{4.2}$$

where $R_{act,cell}$ is the equivalent resistance of activation, $R_{conc,cell}$ is the equivalent resistance of the voltage drop duet to the cell concentration, and C is the equivalent capacitance of the double-layer charging effect (Wang & Nehrir, 2007). The output voltage

University of Malaya

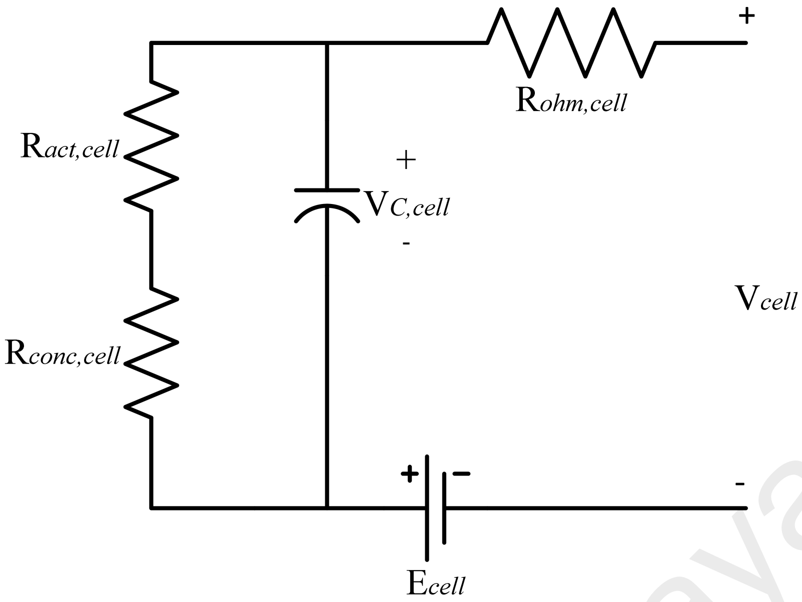

Figure 4.5: Fuel cell equivalent circuit.

of a cell (V_{cell}) is:

$$V_{cell} = E_{cell} - V_{act,cell} - V_{ohm,cell} - V_{conc,cell} \tag{4.3}$$

where E_{cell} is the open-circuit voltage; $V_{act,cell}$ is the activation drop affected by the fuel-cell internal temperature and current; $V_{ohm,cell}$ is the ohmic voltage drop comprising the resistance of the electrodes, the electrolyte, and the interconnection between fuel cells; and $V_{conc,cell}$ is the cell-concentration voltage (drop due to mass diffusion) from the flow channels to the reaction sites (the catalyst surfaces).

4.1.2 The Large-Scale Microgrid

In microgrid implementation, a DER is integrated without interrupting public-grid operation. A lot of DERs can be installed without reforming or rewiring the distribution network (Duan et al., 2008; R. H. Lasseter, 2011). A microgrid enables a power system to observe and control faults more effectively and reduce the damage caused by a DER outage. This boosts the power system's smart grid capability (J. Lopes et al., 2007), allowing load transfer and automated switching through control algorithms to shorten

University of Malaya

outage and power restoration time. The faulted section of the distribution line remains isolated until utility crews get to it (Shamshiri et al., 2012). A microgrid set-up is capable of operating in either grid-connected or off-grid mode according to economy or a planned disconnection, it can also restore grid power quality when the quality drops to below specific standards (Alsayegh et al., 2010; Duan et al., 2008; Kamel et al., 2011; Serban & Serban, 2010). It can improve system reliability and flexibility, through the many options of DER (Driesen & Katiraei, 2008; Silva et al., 2012; Yunwei et al., 2004), also use DER waste heat to improve generation efficiency (Ahn et al., 2010; Blaabjerg et al., 2004; Kroposki et al., 2008; Mao et al., 2008).

The penetration of renewable DERs into power systems increased dramatically in the past few years. Even though micro-DERs are used widely in microgrids for their simplicity and low capital cost, large-scale DERs attract investors and operators through their competitive features such as high integration of clean energy and lower cost per installed Watt. Many large-scale projects all over the world integrate different types of DERs, storage devices, and loads. The consortium for Electric Reliability Technology Solutions (CERTS) has a large-scale microgrid project established in Alameda County Santa Rita Jail in California, USA. This microgrid comprises three DERs: one 1.2 MW PV, one 1 MW FC and two 1.2 MW diesel generators (Alegria, Brown, Minear, & Lasseter, 2014). In Ontario Canada, two DERs are used: 2.5 MVA wind turbine and 2.5 MVA synchronous generator with droop and excitation control systems (Arani & Mohamed, 2015). Both projects are grid-connected systems. Only the California project has an energy storage system: a 2 MW, 4 MWh battery. The parameters and components of the proposed large-scale microgrid are shown in the next sections.

University of Malaya

4.1.3 Large-Scale Fuel Cell Distributed Generator

A physical dynamic model for a 5.5 kW tubular SOFC stack, reported in (Wang & Nehrir, 2007; Colson, Nehrir, & Wang, 2008), is used to simulate the 1.1 MW FC source. The FC power plant contains 50 FC stacks. There are 10 strings, each containing 5 FC stacks connected in series to produce 1100 V. Each FC stack produces 220 V, 22 kW, and 100 A. The voltage versus current and the power versus current characteristics for the 5.5 kW SOFC stack are as shown in Figure 4.6.

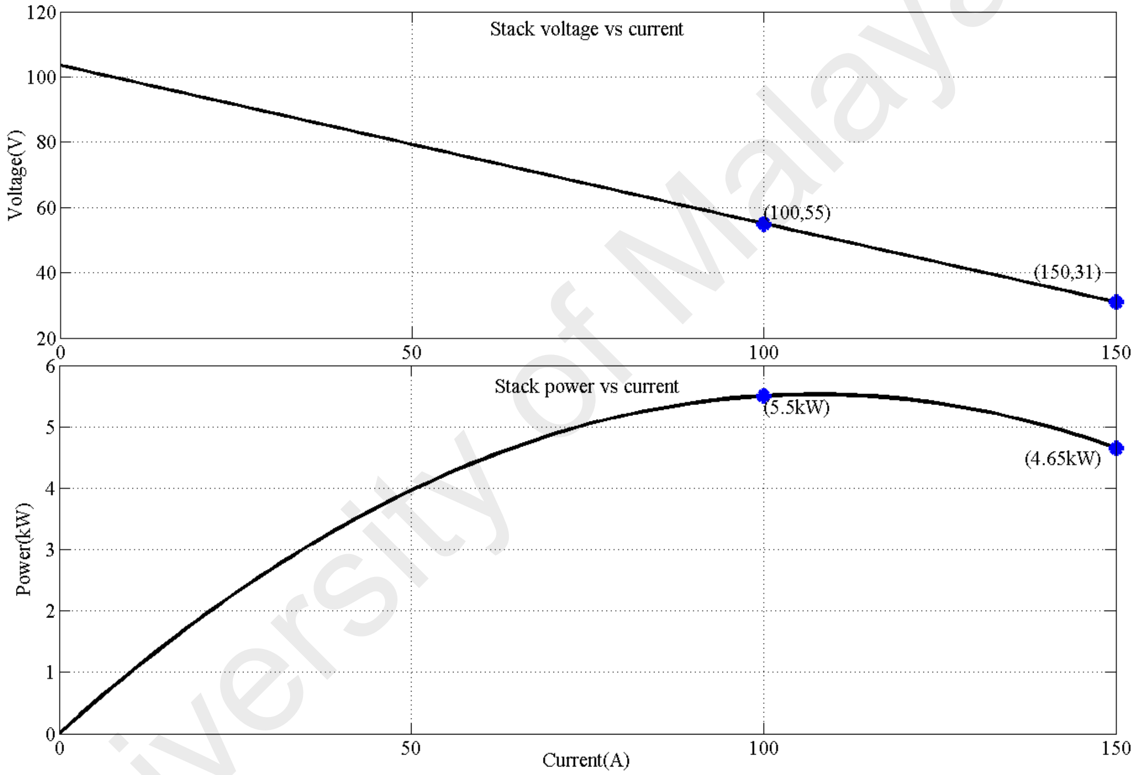

Figure 4.6: Fuel cell voltage and Power vs current.

4.1.4 Large-Scale Photovoltaic Distributed Generator

A PV plant is built on 9 DER combinations connected in parallel. Each combination produces 1.037 MW, so the total capacity at 1000 W/m^2 is 9.3 MW. The PV panels used are SunPower model SPR-305-WHT. The number of series-connected modules per string is 17, whereas the number of parallel strings is 200. The Open Circuit Voltage (V_{OC}), Short Circuit Current (I_{SC}), Maximum Power Voltage (V_{mp}), and Maximum Power

University of Malaya

Current (I_{mp}) are 64.2 V, 5.96 A, 54.7 V, and 5.58 A, respectively. In (Mirhosseini et al., 2012) the inverter used is 1.1 MVA, so in this study each PV source is connected to one inverter. Figure 4.7 shows the curves of the current and the power vs voltage for the PV RES.

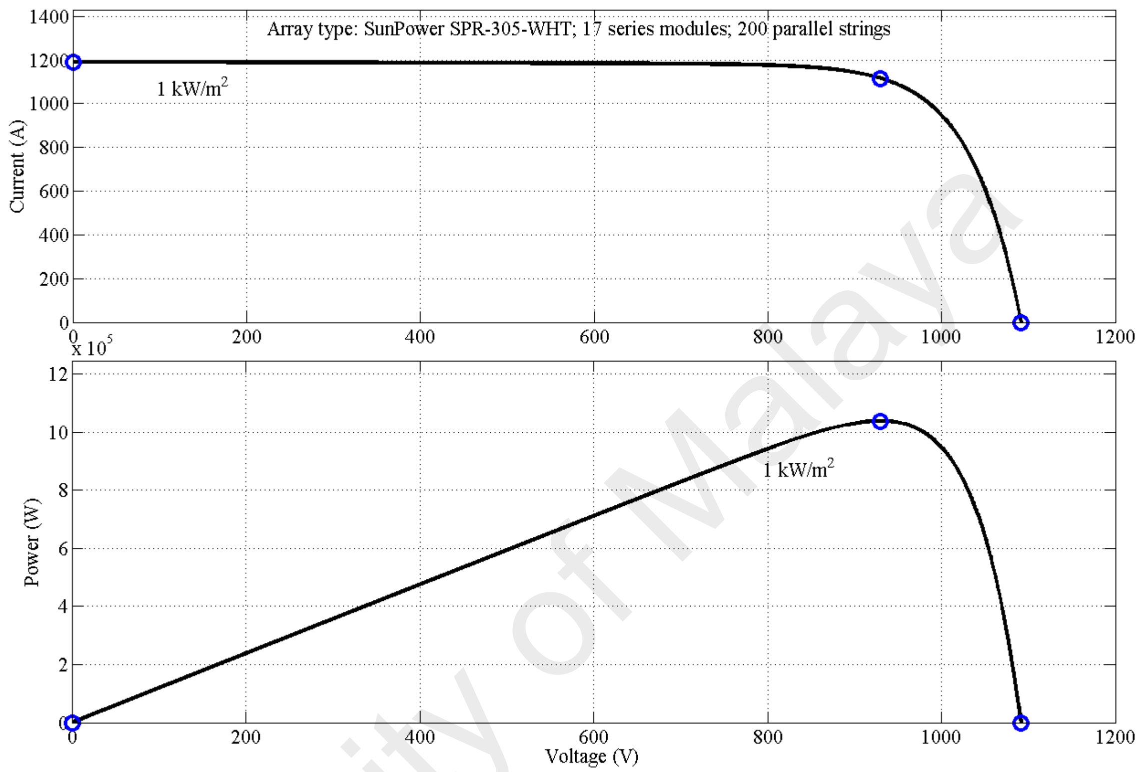

Figure 4.7: Photovoltaic current and power vs voltage for DER.

4.2 Configuration 1

The configuration shown in Figure 4.1 is the configuration 1, connected to 2 MW, 1 MVar load. FC and PV plants described in 4.1.3 and 4.1.4 were used in this system. At the normal operation the solar radiation is 1000 W/m^2. Transformer (T) is step up transformer from 415 at B$_b$ to 11 kV at PCC. In this simulation the impedance (Z$_L$) of the distribution line is resistive which equals 0.1 mΩ. The system runs for 5 s in all cases below.

University of Malaya

4.2.1 Simulation Results and Discussion

The simulated cases are summarized in Table 4.1. Configuration (Cnfg) 1 has 6 cases, the first two cases are ideal conditions so it is not required to be repeated. In configurations 2 and 3 there are 4 cases each. First two cases are without reactive power controller whereas the second two are with reactive power controller. Each case studied different type of disturbances so in cases 1 and 3 radiation variation and load variation have been investigated. Whereas in cases 2 and 4, feeder removal and partial shading have been studied. During these cases the active power, reactive power and the RMS voltage are measured and studied.

Table 4.1: Summary of the cases simulated for each configuration

Cnfgs	Cases	Radiation Variation	Load Variation	Variable Voltage ref	Partial Shading	Feeder Removal	Voltage Regulator
1	1	no	no	no	no	no	no
1	2	yes	yes	no	no	no	no
1	3	yes	yes	yes	no	no	no
1	4	no	no	yes	yes	yes	no
1	5	yes	yes	yes	no	no	yes
1	6	no	no	yes	yes	yes	yes
2	1	yes	yes	yes	no	no	no
2	2	no	no	yes	yes	yes	no
2	3	yes	yes	yes	no	no	yes
2	4	no	no	yes	yes	yes	yes
3	1	yes	yes	yes	no	no	no
3	2	no	no	yes	yes	yes	no
3	3	yes	yes	yes	no	no	yes
3	4	no	no	yes	yes	yes	yes

4.2.2 Case One: Ideal Condition

In this case, the inverter controller fixed the DC V_{ref} at 950 V for the PV source and 1100 V for the FC source. The reactive power dispatched to the PCC was set to zero in the both sources. Series 0.5+j0.5 mΩ impedance was connected to the PV source, and a DC-link capacitor was 24 mF for both DER. The active and reactive power as well as voltage profile of buses; photovoltaic buses (B_{pv}), fuel cell bus (B_{FC}), load bus (B_L), main

University of Malaya

bus (B_b), and PCC were illustrated as follow.

Figure 4.8 illustrates the DC voltage and current for the PV source. The controller stabilized the voltage at 950 V whereas the current was at 1086 A to produce the total of 1.03 MW. Figure 4.9 illustrates the DC voltage and current for the FC source. The controller regulated the voltage at 1100 V whereas the current was at 1000 A to produce the total of 1.1 MW.

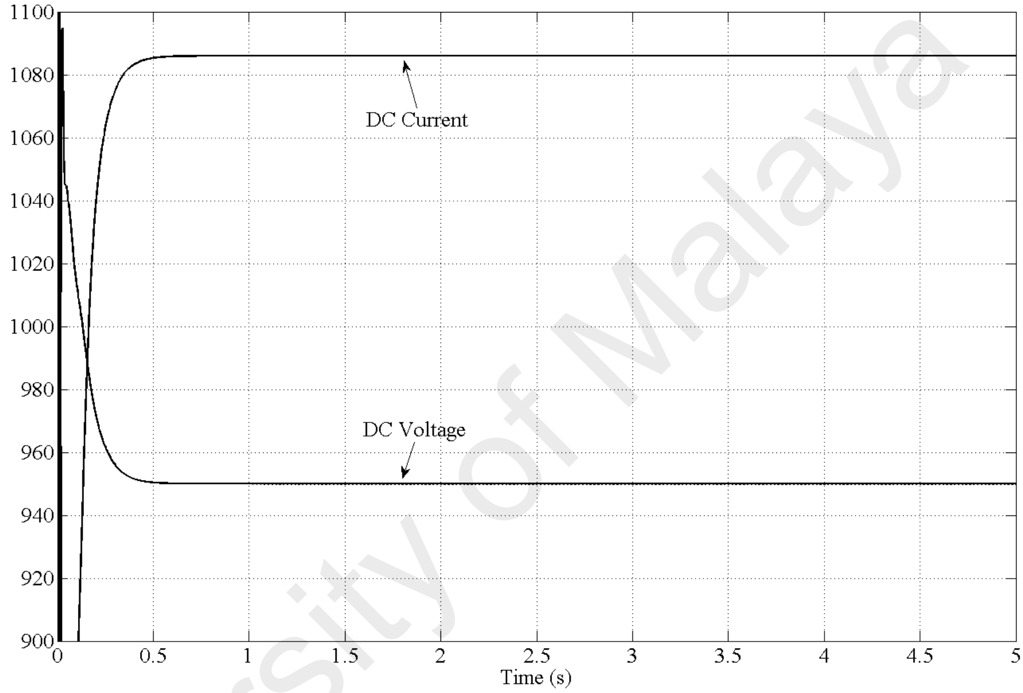

Figure 4.8: Photovoltaic DC voltage and current in configuration 1 case one.

Figure 4.10 shows the active power at all the buses. B_b dispatched 10.33 MW, B_{pv} dispatched 9.28 MW from the 9 inverters, PCC dispatched 8.32 MW to the grid, B_L consumed 1.92 MW and B_{FC} dispatched 1.1 MW. From above values it is shown that total production from PV and FC is 10.33 MW, the load consumed 1.92 MW, and the rest of the active power dispatched to the grid (8.32 MW) with some losses at distribution line. The active power equations are:

$$P_b = P_{PV} + P_{FC} - P_{loss} \tag{4.4}$$

University of Malaya

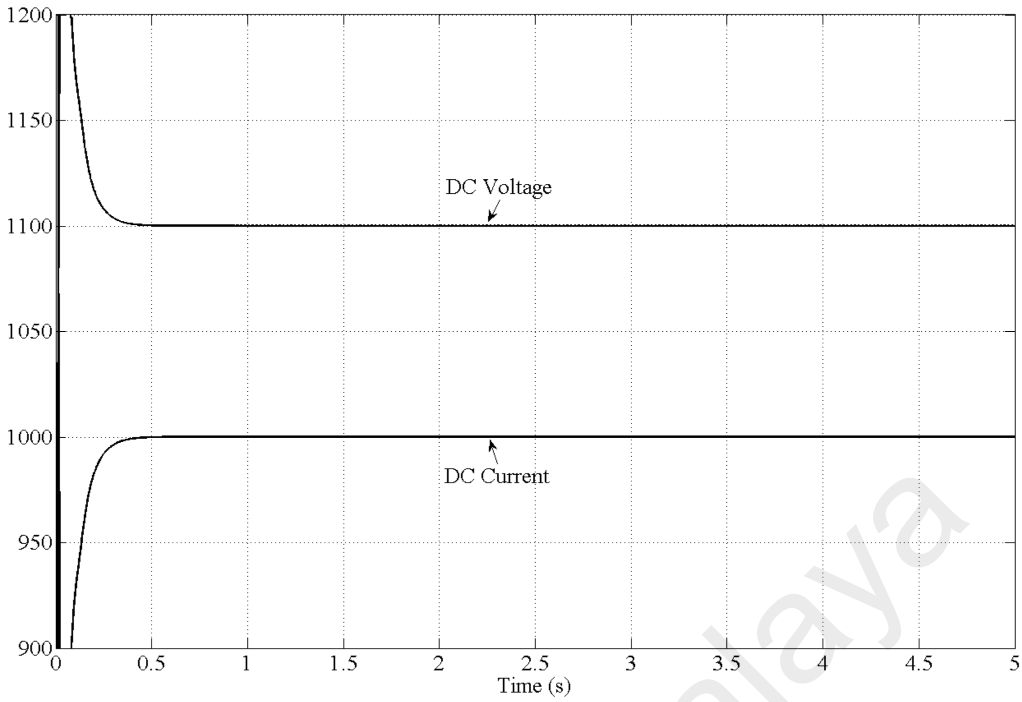

Figure 4.9: Fuel cell DC voltage and current in configuration 1 case one.

$$P_{PCC} = P_b - P_L - P_{loss} \tag{4.5}$$

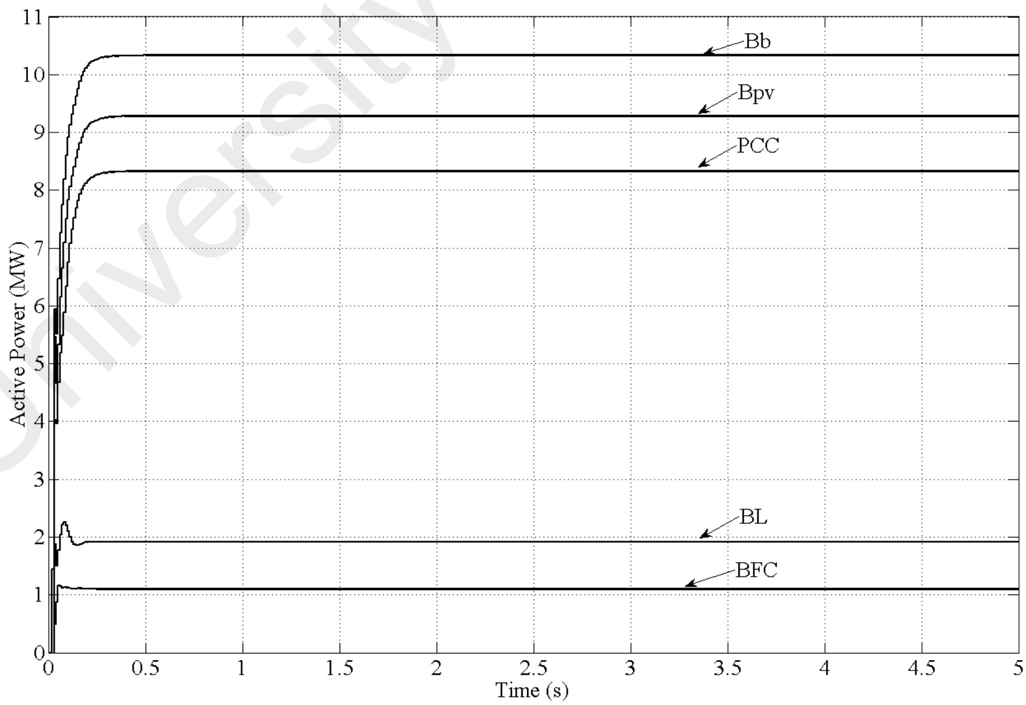

Figure 4.10: Active power of buses B_{pv}, B_{FC}, B_L, B_b, and PCC, in configuration 1 case one.

Figure 4.11 shows the reactive power of buses B_{pv}, B_{FC}, B_L, B_b, and PCC. Buses

University of Malaya

B_{pv}, B_{FC} were set to produce zero reactive power. At B_L the local load was 0.96 MVar where the PCC absorbed 1.18 MVar from the grid to cover the local reactive power. Figure 4.12 shows the voltage of buses PCC, B_{pv}, B_{FC}, B_b, B_L, the RMS values were 6203.3, 236.5, 235.5, 235.3, 234.7 V respectively. B_L had the lower voltage.

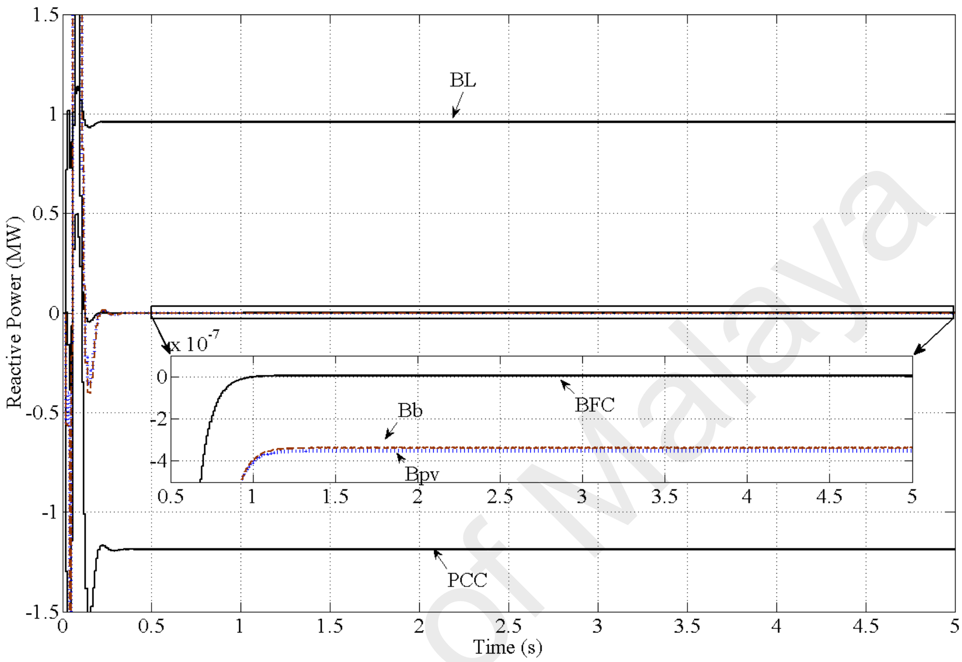

Figure 4.11: Reactive power of buses B_{pv}, B_{FC}, B_L, B_b, and PCC, configuration 1 case one.

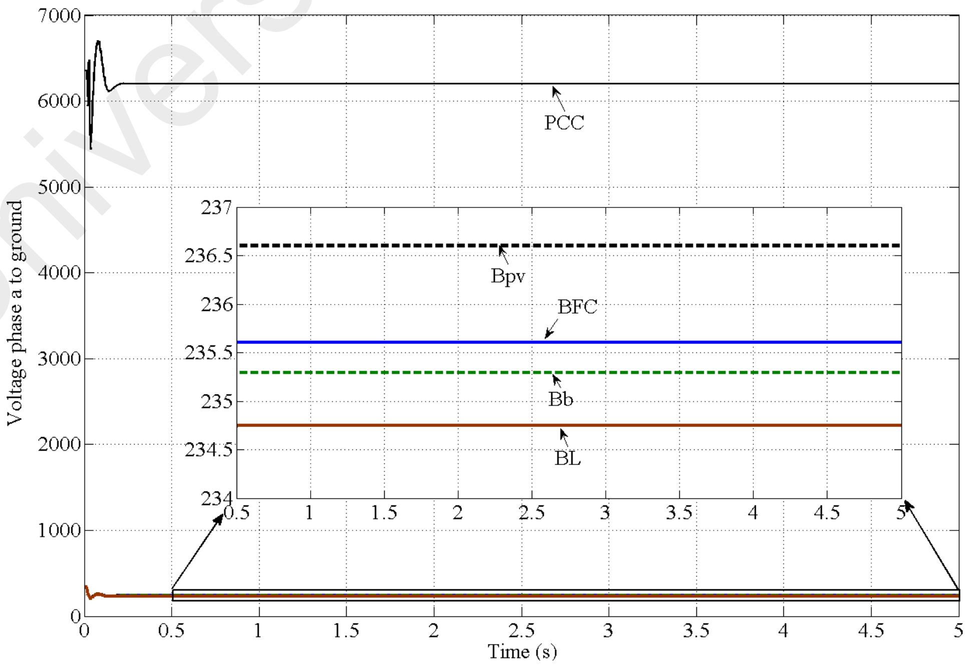

Figure 4.12: Phase-A to ground voltage RMS of buses B_{pv}, B_{FC}, B_L, B_b, and PCC, in configuration 1 case one.

University of Malaya

4.2.3 Case Two: Variation in Solar Radiation and Load

In this case, the reference DC-voltage and reference reactive power were same as in case one. The solar radiation dropped to 700 W/m^2 between 2 s and 4 s, then increased to 900 W/m^2 as shown in table 4.2. A 1 MW active power and 0.5 reactive MVar was connected at 2.5 s then removed from the load at 3.5 s to investigate load changing effect. The active and reactive power as well as voltage profile of buses B$_{pv}$, B$_{FC}$, B$_L$, B$_b$, and PCC are illustrated below.

Table 4.2: The solar radiation on the PV panel for different configuration cases.

Solar radiation (W/m)^2	Time (s)	
	From	To
1000	0	2
700	2	4
900	4	5

Figure 4.13 illustrates the DC voltage and current for the PV source during solar radiation variation and load disturbance. The controller regulated the voltage at 950 V. Although the current changed dramatically with solar radiation variation, load disturbances doesn't affect the DC source current. Figure 4.14 illustrates the DC voltage and current for the FC source. The controller regulated the voltage at 1100 V whereas the current was stable at 1000 A regardless the solar radiation and local load. That owe to the reactive power controller was disabled.

Figure 4.15 shows the active power depicted from the buses. In B$_b$ and B$_{pv}$ the power decreased when the solar radiation dropped, whereas they did not affect during load disturbance. B$_{FC}$ was stable at 1.1 MW, B$_L$ consumed more active power during the load connection. The power dispatched to grid at PCC dropped during solar radiation drop and during load connection, since some of the power absorbed at the load instead of export to the grid.

Figure 4.16 shows the reactive power of buses B$_{pv}$, B$_{FC}$, B$_L$, B$_b$, and PCC. The

University of Malaya

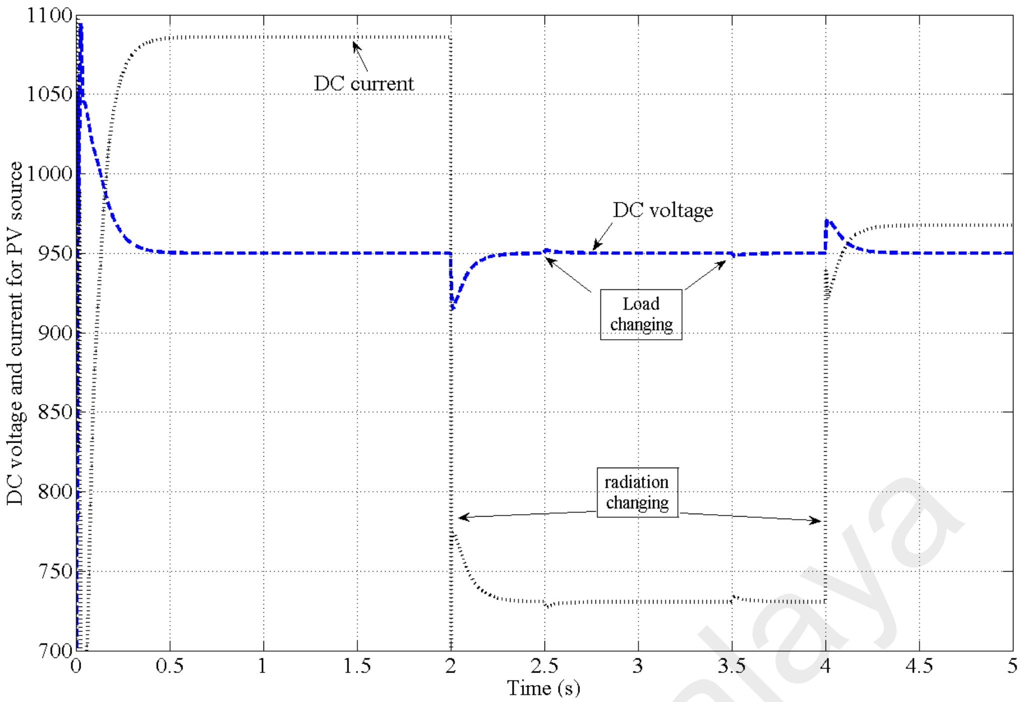

Figure 4.13: Photovoltaic DC voltage and current, in configuration 1 case two.

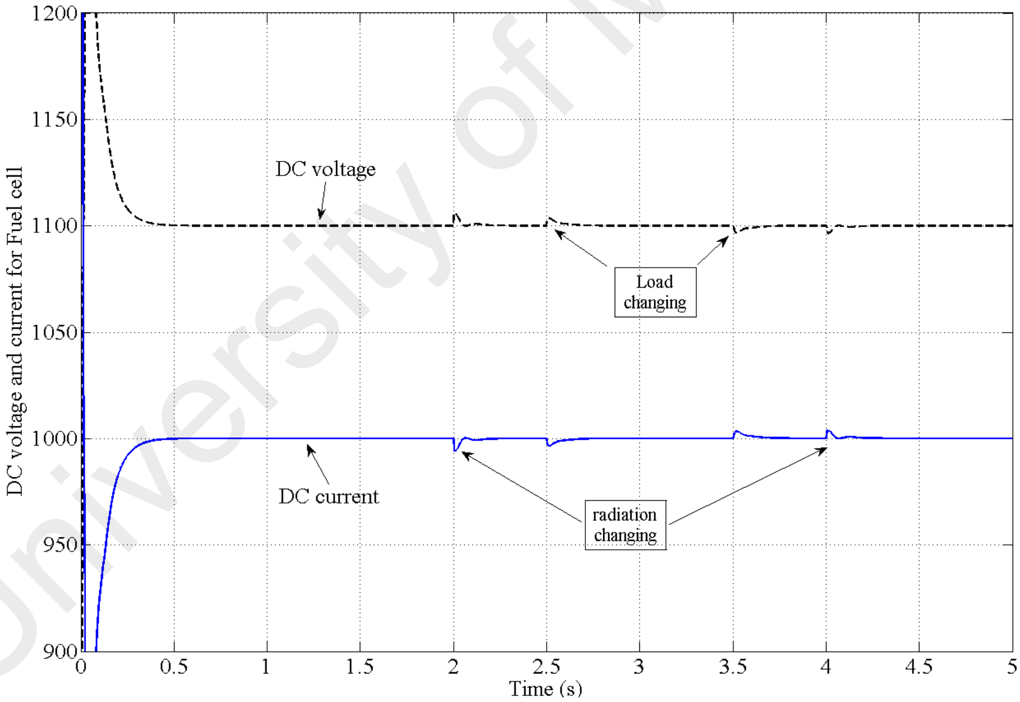

Figure 4.14: Fuel cell DC voltage and current, in configuration 1 case two.

produced reactive power was same as in Figure 4.11, although the solar radiation variation affected PCC and B_L, the main changing in reactive power occurred due to load disturbance.

Figure 4.17 shows the RMS voltages of buses PCC, B_{pv}, B_{FC}, B_b, B_L. Because the

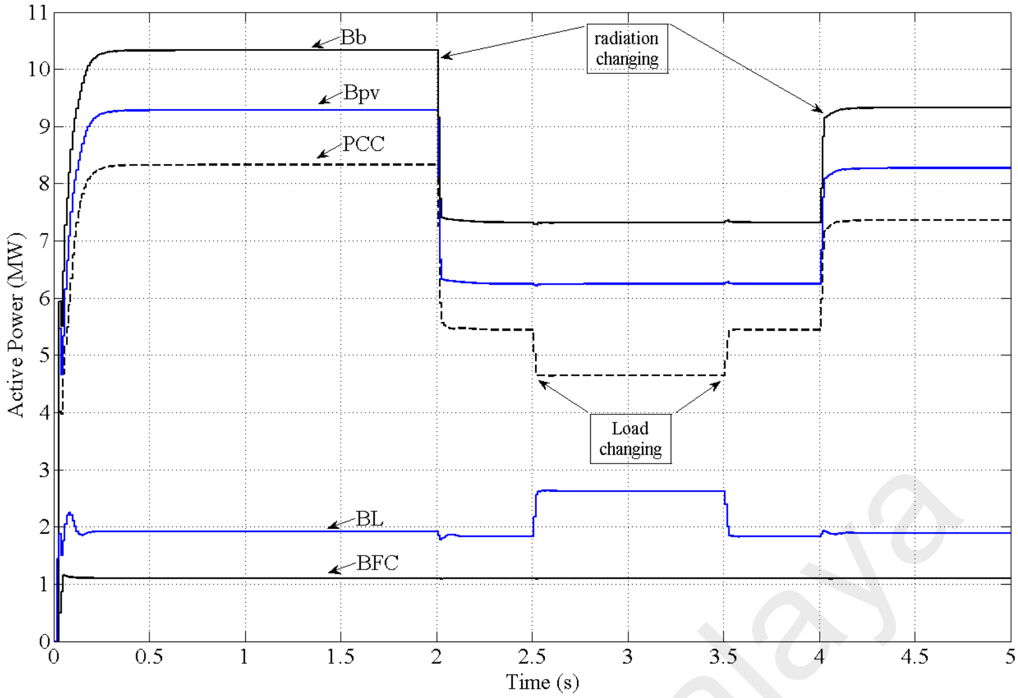

Figure 4.15: Active power of buses B_{pv}, B_{FC}, B_L, B_b, and PCC, in configuration 1 case two.

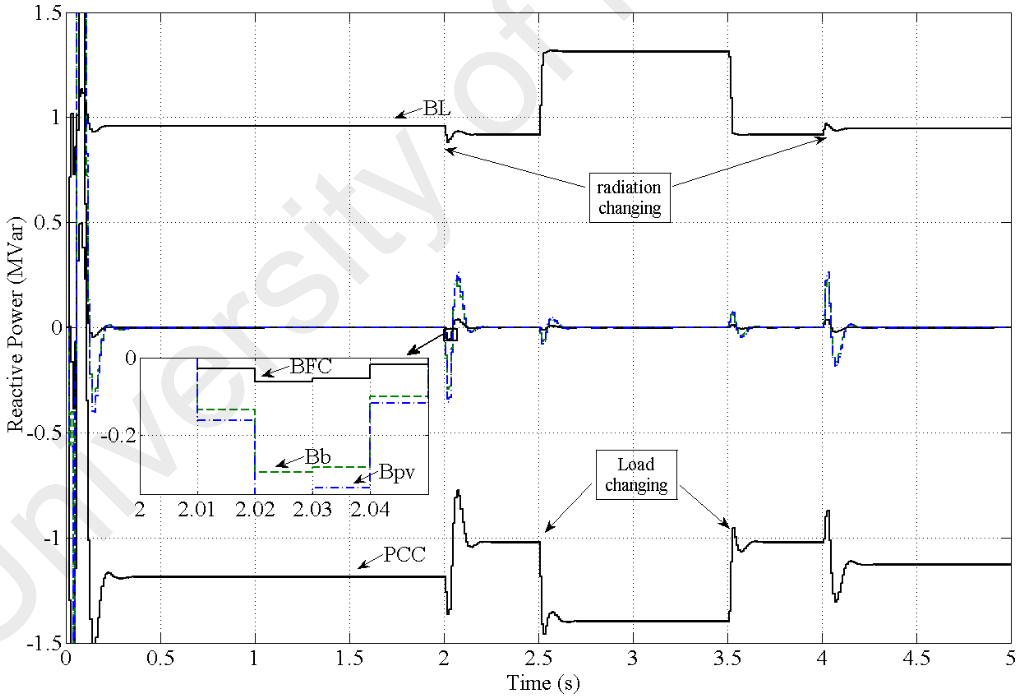

Figure 4.16: Reactive power of buses B_{pv}, B_{FC}, B_L, B_b, and PCC, in configuration 1 case two.

voltage was uncontrollable in this case, the buses voltages were following the grid voltage. When the sun radiation dropped, the voltage dropped as well, owing to the increase in the active power was required to transfer via transmission line to supply the load at the grid

University of Malaya

side. Thus more power losses at transmission line. The same occurred when the load increased.

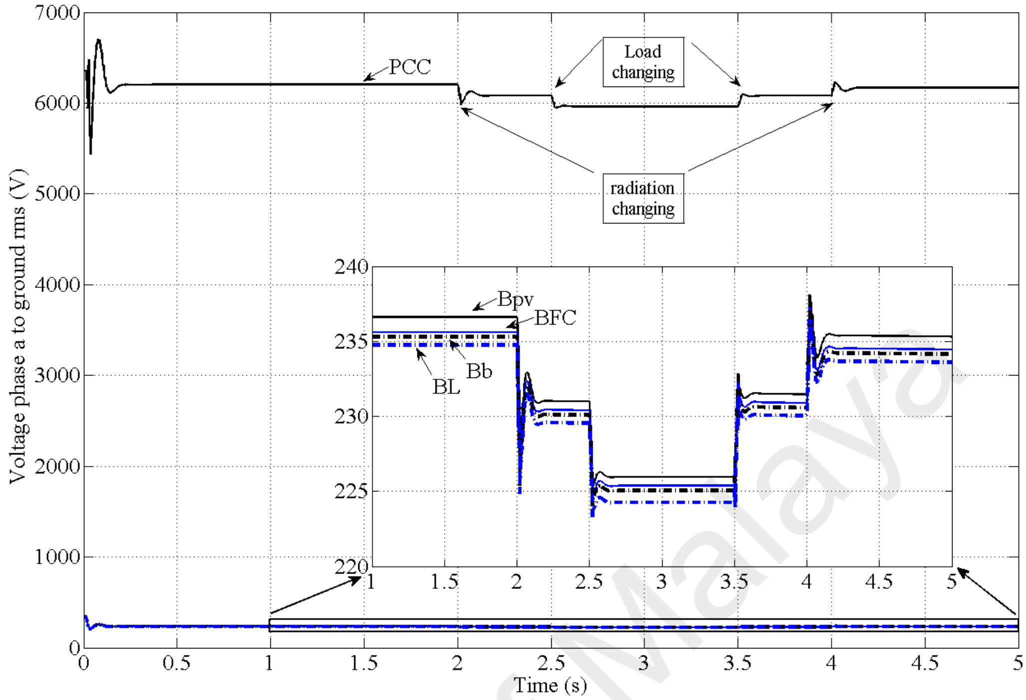

Figure 4.17: Phase-A to ground voltage RMS of buses B_{pv}, B_{FC}, B_L, B_b, and PCC, in configuration 1 case two.

University of Malaya

4.2.4 Case Three: Variation in Solar Radiation and Load With Variable Voltage Ref

In this case, the outer voltage control loop regulates the DC-link voltage to extract maximum power from the PV as Figure 3.7 shows. All other parameters were as in case two. Figure 4.18 shows the difference between dispatched active power with and without variable DC V_{ref}. In this case, the maximum power from the PV was extracted and the power was higher during all radiation levels. Due to increase in PV active power, power increased in B_b and PCC as well.

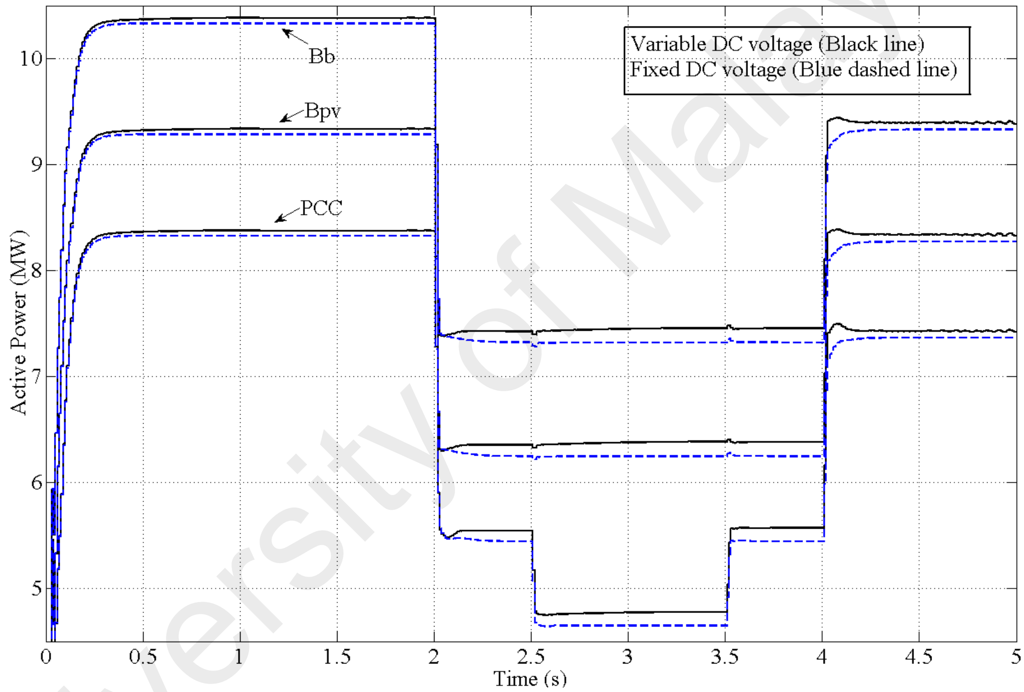

Figure 4.18: Active power (MW) at variable and fixed DC V_{ref}, in configuration 1 case three.

University of Malaya

Figure 4.19 compares voltage and current produced from PV source at variable and fixed DC V_{ref}, it was shown that when variable V_{ref} enabled, the current was dispatched to the grid increased.

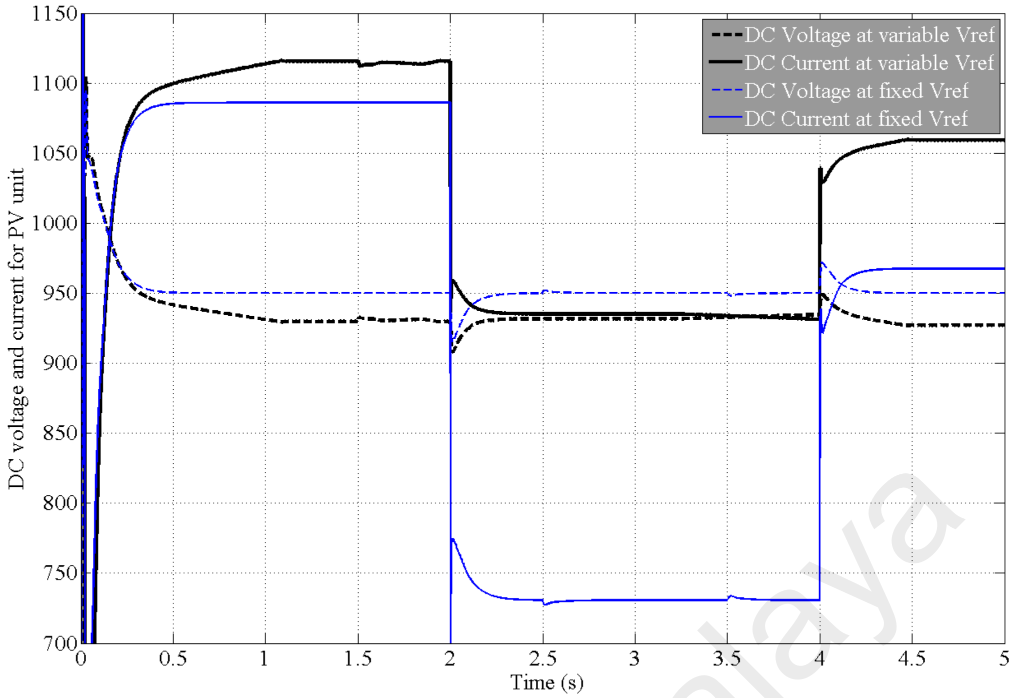

Figure 4.19: DC voltage and current for PV unit with and without variable DC V_{ref}, configuration 1 case three.

4.2.5 Case Four: Partial Shading and Feeder Removal

In this case, the variable V_{ref} enabled for PV controller as in case three. Other parameters were the same as in the case two. Partial shading occurred in one of the PV sources, when 100 strings out of 200 exposed to solar radiation decline from 1000 W/m^2 to 700 W/m^2 at 2 s, then increased to 900 W/m^2 at 4 s. Then FC feeder disconnected at 1.5 s. Figure 4.20 illustrates the DC voltage and current for the PV source during partial shading and FC feeder removal. The controller regulated the voltage at a desired value that extracted maximum power. Although the current changed dramatically with solar radiation variation, feeder removal did not affect the DC current or voltage.

Figure 4.21 illustrates the DC voltage and current for the FC source when the FC feeder removed. The controller regulated the voltage at 1100 V and the current was at 1000 A. When FC feeder removed the current dropped to zero.

Figure 4.22 shows the active power at the buses. At 1.5 s the feeder B_{FC} was removed, so the power dropped to zero. After the feeder removed the active power at B_b

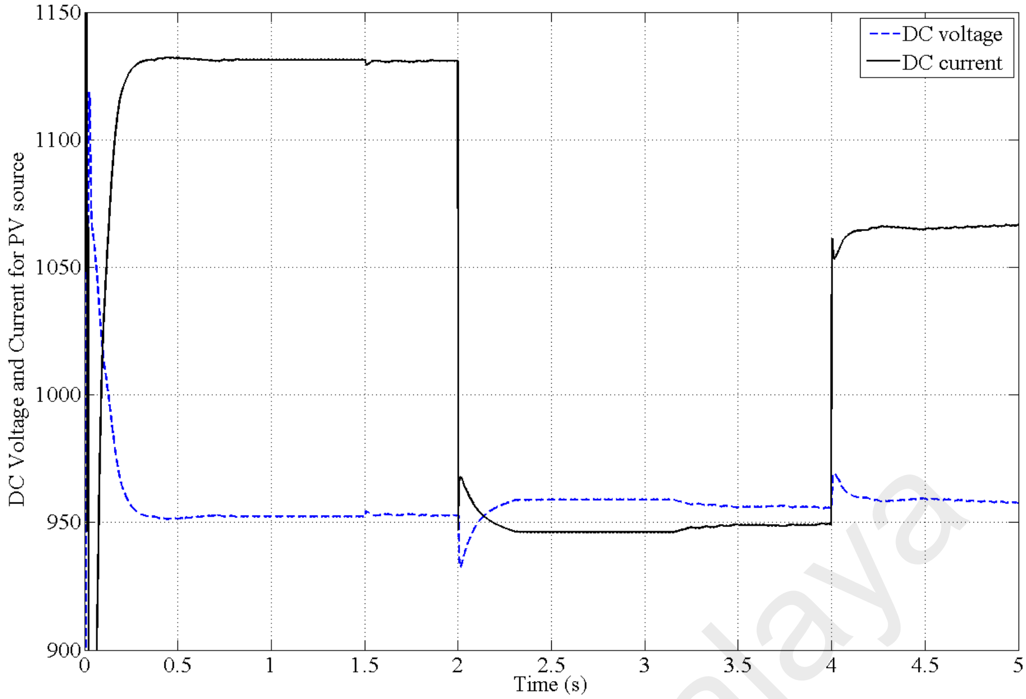

Figure 4.20: DC voltage and current at the PV unit with the partial shading, in configuration 1 case four.

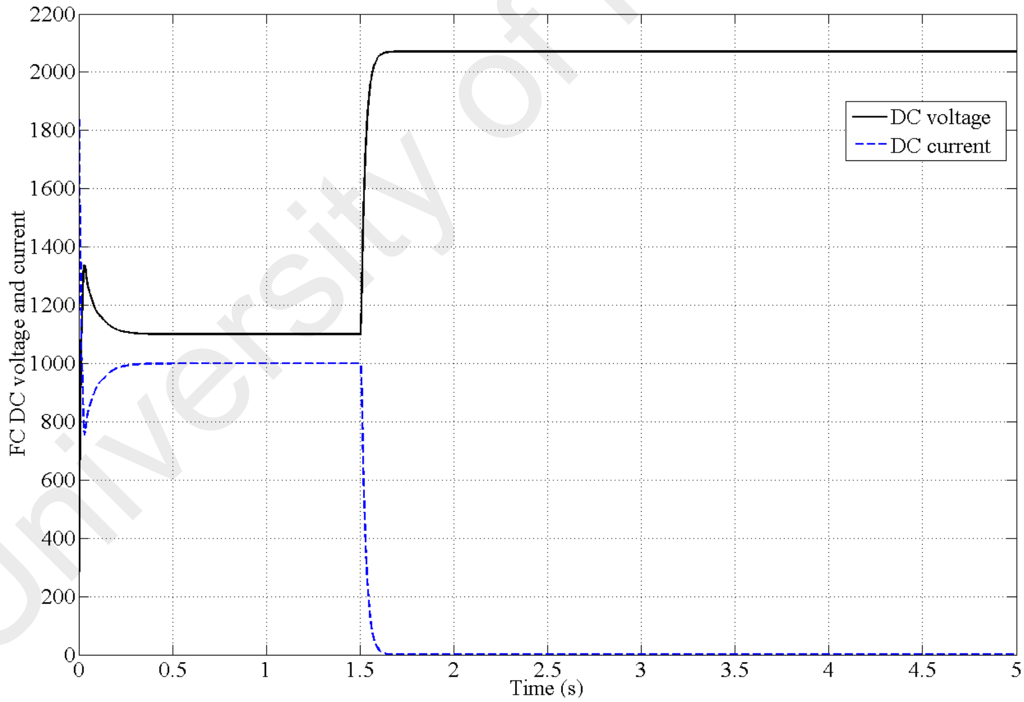

Figure 4.21: Fuel cell DC voltage and current with feeder removal, in configuration 1 case four.

and PCC decreased by 1.1 MW. As the partial shading occurred only in one of the PV sources, the drop in the active power due to radiation decline was insignificant as shown at 2 s.

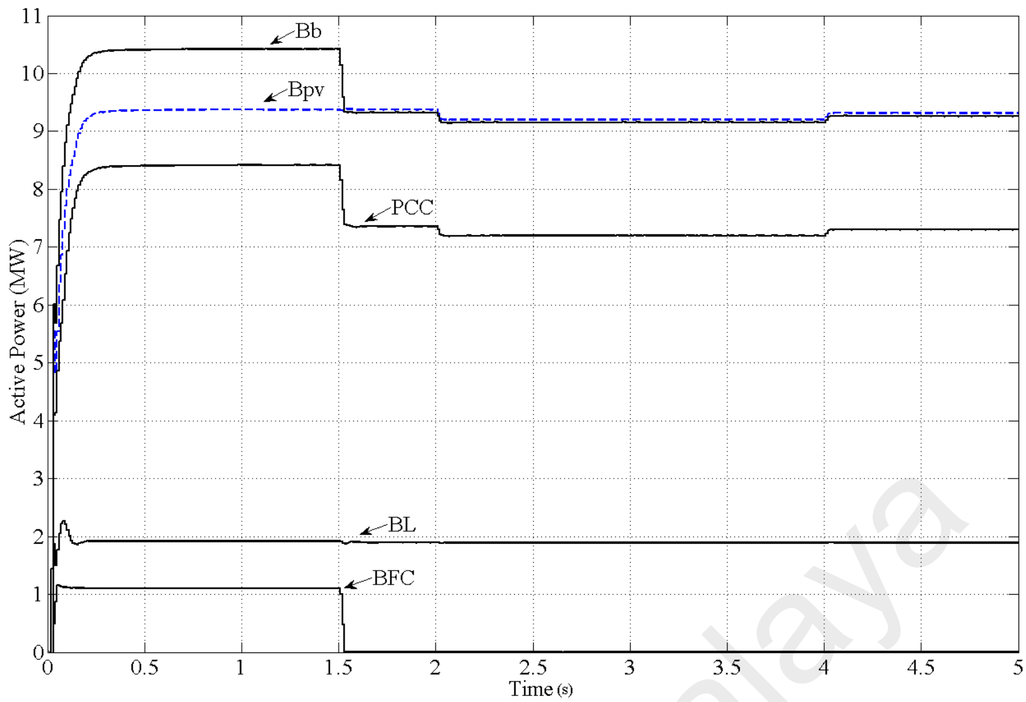

Figure 4.22: Active power with partial shading and feeder losing, in configuration 1 case four.

Figure 4.23 shows the reactive power at all buses. At B_{pv}, B_{FC}, B_L, B_b, and PCC, although the solar radiation variation affected the buses PCC and B_L, the significant change in the reactive power occurred due to feeder removal.

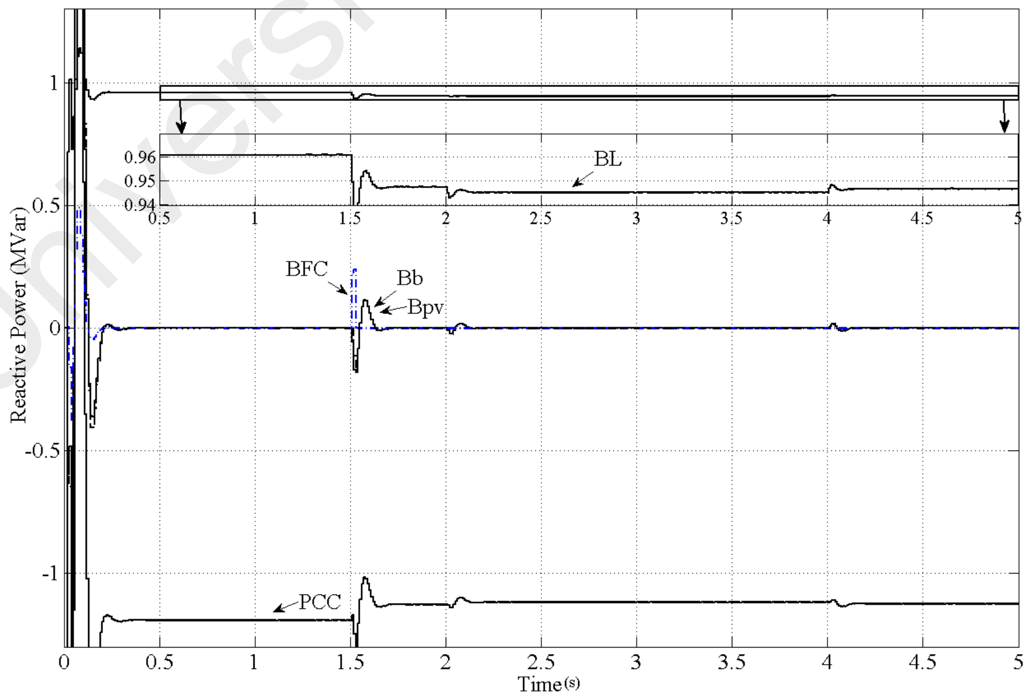

Figure 4.23: Reactive power of buses with partial shading and feeder FC removal, in configuration 1 case four.

University of Malaya

Figure 4.24 shows the voltage of buses PCC, B_{pv}, B_{FC}, B_b, B_L. When FC feeder removed at 1.5 s the voltage dropped at all buses, due to voltage drop at PCC. This occurred as a result of transferring more power via transmission line which causing more power losses at transmission line at the grid.

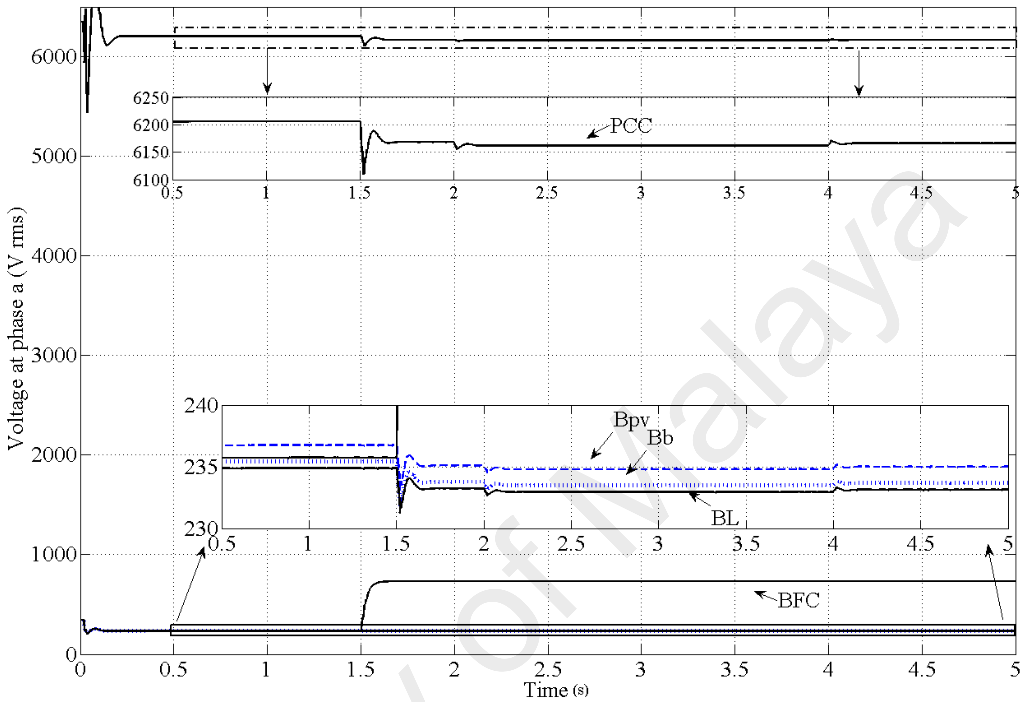

Figure 4.24: Voltage at Phase-A (V rms) at all buses with FC feeder removal and partial shading in PV source, in configuration 1 case four.

University of Malaya

4.3 Configuration 1 With Reactive Power Control

In this section, all the sources and load connect to B_b. The line distance (Z_L), represented by the π model is 10 m. Active power, reactive power, and RMS voltage at photovoltaic bus (B_{pv1}), B_{FC}, B_L, B_b, and PCC are presented in the next sections.

4.3.1 Case Five: Variable Radiation and Variable Load with Q controlling

The inverter controller fixed the DC V_{ref} at 930 V for the PV source and 1100 V for the FC source. The reactive power dispatched to the PCC was set to zero in the PV whereas the FC dispatches the desired amount to regulate the voltage. The solar radiation in this case is illustrated in Table 4.2. The load's initial value was 2 MW. At 2.5 s, a 0.4 MW and 0.2 MVar load was connected then removed at 3.5 s. The DC-link capacitor is 24 mF.

In configuration 1 case five, the active power (MW) of buses B_{pv1}, B_{FC}, B_L, B_b, and PCC are as shown in Figure 4.25. The results are summarized in Table 4.3 in (MW); B_b had the maximum amount of active power as it forms from the power produced at PV and FC. The power dispatched to the PCC decreased when the radiation reduced and when the local load increased. Power consumption by the local load was 2 MW initially before a 0.4 MW load was connected at 2.5 s then removed at 3.5 s. B_{FC} dispatched 1.1 MW regularly. B_{pv1} was initially 1 MW before it dropped when the solar radiation dropped at 2 s. The active power produced by any AC system actually represents the average power, as Equation 4.6 from (Saadat, 2002) shows:

$$p_R(t) = |V||I|cos\theta + |V||I|cos\theta cos2(wt + \theta_v) \tag{4.6}$$

The average active power is thus as in Equation 4.7

$$P = |V||I|cos\theta \tag{4.7}$$

University of Malaya

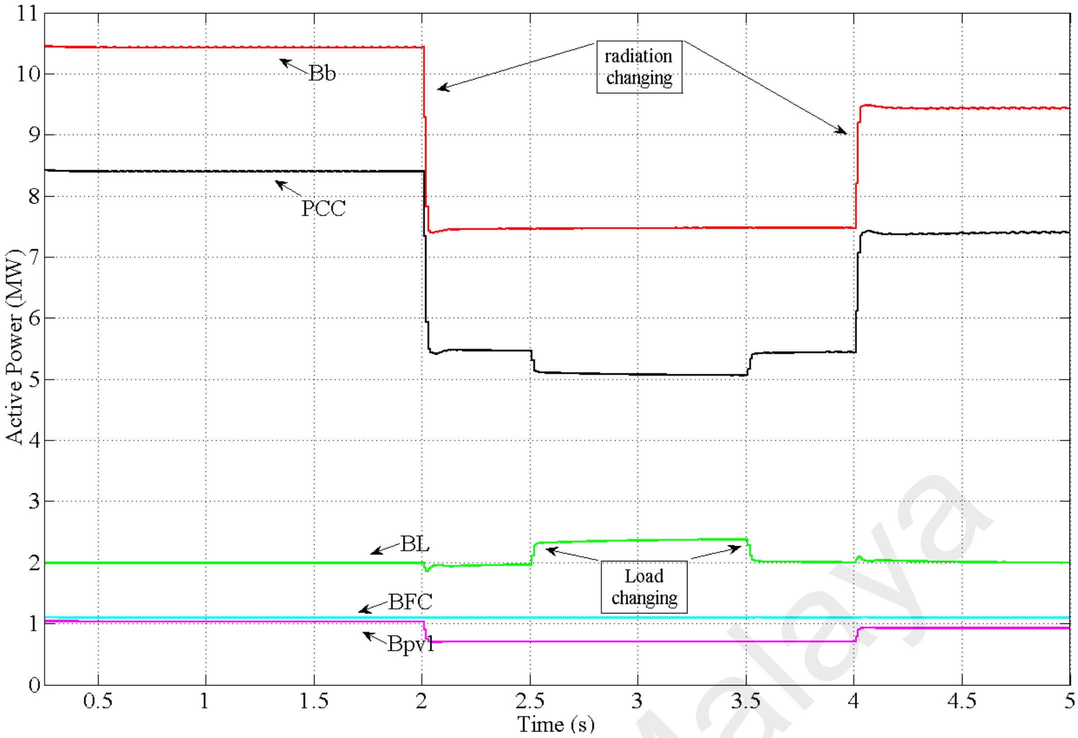

Figure 4.25: Active power of buses B_{pv1}, B_{FC}, B_L, B_b, and PCC, in configuration 1 case five.

Figure 4.26 shows the reactive power of buses B_{pv1}, B_{FC}, B_L, B_b, and PCC. B_{pv1} produced zero reactive power following the inner controller preset value. B_L consumed 0.2 MVar between 2.5 s and 3.5 s when the reactive load connected. A significant amount of reactive power was dispatched to PCC. The high amount of reactive power was required to be dispatched at B_{FC} to regulate the voltage at B_L. The values of the reactive power are as summarized in Table 4.3 in MVar. The reactive power produced by any AC system actually shows the amplitude of the pulsating power, as given by Equation 4.8 (Saadat, 2002):

$$p_X(t) = |V||I|sin\theta sin2(wt + \theta_v) \tag{4.8}$$

The measured reactive power is as in Equation 4.9

$$Q = |V||I|sin\theta \tag{4.9}$$

University of Malaya

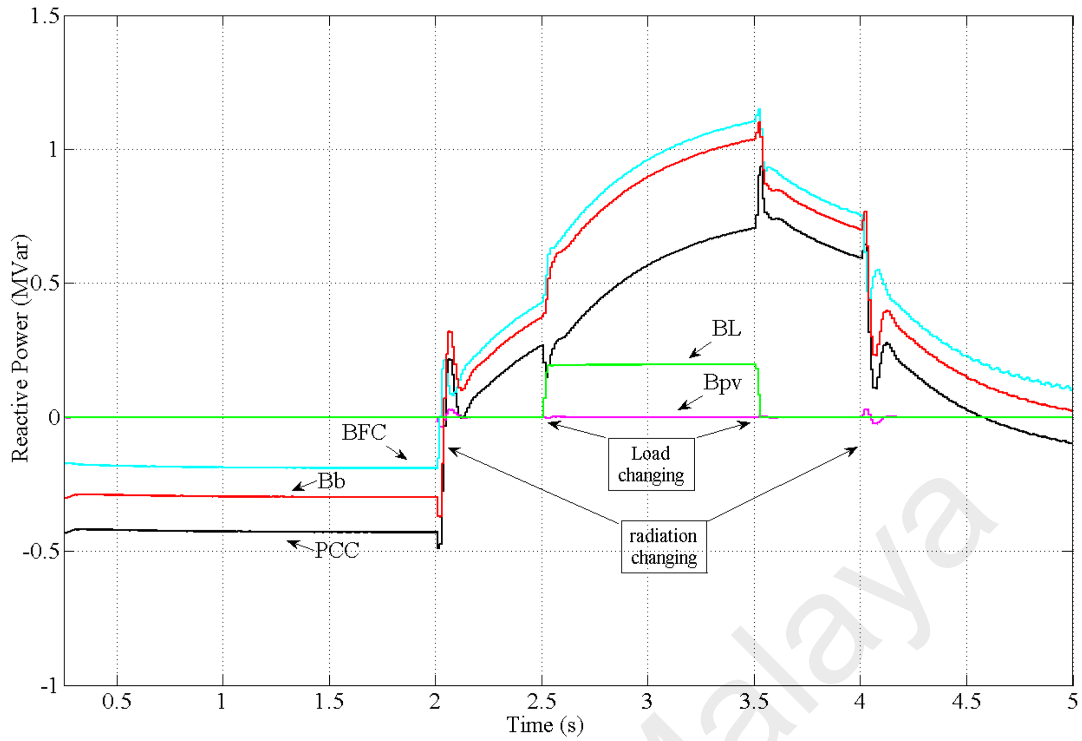

Figure 4.26: Reactive power of buses B_{pv1}, B_{FC}, B_L, B_b, and PCC, in configuration 1 case five.

Figure 4.27 shows the phase-A RMS voltage of buses B_{pv1}, B_{FC}, B_L, B_b, and PCC in configuration 1 case five. At initial condition, all the voltages had similar values. Upon radiation variation and load disturbance, the voltage difference between B_{FC} and B_L increases. Voltage at B_{FC} was regulated to dispatch the desired reactive power. Voltage at B_L was regulated at 239 V, but the interval time between the disturbances had to be longer to allow the voltage to reach steady state. Table 4.3 summarizes the voltage values in (V).

4.3.2 Case Six: Feeder Removal and Partial Shading

In this case, partial shading occurred at one of the PV sources, so the sun radiation changed as shown in Table 4.2. When the FC source was removed at 1.5 s the active and reactive power dropped to zero. Figure 4.28 depicts the active power of buses B_{pv1}, B_{FC}, B_L, B_b, and PCC, in configuration 1 case six.

A significant drop in the power occurred at 1.5 s at B_{FC}, PCC, and B_b owing to feeder removal. A minor drop occurred at 2 s and 4 s upon partial shading of one of the

University of Malaya

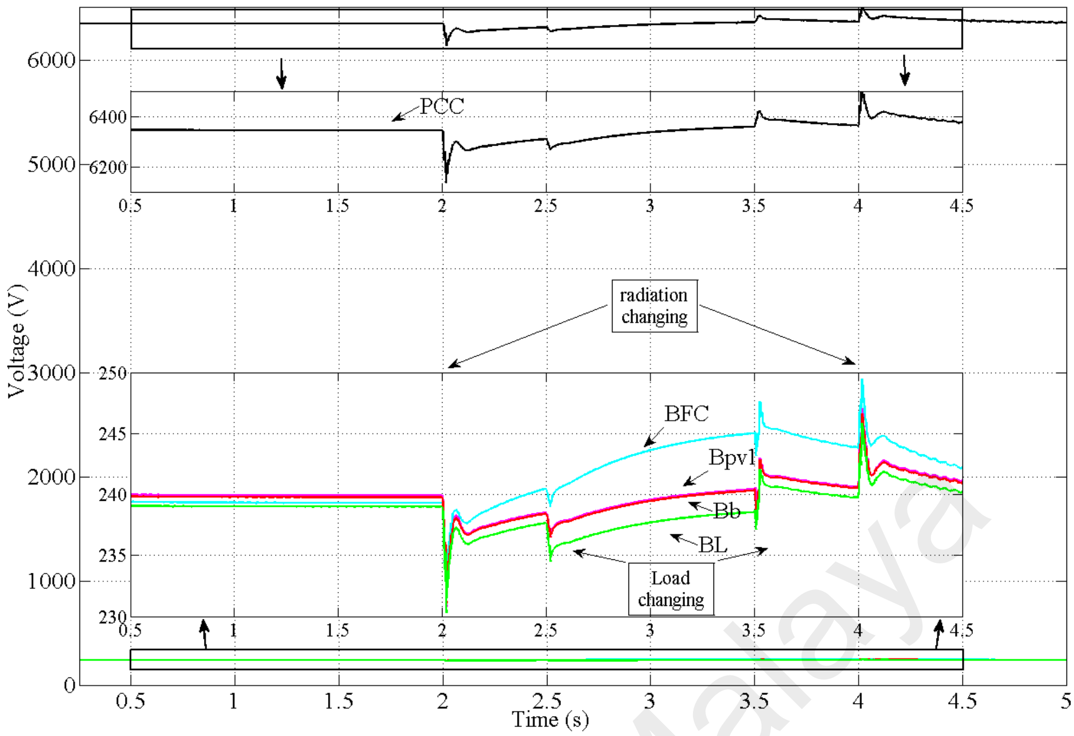

Figure 4.27: Phase-A RMS voltage of buses B_{pv1}, B_{FC}, B_L, B_b, and PCC, in configuration 1 case five.

Table 4.3: Summary of the results of configuration 1 case five, (R stands for Radiation)

Item	Initial Value	R Drop	Load Rise	Load Drop	R Rise
P_{pcc}	8.4	5.465	5.066	5.446	7.41
P_{Bpv1}	1.037	0.707	0.709	0.709	0.926
P_{BFC}	1.1	1.1	1.1	1.1	1.1
P_{Bb}	10.43	7.465	7.477	7.48	9.44
P_{BL}	1.99	1.97	2.379	2	1.995
Q_{pcc}	-0.429	0.27	0.706	0.59	-0.1
Q_{Bpv1}	0	0	0	0	0
Q_{BFC}	-0.19	0.428	1.105	0.75	0.1
Q_{Bb}	-0.2985	0.375	1.037	0.7	0.025
Q_{BL}	0	0	0.198	0	0
V_{pcc}	6345	6312	6360	6365	6355
V_{Bpv1}	239.9	238.5	240.4	240.6	240.2
V_{BFC}	239.3	240.5	245	243.8	240.8
V_{Bb}	239.7	238.4	240.3	240.5	240.1
V_{BL}	239	237.7	238.6	239.7	239.3

PV sources. Table 4.4 summarizes the active power values at all buses.

Figure 4.29 shows the reactive power of buses B_{pv1}, B_{FC}, B_L, B_b, and PCC in configuration 1 case six. B_{pv1} produced zero reactive power following the inner controller preset value. B_L did not consume any reactive power. Before the feeder removal at 1.5

University of Malaya

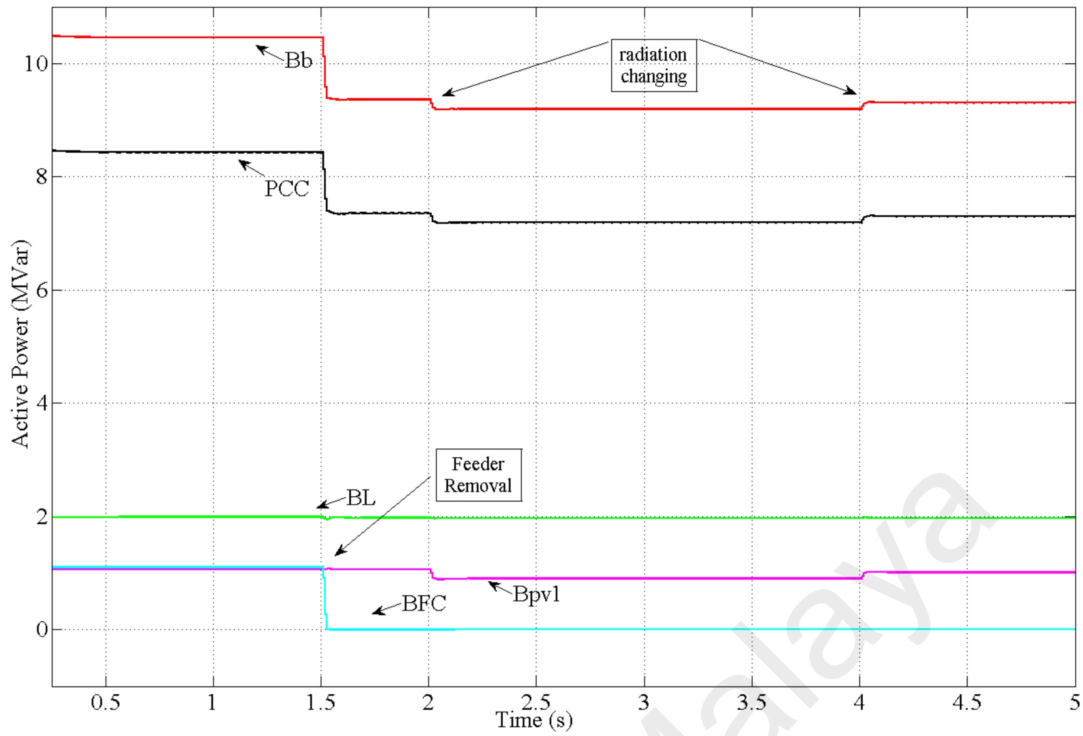

Figure 4.28: Active power of buses B_{pv1}, B_{FC}, B_L, B_b, and PCC, in configuration 1 case six.

s, B_{FC} consumed reactive power to regulate the voltage at B_L. Upon B_{FC} removal, the reactive power at B_b dropped to -0.167 MVar, whereas some reactive power continued being imported from the PCC to supply reactive power consumed at the distribution lines and transformer. Table 4.4 summarizes the reactive power values of all the buses.

Figure 4.30 shows the phase-A RMS voltage of buses B_{pv1}, B_{FC}, B_L, B_b, and PCC in configuration 1 case six. At initial condition, all the voltages had similar values close to 239 V, then when B_{FC} was removed the voltage regulator disconnected. The disturbances were minor at B_{pv1} owing to partial shading, so the voltage at B_{pv1}, B_L, B_b remained stable at 239 V. A drop occurred in the PCC voltage owing to partial shading between 2 s and 4 s. Table 4.4 summarizes the voltage values of all the buses.

University of Malaya

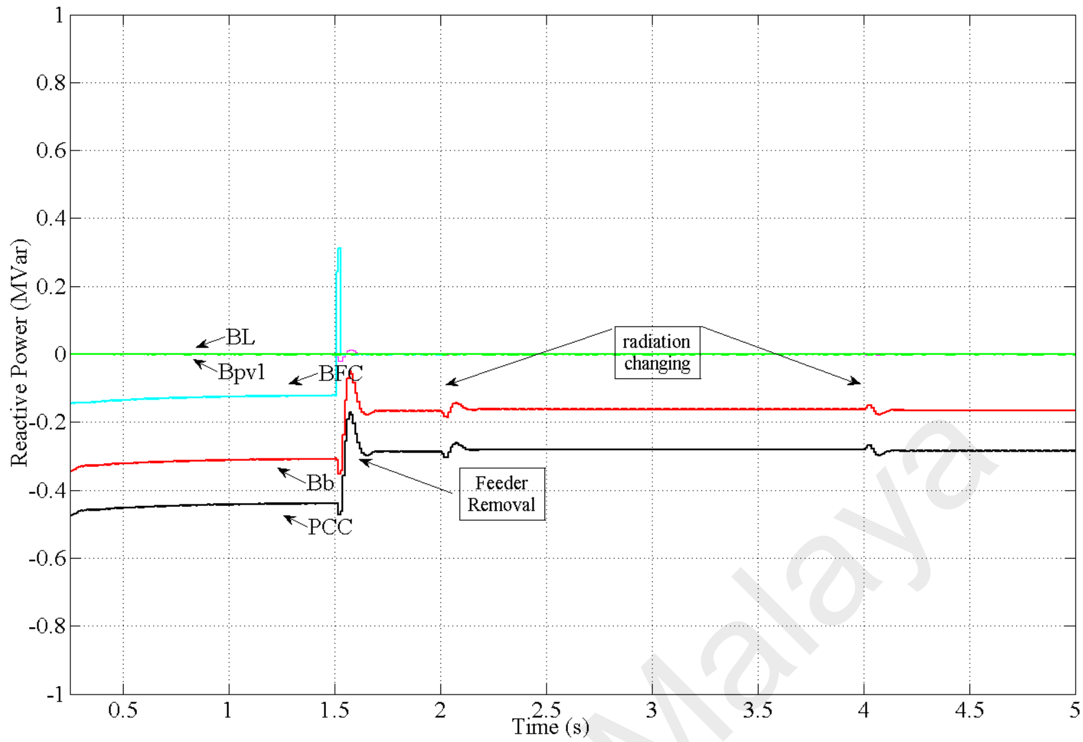

Figure 4.29: Reactive power of buses B_{pv1}, B_{FC}, B_L, B_b, and PCC, in configuration 1 case six.

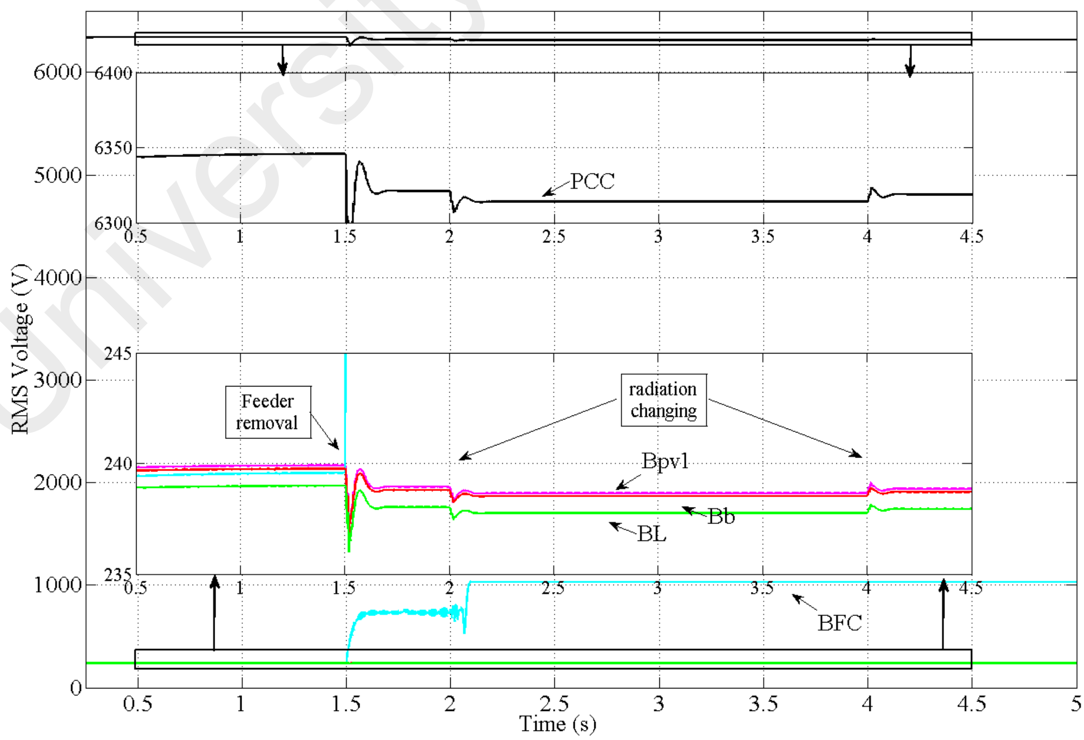

Figure 4.30: Phase-A voltage RMS of buses B_{pv1}, B_{FC}, B_L, B_b, and PCC, in configuration 1 case six.

University of Malaya

Table 4.4: Summary of the results of configuration 1 case six, (R stands for Radiation)

Item	Initial Value	Feeder Removal	Partial R Drop	Partial R Rise
P_{pcc}	8.431	7.353	7.193	7.3
P_{Bpv}	1.067	1.067	0.902	1.012
P_{BFC}	1.1	0	0	0
P_{Bb}	10.46	9.362	9.197	9.307
P_{BL}	1.99	1.974	1.969	1.972
Q_{pcc}	-0.438	-0.287	-0.28	-0.285
Q_{Bpv}	0	0	0	0
Q_{BFC}	-0.1215	0	0	0
Q_{Bb}	-0.308	-0.167	-0.162	-0.165
Q_{BL}	0	0	0	0
V_{pcc}	6346	6321	6314	6318.8
V_{Bpv}	239.92	238.95	238.65	238.85
V_{BFC}	239.55	1031	1031	1031
V_{Bb}	239.78	238.8	238.52	239.7
V_{BL}	239	238	237.78	237.94

4.4 Configuration 2

Figure 4.31 shows the configuration 2, connected to 2 MW, 1 MVar load. At the normal operation the solar radiation was 1000 W/m^2. FC and PV sources as described in 4.1.3 and 4.1.4 were used in this configuration. Transformer (T) is step up transformer from 415 V to 11 kV (RMS line to line voltage). In this simulation the impedance (Z_L) of the distribution line is resistive which equals 0.1 mΩ. The system ran for 5 s in all cases below.

4.4.1 Case One: Variation in Solar radiation and Load With Variable Voltage Reference

The solar radiation and the load variation were as in case two configuration 1. Figure 4.32 illustrates the DC voltage and DC current for the PV source during solar radiation variation and load disturbance. The controller changed the reference DC-link voltage to a value that extracted maximum power from PV.

Figure 4.33 shows the FC source DC voltage and current. It is clear that the controller stabilize the voltage at 1100 V where the current is at 1000 A regardless the solar radiation

University of Malaya

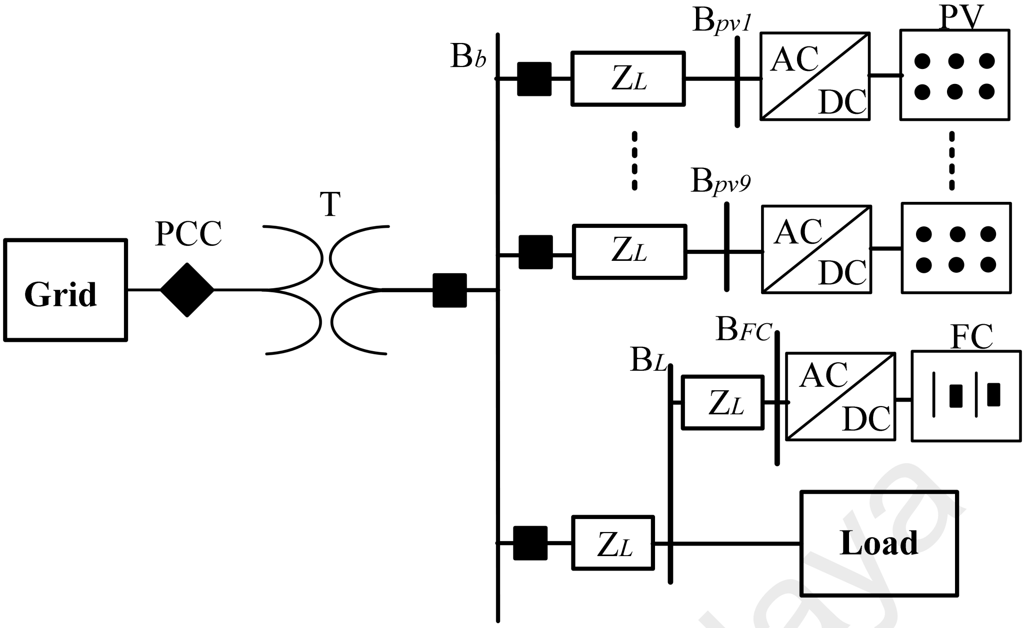

Figure 4.31: Configuration 2.

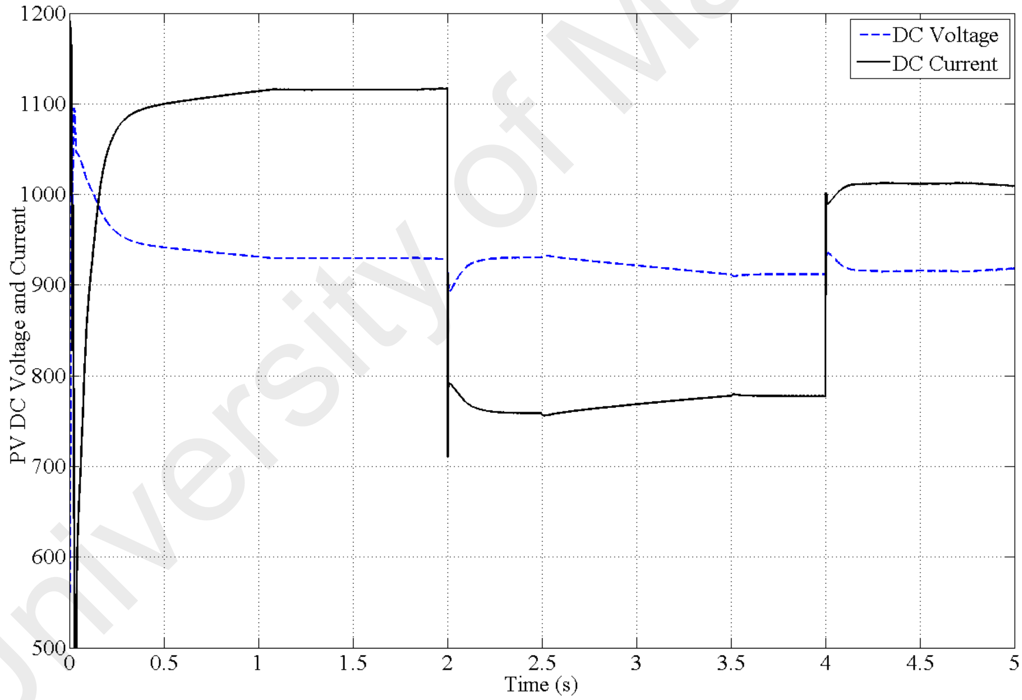

Figure 4.32: Photovoltaic DC voltage and current, in configuration 2 case one.

and local load.

Figure 4.34 illustrates the active power with variable DC V_{ref} in all buses. Active power at B_{FC} did not change by radiation variation neither by load variation, that because the controller was set to dispatch the maximum power regardless the other factors. B_{PV}, B_b, and PCC dropped when the radiation dropped, where only PCC active power

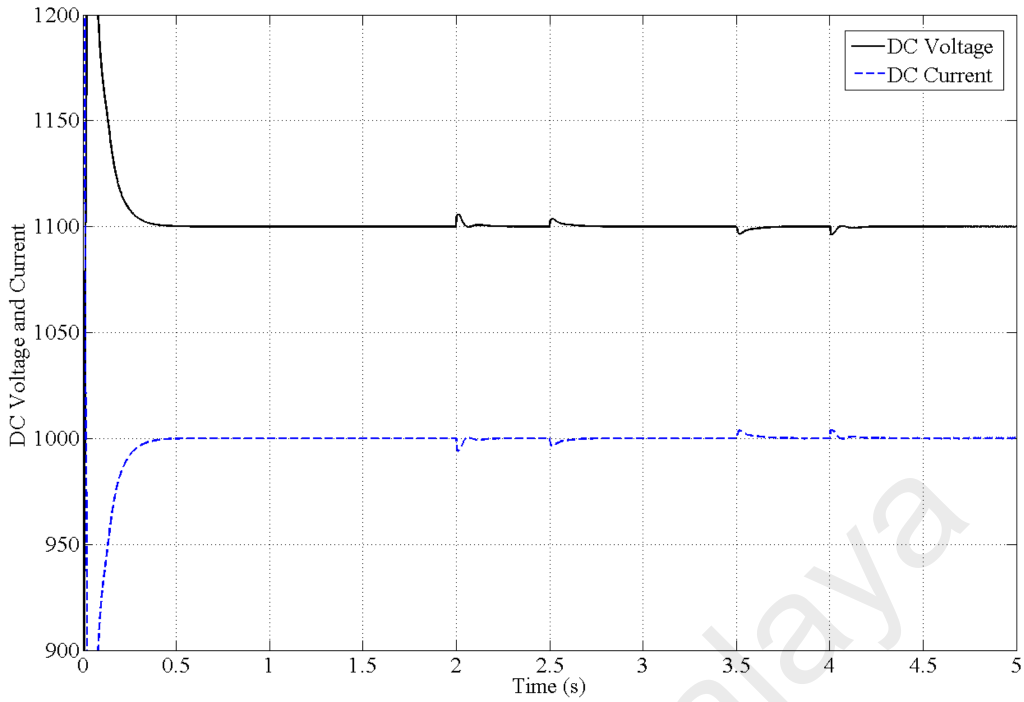

Figure 4.33: Fuel cell DC voltage and current, in configuration 2 case one.

decreased during the increasing of B$_L$.

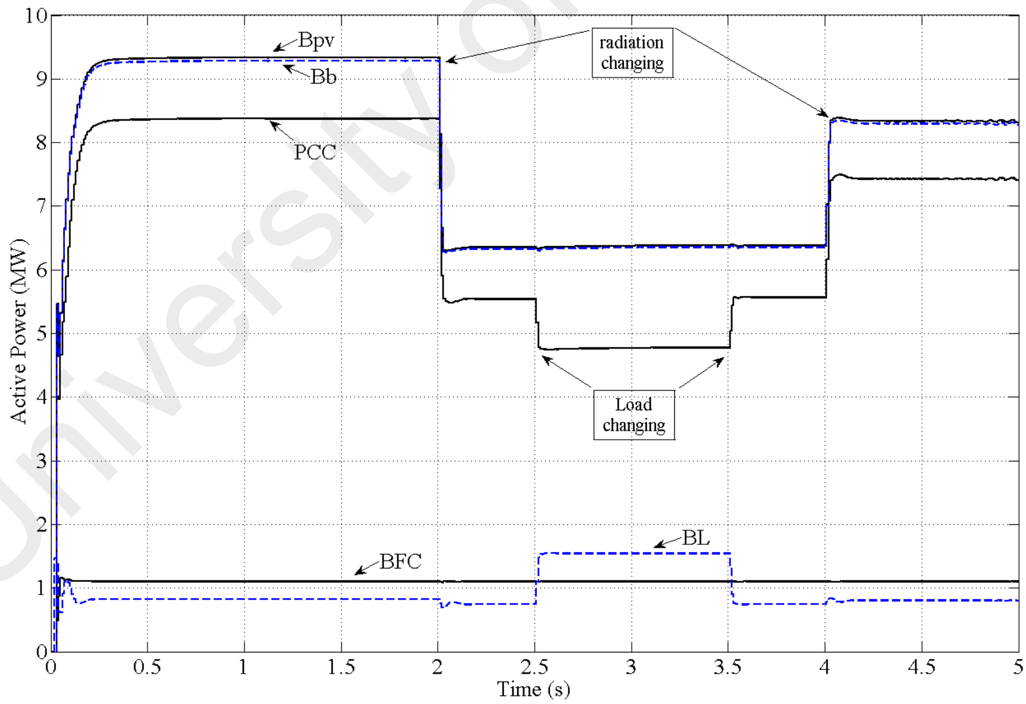

Figure 4.34: Active power (MW) at variable DC V_{ref}, in configuration 2 case one.

Figure 4.35 shows the reactive power dispatched from all buses at configuration 2. In B$_{pv}$, B$_{FC}$, reactive power were set to zero. B$_b$ follows B$_{pv}$. At B$_L$ and PCC, although, the solar radiation variation affected PCC and B$_L$, a significant change occurred in reac-

University of Malaya

tive power during load disturbance. Negative reactive power at PCC illustrates that the microgrid absorbed reactive power from the grid.

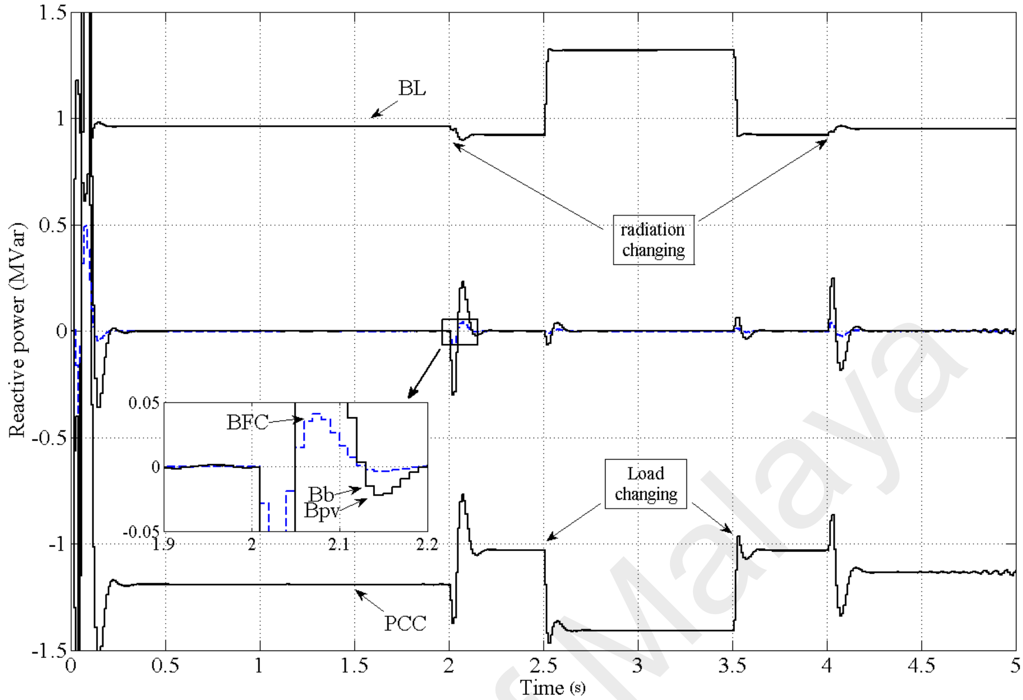

Figure 4.35: Reactive power of buses B_{pv}, B_{FC}, B_L, B_b, and PCC, in configuration 2 case one.

Figure 4.36 shows the voltage of buses PCC, B_{pv}, B_{FC}, B_b, B_L, as the voltage was uncontrollable, the voltages were following the grid voltage. When the radiation dropped the voltage dropped due to the increase of power was required to be transfered via transmission line (at the grid side) to supply the load at grid side. The same thing occurred when the load increased.

4.4.2 Case Two: Partial Shading, Feeder Removal

Partial shading occurred in one of the PV sources, when 100 strings out of 200 exposed to solar radiation decline from 1000 W/m^2 to 700 W/m^2 at 2 s, then increased to 900 W/m^2 at 4 s as shown in table 4.2. Also in this case FC feeder disconnected at 1.5 s. The load increased 1 MW and 0.5 MVar at 2.5 s then removed at 3.5 s.

Figure 4.37 illustrates the DC voltage and current for the PV source. FC feeder removal at 1.5 s and the load disturbance at 2.5 s and 3.5 s had minor effect on voltage

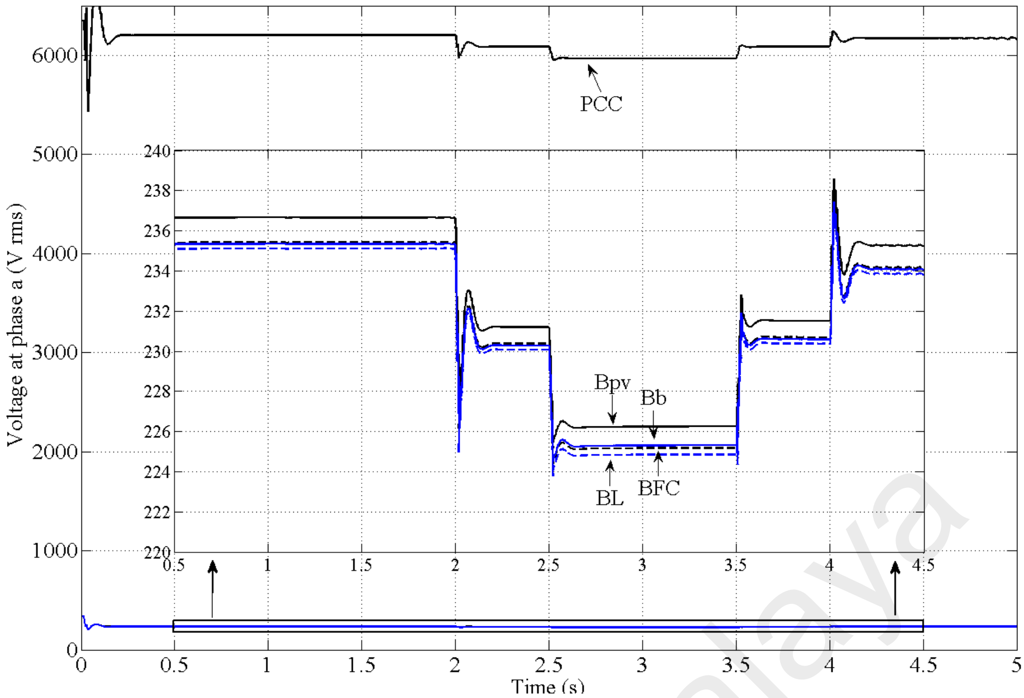

Figure 4.36: Phase-A to ground voltage RMS of buses B_{pv}, B_{FC}, B_L, B_b, and PCC, in configuration 2 case one.

and current. Whereas during solar radiation variation current changed dramatically. The controller regulated the voltage at a value which extracted maximum power from PV source.

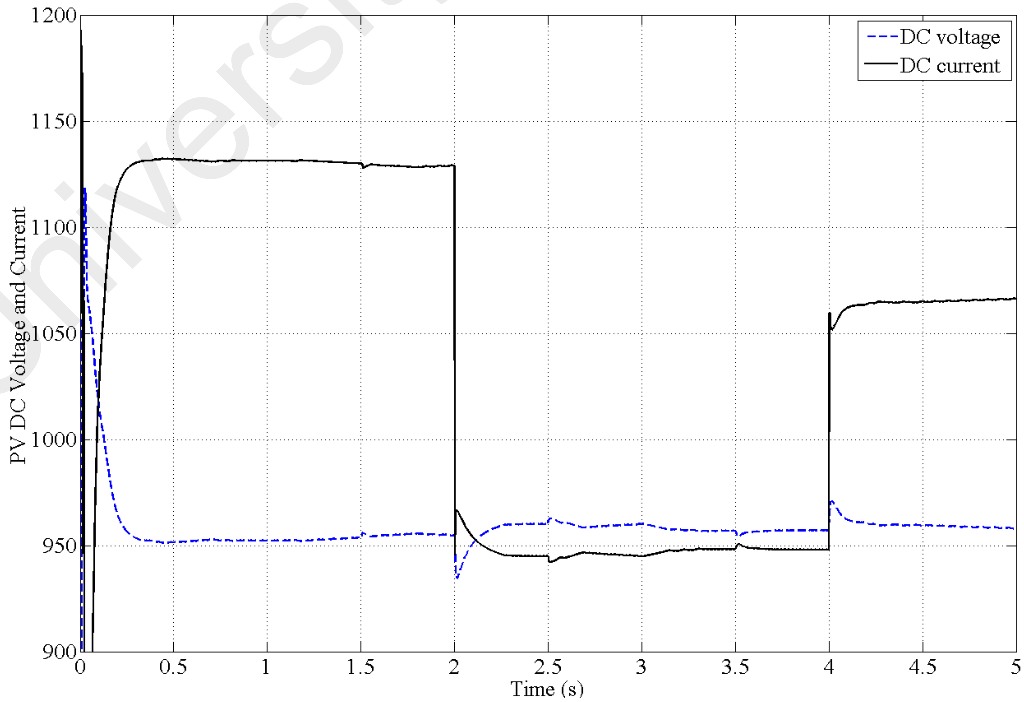

Figure 4.37: Photovoltaic DC voltage and current at the unit where the partial shading occurs, in configuration 2 case two.

University of Malaya

Figure 4.38 illustrates the DC voltage and current for the FC source when the FC feeder removed. The controller regulated the voltage at 1100 V and the current at 1000 A. After the feeder removed the current dropped to zero.

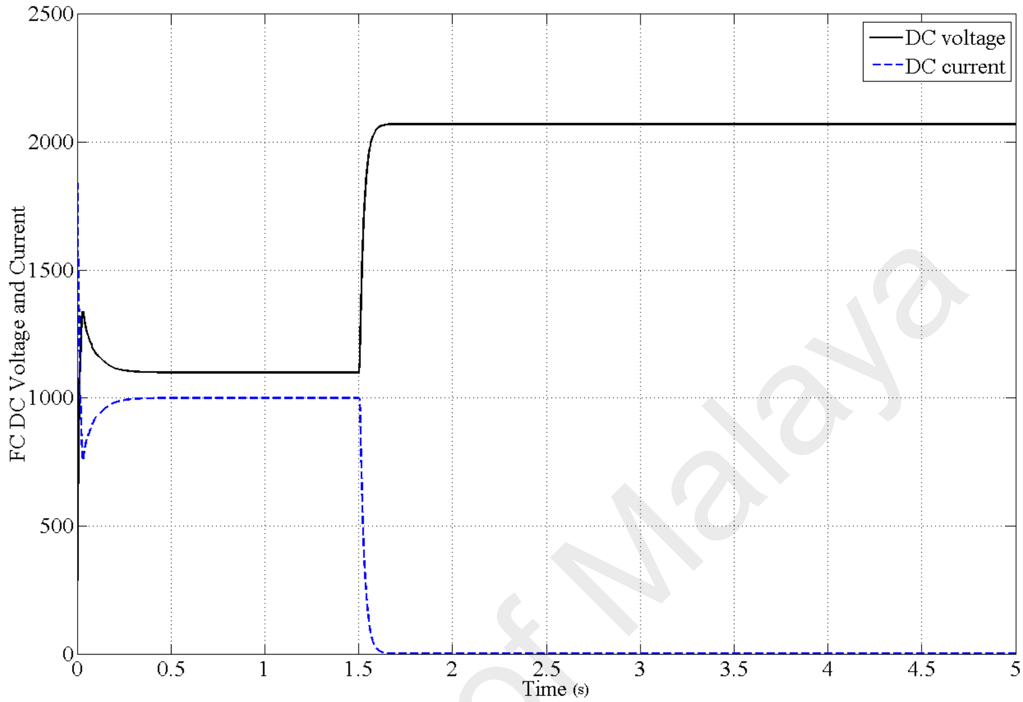

Figure 4.38: Fuel cell DC voltage and current, in configuration 2 case two.

Figure 4.39 illustrates the active power with variable DC V_{ref} in all buses. B_{PV}, B_b, and PCC dropped when the radiation dropped, whereas only PCC active power decreased during the increasing of B_L. At 1.5 s the feeder B_{FC} was removed, causing the power to drop to zero, at the same time the power at PCC decreased by 1.1 MW. As the partial shading occurred at only one of the PV source, the drop in active power due to radiation decline was insignificant.

Figure 4.40 shows the reactive power in all buses at configuration 2. Reactive power in B_{pv}, B_{FC} were set to zero, showing that the controller was regulating the reactive power effectively. B_b just follows B_{pv}. Although FC feeder removal affects PCC and B_L, the significant change in reactive power occurs due to load disturbance. Partial shading did not affect the reactive power drastically.

Figure 4.41 shows the voltage at all buses. Since the voltage was uncontrollable,

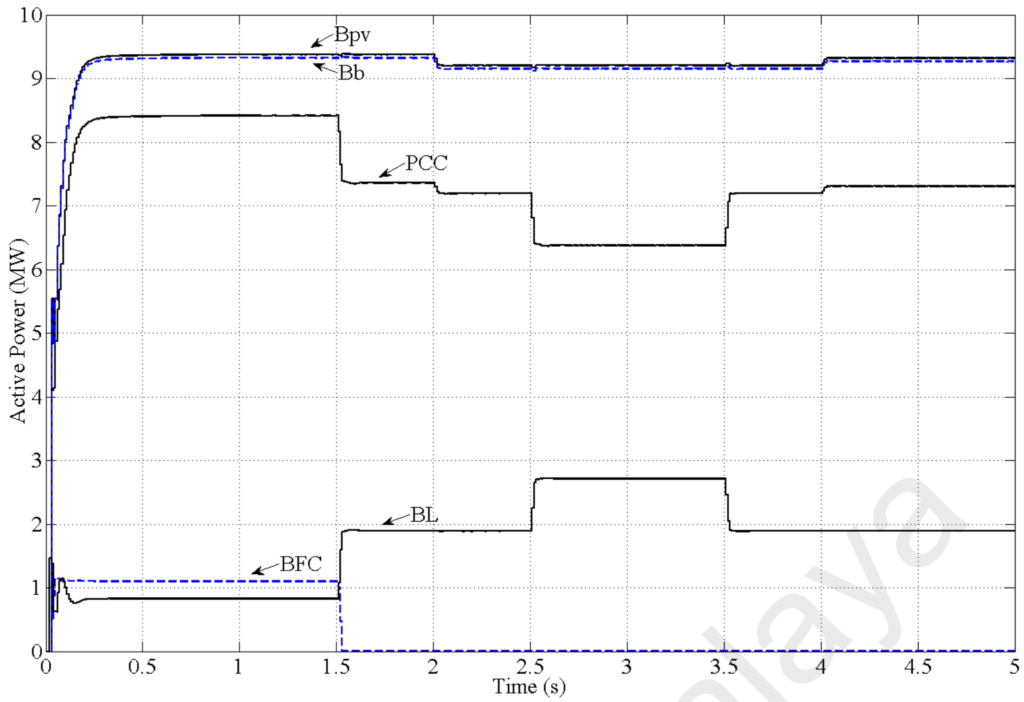

Figure 4.39: Active power (MW) at variable DC V_{ref}, in configuration 2 case two.

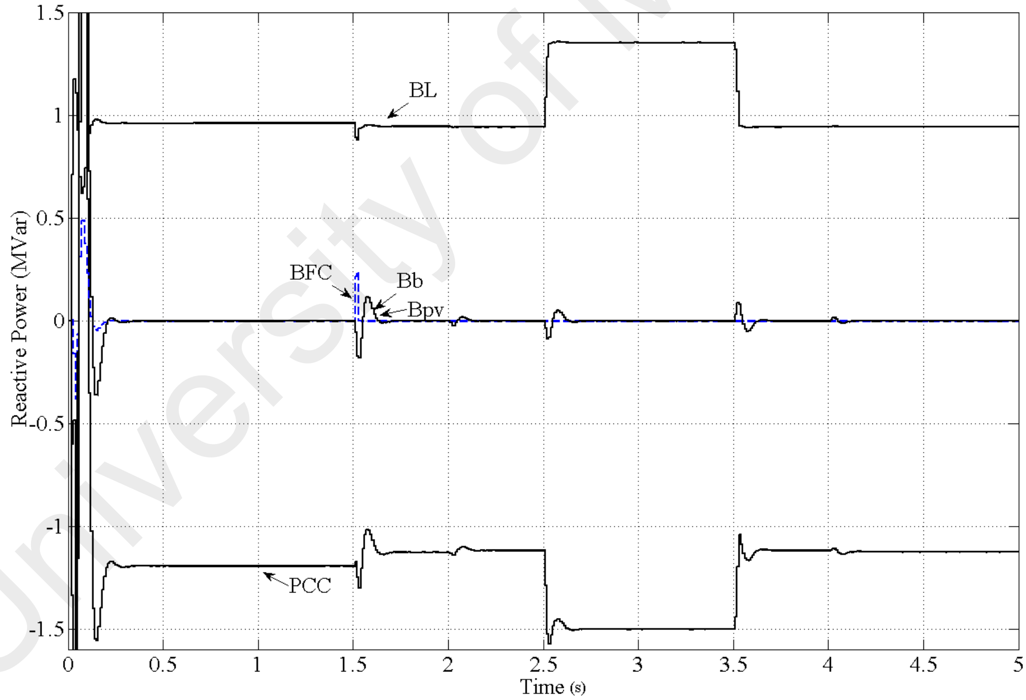

Figure 4.40: Reactive power of buses B_{pv}, B_{FC}, B_L, B_b, and PCC, in configuration 2 case two.

it was following the grid voltage. When FC feeder removed, voltages drooped because less power dispatched to the grid so more power losses taken place at transmission line to supply the load at the grid. Radiation effect was not signification, whereas the load disturbance changed the voltage obviously.

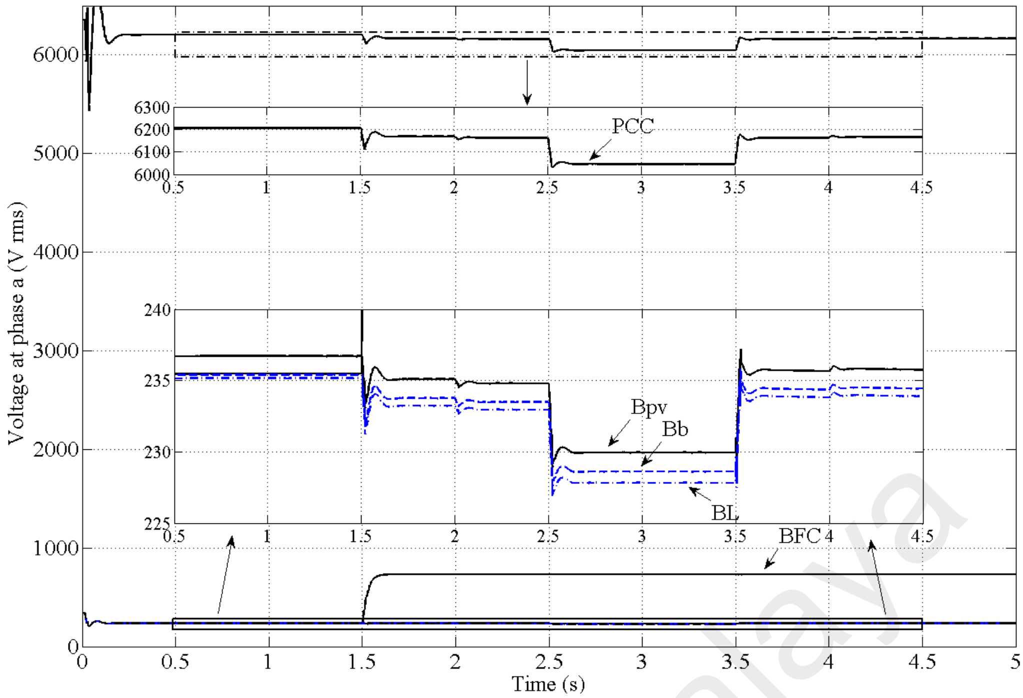

Figure 4.41: Phase-A to ground voltage RMS of buses B_{pv}, B_{FC}, B_L, B_b, and PCC, in configuration 2 case two.

4.5 Configuration 2 With Reactive Power Control

In this section, the distribution line between B_{FC} and B_L is 10 m, and Z_L is represented by the π model (see Figure 4.31). The active power, reactive power, and RMS voltage at B_{pv1}, B_{FC}, B_L, B_b, and PCC are as shown in below Figures. The four conditions investigated are summarized next.

4.5.1 Case Three: Variable Radiation and Variable Load with Q controlling

The inverter controller fixed DC V_{ref} to 930 V for the PV source and 1100 V for the FC source. The reactive power dispatched to the PCC was set to zero in the PV whereas the FC dispatched the desired amount to regulate the voltage. The solar radiation for this case was as presented in Table 4.2. The load initial value was 2 MW. At 2.5 s, a 0.4 MW and 0.2 MVar load was connected then removed at 3.5 s. The DC-link capacitor was 24 mF. Figure 4.42 shows the active power (MW) of buses B_{pv1}, B_{FC}, B_L, B_b, and PCC. The power at B_b equaled the sum of PV sources only since the FC source was connected to B_L. The power at B_L was less than 2 MW (the connected load) because the FC source was

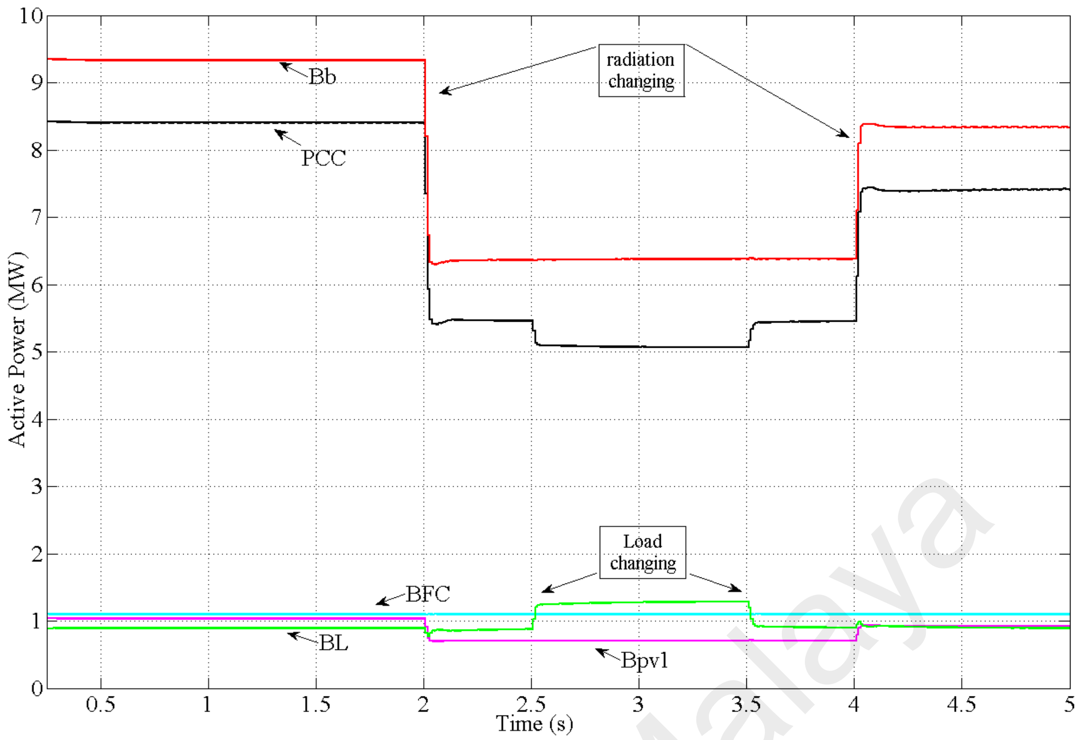

Figure 4.42: Active power of buses B_{pv1}, B_{FC}, B_L, B_b, and PCC, in configuration 2 case three.

connected to B_L so it supplied some of the loads locally. The results are as summarized in Table 4.5.

Figure 4.43 shows the reactive power of buses B_{pv1}, B_{FC}, B_L, B_b, and PCC. B_{pv1}produced zero reactive power following the inner controller preset value. B_L consumed 0.2 MVar between 2.5 s and 3.5 s when the reactive load was connected. A significant amount of reactive power was dispatched to the PCC because it was required for regulating the voltage at B_L. The results are as summarized in Table 4.5.

Figure 4.44 shows the phase-A RMS voltage of buses B_{pv1}, B_{FC}, B_L, B_b, and PCC in configuration 2 case one. Voltage at B_L was higher than at B_{pv1} and B_b, since the voltage regulation bus (B_{FC}) (which had the highest voltage) was connected to B_L. B_{pv1} and B_b had similar voltages during all the intervals. Voltage at B_L was regulated to 239 V as shown by Table 4.5 (which summarizes all the voltage values).

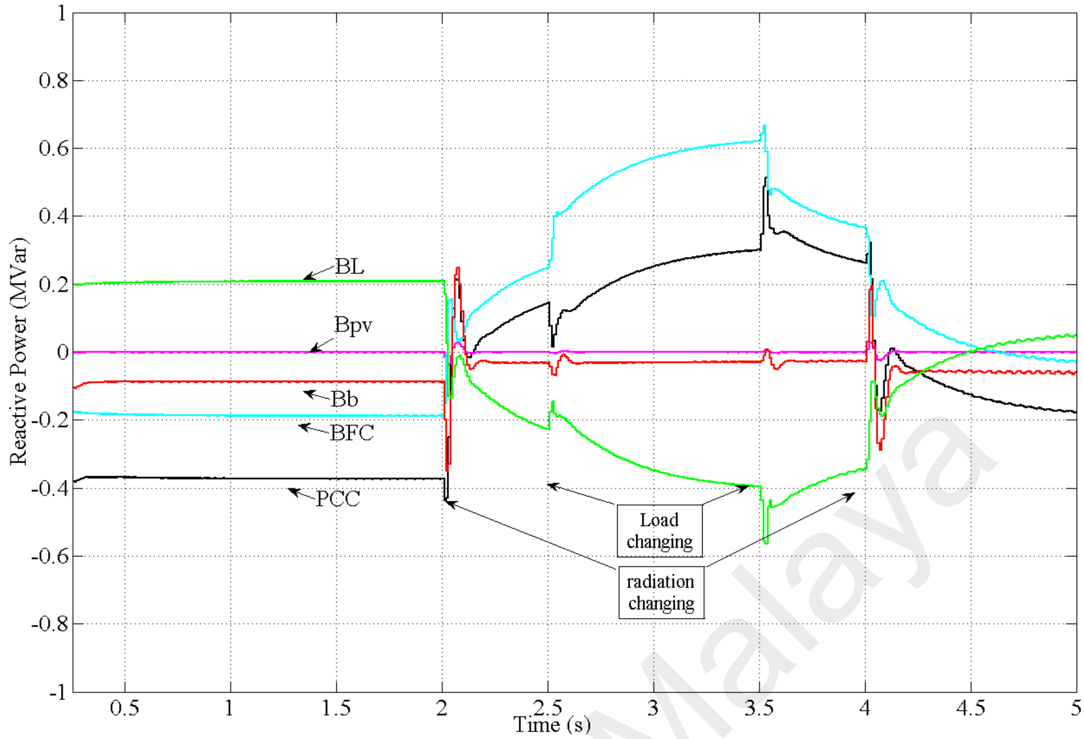

Figure 4.43: Reactive power of buses B_{pv1}, B_{FC}, B_L, B_b, and PCC, in configuration 2 case three.

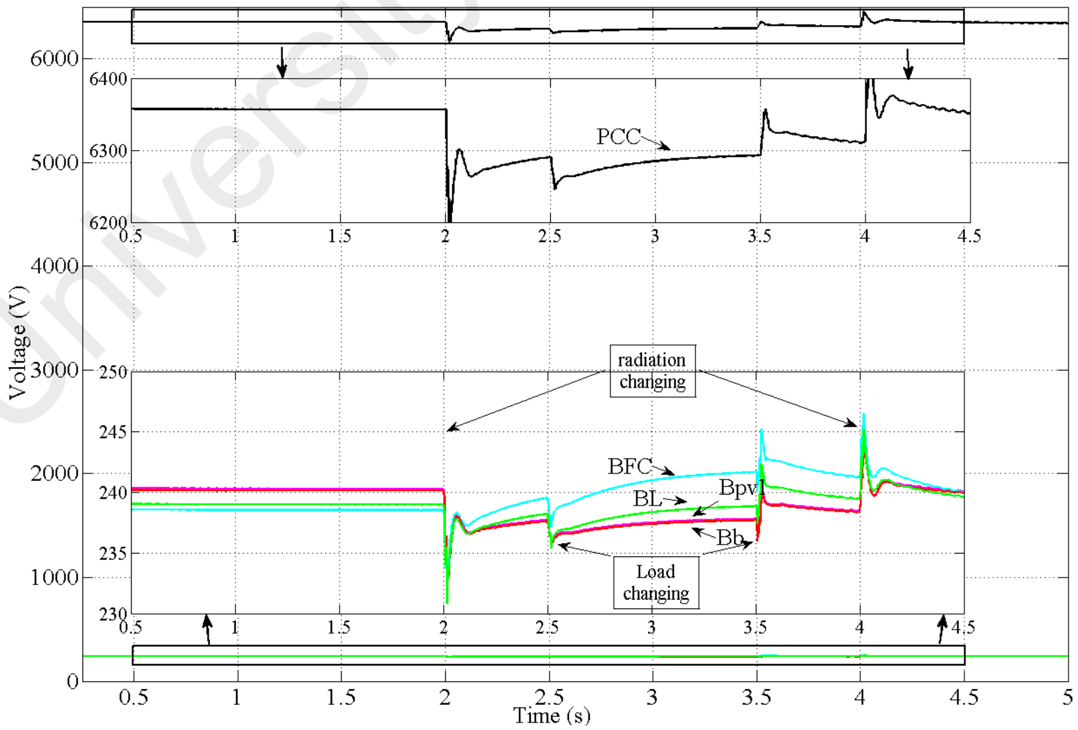

Figure 4.44: Phase-A RMS voltage of buses B_{pv1}, B_{FC}, B_L, B_b, and PCC, in configuration 2 case three.

University of Malaya

Table 4.5: Summary of the results of configuration 2 case three, (R stands for Radiation)

Item	**Initial**	**R**	**Load**		**R**
	Value	**Drop**	**Rise**	**Drop**	**Rise**
P_{pcc}	8.405	5.46	5.066	5.455	7.413
P_{Bpv1}	1.037	0.707	0.709	0.7093	0.926
P_{BFC}	1.1	1.1	1.1	1.1	1.1
P_{Bb}	9.333	6.365	6.38	6.381	8.34
P_{BL}	0.892	0.879	1.287	0.9	0.892
Q_{pcc}	-0.373	0.144	0.301	0.262	-0.18
Q_{Bpv1}	0	0	0	0	0
Q_{BFC}	-0.188	0.25	0.621	0.365	-0.03
Q_{Bb}	-0.087	-0.031	-0.029	-0.026	-0.06
Q_{BL}	0.209	-0.227	-0.396	-0.344	0.062
V_{pcc}	6356.4	6290	6293	6311	6345
V_{Bpv1}	240.3	237.7	237.8	238.4	239.8
V_{Bpv}	238.5	239.5	241.6	241.2	239.3
V_{Bb}	240.1	237.6	238.7	238.3	239.6
V_{BL}	239	238.2	238.9	239.4	239

4.5.2 Case Four: Feeder Removal and Partial Shading

In this case, partial shading occurred at one of the PV sources, owing to a variation in the sun's radiation (see Table 4.2). The FC source feeder (B_{FC}) removed at 1.5 s shows the active and reactive powers dropping to zero. Figure 4.45 depicts the active power of buses B_{pv1}, B_{FC}, B_L, B_b, and PCC in configuration 2 case four. A significant drop in power occurred at 1.5 s, at B_{FC}, and PCC, owing to feeder removal. B_b continued at the same level since B_{FC} was not connected to this bus. At 2 s and 4 s a minor change occurred at B_{pv1}, B_b, and PCC upon partial shading of one of the PV sources. The power at B_L increased to 2 MW (the initial load value) at 1.5 s owing to removal of local source (FC source) which was connected to B_L. Table 4.6 summarizes the active power values of all the buses.

Figure 4.46 shows the reactive power of buses B_{pv1}, B_{FC}, B_L, B_b, and PCC in configuration 2 case four. B_{pv1} produced zero reactive power following the inner controller preset value. B_L did not consume any reactive power but before 1.5 s some reactive power was dispatched from it owing to the B_{FC} connection. Before the feeder removal at 1.5

University of Malaya

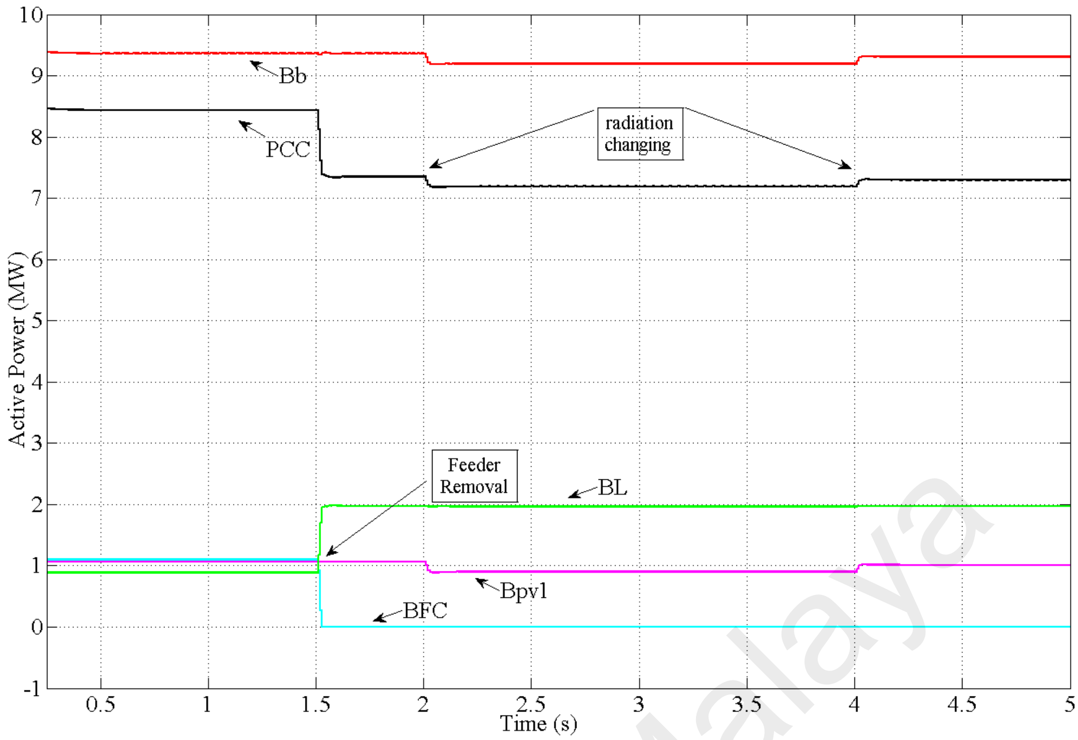

Figure 4.45: Active power of buses B_{pv1}, B_{FC}, B_L, B_b, and PCC, in configuration 2 case four.

s, B_{FC} consumed reactive power to regulate the voltage at B_L. Upon B_{FC} removal, the reactive power at B_L became close to zero, whereas some reactive power continued being imported from PCC to supply reactive power required at the distribution lines and transformer. Table 4.6 summarizes the reactive power values of all the buses.

Figure 4.47 shows the phase-A RMS voltage of buses B_{pv1}, B_{FC}, B_L, B_b, and PCC in configuration 2 case four. At initial condition, all the voltages had similar values close to 239 V. When B_{FC} was removed, the voltage regulator disconnected. Since the disturbances were minor at B_{pv1} owing to the partial shading, the voltage at B_{pv1}, B_L, B_b remained stable at around 239 V. A drop occurred in the PCC voltage owing to the feeder removal at 1.5 s and partial shading between 2 s and 4 s. Table 4.6 summarizes the voltage values of at all the buses.

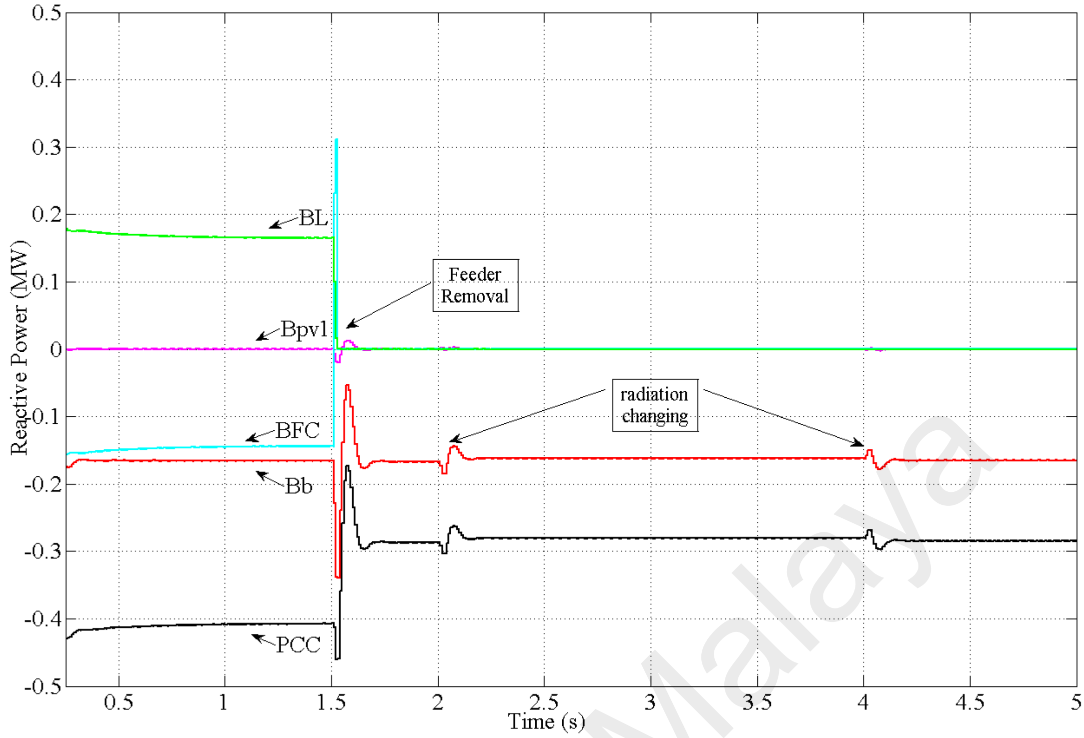

Figure 4.46: Reactive power of buses B_{pv1}, B_{FC}, B_L, B_b, and PCC, in configuration 2 case four.

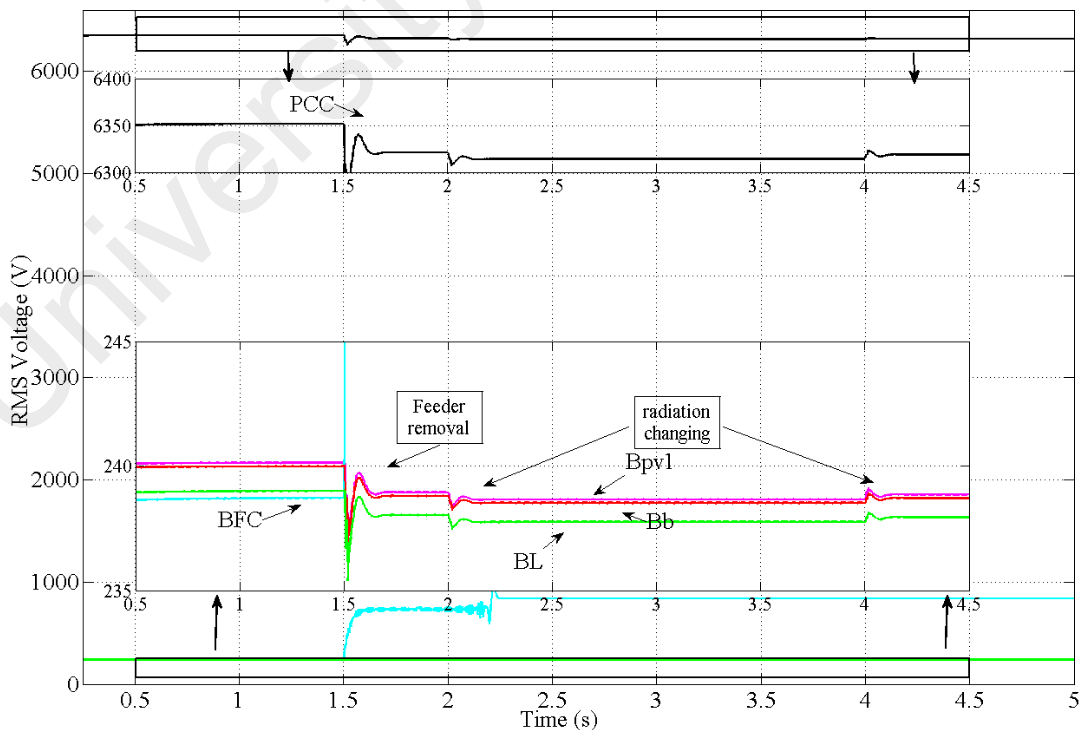

Figure 4.47: Phase-A voltage RMS of buses B_{pv1}, B_{FC}, B_L, B_b, and PCC, in configuration 2 case four.

University of Malaya

Table 4.6: Summary of the results of configuration 2 case four, (R stands for Radiation)

Item	Initial Value	Feeder Removal	Partial R Drop	Partial R Rise
P_{pcc}	8.435	7.352	7.192	7.3
P_{Bpv}	1.0674	1.0674	0.902	1.0123
P_{BFC}	1.1	0	0	0
P_{Bb}	9.363	9.363	9.197	9.307
P_{BL}	0.8915	1.974	1.969	1.9725
Q_{pcc}	-0.403	-0.287	-0.28	-0.285
Q_{Bpv}	0	0	0	0
Q_{BFC}	-0.144	0	0	0
Q_{Bb}	-0.166	-0.167	-0.162	-0.166
Q_{BL}	0.165	0	0	0
V_{pcc}	6351.5	6321	6314	6318.8
V_{Bpv}	240.13	238.95	238.65	238.85
V_{BFC}	238.7	840	840	840
V_{Bb}	239.98	238.8	238.52	238.7
V_{BL}	239	238.03	237.75	237.94

4.6 Configuration 3

Figure 4.48 shows the configuration 3, connected to 2 MW, 1 MVar load. At the normal operation the solar radiation was 1000 W/m^2. FC and PV sources as described in 4.1.3 and 4.1.4 were used in this configuration. Transformer (T) is step up transformer from 415 V to 11 kV (RMS line to line voltage). In this simulation the impedance (Z_L) of the distribution line is resistive which equals 0.1 mΩ. The system ran for 5 s in all cases below.

4.6.1 Case One: Variation in Solar Radiation and Load With Variable Voltage Ref

Solar radiation was as shown in Table 4.2, and the load was increased by 1 MW active power and 0.5 reactive MVar at 2.5 s then removed at 3.5 s. The DC voltage regulator used here was as in Figure 3.7. Figure 4.49 illustrates the DC voltage and current for the PV source during solar radiation variation and load disturbance. The controller changed the reference DC-link voltage to a value that extracted maximum power from PV.

Figure 4.50 illustrates the DC voltage and current for the FC source. It is clear that

University of Malaya

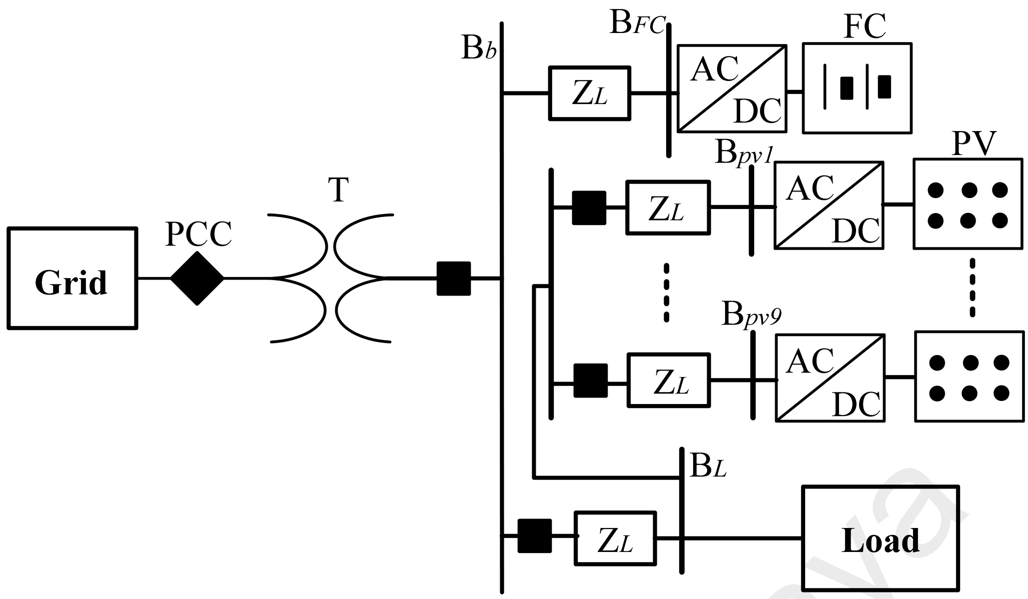

Figure 4.48: configuration 3.

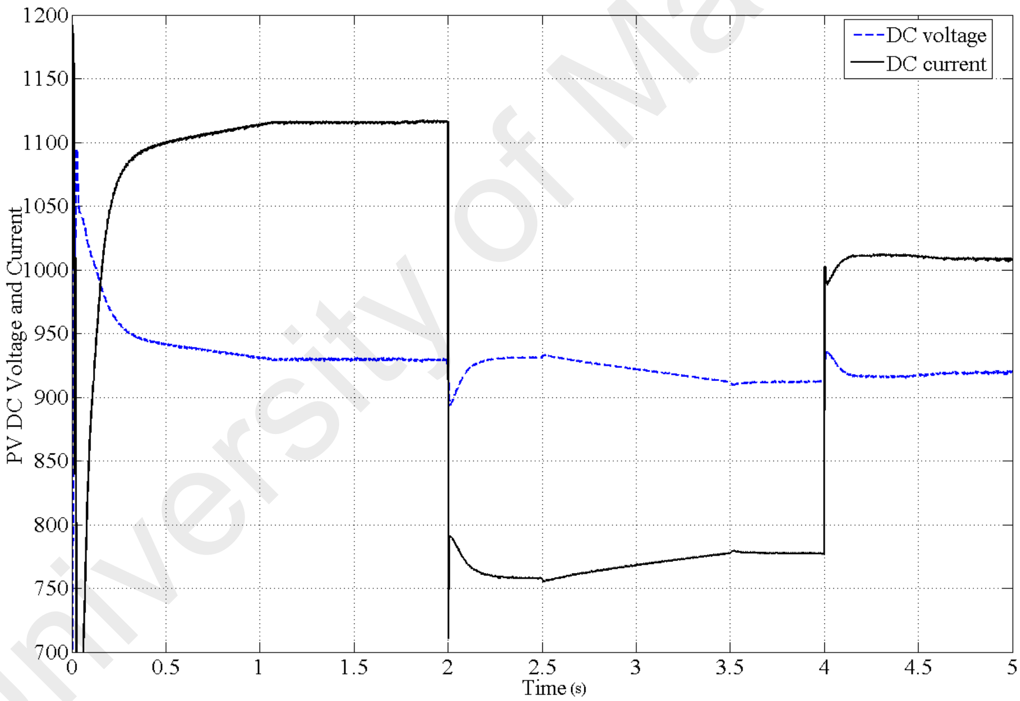

Figure 4.49: Photovoltaic DC voltage and current, in configuration 3 case one.

the controller regulates the voltage at 1100 V while the current at 1000 A, regardless the solar radiation and the load disturbance.

Figure 4.51 illustrates the active power with variable DC V_{ref} in all buses. Active power at B_{FC} was not affected by radiation variation neither by load variation, that because the controller set to dispatch the maximum power regardless the other factors, B_b

University of Malaya

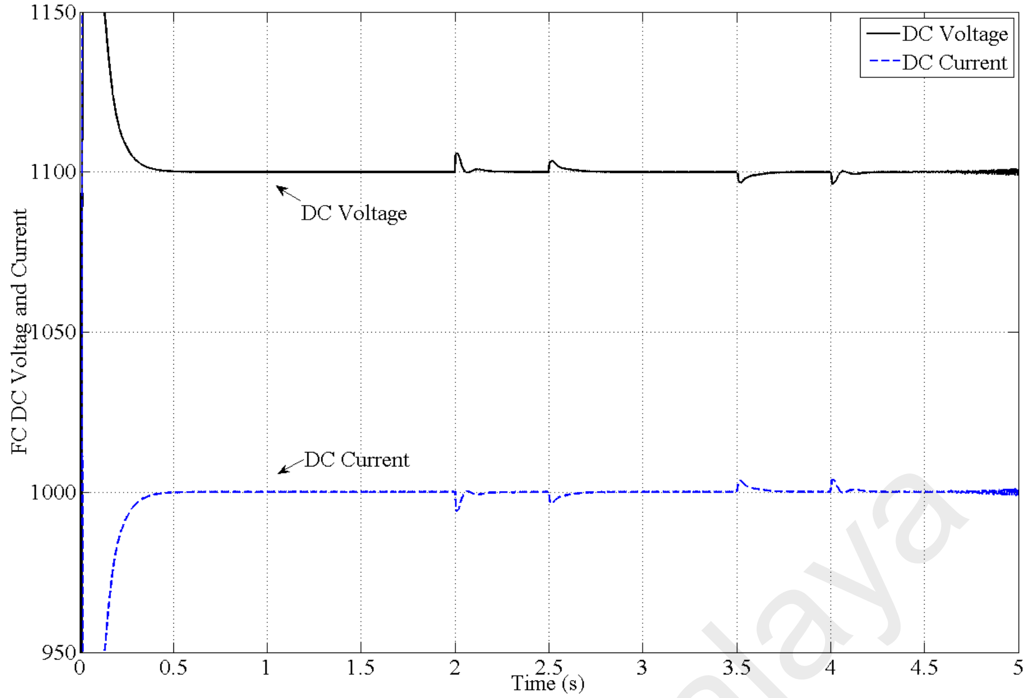

Figure 4.50: Fuel cell DC voltage and current, in configuration 3 case one.

was just following B_{FC} in configuration 3. As the PV source was connected to the load, B_{PV} power was dispatched directly to the load then the non consumed power dispatched through B_L, this explained why the power at B_L was negative.

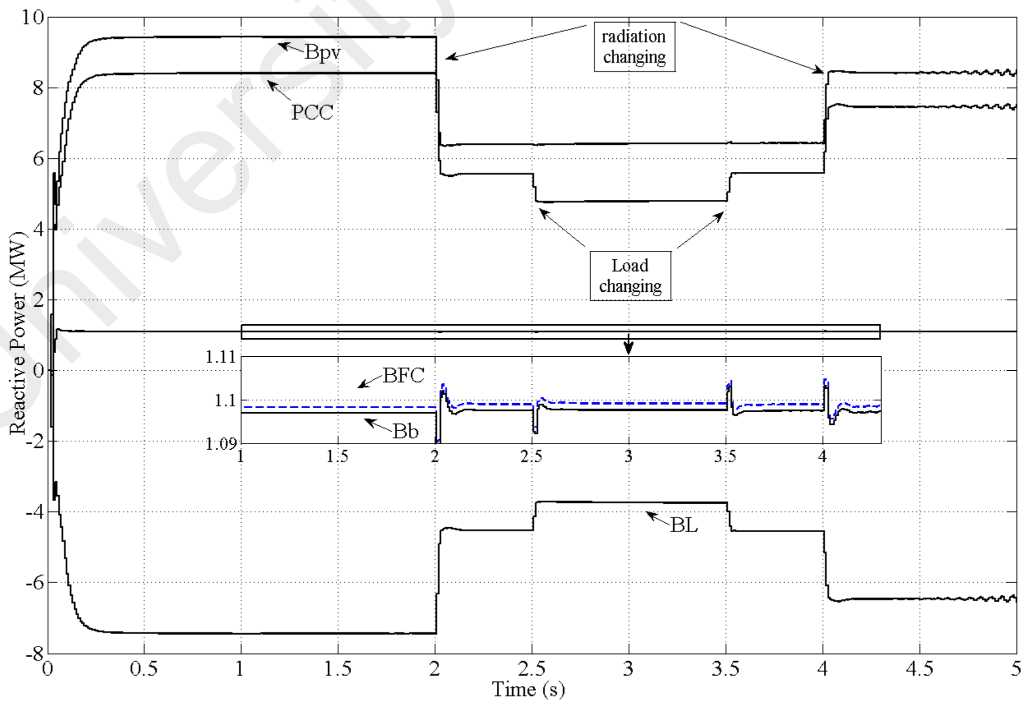

Figure 4.51: Active power (MW) at variable DC V_{ref}, in configuration 3 case one.

Figure 4.52 shows the reactive power in all buses at configuration 3. Reactive power

University of Malaya

in B_{pv}, B_{FC} were set to zero, showing that the controller was regulating the reactive power effectively. B_b just followed B_{FC}. At B_L, and PCC although the solar radiation variation affects PCC and B_L, the significant change in reactive power occurred due to load disturbance, negative reactive power at PCC depicted that the microgrid absorbed reactive power from the grid.

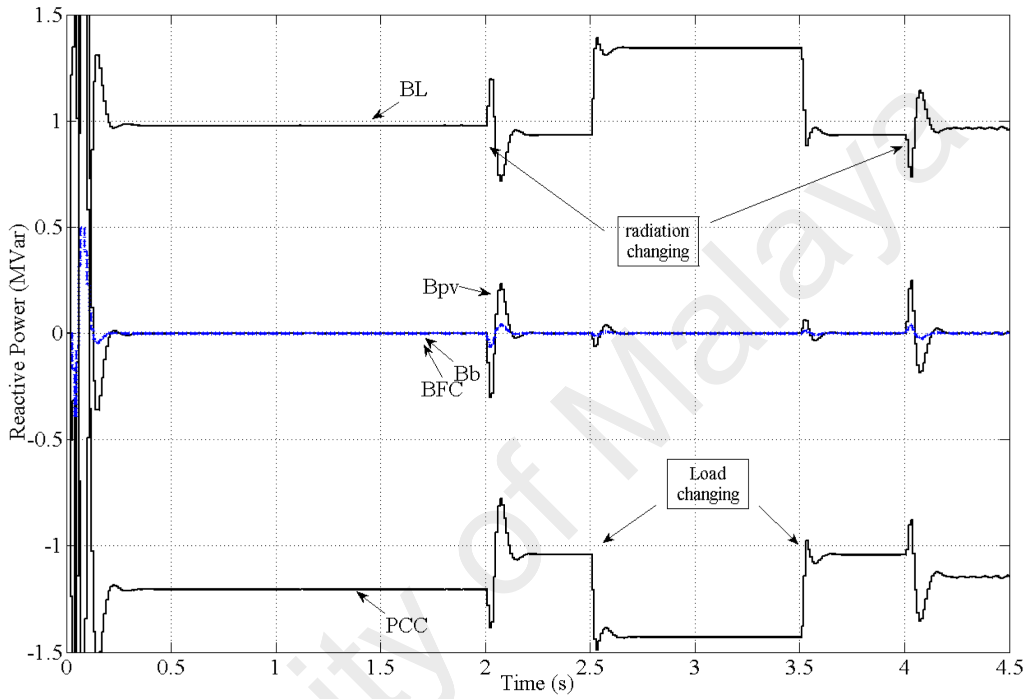

Figure 4.52: Reactive power of buses B_{pv}, B_{FC}, B_L, B_b, and PCC, in configuration 3 case one.

Figure 4.53 shows the voltage of buses PCC, B_{pv}, B_{FC}, B_b, B_L, as the voltage was uncontrollable, the buses voltages were following the grid voltage. When the radiation reduced the voltage dropped due to increase of the power was required to transfer from transmission line (at the grid side) to supply the load. The same thing occurred when the load increases.

4.6.2 Case Two: Partial Shading, Feeder Removal

In this case, partial shading occurred in one of the PV sources, when 100 strings out of 200 exposed to solar radiation decline from 1000 W/m^2 to 700 W/m^2 at 2 s, then increased to 900 W/m^2 at 4 s as shown in table 4.2. In this case FC feeder disconnected

University of Malaya

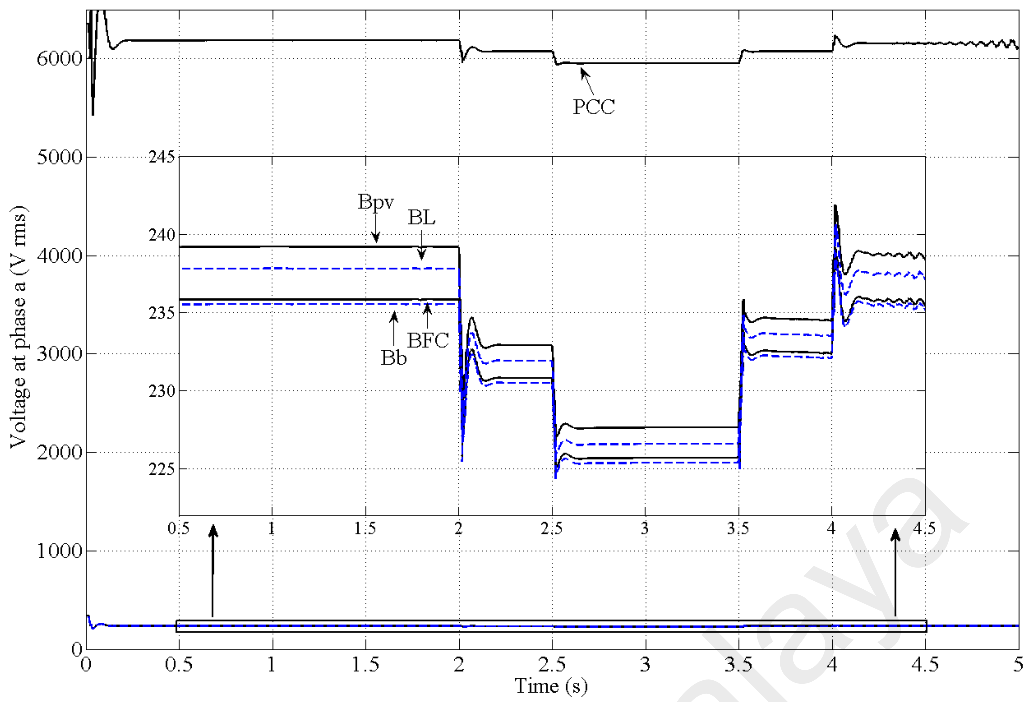

Figure 4.53: Phase-A to ground voltage RMS of buses B_{pv}, B_{FC}, B_L, B_b, and PCC, in configuration 3 case one.

at 1.5 s. Figure 4.54 illustrates the DC voltage and current for the PV source. FC feeder removal at 1.5 s had insignificant effect on the voltage and current. Whereas during solar radiation variation the current changed dramatically and controller regulated the voltage at a value that extracted maximum power from PV source.

Figure 4.55 illustrates the DC voltage and current for the FC source when the FC feeder removed. The controller regulated the voltage at 1100 V and the current at 1000 A. After the FC feeder removed the current dropped to zero.

Figure 4.56 illustrates the active power with variable DC V_{ref} dispatched from all buses. PCC and B_L dropped when the radiation decreased. At 1.5 s the feeder B_{FC} was removed so the power dropped to zero, at the same time the power at PCC decreased by 1.1 MW. As the partial shading occurred at only one of the PV source, the change in active power due to radiation disturbance wa insignificant as shown at 2 s and 4 s.

Figure 4.57 shows the reactive power in all buses at configuration 3. Reactive power in B_{pv}, B_{FC} were zero showing that the controller was regulating the reactive power effec-

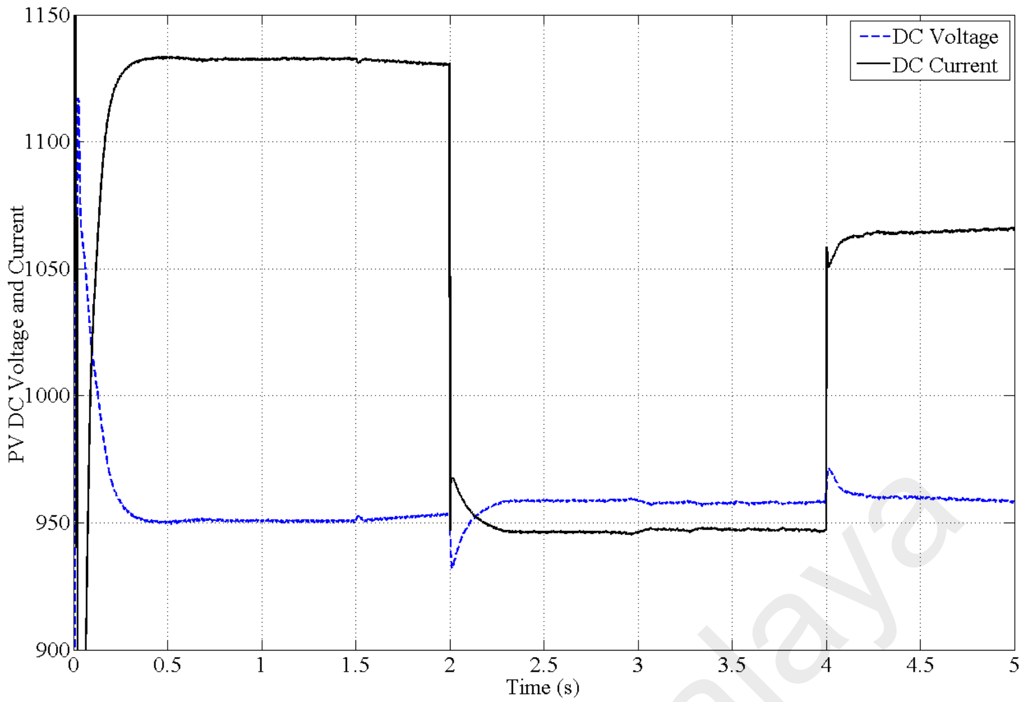

Figure 4.54: Photovoltaic DC voltage and current at the unit where the partial shading occurs, in configuration 3 case two.

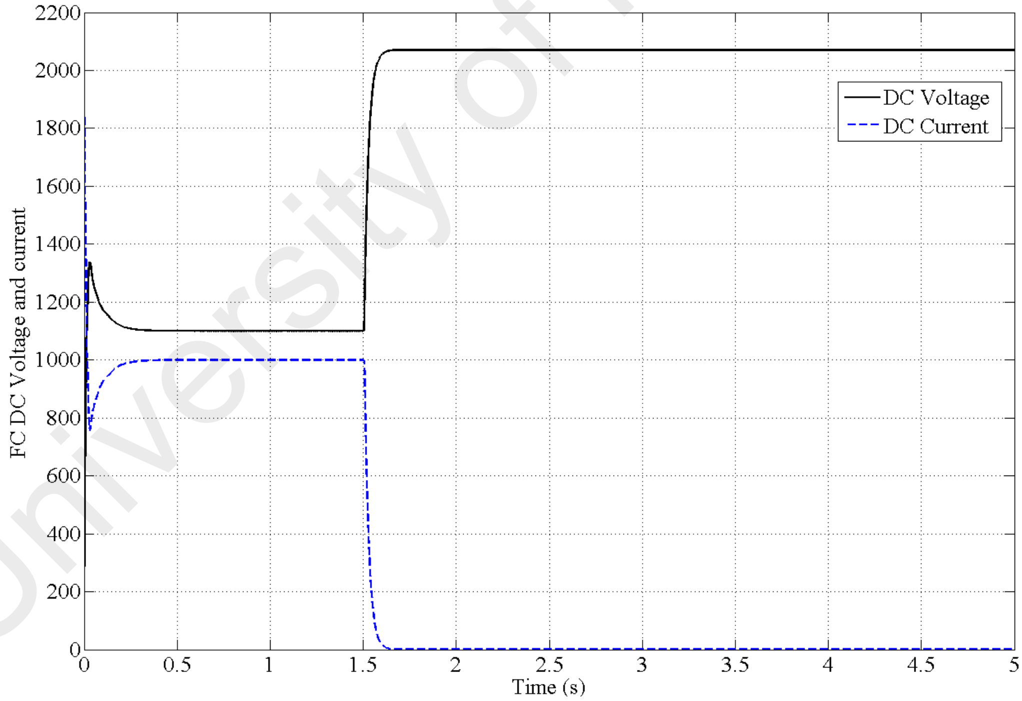

Figure 4.55: Fuel cell DC voltage and current, in configuration 3 case two.

tively. B_b just follows B_{pv}. FC feeder removal affected PCC and B_L only. Partial shading had insignificant effect on the reactive power.

Figure 4.58 shows the voltage at all buses. Since the voltage ws uncontrollable, the voltages were following the grid voltage. After FC feeder removed, voltages dropped

University of Malaya

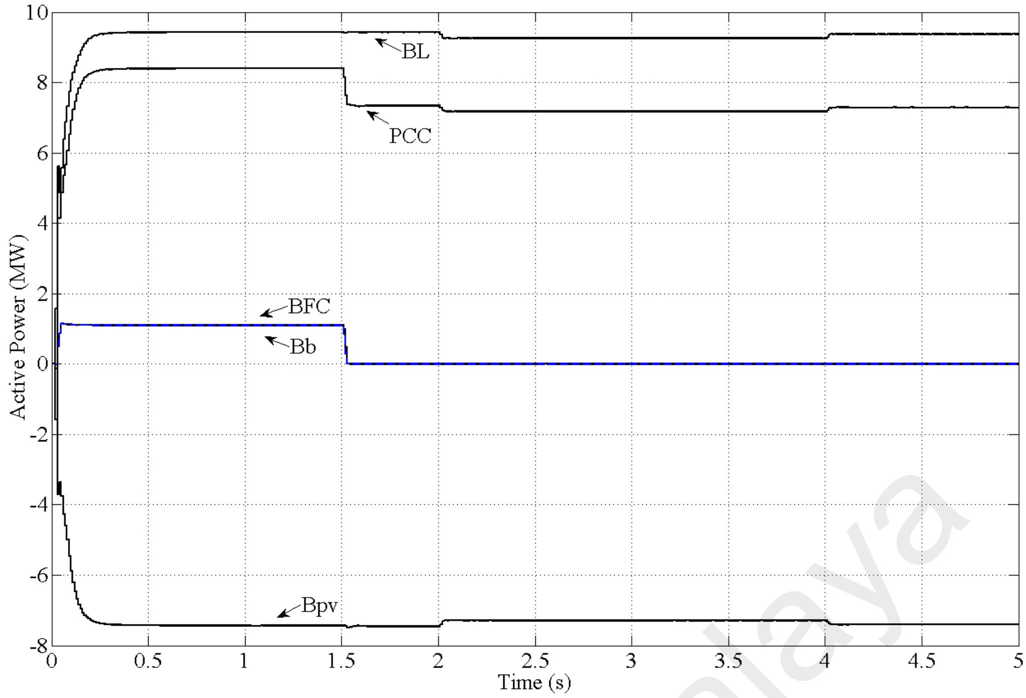

Figure 4.56: Active power (MW) at variable DC V_{ref}, in configuration 3 case two.

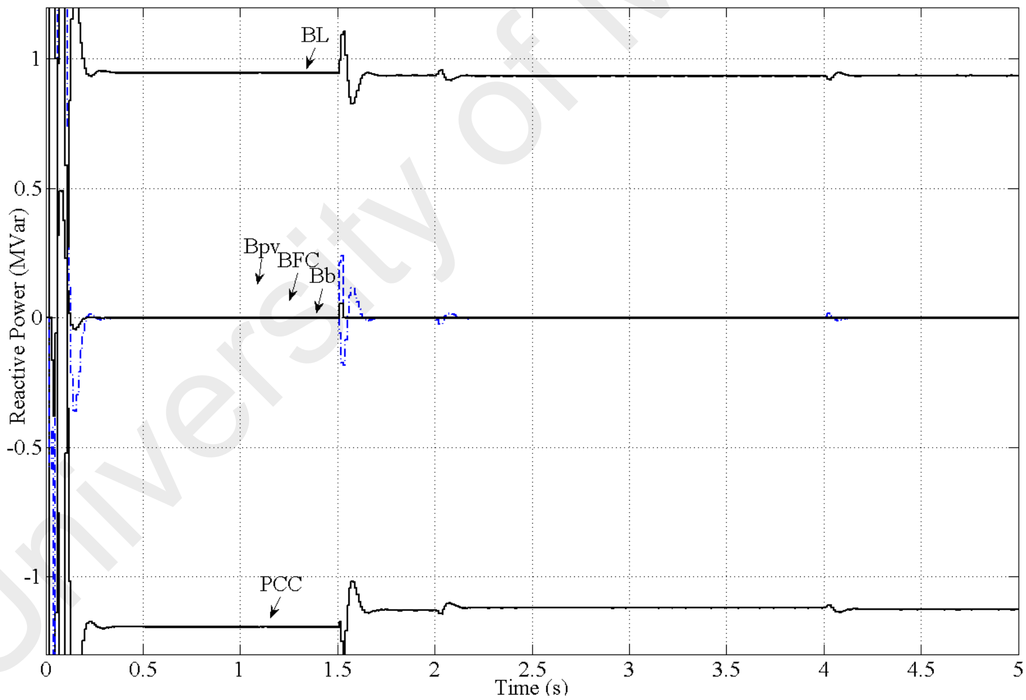

Figure 4.57: Reactive power of buses B_{pv}, B_{FC}, B_L, B_b, and PCC, in configuration 3 case two.

because less power dispatched to the grid so more power losses were taken place at transmission line to supply the load at the grid side. Radiation effect was not significant, whereas the load disturbance changed the voltage obviously.

University of Malaya

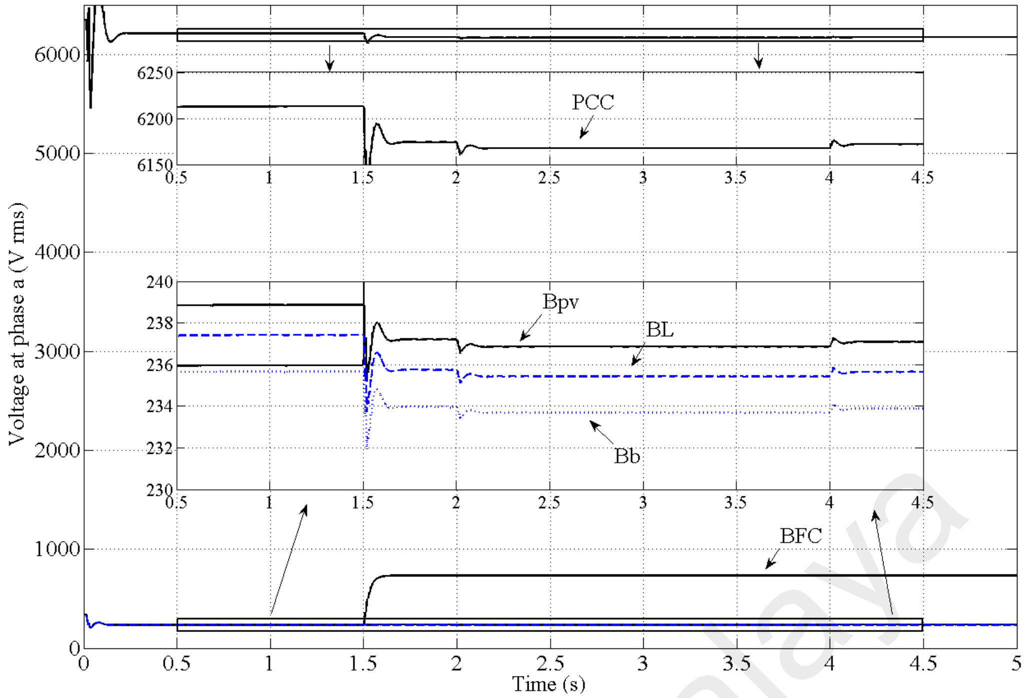

Figure 4.58: Phase-A to ground voltage RMS of buses B_{pv}, B_{FC}, B_L, B_b, and PCC, in configuration 3 case two.

4.7 Configuration 3 With Reactive Power Control

In this section, B_{pv} buses were connected to B_L the distribution line between B_{PV} and B_L is 10 m, Z_L is represented by π model (see Figure 4.3). Active power, reactive power and RMS voltage at B_{pv1}, B_{FC}, B_L, B_b, and PCC are as shown in below Figures. The four conditions investigated are summarized next.

4.7.1 Case Three: Variable Radiation and Variable Load with Q controlling

The inverter controller fixed the DC V_{ref} at 930 V for the PV source and 1100 V for the FC source. The reactive power dispatched to the PCC was set to zero in the PV whereas th FC dispatched the desired amount to regulate the voltage. The solar radiation in this case was as illustrated in Table 4.2. The load's initial value was 2 MW. Between 2.5 s and 3.5 s, a 0.4 MW 0.2 MVar load was connected. The DC-link capacitor was 24 mF. Fig. 4.59 shows the active power (MW) of buses B_{pv1}, B_{FC}, B_L, B_b, and PCC in configuration 3 case three. The power at B_b and B_{FC} had close values because B_{pv1} was not connected to B_b. The negative power at B_L was due to the connection of the

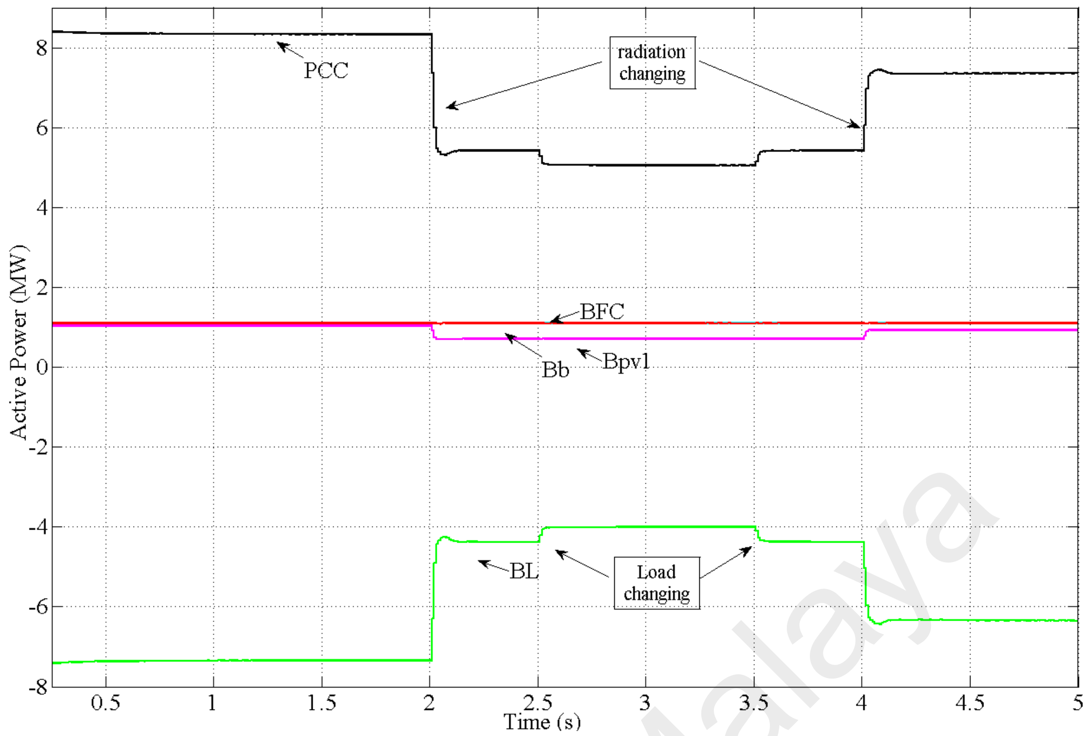

Figure 4.59: Active power of buses B_{pv1}, B_{FC}, B_L, B_b, and PCC, in configuration 3 case three.

PV sources to B_L, so the local load was supplied first before the rest of the power was dispatched to the PCC. The power consumed by the local load was 2 MW before the radiation disturbance. Between 2.5 s and 3.5 s, a 0.4 MW load was connected. B_{FC} dispatched 1.1 MW regularly. B_{pv1} was initially 1 MW before it dropped when the solar radiation dropped at 2 s. The results are as summarized in Table 4.7

Figure 4.60 shows the reactive power of buses B_{pv1}, B_{FC}, B_L, B_b, and PCC. B_{pv1} had zero reactive power as preset by the inner controller. B_L consumed 0.2 MVar between 2.5 s and 3.5 s when the reactive load was connected. Before and after this time interval the reactive power consumed at B_L was actually at distribution line between B_L and PV sources. A significant amount of reactive power was dispatched to the PCC because it was required for regulating the voltage at B_L. The results are as summarized in Table 4.7.

Figure 4.61 shows the phase-A RMS voltage of buses B_{pv1}, B_{FC}, B_L, B_b, and PCC in configuration 3 case three. Voltages at B_{pv1}, B_L, B_b had similar values during all

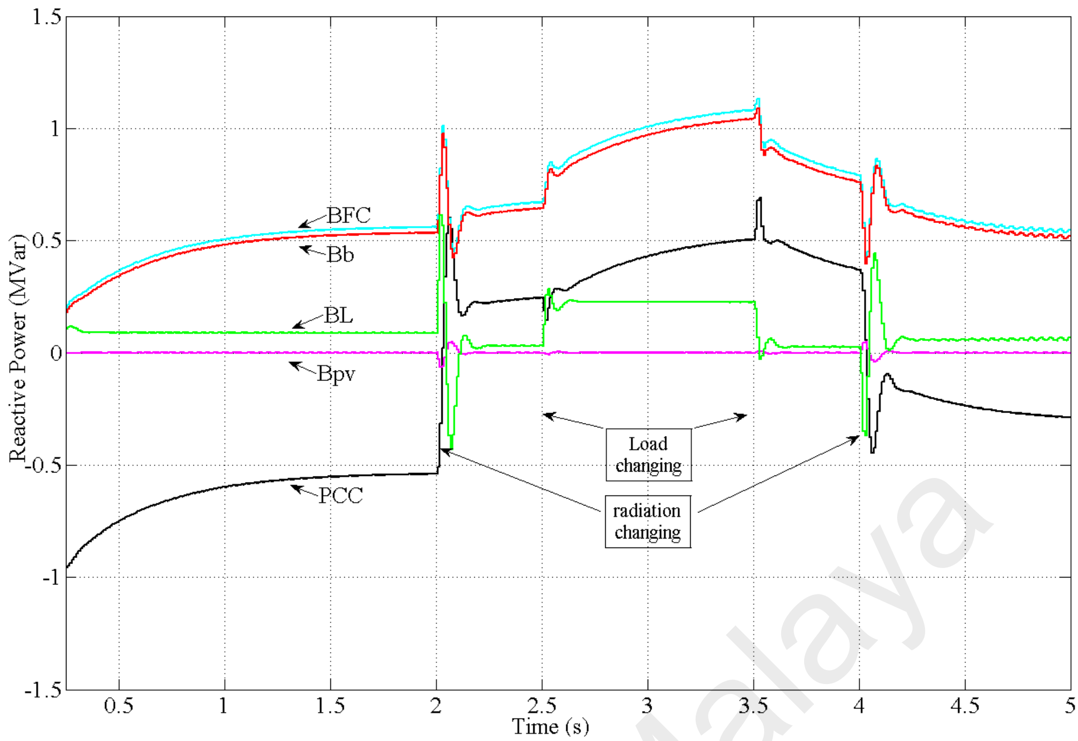

Figure 4.60: Reactive power of buses B_{pv1}, B_{FC}, B_L, B_b, and PCC, in configuration 3 case three.

the disturbances. Voltage at B_{FC} had to be higher than the others to be able to dispatch reactive power and regulate the B_L voltage. The highest voltage difference between B_{FC} and B_L was when the radiation dropped and the load increased. Table 4.7 summarizes the voltage values.

Table 4.7: Summary of the results of configuration 3 case three, (R stands for Radiation)

Item	Initial Value	R Drop	Load Rise	Load Drop	R Rise
P_{pcc}	8.334	5.425	5.048	5.426	7.36
P_{Bpv1}	1.037	0.707	0.709	0.709	0.926
P_{BFC}	1.1	1.1	1.1	1.1	1.1
P_{Bb}	1.098	1.097	1.097	1.097	1.098
P_{BL}	-7.34	-4.38	-3.99	-4.38	-6.35
Q_{pcc}	-0.537	0.247	0.507	0.367	-0.288
Q_{Bpv1}	0	0	0	0	0
Q_{BFC}	0.561	0.672	1.08	0.79	0.535
Q_{Bb}	0.5354	0.644	1.045	0.76	0.51
Q_{BL}	0.088	0.031	0.226	0.026	0.06
V_{pcc}	6323.5	6306	6326.5	6326	6318
V_{Bpv1}	239.1	238.9	238.8	239.6	239.2
V_{BFC}	241.4	241.2	243.6	242.4	241.2
V_{Bb}	238.9	238.2	239	238.9	238.7
V_{BL}	238.9	238.8	238.7	239.6	239

University of Malaya

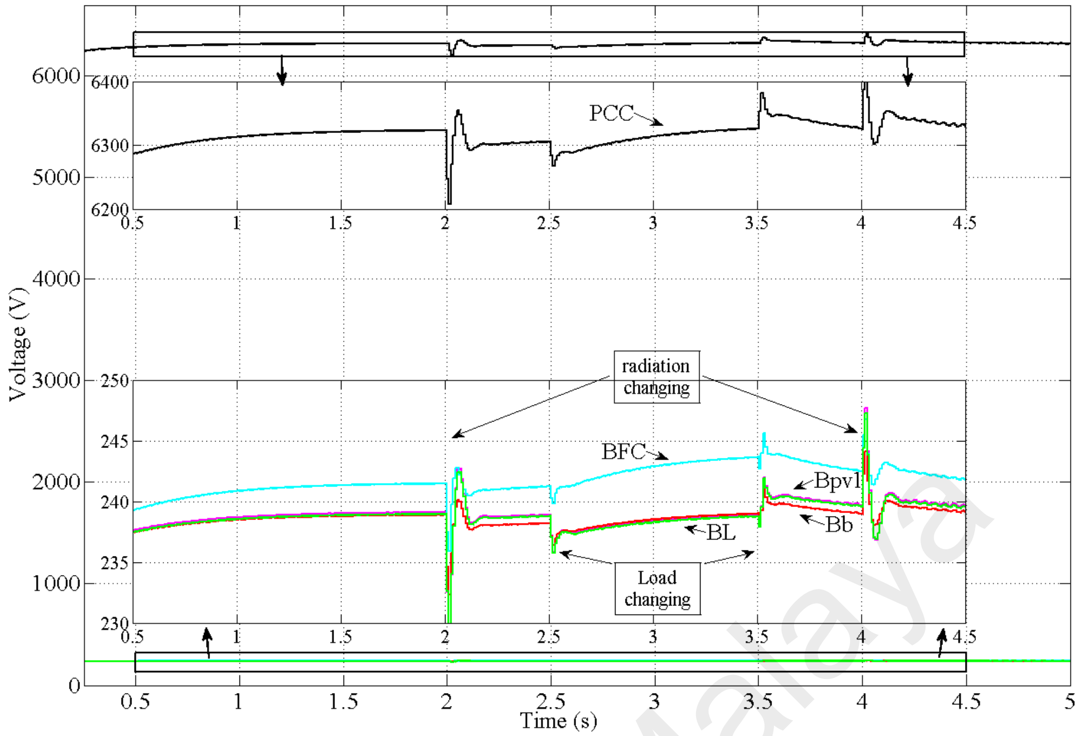

Figure 4.61: Phase-A voltage RMS of buses B_{pv1}, B_{FC}, B_L, B_b, and PCC, in configuration 3 case three.

4.7.2 Case Four: Feeder Removal and Partial Shading

In this case, partial shading occurred at one of the PV sources, owing to variation in the sun radiation (see Table 4.2). FC source feeder (B_{FC}) removed at 1.5 s resulted in zero active and reactive powers. Figure 4.62 depicts active power of buses B_{pv1}, B_{FC}, B_L, B_b, and PCC in configuration 3 case four. A significant drop in the power occurred at 1.5 s at B_{FC}, B_b, and PCC owing to feeder removal. At 2 s and 4 s minor drop occurred in the PCC and B_{pv1} upon the partial shading of one of the PV sources. The power at B_b equaled that at B_{FC} because the PV source was connected directly to B_L and not to B_b as in the previous configurations. Table 4.7 summarizes the active power values of all the buses.

Figure 4.63 shows the reactive powers of buses B_{pv1}, B_{FC}, B_L, B_b, and PCC in configuration 3 case four. B_{pv1} and B_L had zero reactive power. B_L consumed 0.17 MVar owing to the inductance of distribution line between B_L and B_{pv1}. Before the feeder removal at 1.5 s, B_{FC} dispatched reactive power to regulate the voltage at B_L. Upon

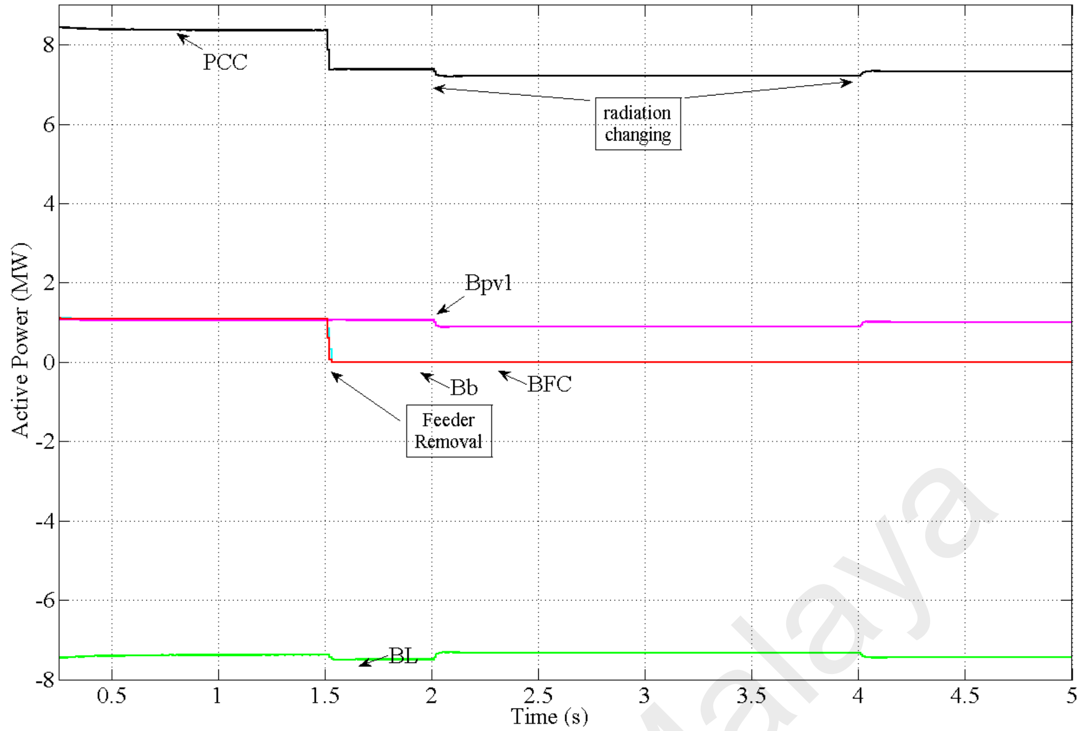

Figure 4.62: Active power of buses B_{pv1}, B_{FC}, B_L, B_b, and PCC, in configuration 3 case four.

B_{FC} removal, the reactive power at B_{FC} and B_b dropped to zero whereas some reactive power continued being imported from PCC to supply the reactive power required at the distribution lines and transformer. Table 4.8 summarizes the reactive power values of all the buses.

Figure 4.64 shows the phase-A RMS voltage of buses B_{pv1}, B_{FC}, B_L, B_b, and PCC in configuration 3 case four. The initial values of the voltages at B_{pv1}, B_L, B_b were similar and close to 239 V. When B_{FC} was removed, the voltage regulator disconnected, thus the voltages dropped to values close to 232 V. Since the disturbances were minor at B_{pv1} owing to the partial shading, the voltage at B_{pv1}, B_L, B_b remained stable around 232 V. A drop occurred in the PCC voltage owing to the feeder removal at 1.5 s. Table 4.8 summarizes the voltage values of all the buses. In configuration 3, owing to the longer distance between B_{FC} and B_L, reactive power and voltage in case three and case four depict a slow response as shown in Figures. 4.60, 4.61, 4.63, and 4.64.

University of Malaya

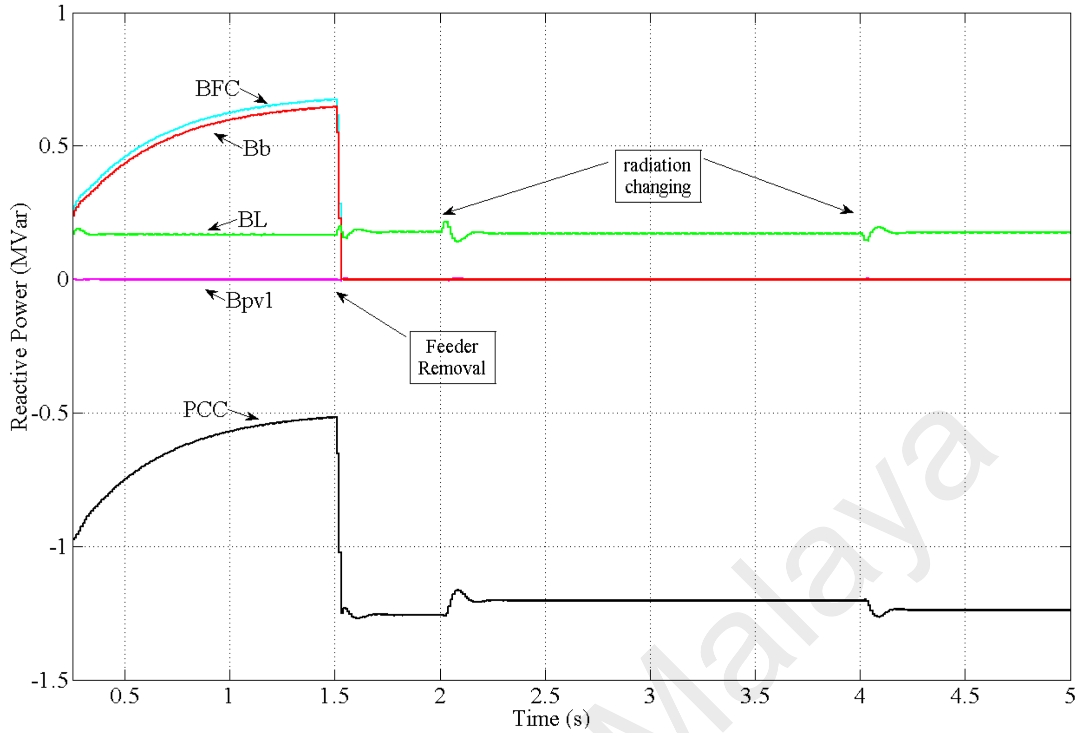

Figure 4.63: Reactive power of buses B_{pv1}, B_{FC}, B_L, B_b, and PCC, in configuration 3 case four.

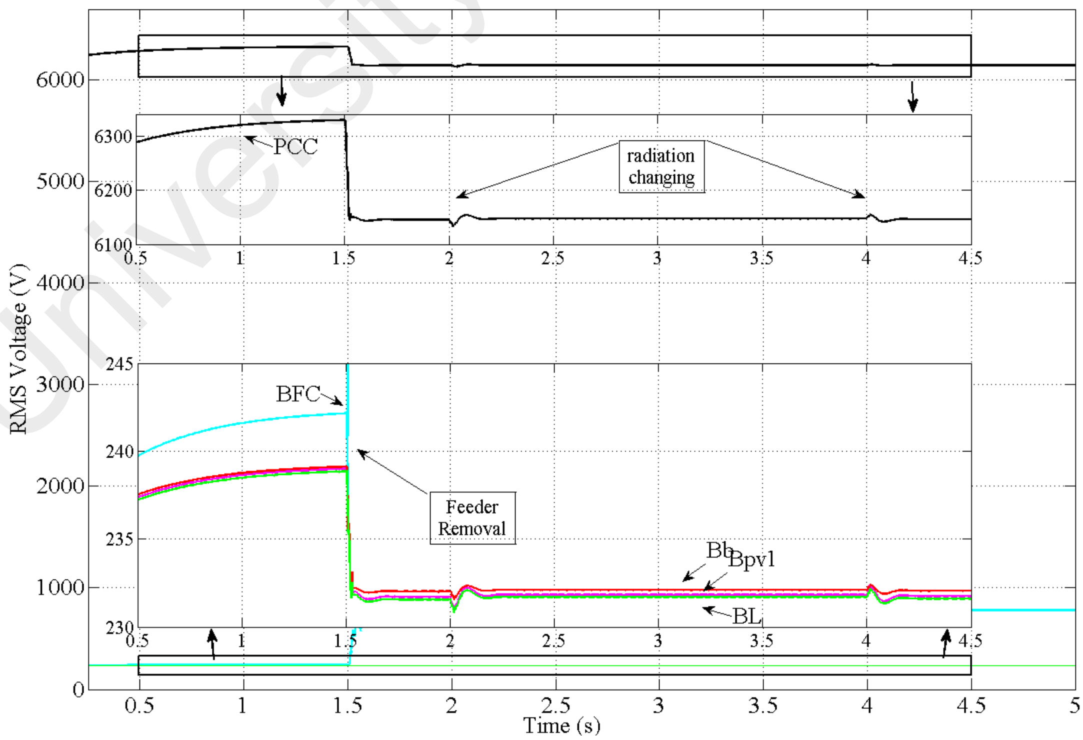

Figure 4.64: Phase-A RMS voltage of buses B_{pv1}, B_{FC}, B_L, B_b, and PCC, in configuration 3 case four.

Table 4.8: Summary of the results of configuration 3 case four, (R stands for Radiation)

Item	Initial Value	Feeder Removal	Partial R Drop	Partial R Rise
P_{pcc}	8.365	7.384	7.22	7.33
P_{Bpv}	1.067	1.067	0.902	1.0122
P_{BFC}	1.1	0	0	0
P_{Bb}	1.098	0	0	0
P_{BL}	-7.37	-7.494	-7.326	-7.438
Q_{pcc}	-0.515	-1.257	-1.203	-1.239
Q_{Bpv}	0	0	0	0
Q_{BFC}	0.674	0	0	0
Q_{Bb}	0.646	0	0	0
Q_{BL}	0.167	0.178	0.172	0.176
V_{pcc}	6329.1	6145.2	6147.2	6145.9
V_{Bpv}	239	231.7	231.84	231.75
V_{BFC}	242.14	781	781	781
V_{Bb}	239.1	232.02	232.1	232.05
V_{BL}	238.85	231.54	231.7	231.6

4.8 Result Comparison and Discussion

The results are summarized in this section. Each configuration has been investigated for four cases, one and three has same disturbances whereas two and four as same disturbances. Case one same as case 3 had five stages organized as follows: normal operation, upon radiation drop, upon load increase, upon load decrease, and upon radiation increase. Case two same as case four has four stages arranged as follows: normal operation, upon feeder removal, upon partial shading at one PV source and when partial shading had passed.

Figure 4.65 shows the active power at PCC in configurations 1, 2 and 3. The power dispatched to the grid from configuration 1 is the highest at normal operation. While the configuration 3 has the highest power dispatching at low radiation and high load.

Figure 4.66 illustrates the RMS voltage at phase-A in buses PCC and B_L, all the configurations has the same voltages at bus B_L, whereas at PCC bus the highest voltage is at configuration 1 and the lowest one is configuration 3.

Figure 4.67 shows the reactive power at PCC and B_{FC} in configurations 1, 2 and

University of Malaya

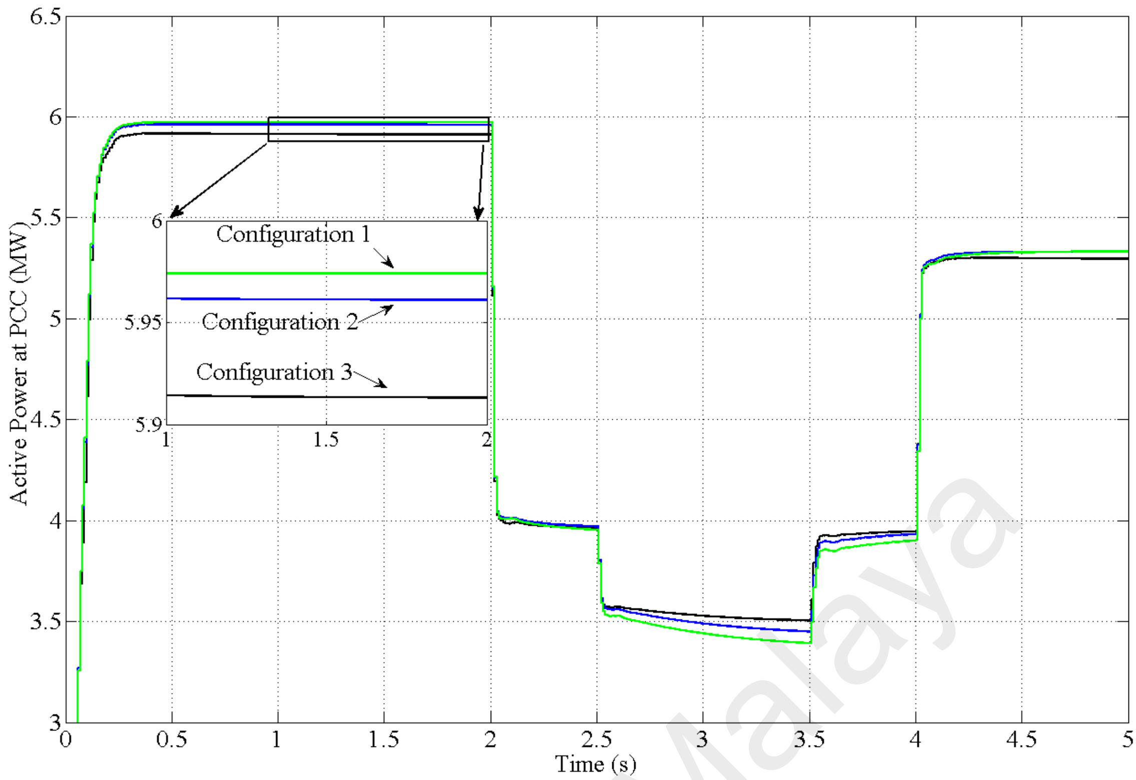

Figure 4.65: Active power at PCC in configurations 1, 2 and 3.

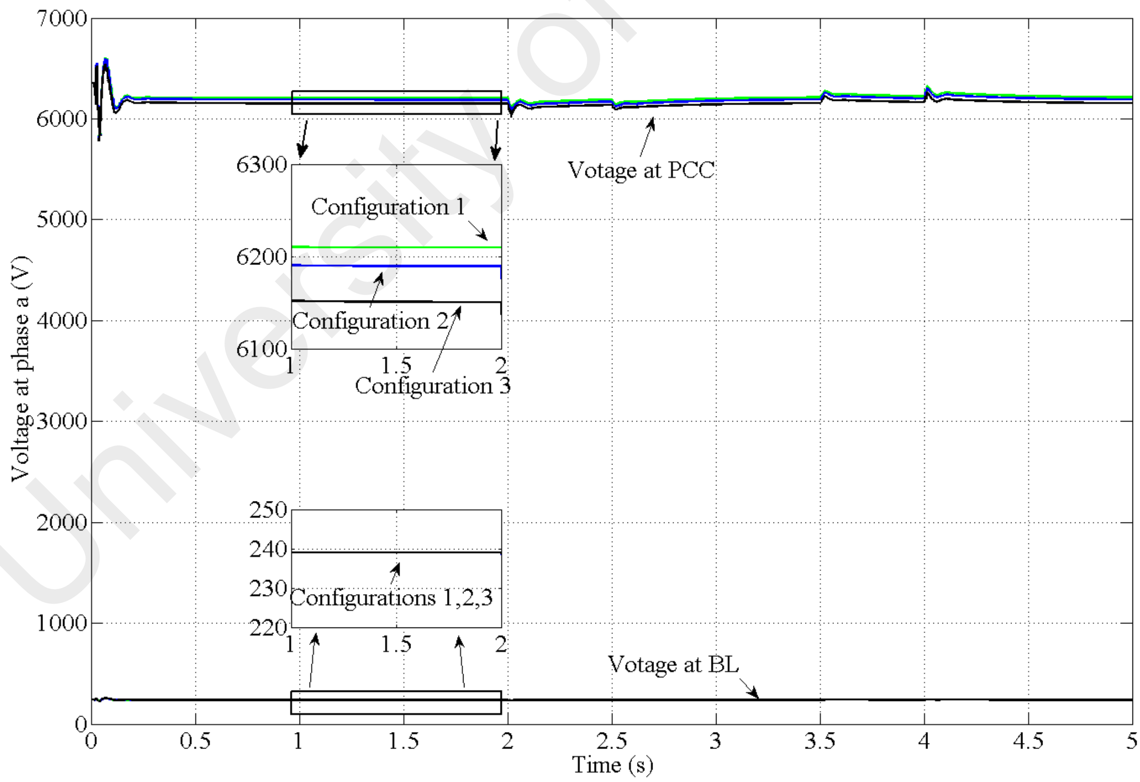

Figure 4.66: RMS voltage at phase-A of buses PCC and B_L in configurations 1, two and 3.

3. For all configurations reactive power in B_{FC} is higher than at PCC. In all graphs the highest injected reactive power is between 2.5 (s) and 3.5 (s).

University of Malaya

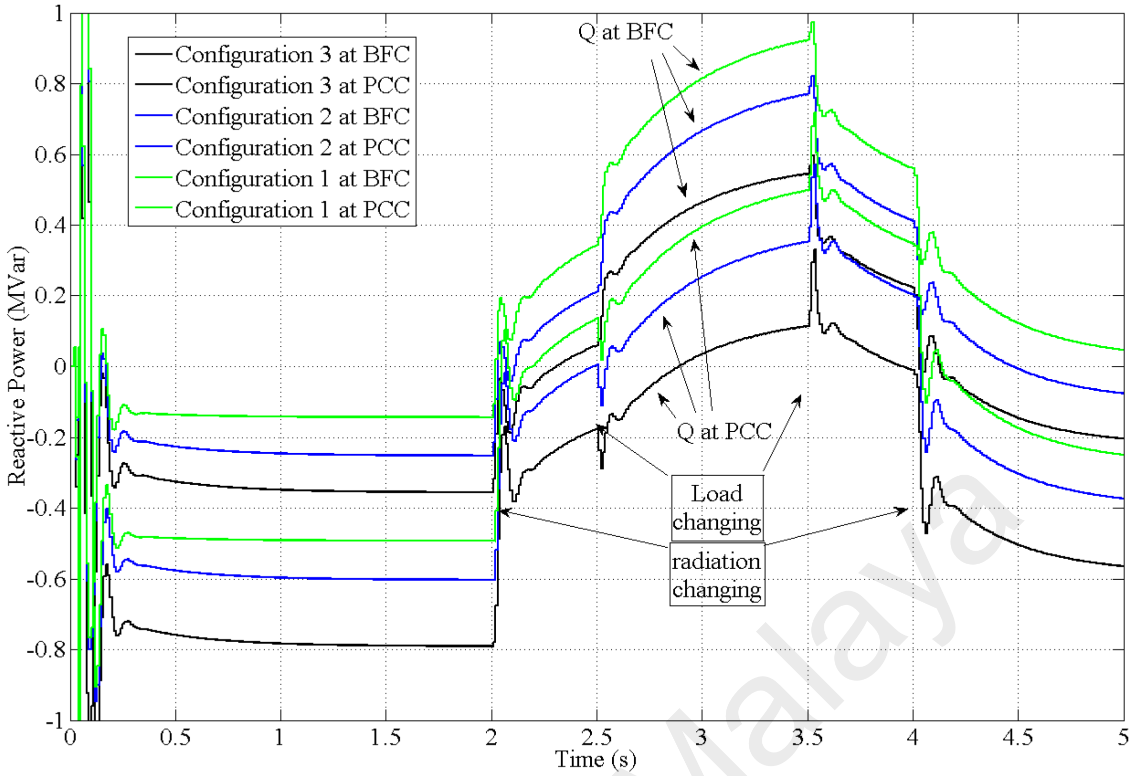

Figure 4.67: Reactive power at PCC and B_{FC} in configurations 1, 2 and 3.

Figure 4.68 compares the reactive power losses of the three configurations in first group of disturbances (case one and three). The highest circulating reactive power was in configuration 3 owing to the longer distance between B_{FC} (the reactive power producer bus) and B_L (where voltage regulation was required). For the same reason, Q loss occurred in configuration 3 for second group of disturbances (case two and four) as shown in Figure 4.69. In general, the Q loss in second group of disturbances was higher because of the higher Q produced without any radiation drop.

Figure 4.70 shows the RMS voltage at B_L for second group of disturbances across the three configurations and the four stages. Upon B_{FC} removal during stages 2 to 4, the voltage dropped slightly in configurations 1 and 2, but significantly in configuration 3 because the dispatched reactive power was significantly higher as shown in Figure 4.69.

Figure 4.71 shows the reactive power exported to the grid in first group of disturbances for the five stages. In stage 1 and true for all the three configurations, the microgrid absorbed reactive power from the grid. In stages 2, 3, and 4 when the radiation

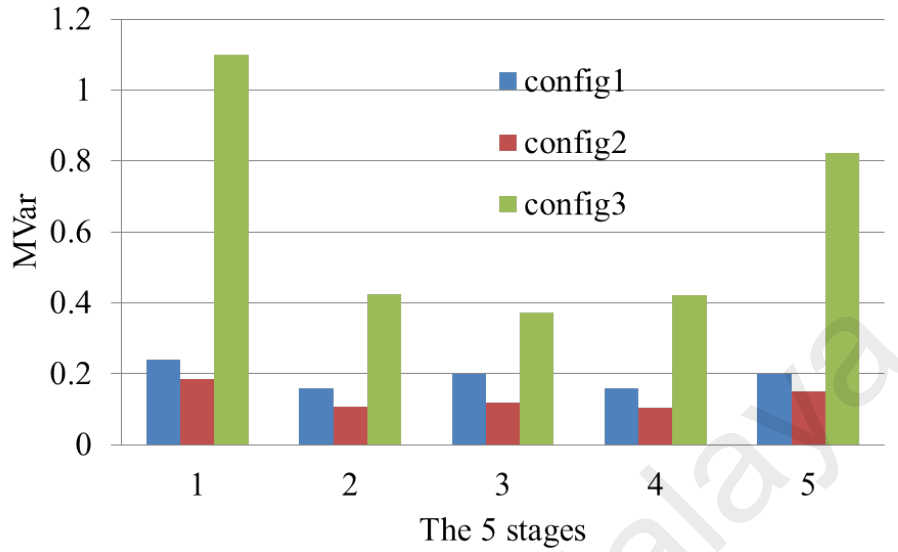

Figure 4.68: Reactive power consumed as loss in the microgrid; all three configurations, first group of disturbances.

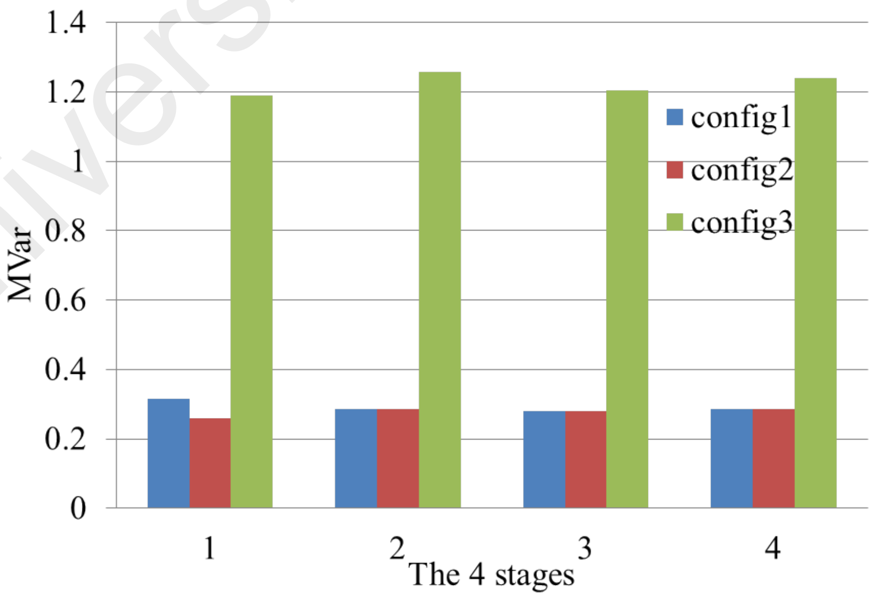

Figure 4.69: Reactive power losses in second group of disturbances across the three configurations.

University of Malaya

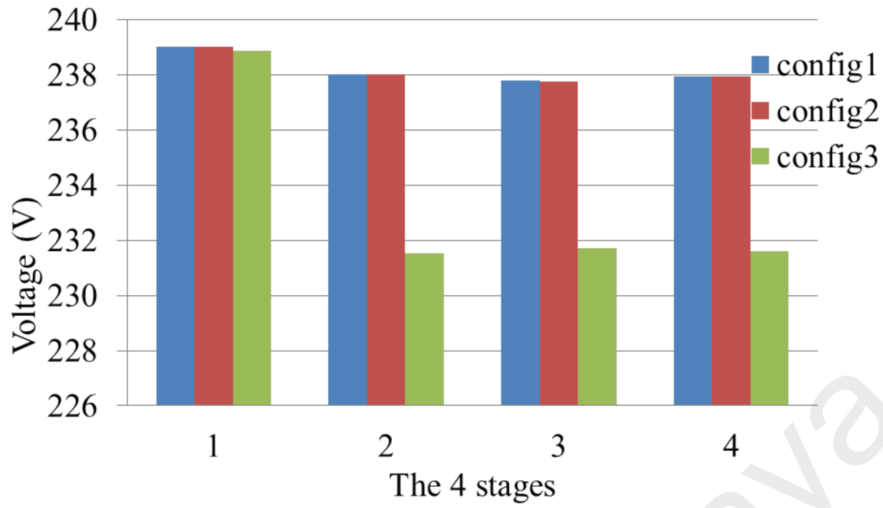

Figure 4.70: RMS Voltage at B_L for second group of disturbances across the three configurations.

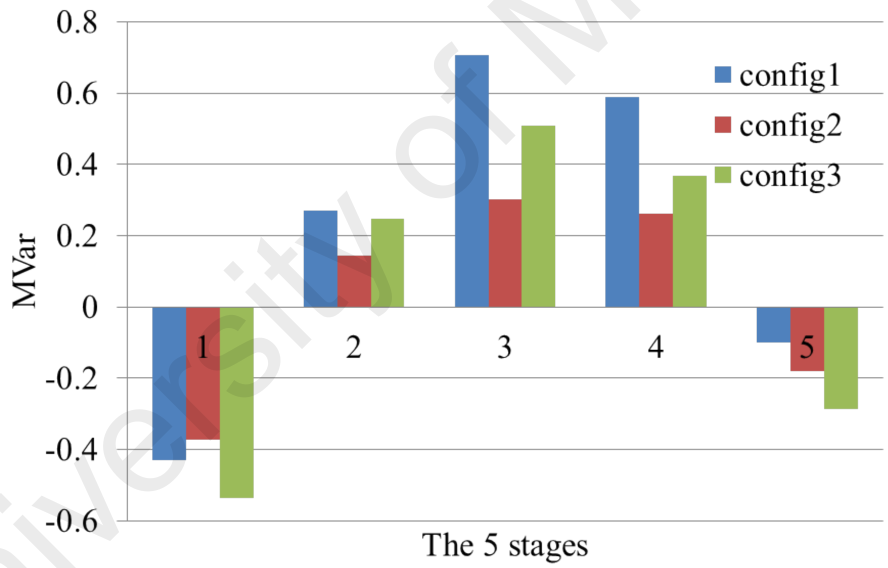

Figure 4.71: Reactive power exported to the grid (PCC); all three configurations, first group of disturbances.

University of Malaya

reduced, the microgrid exported reactive power to the grid. In all the stages the reactive power imported/exported to the grid was least in configuration 2, owing to the connection of the FC source to B_L.

Figure 4.72 shows the reactive power dispatched from B_{FC} in the three configurations (first group of disturbances for the five stages). The highest reactive power was in configuration 3 whereas the lowest was in configuration 2. The distance between B_{FC}

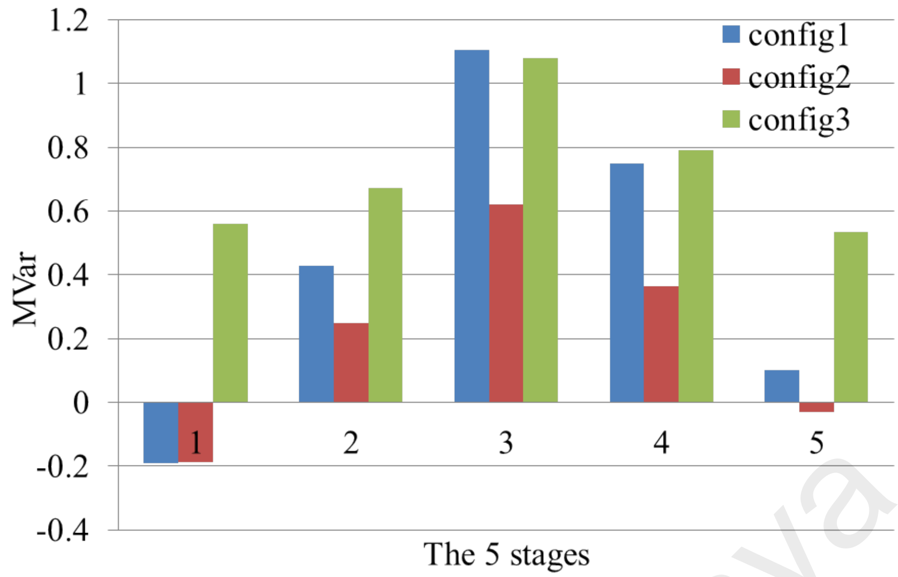

Figure 4.72: Reactive power dispatched from B_{FC} in the three configurations, first group of disturbances.

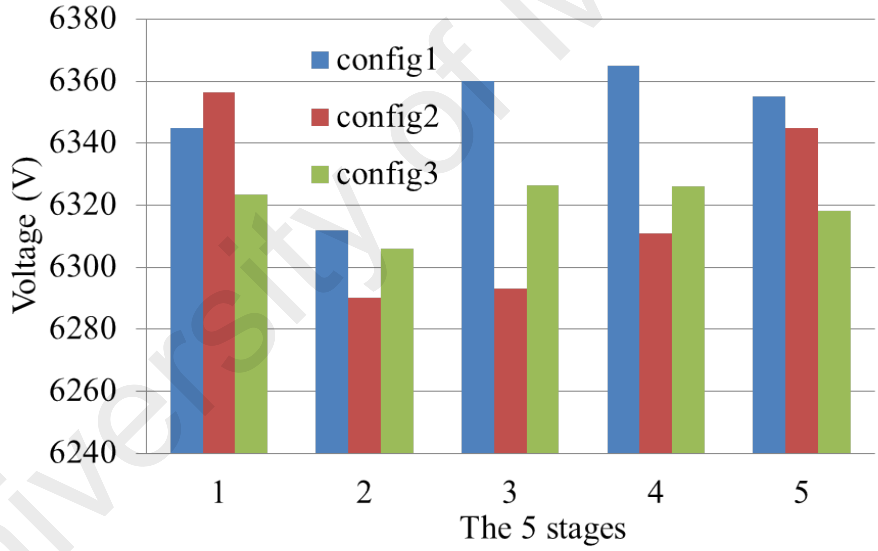

Figure 4.73: RMS Voltage at PCC, first group of disturbances all three configurations.

and B_L played a main role in determining the amount of reactive power.

Figure 4.73 shows the RMS voltage at the PCC: first group of disturbances in all three configurations. The closest voltage to the rated value (6350 V) in all the stages occurred in configuration 1, so this is the configuration with less disturbance on the grid side (the PCC).

Figure 4.74 shows the RMS voltage at B_L in the all configurations and the five stages.

University of Malaya

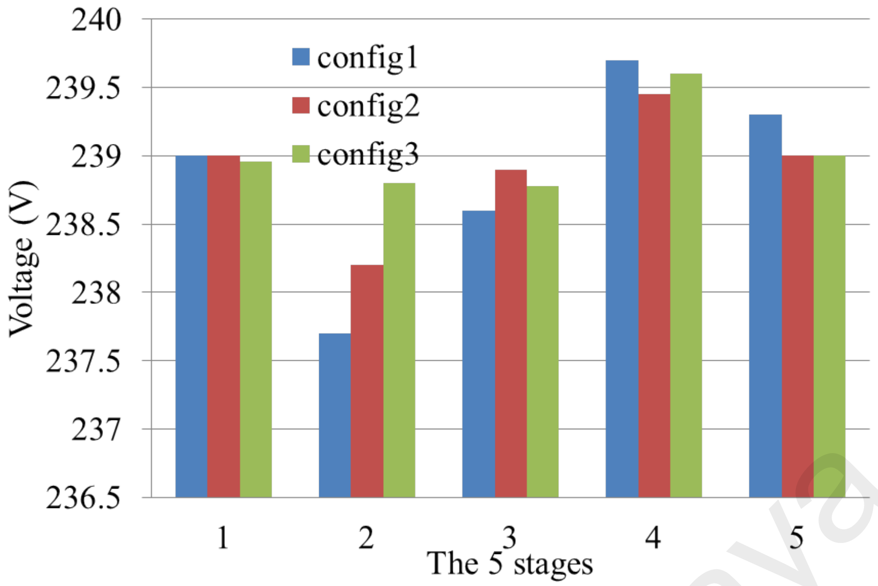

Figure 4.74: RMS Voltage at load, first group of disturbances all three configurations.

The voltage regulator worked properly in all the configurations. Configuration 1 required more time to reach steady state.

The penetration of large-scale renewable DERs into power systems have been studied in this work. A single-stage power conversion system is proposed to convert the DC to AC, due to it's simplicity and efficiency. The combination between PV and FC sources demonstrated a good combination in terms of voltage stability and reactive power dispatching flexibility. Many factors affect the power management network stability, such as the microgrid configuration, distance between the sources and the PCC, and the ambient disturbances. The power management strategies implemented in this work revealed the importance of power management for the microgrid and showed how the robust power management is able to regulate the voltage and increase/decrease the circulating reactive power in the microgrid.

University of Malaya

4.8.1 Point of Microgrid Connection

The electrical power system lines and buses have different voltage profiles and active and reactive power flows. To connect a microgrid system to a grid, the critical lines and buses have to be specified. Microgrid connection to a properly chosen bus reduces the total power losses of the grid and increases the grid stability. The standard IEEE 30-bus test system represents the grid, as many previous works show (Zabaiou et al., 2014). This study considers the standard IEEE 30-bus test system for the connection of the proposed microgrid (see Figure 4.75). The IEEE test system bus and line data are shown in appendix 5.2 (Saadat, 2002). The system's total loss is 16.394 MW 16.560 MVar. An investigation by (Zabaiou et al., 2014) shows that the most critical line is the 2-5 line. It also shows the line as having the highest active power loss (2.934 MW). The active and reactive powers from buses 5 to 2 are -79.201 MW 6.15 MVar with 7.922 MVar reactive power loss. This work recommends connecting a microgrid to bus 5 to reduce system power loss and increase stability. The initial active and reactive power values were connected to bus 5 (8.4 MW and -0.429 MVar). Line 2-5 was the most critical line in the system, the line power loss was reduced from 2.934 MW and 7.922 MVar to 2.577 MW and 6.422 MVar by the microgrid connection to bus 5. The integration of the microgrid reduced the total active power loss from 16.394 MW to 15.149 MW and reduced the reactive power from 16.56 MVar to 12.23 MVar through the same calculations shown in (Saadat, 2002).

University of Malaya

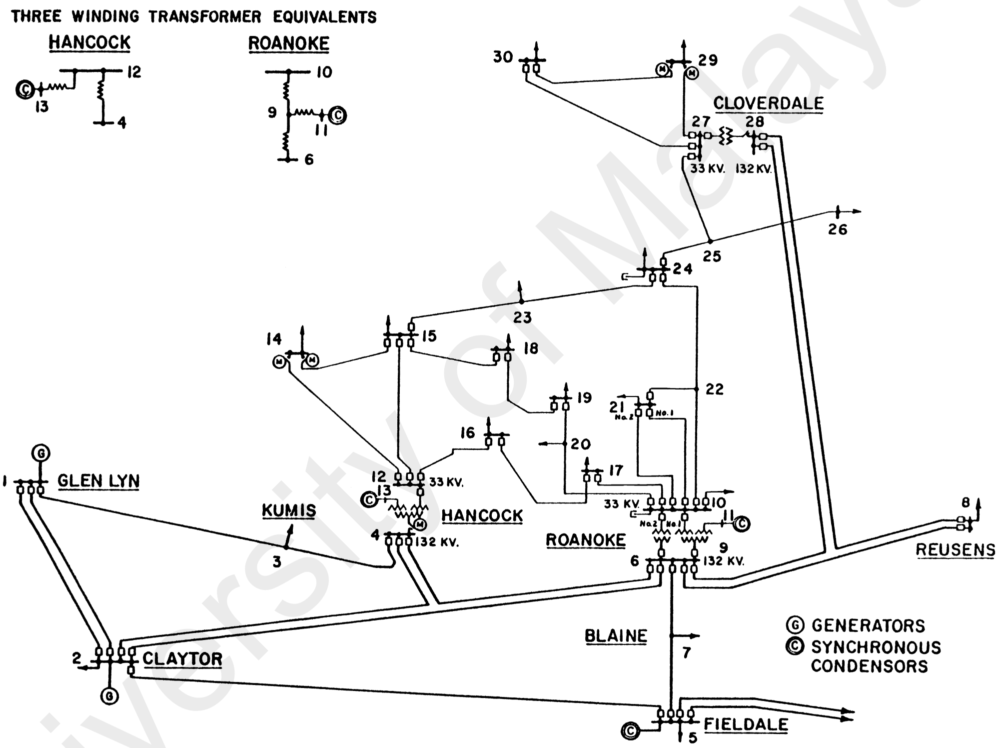

Figure 4.75: IEEE 30-Bus Test System.

University of Malaya

CHAPTER 5: CONCLUSIONS AND FUTURE WORKS

5.1 Conclusions

The microgrid has many attractive features that boost its competitiveness in penetrating the renewable energy market. Microgrid architecture and classifications were reviewed here along with the control techniques and strategies. A robust control for microgrid ensures seamless import/export of active and reactive powers by the grid and continuous supply of the critical load during islanded mode. These lead to a flexible and smart power system. This work examined a single-stage power conversion system. An inverter was the only power conversion component used. Two aims were achieved: MPPT and unity power factor dispatching to the grid. The active power dispatched was higher than that dispatched by a two-stage power conversion system. A dynamic reference voltage was used to extract maximum power from the system. This technique can extract high active power from the PV panel despite variable solar radiation and variable cell temperature. A large-scale PV DER was also studied. The effect of the distance between the PV's DER at B_{inv} and B_b was studied at 10 m, 100 m and 200 m and with variable sun radiation and variable local load. The voltage controller was able to regulate the voltage for a 200 m distance. However for longer distance connecting the DER to an 11 kV distribution network is recommended to prevent high power losses in the distribution line. Three large-scale microgrid configurations were investigated for their effects on distribution networks under the conditions of solar radiation with severe disturbances, load disturbances, feeder removal, and partial shading. Each microgrid, comprised of PV and FC sources with a local load, was connected to a low-voltage distribution network. The microgrids had a control strategy for managing the reactive power generated by the sources which improved the voltage stability of the load bus. One of the three micro-

University of Malaya

grid configurations (configuration 2) showed a fast response and low circulating reactive power during all disturbances. The active power losses were similar in all configurations. This study also revealed how using FC as a dispatchable source can enhance power flow. The voltage regulator implemented in the FC inverter improved the voltage stability at the local load in all three microgrid configurations studied. .

5.2 Future Works

The following future works are possible, consequent to this study: a methodology to define the optimal reactive power references for every PV and FC unit connected to various microgrid configurations, an investigation for unbalance load effects for the different configurations and how reactive power controller can mitigate them. A study of transformer tap changer effect on reducing the reactive power required to regulate voltage, and an investigation into the effect of microgrid connection on all buses of a 30-bus test system.

University of Malaya

REFERENCES

Abusorrah, A., Al-Hindawi, M. M., Al-Turki, Y., Mandal, K., Giaouris, D., Banerjee, S., ... Papadopoulou, S. (2013). Stability of a boost converter fed from photovoltaic source. *Solar Energy*, *98*, 458–471.

Acuna, P. F., Morán, L. A., Weishaupt, C. A., & Dixon, J. W. (n.d.). An active power filter implemented with multilevel single-phase npc converters. In *Iecon 2011-37th annual conference on ieee industrial electronics society* (p. 4367-4372). IEEE.

Ahn, S., Park, J., Chung, I., Moon, S., Kang, S., & Nam, S. (2010). Power-sharing method of multiple distributed generators considering control modes and configurations of a microgrid. *Power Delivery, IEEE Transactions on*, *25*(3), 2007-2016.

Alajmi, B., Ahmed, K., Adam, G., & Williams, B. (2013, June). Single-phase single-stage transformer less grid-connected pv system. *Power Electronics, IEEE Transactions on*, *28*(6), 2664-2676. doi: 10.1109/TPEL.2012.2228280

Alegria, E., Brown, T., Minear, E., & Lasseter, R. H. (2014). Certs microgrid demonstration with large-scale energy storage and renewable generation. *Smart Grid, IEEE Transactions on*, *5*(2), 937–943.

Alsayegh, O., Alhajraf, S., & Albusairi, H. (2010). Grid-connected renewable energy source systems: Challenges and proposed management schemes. *Energy Conversion and Management*, *51*(8), 1690-1693.

Aman, M. M., Jasmon, G. B., Mokhlis, H., & Bakar, A. H. A. (2012). Optimal placement and sizing of a dg based on a new power stability index and line losses. *International Journal of Electrical Power and Energy Systems*, *43*(1), 1296-1304.

Arani, M. F., & Mohamed, Y.-R. (2015). Analysis and impacts of implementing droop control in dfig-based wind turbines on microgrid/weak-grid stability.

Azmi, S. A., Adam, G. P., Ahmed, K. H., Finney, S. J., & Williams, B. W. (2013). Grid interfacing of multimegawatt photovoltaic inverters. *Power Electronics, IEEE Transactions on*, *28*(6), 2770-2784.

Balathandayuthapani, S., Edrington, C., Henry, S., & Cao, J. (2012, June). Analysis and control of a photovoltaic system: Application to a high-penetration case study. *Systems Journal, IEEE*, *6*(2), 213-219. doi: 10.1109/JSYST.2011.2162889

Barklund, E., Pogaku, N., Prodanovic, M., Hernandez-Aramburo, C., & Green, T. C. (2008). Energy management in autonomous microgrid using stability-constrained droop control of inverters. *Power Electronics, IEEE Transactions on*, *23*(5), 2346-2352.

Barsali, S., Ceraolo, M., Pelacchi, P., & Poli, D. (2002). Control techniques of dispersed generators to improve the continuity of electricity supply. In *Power engineering society winter meeting, 2002. ieee* (Vol. 2, p. 789-794). IEEE.

University of Malaya

Bastos, R., Aguiar, C., Goncalves, A., & Machado, R. (2014, Sept). An intelligent control system used to improve energy production from alternative sources with dc/dc integration. *Smart Grid, IEEE Transactions on*, *5*(5), 2486-2495. doi: 10.1109/TSG.2014.2309491

Blaabjerg, F., Chen, Z., & Kjaer, S. (2004). Power electronics as efficient interface in dispersed power generation systems. *Power Electronics, IEEE Transactions on*, *19*(5), 1184-1194.

Bo, Z., Xuesong, Z., & Jian, C. (2012). Integrated microgrid laboratory system. *Power Systems, IEEE Transactions on*, *27*(4), 2175-2185.

Bogart Jr, T. F. (1986). *Electronic devices and circuits.* Merrill Publishing Company.

Borup, U., Blaabjerg, F., & Enjeti, P. N. (2001). Sharing of nonlinear load in parallel-connected three-phase converters. *Industry Applications, IEEE Transactions on*, *37*(6), 1817-1823.

Canada, N. R. (2012). Self-healing grid project. *Natural Resources Canada*.

Carvalho, P. M., Correia, P. F., & Ferreira, L. (2008). Distributed reactive power generation control for voltage rise mitigation in distribution networks. *Power Systems, IEEE Transactions on*, *23*(2), 766-772.

Chandorkar, M., & Divan, D. (1996). Decentralized operation of distributed ups systems. In *Power electronics, drives and energy systems for industrial growth, 1996., proceedings of the 1996 international conference on* (Vol. 1, p. 565-571). IEEE.

Chandorkar, M. C., Divan, D. M., & Adapa, R. (1993). Control of parallel connected inverters in standalone ac supply systems. *Industry Applications, IEEE Transactions on*, *29*(1), 136-143.

Chen, Y.-K., Wu, Y.-E., Wu, T.-F., & Ku, C.-P. (2003). Acss for paralleled multi-inverter systems with dsp-based robust controls. *Aerospace and Electronic Systems, IEEE Transactions on*, *39*(3), 1002–1015.

Chen, Z. (2012). A review of power electronics based microgrids. *Journal of Power Electronics*, *12*(1).

Cheng, P.-T., Chen, C.-A., Lee, T.-L., & Kuo, S.-Y. (2009). A cooperative imbalance compensation method for distributed-generation interface converters. *Industry Applications, IEEE Transactions on*, *45*(2), 805-815.

Cheng, Y. J., & Sng, E. K. K. (2006). A novel communication strategy for decentralized control of paralleled multi-inverter systems. *Power Electronics, IEEE Transactions on*, *21*(1), 148-156.

Chiang, S., Lin, C., & Yen, C. (2004). Current limitation control technique for parallel operation of ups inverters. In *Power electronics specialists conference, 2004. pesc 04. 2004 ieee 35th annual* (Vol. 3, p. 1922-1926). IEEE.

University of Malaya

Chiang, S., Yen, C., & Chang, K. (2001). A multimodule parallelable series-connected pwm voltage regulator. *Industrial Electronics, IEEE Transactions on*, *48*(3), 506-516.

Chong, B., & Zhang, L. (2013). Controller design for integrated pv–converter modules under partial shading conditions. *Solar Energy*, *92*, 123–138.

Chung, I.-Y., Park, S.-W., Kim, H.-J., Moon, S.-I., Han, B.-M., Kim, J.-E., & Choi, J.-H. (2005). Operating strategy and control scheme of premium power supply interconnected with electric power systems. *Power Delivery, IEEE Transactions on*, *20*(3), 2281-2288.

Coelho, E., Cortizo, P., & Garcia, P. (1999). Small signal stability for single phase inverter connected to stiff ac system. In *Industry applications conference, 1999. thirty-fourth ias annual meeting. conference record of the 1999 ieee* (Vol. 4, p. 2180-2187). IEEE.

Colet-Subirachs, A., Ruiz-Alvarez, A., Gomis-Bellmunt, O., Alvarez-Cuevas-Figuerola, F., & Sudria-Andreu, A. (2012). Centralized and distributed active and reactive power control of a utility connected microgrid using iec61850. *Systems Journal, IEEE*, *6*(1), 58-67.

Colson, C., Nehrir, M., & Wang, C. (2008, Sept). Modeling a large-scale utility-interconnected solid oxide fuel cell power plant. In *Power symposium, 2008. naps '08. 40th north american* (p. 1-5). doi: 10.1109/NAPS.2008.5307333

Das, M., & Agarwal, V. (2012). Novel pv fed three phase single power stage system for stand-alone applications. In *Photovoltaic specialists conference (pvsc), 2012 38th ieee* (pp. 001405–001410).

De, D., & Ramanarayanan, V. (2010). Decentralized parallel operation of inverters sharing unbalanced and nonlinear loads. *Power Electronics, IEEE Transactions on*, *25*(12), 3015-3025.

De Brabandere, K., Bolsens, B., Van den Keybus, J., Woyte, A., Driesen, J., & Belmans, R. (2007a). A voltage and frequency droop control method for parallel inverters. *Power Electronics, IEEE Transactions on*, *22*(4).

De Brabandere, K., Bolsens, B., Van den Keybus, J., Woyte, A., Driesen, J., & Belmans, R. (2007b). A voltage and frequency droop control method for parallel inverters. *Power Electronics, IEEE Transactions on*, *22*(4), 1107-1115.

de Brito, M., Sampaio, L., Luigi, G., e Melo, G., & Canesin, C. (2011). Comparative analysis of mppt techniques for pv applications. In *Clean electrical power (iccep), 2011 international conference on* (p. 99-104). doi: 10.1109/ICCEP.2011.6036361

Delghavi, M. B., & Yazdani, A. (2012). A unified control strategy for electronically interfaced distributed energy resources. *Power Delivery, IEEE Transactions on*, *27*(2), 803-812.

Dimeas, A. L., & Hatziargyriou, N. D. (2005). Operation of a multiagent system for microgrid control. *Power Systems, IEEE Transactions on*, *20*(3), 1447-1455.

University of Malaya

Dixon, J., Moran, L., Rodriguez, J., & Domke, R. (2005). Reactive power compensation technologies: state-of-the-art review. *Proceedings of the IEEE*, *93*(12).

Driesen, J., & Katiraei, F. (2008). Design for distributed energy resources. *Power and Energy Magazine, IEEE*, *6*(3), 30-40.

Du, W., Jiang, Q., Erickson, M., & Lasseter, R. (2014, Aug). Voltage-source control of pv inverter in a certs microgrid. *Power Delivery, IEEE Transactions on*, *29*(4), 1726-1734. doi: 10.1109/TPWRD.2014.2302313

Duan, Y., Gong, Y., Li, Q., & Wang, H. (2008). Modelling and simulation of the microsources within a microgrid. In *Electrical machines and systems, 2008. icems 2008. international conference on* (p. 2667-2671).

Eid, B. (2012). Microgird system with multi distributed energy resources using matalb/simulink. In *power and energy conversion symposium pecs2012* (p. 194-196). Fakulti Kejuruteraan Elektrik, Universiti Teknikal Malaysia Melaka Hang Tuah Jaya, 76100 Durian Tunggal, Melaka, Malaysia.

Eid, B., Rahim, N., & Selvaraj, J. (2013, Nov). Distributed photovoltaic generator performing reactive power compensation. In *Clean energy and technology (ceat), 2013 ieee conference on* (p. 38-41). doi: 10.1109/CEAT.2013.6775596

Eid, B., Rahim, N., Selvaraj, J., & El Khateb, A. (2014). Control methods and objectives for electronically coupled distributed energy resources in microgrids: A review. *Systems Journal, IEEE*, *PP*(99), 1-13. doi: 10.1109/JSYST.2013.2296075

El Khateb, A., Rahim, N., Selvaraj, J., & Uddin, M. (2014). Fuzzy logic controller based sepic converter for maximum power point tracking. *Industry Applications, IEEE Transactions on*, *PP*(99), 1-1. doi: 10.1109/TIA.2014.2298558

El Khateb, A., Rahim, N. A., Selvaraj, J., & Uddin, M. N. (2013). Maximum power point tracking of single-ended primary-inductor converter employing a novel optimisation technique for proportional-integral-derivative controller. *IET Power Electronics*, *6*(6), 1111-1121.

Elsied, M., Oukaour, A., Gualous, H., & Hassan, R. (2015). Energy management and optimization in microgrid system based on green energy. *Energy*, *84*, 139–151.

Engler, A. (2005). Applicability of droops in low voltage grids. *International Journal of Distributed Energy Resources*, *1*(1), 3-15.

Farhangi, H. (2010, January). The path of the smart grid. *Power and Energy Magazine, IEEE*, *8*(1), 18-28. doi: 10.1109/MPE.2009.934876

Georgakis, D., Papathanassiou, S., Hatziargyriou, N., Engler, A., & Hardt, C. (2004). Operation of a prototype microgrid system based on micro-sources quipped with fast-acting power electronics interfaces. In *Power electronics specialists conference, 2004. pesc 04. 2004 ieee 35th annual* (Vol. 4, p. 2521-2526 Vol.4).

Green, T. C., & Prodanović, M. (2007). Control of inverter-based micro-grids. *Electric*

University of Malaya

Power Systems Research, *77*(9), 1204-1213.

Guerrero, J., de Vicuña, L., Matas, J., Castilla, M., & Miret, J. (2004). A wireless controller to enhance dynamic performance of parallel inverters in distributed generation systems. *Power Electronics, IEEE Transactions on*, *19*(5), 1205-1213.

Guerrero, J., Matas, J., de Vicuña, L., Castilla, M., & Miret, J. (2007). Decentralized control for parallel operation of distributed generation inverters using resistive output impedance. *Industrial Electronics, IEEE Transactions on*, *54*(2), 994-1004.

Guerrero, J., Matas, J., De Vicuna, L., Berbel, N., & Sosa, J. (2005). Wireless-control strategy for parallel operation of distributed generation inverters. In *Industrial electronics, 2005. isie 2005. proceedings of the ieee international symposium on* (Vol. 2, p. 845-850). IEEE.

Guerrero, J., Vasquez, J., Matas, J., Castilla, M., & de Vicuna, L. (2009). Control strategy for flexible microgrid based on parallel line-interactive ups systems. *Industrial Electronics, IEEE Transactions on*, *56*(3), 726-736.

Guerrero, J., Vasquez, J., Matas, J., de Vicuña, L., & Castilla, M. (2011). Hierarchical control of droop-controlled ac and dc microgrids—a general approach toward standardization. *Industrial Electronics, IEEE Transactions on*, *58*(1), 158-172.

Guerrero, J. M., GarciadeVicuna, L., Matas, J., Castilla, M., & Miret, J. (2005). Output impedance design of parallel-connected ups inverters with wireless load-sharing control. *Industrial Electronics, IEEE Transactions on*, *52*(4).

Guerrero, J. M., Hang, L., & Uceda, J. (2008). Control of distributed uninterruptible power supply systems. *Industrial Electronics, IEEE Transactions on*, *55*(8), 2845-2859.

Gurrero, J., De Vicuna, L. G., & Uceda, J. (2007). Uninterruptible power supply systems provide protection. *Industrial Electronics Magazine, IEEE*, *1*(1), 28-38.

Hanaoka, H., Nagai, M., & Yanagisawa, M. (2003). Development of a novel parallel redundant ups. In *Telecommunications energy conference, 2003. intelec'03. the 25th international* (p. 493-498). IEEE.

Hatziargyriou, N., Dimeas, A., Tsikalakis, A., Lopes, J., Karniotakis, G., & Oyarzabal, J. (2005). Management of microgrids in market environment. In *Future power systems, 2005 international conference on* (p. 7 pp.-7). IEEE.

Hatziargyriou, N. D., & Sakis Meliopoulos, A. P. (2002). Distributed energy sources: technical challenges. In *Power engineering society winter meeting, 2002. ieee* (Vol. 2, p. 1017-1022 vol.2).

He, Z., Xing, Y., & Hu, Y. (2004). Low cost compound current sharing control for inverters in parallel operation. In *Power electronics specialists conference, 2004. pesc 04. 2004 ieee 35th annual* (Vol. 1, p. 222-227). IEEE.

Hien, N. C., Mithulananthan, N., & Bansal, R. C. (2013). Location and sizing of dis-

University of Malaya

tributed generation units for loadabilty enhancement in primary feeder. *IEEE Systems Journal*, *7*(4), 797–806.

Holtz, J., Lotzkat, W., & Werner, K.-H. (1988). A high-power multitransistor-inverter uninterruptable power supply system. *Power Electronics, IEEE Transactions on*, *3*(3), 278-285.

Holtz, J., & Werner, K.-H. (1990). Multi-inverter ups system with redundant load sharing control. *Industrial Electronics, IEEE Transactions on*, *37*(6), 506-513.

Hong, T., & De Leon, F. (2015). A reconfigurable auto-loop micro-grid.

Hua, C.-C., Liao, K.-A., & Lin, J.-R. (2002). Parallel operation of inverters for distributed photovoltaic power supply system. In *Power electronics specialists conference, 2002. pesc 02. 2002 ieee 33rd annual* (Vol. 4, p. 1979-1983). IEEE.

Hussein, K., Muta, I., Hoshino, T., & Osakada, M. (1995, Jan). Maximum photovoltaic power tracking: an algorithm for rapidly changing atmospheric conditions. *Generation, Transmission and Distribution, IEE Proceedings-*, *142*(1), 59-64. doi: 10.1049/ip-gtd:19951577

Ito, Y., & Iyama, O. (1997). Parallel redundant operation of ups with robust current minor loop. In *Power conversion conference-nagaoka 1997., proceedings of the* (Vol. 1, p. 489-494). IEEE.

Iwade, T., Komiyama, S., Tanimura, Y., Yamanaka, M., Sakane, M., & Hirachi, K. (2003). A novel small-scale ups using a parallel redundant operation system. In *Telecommunications energy conference, 2003. intelec'03. the 25th international* (p. 480-484). IEEE.

Jang, M., & Agelidis, V. (2011, May). A minimum power-processing-stage fuel-cell energy system based on a boost-inverter with a bidirectional backup battery storage. *Power Electronics, IEEE Transactions on*, *26*(5), 1568-1577. doi: 10.1109/TPEL.2010.2086490

Jiayi, H., Chuanwen, J., & Rong, X. (2008). A review on distributed energy resources and microgrid. *Renewable and Sustainable Energy Reviews*, *12*(9), 2472-2483.

Kadri, R., Gaubert, J.-P., & Champenois, G. (2011). An improved maximum power point tracking for photovoltaic grid-connected inverter based on voltage-oriented control. *Industrial Electronics, IEEE Transactions on*, *58*(1), 66–75.

Kakigano, H., Miura, Y., Ise, T., & Uchida, R. (2006). Dc micro-grid for super high quality distribution—system configuration and control of distributed generations and energy storage devices—. In *Power electronics specialists conference, 2006. pesc'06. 37th ieee* (p. 1-7). IEEE.

Kamel, R. M., Chaouachi, A., & Nagasaka, K. (2011). Enhancement of micro-grid performance during islanding mode using storage batteries and new fuzzy logic pitch angle controller. *Energy Conversion and Management*, *52*(5).

University of Malaya

Katiraei, F., & Iravani, M. R. (2006). Power management strategies for a microgrid with multiple distributed generation units. *Power Systems, IEEE Transactions on*, *21*(4).

Katiraei, F., Iravani, R., Hatziargyriou, N., & Dimeas, A. (2008). Microgrids management. *Power and Energy Magazine, IEEE*, *6*(3).

Khanh, L. N., Seo, J.-J., Kim, Y.-S., & Won, D.-J. (2010). Power-management strategies for a grid-connected pv-fc hybrid system. *Power Delivery, IEEE Transactions on*, *25*(3), 1874–1882.

Khosrow Moslehi, R. K. (2006). vision for a self-healing power grid. *ABB Review*.

Kim, H., Yu, T., & Choi, S. (2008). Indirect current control algorithm for utility interactive inverters in distributed generation systems. *Power Electronics, IEEE Transactions on*, *23*(3).

Kish, G., Lee, J., & Lehn, P. (2012, July). Modelling and control of photovoltaic panels utilising the incremental conductance method for maximum power point tracking. *Renewable Power Generation, IET*, *6*(4), 259-266. doi: 10.1049/iet-rpg.2011.0052

Knazkins, V. (2004). *Stability of power systems with large amounts of distributed generation* (Unpublished doctoral dissertation).

Koohi-Kamali, S., Rahim, N., & Mokhlis, H. (2014). Smart power management algorithm in microgrid consisting of photovoltaic, diesel, and battery storage plants considering variations in sunlight, temperature, and load. *Energy Conversion and Management*, *84*, 562–582.

Kroposki, B., Lasseter, R., Ise, T., Morozumi, S., Papatlianassiou, S., & Hatziargyriou, N. (2008). Making microgrids work. *Power and Energy Magazine, IEEE*, *6*(3).

Lasseter, R., & Piagi, P. (2006). Control and design of microgrid components. *PSERC Publication 06*, *3*.

Lasseter, R. H. (2002). Microgrids. In *Power engineering society winter meeting, 2002. ieee* (Vol. 1, p. 305-308). IEEE.

Lasseter, R. H. (2011). Smart distribution: Coupled microgrids. *Proceedings of the IEEE*, *99*(6).

Lee, C., Kim, S., Kim, C., Hong, S., Yoo, J., Kim, S., ... Sun, S. (1998). Parallel ups with a instantaneous current sharing control. In *Industrial electronics society, 1998. iecon'98. proceedings of the 24th annual conference of the ieee* (Vol. 1, p. 568-573). IEEE.

Li, S., Gao, X., Wang, L., & Liu, S. (2013). A novel maximum power point tracking control method with variable weather parameters for photovoltaic systems. *Solar Energy*, *97*, 529–536.

Lopes, J., Hatziargyriou, N., Mutale, J., Djapic, P., & Jenkins, N. (2007). Integrating distributed generation into electric power systems: A review of drivers, challenges

University of Malaya

and opportunities. *Electric Power Systems Research*, *77*(9).

Lopes, J. A. P., Moreira, C. L., & Madureira, A. G. (2006). Defining control strategies for microgrids islanded operation. *Power Systems, IEEE Transactions on*, *21*(2).

Madureira, A., Moreira, C., & Lopes, J. P. (2005). Secondary load-frequency control for microgrids in islanded operation. In *Proc. international conference on renewable energy and power quality icrepq '05, spain.*

Mao, M., Liuchen, C., & Ding, M. (2008). Integration and intelligent control of micro-grids with multi-energy generations: A review. In *Sustainable energy technologies, 2008. icset 2008. ieee international conference on* (p. 777-780).

Marei, M. I. (2012). A unified control strategy based on phase angle estimation for matrix converter interface system. *Systems Journal, IEEE*, *6*(2).

Martins, A. P., Carvalho, A. S., & Araujo, A. (1995). Design and implementation of a current controller for the parallel operation of standard upss. In *Industrial electronics, control, and instrumentation, 1995., proceedings of the 1995 ieee iecon 21st international conference on* (Vol. 1, p. 584-589). IEEE.

Marwali, M. N., Jung, J.-W., & Keyhani, A. (2004). Control of distributed generation systems-part ii: Load sharing control. *Power Electronics, IEEE Transactions on*, *19*(6).

Masters, C. (2002). Voltage rise: the big issue when connecting embedded generation to long 11 kv overhead lines. *Power Engineering Journal*, *16*(1).

Mazumder, S. K., Tahir, M., & Acharya, K. (2008). Master–slave current-sharing control of a parallel dc–dc converter system over an rf communication interface. *Industrial Electronics, IEEE Transactions on*, *55*(1).

Mehta, G., & Singh, S. (2013). Electrical engineering department, indian institute of technology, roorkee, india. In *Photovoltaic specialists conference (pvsc), 2013 ieee 39th* (pp. 3147–3152).

Mihalache, L. (2003). Paralleling control technique with no intercommunication signals for resonant controller-based inverters. In *Industry applications conference, 2003. 38th ias annual meeting. conference record of the* (Vol. 3, p. 1882-1889). IEEE.

Mikati, M., Santos, M., & Armenta, C. (2013). Electric grid dependence on the configuration of a small-scale wind and solar power hybrid system. *Renewable Energy*, *57*, 587–593.

Mirhosseini, M., Agelidis, V. G., & Ravishankar, J. (2012). Modelling of large-scale grid-connected photovoltaic systems: Static grid support by reactive power control. In *Power engineering society conference and exposition in africa (powerafrica), 2012 ieee* (pp. 1–8).

Miveh, M. R., Mirsaeidi, S., & Gandomkar, M. (2012). Fundamental key issues and analysis of symmetrical current components in micro-grids.

University of Malaya

Moreira, C., Resende, F., & Peas Lopes, J. (2007). Using low voltage microgrids for service restoration. *Power Systems, IEEE Transactions on*, *22*(1), 395–403.

Norton, B., Eames, P. C., Mallick, T. K., Huang, M. J., McCormack, S. J., Mondol, J. D., & Yohanis, Y. G. (2011). Enhancing the performance of building integrated photovoltaics. *Solar Energy*, *85*(8), 1629–1664.

Ozdemir, S., Altin, N., & Sefa, I. (2014). Single stage three level grid interactive {MPPT} inverter for {PV} systems. *Energy Conversion and Management*, *80*(0), 561 - 572. doi: http://dx.doi.org/10.1016/j.enconman.2014.01.048

Pei, Y., Jiang, G., Yang, X., & Wang, Z. (2004). Auto-master-slave control technique of parallel inverters in distributed ac power systems and ups. In *Power electronics specialists conference, 2004. pesc 04. 2004 ieee 35th annual* (Vol. 3, p. 2050-2053). IEEE.

Peng, F., Li, Y., & Tolbert, L. (2009). Control and protection of power electronics interfaced distributed generation systems in a customer-driven microgrid. In *Power and energy society general meeting, 2009. pes'09. ieee* (p. 1-8). IEEE.

Piagi, P., & Lasseter, R. H. (2006). Autonomous control of microgrids. In *Power engineering society general meeting, 2006. ieee.*

Pogaku, N. (2006). *Analysis, control and testing of inverter-based distributed generation in standalone and grid-connected applications* (Unpublished doctoral dissertation).

Pogaku, N., Prodanovic, M., & Green, T. C. (2007). Modeling, analysis and testing of autonomous operation of an inverter-based microgrid. *Power Electronics, IEEE Transactions on*, *22*(2).

Ponnaluri, S., Linhofer, G., Steinke, J., & Steimer, P. (2005). Comparison of single and two stage topologies for interface of bess or fuel cell system using the abb standard power electronics building blocks. In *Power electronics and applications, 2005 european conference on* (p. 9 pp.-P. 9). IEEE.

Prodanovic, M., & Green, T. C. (2006). High-quality power generation through distributed control of a power park microgrid. *Industrial Electronics, IEEE Transactions on*, *53*(5).

Rahman, S., & Tam, K.-s. (1988). A feasibility study of photovoltaic-fuel cell hybrid energy system. *Energy Conversion, IEEE Transactions on*, *3*(1), 50–55.

Rekik, M., Abdelkafi, A., & Krichen, L. (2015). A micro-grid ensuring multi-objective control strategy of a power electrical system for quality improvement. *Energy*, *88*, 351–363.

Rocabert, J., Luna, A., Blaabjerg, F., Rodri, x, & guez, P. (2012). Control of power converters in ac microgrids. *Power Electronics, IEEE Transactions on*, *27*(11).

Saadat, H. (2002). *Power system analysis*. McGraw-Hill Primis Custom.

University of Malaya

Salam, A., Mohamed, A., & Hannan, M. (2008). Technical challenges on microgrids. *ARPN Journal of engineering and applied sciences*, *3*(6).

Sao, C., & Lehn, P. (2006). Intentional islanded operation of converter fed microgrids. In *Power engineering society general meeting, 2006. ieee* (p. 6 pp.). IEEE.

Sao, C., & Lehn, P. (2008). Control and power management of converter fed microgrids. *Power Systems, IEEE Transactions on*, *23*(3).

Savaghebi, M., Jalilian, A., Vasquez, J. C., & Guerrero, J. M. (2013). Autonomous voltage unbalance compensation in an islanded droop-controlled microgrid. *Ieee Transactions on Industrial Electronics*, *60*(4).

Schenk, T., & Stokes, L. (2013, May). The power of collaboration: Engaging all parties in renewable energy infrastructure development. *Power and Energy Magazine, IEEE*, *11*(3), 56-65. doi: 10.1109/MPE.2013.2246736

Serban, E., & Serban, H. (2010). A control strategy for a distributed power generation microgrid application with voltage- and current-controlled source converter. *Power Electronics, IEEE Transactions on*, *25*(12).

Shahnia, F., Majumder, R., Ghosh, A., Ledwich, G., & Zare, F. (2010). Operation and control of a hybrid microgrid containing unbalanced and nonlinear loads. *Electric Power Systems Research*, *80*(8), 954–965.

Shamshiri, M., Chin Kim, G., & Chee Wei, T. (2012). A review of recent development in smart grid and micro-grid laboratories. In *Power engineering and optimization conference (pedco) melaka, malaysia, 2012 ieee international* (p. 367-372).

Silva, M., Morais, H., & Vale, Z. (2012). An integrated approach for distributed energy resource short-term scheduling in smart grids considering realistic power system simulation. *Energy Conversion and Management*, *64*(0).

Skjellnes, T., Skjellnes, A., & Norum, L. E. (2002). Load sharing for parallel inverters without communication. In *Nordic workshop on power and industrial electronics (norpie 2002), stockholm, sweden.*

Song, Y., Chung, S., & Enjeti, P. (2004). A current-fed hf link direct dc/ac converter with active harmonic filter for fuel cell power systems. In *Industry applications conference, 2004. 39th ias annual meeting. conference record of the 2004 ieee* (Vol. 1). IEEE.

Sontidpanya, C., Radman, G., & Craven, R. (2011). An island detection demonstration on a laboratory sized power grid (labgrid). In *Southeastcon, 2011 proceedings of ieee* (p. 158-163). IEEE.

Srivastava, A. K., Kumar, A. A., & Schulz, N. N. (2012). Impact of distributed generations with energy storage devices on the electric grid. *Systems Journal, IEEE*, *6*(1).

Sun, X., Lee, Y.-S., & Xu, D. (2003). Modeling, analysis, and implementation of parallel

University of Malaya

multi-inverter systems with instantaneous average-current-sharing scheme. *Power Electronics, IEEE Transactions on*, *18*(3).

Tamai, S., & Kinoshita, M. (1991). Parallel operation of digital controlled ups system. In *Industrial electronics, control and instrumentation, 1991. proceedings. iecon'91., 1991 international conference on* (p. 326-331). IEEE.

Tan, J., Lin, H., Zhang, J., & Ying, J. (2003). A novel load sharing control technique for paralleled inverters. In *Power electronics specialist conference, 2003. pesc'03. 2003 ieee 34th annual* (Vol. 3, p. 1432-1437). IEEE.

Teimourzadeh Baboli, P., Shahparasti, M., Parsa Moghaddam, M., Haghifam, M. R., & Mohamadian, M. (2014). Energy management and operation modelling of hybrid ac–dc microgrid. *Generation, Transmission & Distribution, IET*, *8*(10), 1700–1711.

Tsang, K., & Chan, W. (2013). Three-level grid-connected photovoltaic inverter with maximum power point tracking. *Energy Conversion and Management*, *65*(0), 221 - 227. (Global Conference on Renewable energy and Energy Efficiency for Desert Regions 2011)

Tuladhar, A., Jin, H., Unger, T., & Mauch, K. (1997). Parallel operation of single phase inverter modules with no control interconnections. In *Applied power electronics conference and exposition, 1997. apec'97 conference proceedings 1997., twelfth annual* (Vol. 1, p. 94-100). IEEE.

Tuladhar, A., Jin, H., Unger, T., & Mauch, K. (2000). Control of parallel inverters in distributed ac power systems with consideration of line impedance effect. *Industry Applications, IEEE Transactions on*, *36*(1).

Turitsyn, K., Sulc, P., Backhaus, S., & Chertkov, M. (2011). Options for control of reactive power by distributed photovoltaic generators. *Proceedings of the IEEE*, *99*(6).

Ustun, T. S., Ozansoy, C., & Zayegh, A. (2011). Recent developments in microgrids and example cases around the world—a review. *Renewable and Sustainable Energy Reviews*, *15*(8).

von Appen, J., Braun, M., Stetz, T., Diwold, K., & Geibel, D. (2013). Time in the sun: the challenge of high pv penetration in the german electric grid. *Power and Energy Magazine, IEEE*, *11*(2), 55–64.

Wang, C., & Nehrir, M. (2007, Dec). A physically based dynamic model for solid oxide fuel cells. *Energy Conversion, IEEE Transactions on*, *22*(4), 887-897. doi: 10.1109/TEC.2007.895468

Wu, J., Botterud, A., Mills, A., Zhou, Z., Hodge, B.-M., & Heaney, M. (2015). Integrating solar pv (photovoltaics) in utility system operations: Analytical framework and arizona case study. *Energy*, *85*, 1–9.

Wu, R., Dewan, S. B., & Slemon, G. R. (1991). Analysis of an ac-to-dc voltage source converter using pwm with phase and amplitude control. *Industry Applications, IEEE*

University of Malaya

Transactions on, *27*(2), 355–364.

Wu, T.-F., Chen, Y.-K., & Huang, Y.-H. (2000). 3c strategy for inverters in parallel operation achieving an equal current distribution. *Industrial Electronics, IEEE Transactions on*, *47*(2).

Xiao, W., Edwin, F. F., Spagnuolo, G., & Jatskevich, J. (2013). Efficient approaches for modeling and simulating photovoltaic power systems. *Photovoltaics, IEEE Journal of*, *3*(1), 500–508.

Ya'acob, M. E., Hizam, H., Khatib, T., Radzi, M. A. M., Gomes, C., Marhaban, M. H., ... others (2014). Modelling of photovoltaic array temperature in a tropical site using generalized extreme value distribution. *Journal of Renewable and Sustainable Energy*, *6*(3), 033134.

Yazdani, A., Di Fazio, A., Ghoddami, H., Russo, M., Kazerani, M., Jatskevich, J., ... Martinez, J. (2011, April). Modeling guidelines and a benchmark for power system simulation studies of three-phase single-stage photovoltaic systems. *Power Delivery, IEEE Transactions on*, *26*(2), 1247-1264. doi: 10.1109/TPWRD.2010.2084599

Yun Tiam, T., Kirschen, D. S., & Jenkins, N. (2004). A model of pv generation suitable for stability analysis. *Energy Conversion, IEEE Transactions on*, *19*(4).

Yunwei, L., Vilathgamuwa, D. M., & Poh Chiang, L. (2004). Design, analysis, and real-time testing of a controller for multibus microgrid system. *Power Electronics, IEEE Transactions on*, *19*(5).

Zabaiou, T., Dessaint, L.-A., & Kamwa, I. (2014). Preventive control approach for voltage stability improvement using voltage stability constrained optimal power flow based on static line voltage stability indices. *IET Generation, Transmission & Distribution*, *8*(5), 924–934.

Zanxuan, F., & Wenlong, Q. (2004). A current share method for parallel single-phase dc/ac inverter without control interconnection. In *Power electronics and motion control conference, 2004. ipemc 2004. the 4th international* (Vol. 2, p. 953-955). IEEE.

Zhang, Z., Huang, X., Jiang, J., & Wu, B. (2010). A load-sharing control scheme for a microgrid with a fixed frequency inverter. *Electric Power Systems Research*, *80*(3).

University of Malaya

LIST OF PUBLICATIONS

C.1 Journals

- Eid, B., Rahim, N., Selvaraj, J., & El Khateb, A. (2014). Control methods and objectives for electronically coupled distributed energy resources in microgrids: a review. Systems Journal, IEEE, PP(99), 1-13.
- Eid, B., Rahim, N., Selvaraj, J., & Williams B. (2015). Electronically coupled distributed generation modeling and control strategies for microgrid applications. Applied Mathematics & Information Sciences.

C.2 Proceedings

- Eid, B., Rahim, N., & Selvaraj, J. (2014). "DISTRIBUTED PHOTOVOLTAIC INVERTER PERFORMING MAXIMUM POWER POINT TRACKING AND DISPATCHING UNITY POWER FACTOR", 3RD IET International Conference on Clean Energy and Technology (CEAT 2014), Kuching, Sarawak, Malaysia
- Alyan, A., Rahim, N., Mubin M., & Eid, B. (2014) "NEW TOPOLOGY THREE PHASE MULTILEVEL INVERTER FOR GRID-CONNECTED PHOTOVOLTAIC SYSTEM", International Symposium on Industrial Electronics (ISIE2014) IEEE, Istanbul, Turkey
- Eid, B., Rahim, N., & Selvaraj, J. (2013). "DISTRIBUTED PHOTOVOLTAIC GENERATOR PERFORMING REACTIVE POWER COMPENSATION", IEEE Conference on Clean Energy and Technology (CEAT 2013), Langkawi, Malaysia
- Eid, B., Rahim, N., & Selvaraj, J. (2012). "MICROGIRD SYSTEM WITH MULTI DISTRIBUTED ENERGY RESOURCES USING MATALB/SIMULINK ", Power and Energy Conversion Symposium (PECS 2012), Melaka, Malaysia

University of Malaya

APPENDIX A

Table 1: Appendix: Electrical specifications of the SunPower PV panels

Parameter	**Value**
Number of cells in series	96
Maximum Power (P_{mp}) [W]	305.2
V_{mp} [V]	54.7
I_{mp} [A]	5.58
V_{OC} [V]	64.2
I_{SC} [A]	5.96
Series resistance of PV model (R_s) [ohms]	3.80e-02
Parallel resistance of PV model (R_{sh}) [ohms]	9.94e+02
Diode reverse saturation current (I_{rsc}) [A]	3.19e-08
Light-generated photo-current (I_{ph}) [A]	5.96
Diode quality factor of PV model (η)	1.3

University of Malaya

APPENDIX B

IEEE 30-BUS TEST SYSTEM (American Electric Power)

B.1 Bus data

```
basemva = 100;  accuracy = 0.001; maxiter = 10;

%         Bus Bus  Voltage Angle   ---Load---- -------Generator----- Injected
%         No  code Mag.    Degree  MW     Mvar  MW  Mvar Qmin Qmax     Mvar
busdata=[1    1    1.06    0.0     0.0    0.0   0.0 0.0   0    0        0
         2    2    1.043   0.0    21.70  12.7  40.0 0.0 -40   50        0
         3    0    1.0     0.0     2.4    1.2   0.0 0.0   0    0        0
         4    0    1.06    0.0     7.6    1.6   0.0 0.0   0    0        0
         5    2    1.01    0.0    94.2   19.0   0.0 0.0 -40   40        0
         6    0    1.0     0.0     0.0    0.0   0.0 0.0   0    0        0
         7    0    1.0     0.0    22.8   10.9   0.0 0.0   0    0        0
         8    2    1.01    0.0    30.0   30.0   0.0 0.0 -10   60        0
         9    0    1.0     0.0     0.0    0.0   0.0 0.0   0    0        0
        10    0    1.0     0.0     5.8    2.0   0.0 0.0  -6   24       19
        11    2    1.082   0.0     0.0    0.0   0.0 0.0   0    0        0
        12    0    1.0     0      11.2    7.5   0   0     0    0        0
        13    2    1.071   0       0      0.0   0   0    -6   24        0
        14    0    1       0       6.2    1.6   0   0     0    0        0
        15    0    1       0       8.2    2.5   0   0     0    0        0
        16    0    1       0       3.5    1.8   0   0     0    0        0
        17    0    1       0       9.0    5.8   0   0     0    0        0
        18    0    1       0       3.2    0.9   0   0     0    0        0
        19    0    1       0       9.5    3.4   0   0     0    0        0
        20    0    1       0       2.2    0.7   0   0     0    0        0
```

University of Malaya

```
21   0   1   0   17.5   11.2   0   0   0   0   0
22   0   1   0   0      0.0    0   0   0   0   0
23   0   1   0   3.2    1.6    0   0   0   0   0
24   0   1   0   8.7    6.7    0   0   0   0   4.3
25   0   1   0   0      0.0    0   0   0   0   0
26   0   1   0   3.5    2.3    0   0   0   0   0
27   0   1   0   0      0.0    0   0   0   0   0
28   0   1   0   0      0.0    0   0   0   0   0
29   0   1   0   2.4    0.9    0   0   0   0   0
30   0   1   0   10.6   1.9    0   0   0   0   0];
```

B.2 line data

```
%                                         Line code
%         Bus bus   R       X      1/2 B   = 1 for lines
%         nl  nr  p.u.    p.u.    p.u.     > 1 or < 1 tr. tap at bus nl
linedata=[1   2   0.0192  0.0575  0.02640   1
          1   3   0.0452  0.1852  0.02040   1
          2   4   0.0570  0.1737  0.01840   1
          3   4   0.0132  0.0379  0.00420   1
          2   5   0.0472  0.1983  0.02090   1
          2   6   0.0581  0.1763  0.01870   1
          4   6   0.0119  0.0414  0.00450   1
          5   7   0.0460  0.1160  0.01020   1
          6   7   0.0267  0.0820  0.00850   1
          6   8   0.0120  0.0420  0.00450   1
          6   9   0.0     0.2080  0.0     0.978
          6  10   0        .5560  0       0.969
          9  11   0        .2080  0         1
          9  10   0        .1100  0         1
```

University of Malaya

```
                  4   12    0          .2560    0      0.932
                 12   13    0          .1400    0          1
                 12   14     .1231     .2559    0          1
                 12   15     .0662     .1304    0          1
                 12   16     .0945     .1987    0          1
                 14   15     .2210     .1997    0          1
                 16   17     .0824     .1923    0          1
                 15   18     .1073     .2185    0          1
                 18   19     .0639     .1292    0          1
                 19   20     .0340     .0680    0          1
                 10   20     .0936     .2090    0          1
                 10   17     .0324     .0845    0          1
                 10   21     .0348     .0749    0          1
                 10   22     .0727     .1499    0          1
                 21   22     .0116     .0236    0          1
                 15   23     .1000     .2020    0          1
                 22   24     .1150     .1790    0          1
                 23   24     .1320     .2700    0          1
                 24   25     .1885     .3292    0          1
                 25   26     .2544     .3800    0          1
                 25   27     .1093     .2087    0          1
                 28   27      0        .3960    0      0.968
                 27   29     .2198     .4153    0          1
                 27   30     .3202     .6027    0          1
                 29   30     .2399     .4533    0          1
                  8   28     .0636     .2000    0.0214     1
                  6   28     .0169     .0599    0.065      1];
lfybus                               % form the bus admittance matrix
lfnewton                % Load load flow solution by Newton-Raphson method
busout                 % Prints the power flow solution on the screen
```

University of Malaya

```
lineflow          % computes and displays the line flow and losses
```

B.3 The program obtains the Bus Admittance Matrix for power flow solution

```
%  This program obtains the Bus Admittance Matrix for power flow solution
%  Copyright (c) 1998 by H. Saadat

j=sqrt(-1); i = sqrt(-1);
nl = linedata(:,1); nr = linedata(:,2); R = linedata(:,3);
X = linedata(:,4); Bc = j*linedata(:,5); a = linedata(:, 6);
nbr=length(linedata(:,1)); nbus = max(max(nl), max(nr));
Z = R + j*X; y= ones(nbr,1)./Z;        %branch admittance
for n = 1:nbr
if a(n) <= 0
    a(n) = 1; else end
Ybus=zeros(nbus,nbus);      % initialize Ybus to zero
               % formation of the off diagonal elements
for k=1:nbr;
       Ybus(nl(k),nr(k))=Ybus(nl(k),nr(k))-y(k)/a(k);
       Ybus(nr(k),nl(k))=Ybus(nl(k),nr(k));
    end
end
              % formation of the diagonal elements
for  n=1:nbus
     for k=1:nbr
         if nl(k)==n
         Ybus(n,n) = Ybus(n,n)+y(k)/(a(k)^2) + Bc(k);
         elseif nr(k)==n
         Ybus(n,n) = Ybus(n,n)+y(k) +Bc(k);
```

University of Malaya

```
        else, end
    end
end
clear Pgg
```

University of Malaya

B.4 Power Flow Solution by Newton-Raphson method

```
%   Power flow solution by Newton-Raphson method
%   Copyright (c) 1998 by  H. Saadat
%   Revision 1 (Aug. 99) To include two or more parallel lines
ns=0; ng=0; Vm=0; delta=0; yload=0; deltad=0;
nbus = length(busdata(:,1));
kb=[];Vm=[]; delta=[]; Pd=[]; Qd=[]; Pg=[]; Qg=[]; Qmin=[]; Qmax=[];  % Added (6-8-00)
Pk=[]; P=[]; Qk=[]; Q=[]; S=[]; V=[]; % Added (6-8-00)
for k=1:nbus
n=busdata(k,1);
kb(n)=busdata(k,2); Vm(n)=busdata(k,3); delta(n)=busdata(k, 4);
Pd(n)=busdata(k,5); Qd(n)=busdata(k,6); Pg(n)=busdata(k,7); Qg(n) = busdata(k,8);
Qmin(n)=busdata(k, 9); Qmax(n)=busdata(k, 10);
Qsh(n)=busdata(k, 11);
    if Vm(n) <= 0
        Vm(n) = 1.0; V(n) = 1 + j*0;
```

University of Malaya

```
    else delta(n) = pi/180*delta(n);
         V(n) = Vm(n)*(cos(delta(n)) + j*sin(delta(n)));
         P(n)=(Pg(n)-Pd(n))/basemva;
         Q(n)=(Qg(n)-Qd(n)+ Qsh(n))/basemva;
         S(n) = P(n) + j*Q(n);
    end
end
for k=1:nbus
if kb(k) == 1, ns = ns+1; else, end
if kb(k) == 2
    ng = ng+1; else, end
ngs(k) = ng;
nss(k) = ns;
end
Ym=abs(Ybus); t = angle(Ybus);
m=2*nbus-ng-2*ns;
maxerror = 1; converge=1;
iter = 0;
```

```
%%%% added for parallel lines (Aug. 99)

mline=ones(nbr,1);

for k=1:nbr

      for m=k+1:nbr

         if((nl(k)==nl(m)) && (nr(k)==nr(m)));

            mline(m)=2;

         elseif ((nl(k)==nr(m)) && (nr(k)==nl(m)));

         mline(m)=2;

         else, end

      end

   end

%%%   end of statements for parallel lines (Aug. 99)


% Start of iterations

clear A  DC   J  DX

while maxerror >= accuracy && iter <= maxiter % Test for max. power mismatch

for ii=1:m

for k=1:m
```

University of Malaya

```
   A(ii,k)=0;      %Initializing Jacobian matrix
end, end
iter = iter+1;
for n=1:nbus
nn=n-nss(n);
lm=nbus+n-ngs(n)-nss(n)-ns;
J11=0; J22=0; J33=0; J44=0;
   for ii=1:nbr
    if mline(ii)==1   % Added to include parallel lines (Aug. 99)
        if nl(ii) == n || nr(ii) == n
            if nl(ii) == n ,  l = nr(ii); end
            if nr(ii) == n , l = nl(ii); end
         J11=J11+ Vm(n)*Vm(l)*Ym(n,l)*sin(t(n,l)- delta(n) + delta(l));
         J33=J33+ Vm(n)*Vm(l)*Ym(n,l)*cos(t(n,l)- delta(n) + delta(l));
                if kb(n)~=1
                J22=J22+ Vm(l)*Ym(n,l)*cos(t(n,l)- delta(n) + delta(l));
                J44=J44+ Vm(l)*Ym(n,l)*sin(t(n,l)- delta(n) + delta(l));
                else, end
```

University of Malaya

```
            if kb(n) ~= 1  && kb(l) ~=1
                lk = nbus+l-ngs(l)-nss(l)-ns;
                ll = l -nss(l);
            % off diagonalelements of J1
                A(nn, ll) =-Vm(n)*Vm(l)*Ym(n,l)*sin(t(n,l)- delta(n) + delta(l));
                if kb(l) == 0  % off diagonal elements of J2
                A(nn, lk) =Vm(n)*Ym(n,l)*cos(t(n,l)- delta(n) + delta(l));end
                if kb(n) == 0  % off diagonal elements of J3
                A(lm, ll) =-Vm(n)*Vm(l)*Ym(n,l)*cos(t(n,l)- delta(n)+delta(l)); end
                if kb(n) == 0 && kb(l) == 0  % off diagonal elements of  J4
                A(lm, lk) =-Vm(n)*Ym(n,l)*sin(t(n,l)- delta(n) + delta(l));end
           else end
        else , end
   else, end
end
Pk = Vm(n)^2*Ym(n,n)*cos(t(n,n))+J33;
Qk = -Vm(n)^2*Ym(n,n)*sin(t(n,n))-J11;
if kb(n) == 1
```

University of Malaya

```
    P(n)=Pk; Q(n) = Qk; end   % Swing bus P
  if kb(n) == 2
      Q(n)=Qk;
      if Qmax(n) ~= 0
        Qgc = Q(n)*basemva + Qd(n) - Qsh(n);
        if iter <= 7                  % Between the 2th & 6th iterations
           if iter > 2                % the Mvar of generator buses are
             if Qgc  < Qmin(n),       % tested. If not within limits Vm(n)
             Vm(n) = Vm(n) + 0.01;    % is changed in steps of 0.01 pu to
             elseif Qgc  > Qmax(n),   % bring the generator Mvar within
             Vm(n) = Vm(n) - 0.01;end % the specified limits.
           else, end
        else,end
      else,end
  end
if kb(n) ~= 1
  A(nn,nn) = J11;  %diagonal elements of J1
  DC(nn) = P(n)-Pk;
```

University of Malaya

```
    end
    if kb(n) == 0
      A(nn,lm) = 2*Vm(n)*Ym(n,n)*cos(t(n,n))+J22;  %diagonal elements of J2
      A(lm,nn)= J33;        %diagonal elements of J3
      A(lm,lm) =-2*Vm(n)*Ym(n,n)*sin(t(n,n))-J44;  %diagonal of elements of J4
      DC(lm) = Q(n)-Qk;
    end
end
DX=A\DC';
for n=1:nbus
  nn=n-nss(n);
  lm=nbus+n-ngs(n)-nss(n)-ns;
    if kb(n) ~= 1
    delta(n) = delta(n)+DX(nn); end
    if kb(n) == 0
    Vm(n)=Vm(n)+DX(lm); end
 end
  maxerror=max(abs(DC));
```

University of Malaya

```
     if iter == maxiter && maxerror > accuracy
   fprintf('\nWARNING: Iterative solution did not converged after ')
   fprintf('%g', iter), fprintf(' iterations.\n\n')
   fprintf('Press Enter to terminate the iterations and print the results \n')
   converge = 0; pause, else, end

end

if converge ~= 1
   tech= ('                      ITERATIVE SOLUTION DID NOT CONVERGE'); else,
   tech=('                   Power Flow Solution by Newton-Raphson Method');
end
V = Vm.*cos(delta)+j*Vm.*sin(delta);
deltad=180/pi*delta;
i=sqrt(-1);
k=0;
for n = 1:nbus
     if kb(n) == 1
```

University of Malaya

```
        k=k+1;
        S(n)= P(n)+j*Q(n);
        Pg(n) = P(n)*basemva + Pd(n);
        Qg(n) = Q(n)*basemva + Qd(n) - Qsh(n);
        Pgg(k)=Pg(n);
        Qgg(k)=Qg(n);     %june 97
        elseif  kb(n) ==2
        k=k+1;
        S(n)=P(n)+j*Q(n);
        Qg(n) = Q(n)*basemva + Qd(n) - Qsh(n);
        Pgg(k)=Pg(n);
        Qgg(k)=Qg(n);  % June 1997
   end
yload(n) = (Pd(n)- j*Qd(n)+j*Qsh(n))/(basemva*Vm(n)^2);
end
busdata(:,3)=Vm'; busdata(:,4)=deltad';
Pgt = sum(Pg);  Qgt = sum(Qg); Pdt = sum(Pd); Qdt = sum(Qd); Qsht = sum(Qsh);
```

University of Malaya

```
%clear A DC DX  J11 J22 J33 J44 Qk delta lk ll lm

%clear A DC DX  J11 J22 J33  Qk delta lk ll lm
```

B.5 The program prints the power flow solution

```
%  This program prints the power flow solution in a tabulated form on the screen.

%

%  Copyright (C) 1998 by H. Saadat.

%clc

disp(tech)

fprintf('                      Maximum Power Mismatch = %g \n', maxerror)

fprintf('                             No. of Iterations = %g \n\n', iter)

head =['    Bus  Voltage  Angle    ------Load------    ---Generation---   Injected'

       '    No.  Mag.     Degree     MW       Mvar       MW       Mvar       Mvar '

       '                                                                          '];

disp(head)
```

University of Malaya

```
for n=1:nbus
     fprintf(' %5g', n), fprintf(' %7.3f', Vm(n)),
     fprintf(' %8.3f', deltad(n)), fprintf(' %9.3f', Pd(n)),
     fprintf(' %9.3f', Qd(n)),  fprintf(' %9.3f', Pg(n)),
     fprintf(' %9.3f ', Qg(n)), fprintf(' %8.3f\n', Qsh(n))
end
    fprintf('      \n'), fprintf('    Total               ')
    fprintf(' %9.3f', Pdt), fprintf(' %9.3f', Qdt),
    fprintf(' %9.3f', Pgt), fprintf(' %9.3f', Q
```

B.6 The program to compute line flow and line losses

```
%  This program is used in conjunction with lf Newton for the computation of line flow and line losses.
%
%  Copyright (c) 1998 H. Saadat
SLT = 0;
```

University of Malaya

```
fprintf('\n')
fprintf('                           Line Flow and Losses \n\n')
fprintf('     --Line--  Power at bus & line flow    --Line loss--  Transformer\n')
fprintf('     from  to    MW      Mvar     MVA       MW      Mvar      tap\n')
for n = 1:nbus
busprt = 0;
   for L = 1:nbr;
       if busprt == 0
       fprintf('   \n'), fprintf('%6g', n), fprintf('      %9.3f', P(n)*basemva)
       fprintf('%9.3f', Q(n)*basemva), fprintf('%9.3f\n', abs(S(n)*basemva))

       busprt = 1;
       else, end
       if nl(L)==n      k = nr(L);
       In = (V(n) - a(L)*V(k))*y(L)/a(L)^2 + Bc(L)/a(L)^2*V(n);
       Ik = (V(k) - V(n)/a(L))*y(L) + Bc(L)*V(k);
       Snk = V(n)*conj(In)*basemva;
       Skn = V(k)*conj(Ik)*basemva;
```


University of Malaya

```
SL  = Snk + Skn;
SLT = SLT + SL;
elseif nr(L)==n  k = nl(L);
In = (V(n) - V(k)/a(L))*y(L) + Bc(L)*V(n);
Ik = (V(k) - a(L)*V(n))*y(L)/a(L)^2 + Bc(L)/a(L)^2*V(k);
Snk = V(n)*conj(In)*basemva;
Skn = V(k)*conj(Ik)*basemva;
SL  = Snk + Skn;
SLT = SLT + SL;
else, end
  if nl(L)==n | nr(L)==n
  fprintf('%12g', k),
  fprintf('%9.3f', real(Snk)), fprintf('%9.3f', imag(Snk))
  fprintf('%9.3f', abs(Snk)),
  fprintf('%9.3f', real(SL)),
      if nl(L) ==n & a(L) ~= 1
      fprintf('%9.3f', imag(SL)), fprintf('%9.3f\n', a(L))
      else, fprintf('%9.3f\n', imag(SL))
```

University of Malaya

```
             end
         else, end
  end
end
SLT = SLT/2;
fprintf('   \n'), fprintf('    Total loss                         ')
fprintf('%9.3f', real(SLT)), fprintf('%9.3f\n', imag(SLT))
clear Ik In SL SLT Skn Snk
```

University of Malaya